Studies on neuroinvasion, susceptibility and long-term persistence of alphaherpesviruses in the murine central nervous system

INAUGURAL-DISSERTATION

zur Erlangung des Grades eines

Dr. med. vet.

beim Fachbereich Veterinärmedizin

der Justus-Liebig-Universität Gießen

Viktoria Korff

Aus dem Institut für Veterinär-Pathologie der Justus-Liebig-Universität in Gießen

und dem

Friedrich-Loeffler-Institut, Bundesforschungsinstitut für Tiergesundheit,

Greifswald – Insel Riems

Betreuer: Prof. Dr. Jens P. Teifke

Studies on neuroinvasion, susceptibility and long-term persistence of alphaherpesviruses in the murine central nervous system

INAUGURAL-DISSERTATION

zur Erlangung des Grades eines

Dr. med. vet.

beim Fachbereich Veterinärmedizin

der Justus-Liebig-Universität Gießen

eingereicht von

Viktoria Korff

Tierärztin aus Freiburg im Breisgau

Gießen 2025

Mit Genehmigung des Fachbereichs Veterinärmedizin
der Justus-Liebig-Universität Gießen

Dekan: Prof. Dr. Dr. Stefan Arnhold

1. Gutachter: Prof. Dr. Jens P. Teifke

2. Gutachter: Prof. Dr. Christiane Herden

Tag der Disputation: 11.05.2026

Table of Contents

Abbreviations

12N	Hypoglossal nucleus
AD	Alzheimer's disease
AI	Agranular insular cortex
Amb	Ambiguus nucleus
aMCI	Amnestic mild cognitive impairment
BoHV-1	Bovid alpha Herpes Virus 1
CCL	C-C chemokine motif ligand
CN	Cranial nerve
CNS	Central nervous system
CSF	Cerebrospinal fluid
CXCL	C-X-C chemokine motif ligand
dpi	Days post infection
dpt	Days post treatment
DRG	Dorsal root ganglion
FR	Reticular formation
Hpc	Hippocampus
HSE	Herpes simplex encephalitis
HSV-1	Herpes Simplex Virus 1
IFN	Interferon
LAT	Latency associated transcript
LEnt	Lateral entorhinal cortex
M1	Primary motor cortex
Me5	Mesencephalic trigeminal nucleus
miRNA	MicroRNA
MO	Medial orbital cortex
MTL	Mesiotemporal lobe

OB	Olfactory bulb
OE	Olfactory epithelium
Pir	Piriform cortex
Pr5	Principal sensory nucleus
PrV	Pseudorabies
PrV-Ka	PrV- Kaplan
RNA-ISH	RNA in situ hybridization
S1	Primary somatosensory cortex
SCG	Superior cervical ganglion
Sol	Nucleus of the solitary tract
Sp5	Spinal trigeminal nucleus
TG	Trigeminal ganglion
U_L	Unique long
U_S	Unique short
V1	Primary visual cortex
V2	Secondary visual cortex
VMO	Vomeronasalorgan
VPM	Ventral posteromedial nucleus
VZV	Varicella Zoster Virus

1 Initial remarks and objectives

Alphaherpesviruses such as Herpes Simplex Virus 1 (HSV-1) and Pseudorabies Virus (PrV) are neurotropic, double-stranded DNA viruses capable of causing severe neurological disease in their natural and incidental hosts (Mettenleiter et al., 2019; Stahl and Mailles, 2019). Following productive infection of the oral or nasal mucosa, virions enter peripheral sensory neurons – most notably via nectin-1 (Spear et al., 2000; Mettenleiter, 2003) – and undergo retrograde axonal transport to peripheral and autonomic ganglia, particularly the trigeminal ganglion (TG). There, the virus either establishes lifelong latency or continues to spread to higher-order brain regions (Hill et al., 1975; Hill et al., 2001; Smith, 2012; Koyuncu et al., 2018; Duarte et al., 2019).

Productive infection proceeds through the canonical immediate-early, early, and late transcriptional cascade (Ben-Porat and Kaplan, 1985; Pomeranz et al., 2005) whereas latency is defined by the persistence of the viral genome in an episomal form, with transcription largely restricted to latency-associated transcripts (LATs) (Pomeranz et al., 2005; Mahjoub et al., 2015; Phelan et al., 2017) and microRNAs (miRNAs) that suppress apoptosis and reactivation (Perng et al., 2000; Gupta et al., 2006; Umbach et al., 2008; Shen et al., 2009). The balance between latency and reactivation is governed by viral–host interactions within neurons and by immune surveillance (Divito et al., 2006).

Physiological or environmental stressors can tip this balance leading to renewed viral replication and spread anterogradely to peripheral sites or retrogradely into the central nervous system (CNS) (Harrison and Jones, 2022).

Two principal neuronal routes have been implicated in CNS invasion:

1) the trigeminal pathway connecting peripheral ganglia with brainstem nuclei and thalamocortical targets (Arbuthnot et al., 1990; Ezure et al., 2001; Held and Derfuss, 2011), and

2) the olfactory pathway, whereby virions detected in the olfactory epithelium (OE) can reach mesiotemporal areas via the olfactory bulb (OB) (Twomey et al., 1979; Esiri, 1982; Shivkumar et al., 2013; Barrios et al., 2014; Verpoest et al., 2017; Menendez and Carr, 2017b; Niemeyer et al., 2024).

Despite extensive research, the relative contribution, timing, and anatomical specificity of these routes remain incompletely resolved.

Once in the brain, alphaherpesviruses elicit robust inflammatory responses. PrV, a close relative of HSV-1, induces fatal encephalitis and severe pruritus in a broad range of non-suid species (Mettenleiter, 2000). HSV-1 is the leading cause of sporadic Herpes Simplex Encephalitis (HSE) in humans, a life-threatening disease with a marked tropism for mesiotemporal and frontal brain regions (Bradshaw and Venkatesan, 2016; Stahl and Mailles, 2019).

The mechanisms underlying this selective vulnerability are poorly understood and may involve differential receptor expression, regional neuroimmune milieus, and systems-level connectivity (Damasio and van Hoesen, 1985; Boggian et al., 2000; Tyler, 2004; Lathe and Haas, 2017; Masuda et al., 2019; Verzosa et al., 2021).

To address these gaps, we employed an attenuated PrV strain — PrV-ΔUL21/US3Δkin — which lacks the tegument protein pUL21 and expresses a kinase-inactive pUS3. In female CD1 mice intranasal infection with this mutant causes non-lethal lymphohistiocytic meningoencephalitis in the frontal and mesiotemporal lobes (MTL), recapitulating clinical, anatomical, and histopathological features of human HSE (Sehl et al., 2020). Prior work indicates a multiphasic disease course with persistent neuroinflammation and late clinical exacerbations, raising the possibility of viral persistence and/or intermittent reactivation within the CNS (Sehl-Ewert et al., 2022).

Objectives

This thesis aims to identify and characterize the major determinants of alphaherpesviral neuroinvasion and persistence in the CNS by combining complementary in vitro and in vivo investigations in the PrV-ΔUL21/US3Δkin mouse model.

1. Regional susceptibility: Determine whether distinct CNS regions and neuronal populations exhibit differential susceptibility to PrV infection.
2. Early entry routes: Define the earliest replication sites and anatomical pathways mediating neuroinvasion after intranasal inoculation, with a focus on olfactory, trigeminal, and additional cranial nerve routes.
3. Long-term infection dynamics: Assess whether prolonged infection entails viral persistence and/or reactivation and characterize associated chronic inflammatory changes.

Approach

- In vitro susceptibility assays using primary neurons derived from cerebral and cerebellar regions to profile region- and cell type–specific specificity (**paper I**).
- Stereotactic intracranial inoculations into the temporal lobe and cerebellum to analyze regional vulnerability and dissemination; receptor-level analyses emphasizing nectin-1 by immunofluorescence (**paper I**).
- Time-resolved mapping of early CNS entry routes after intranasal inoculation using immunofluorescence and RNA in situ hybridization (RNA-ISH) to track olfactory, trigeminal, and additional cranial nerve pathways (**paper II**).
- Long-term study up to 105 days post infection (dpi) integrating RNA-ISH, RT-qPCR, and histopathology to evaluate viral transcripts, immune cell infiltration, and lesion development (**paper III**).

By integrating molecular, anatomical, and histopathological readouts, we validate PrV-ΔUL21/US3Δkin as a robust experimental platform and delineate critical mechanisms of alphaherpesviral neuroinvasion and persistence in the murine CNS.

2 Introduction

2.1 The central nervous system

The nervous system is divided into two major components: the peripheral nervous system (PNS), which consists of peripheral nerves and ganglia, and the CNS, which comprises the brain and spinal cord.

2.1.1 Cells of the CNS

Neural tissue is composed of two principal cell types: neurons, which generate and transmit electrical impulses, and glial cells, which provide structural, metabolic, and immunological support (Fig. 1).

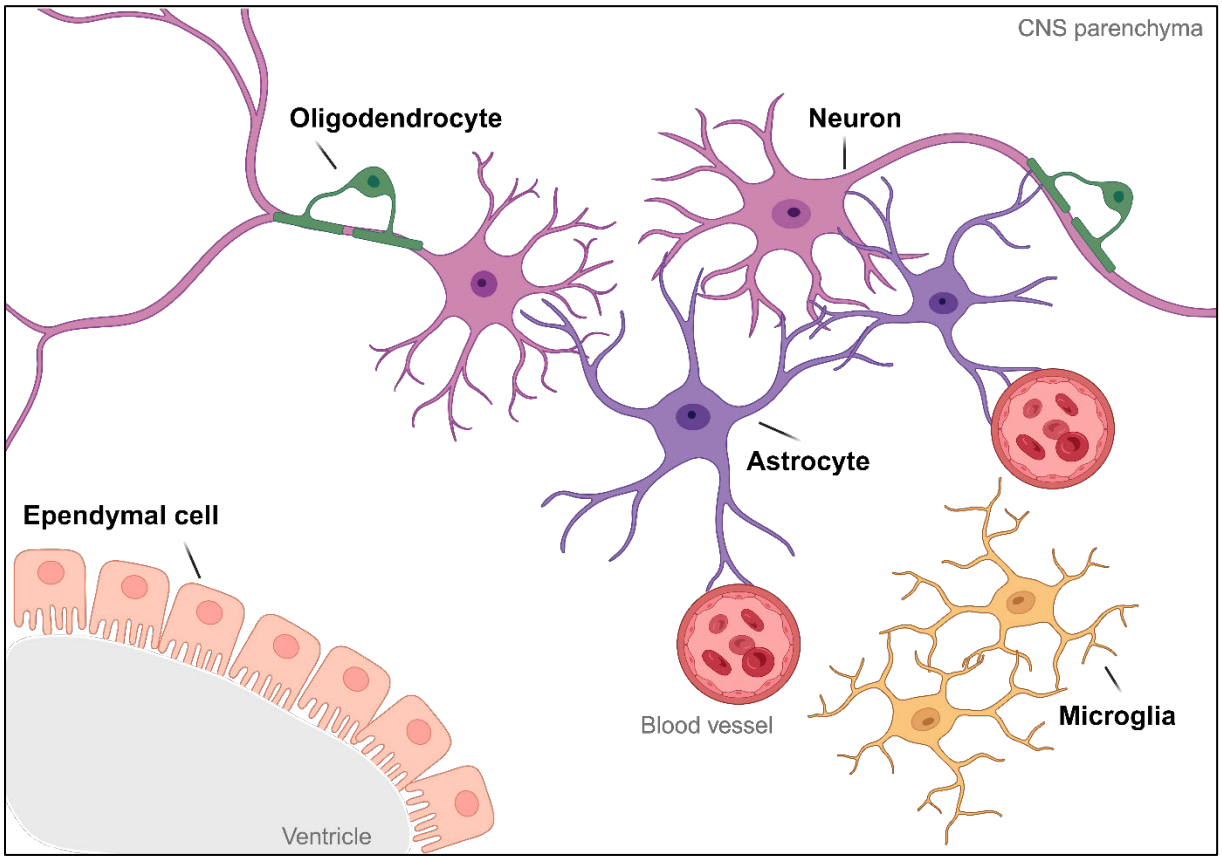

Fig. 1 Cellular composition of the CNS. *Schematic representation of major CNS cell types, including ependymal cells lining the ventricular system, neurons with myelinated axons ensheathed by oligodendrocytes, astrocytes forming the blood-brain barrier at vascular interfaces, and microglia serving as resident immune cells. Created with BioRender.com.*

Among the neuroglia of the CNS, ependymal cells line the ventricular system and contribute to the production and circulation of cerebrospinal fluid (CSF) through their ciliated apical surfaces (Deng et al., 2023). Astrocytes play a key role in maintaining ionic homeostasis, regulating neurotransmitter uptake, and forming the blood-brain barrier, thereby supporting neuronal function and synaptic transmission (Cabezas et al., 2014)**.** Microglia serve as the resident immune cells of the CNS, engaging in phagocytosis, antigen presentation, and mediating inflammatory responses during injury or disease (Colonna and Butovsky, 2017; Qin et al., 2023). Oligodendrocytes are responsible for myelinating axons within the CNS, thereby increasing the speed and efficiency of action potential conduction (Simons and Nave, 2015).

Neurons consist of a cell body (soma) containing the nucleus, an axon, and proximal and distal dendrites. The axon is specialized for impulse conduction and differs from the soma and dendrites by lacking rough endoplasmic reticulum and ribosomes (Raine, 1999). Neurons are morphologically classified based on the number and arrangement of their processes (Fig. 2). Multipolar neurons, the most prevalent type in the CNS, possess a single axon and multiple dendrites that branch extensively near the soma, allowing complex synaptic integration and motor output (Rolls and Jegla, 2015). Bipolar neurons have one axon and one dendrite emerging from opposite poles of the soma and are typically found in specialized sensory systems, such as the retina and olfactory epithelium (Remington, 2012; Brozzetti et al., 2020). Pseudounipolar neurons, which originate as bipolar during development, exhibit a single process that bifurcates into peripheral and central branches and are primarily located in peripheral sensory ganglia, where they mediate signal transmission from the periphery to the CNS (Fitzgerald, 2005).

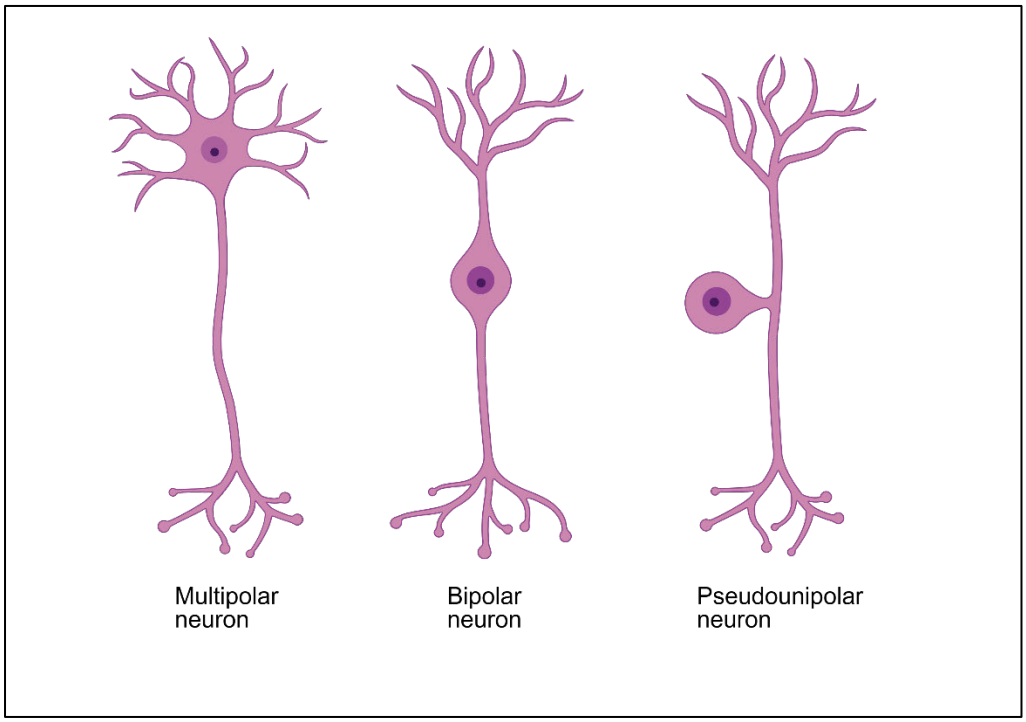

***Fig. 2 Structural classification of neurons**. Schematic illustration depicting three principal neuronal types based on morphological characteristics: (i) multipolar neurons, characterized by multiple dendrites and a single axon; (ii) bipolar neurons, with one dendrite and one axon emerging from opposite poles of the soma; and (iii) pseudounipolar neurons, exhibiting a single process that bifurcates into peripheral and central branches. Created with BioRender.com.*

Functionally, neurons are generally classified into three main types: sensory neurons, motor neurons, and interneurons. Sensory neurons transmit signals from peripheral receptors toward the CNS (afferent pathway). Motor neurons convey signals from the CNS to effectors such as muscles or glands (efferent pathway). Interneurons, located entirely within the CNS, mediate communication between sensory and motor neurons and are essential for reflexes and higher-order processing (Sunderland, 2001).

2.1.2 Structural and functional organization

The CNS is organized into gray and white matter. Gray matter consists primarily of neuronal cell bodies, dendrites, and unmyelinated axons, forming the cortical surface and deep nuclei of the brain. In contrast, white matter is composed predominantly of myelinated axonal tracts and lies beneath the cortex. In the spinal cord, this arrangement is reversed, with gray matter occupying the central region and white matter surrounding it (Liebich, 2010).

Structurally, the brain is hierarchically organized into the hindbrain, midbrain, and forebrain (Wurst and Bally-Cuif, 2001) (Fig. 3A).

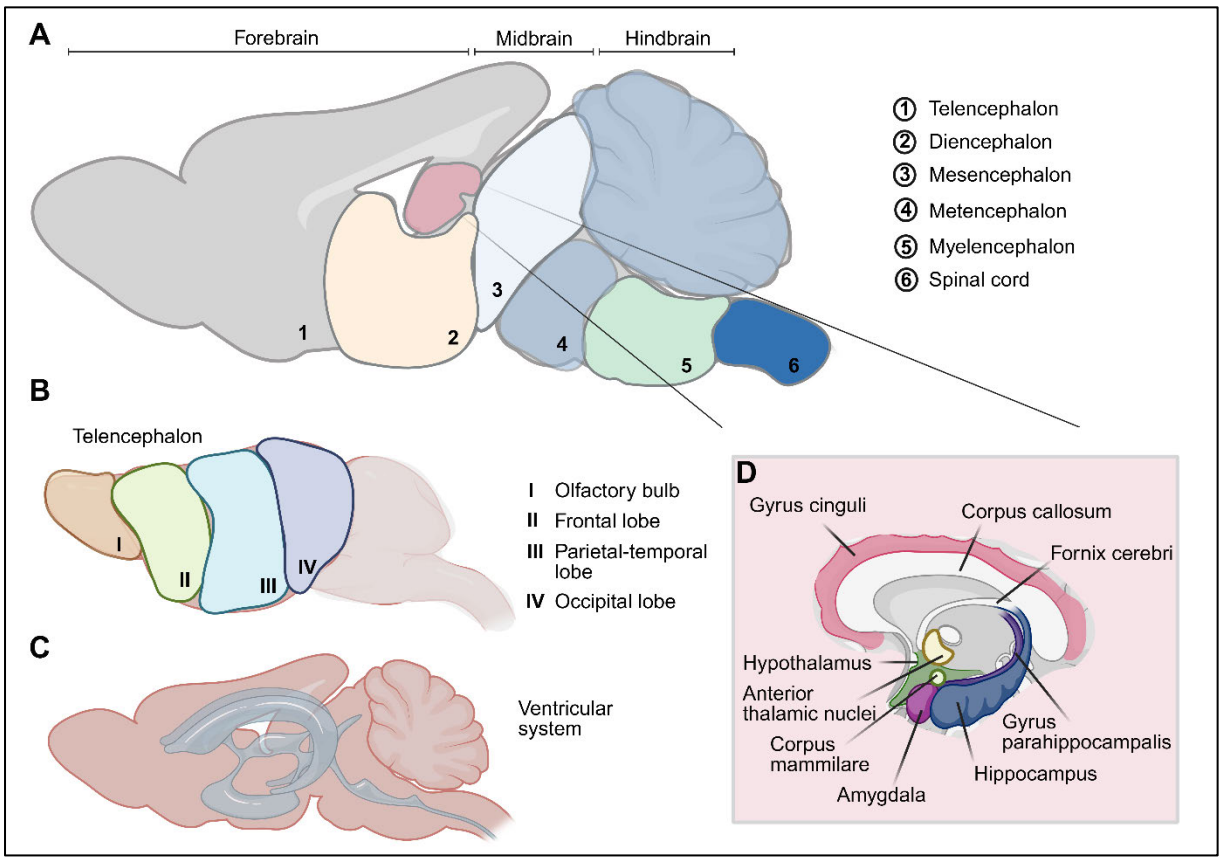

Fig. 3 Anatomical and functional organization of the murine brain. *A) The CNS is subdivided into three primary regions: the forebrain, midbrain, and hindbrain. These correspond to the major developmental subdivisions — the telencephalon (1) and diencephalon (2) forming the forebrain; the mesencephalon (3) constituting the midbrain; and the metencephalon (4) and myelencephalon (5) comprising the hindbrain. The spinal cord (6) represents the caudal continuation of the CNS. B) Telencephalic subdivisions, comprising olfactory bulb (I), frontal (II), parietal-temporal (III), and occipital (IV) regions. C) Ventricular system composed of cerebrospinal fluid-filled cavities. D) Limbic system architecture, highlighting key structures involved in emotion and memory processing, including the cingulate gyrus, corpus callosum, fornix, hypothalamus, anterior thalamic nuclei, mammillary bodies, amygdala, parahippocampal gyrus, and hippocampus. Created with BioRender.com*

The hindbrain, comprising the myelencephalon and metencephalon, represents an evolutionarily conserved region fundamental for autonomic regulation, sensorimotor integration, and basic survival functions (Horn-Bochtler and Büttner-Ennever, 2011). The myelencephalon includes the medulla oblongata, which transitions caudally into the spinal cord, forming a continuous axis for neural transmission (Johns, 2014). This

region governs vital autonomic processes such as respiration and cardiovascular control (Diek et al., 2022).

The metencephalon comprises the pons and cerebellum. The pons serves as a relay between the cerebrum and cerebellum and contains parts of the reticular formation (FR), which plays a crucial role in autonomic control, including cardiovascular and respiratory regulation (Traurig, 2008). The cerebellum is critical for motor coordination, balance, and procedural learning (Narayanan and Thirumalai, 2019).

The midbrain (mesencephalon), contains the periaqueductal gray, ventral tegmental area, substantia nigra, parts of the FR, and the cerebral peduncles (Moreno-Bravo et al., 2012). These structures are involved in pain modulation, reward processing, and voluntary motor control (Gebhart and Schmidt, 2013).

Together, these three subdivisions form the brainstem, a central hub for integrative neural pathways and cranial nerve activity. The brainstem houses distinct cranial nerve (CN) nuclei responsible for a wide range of sensory and motor functions (Johns, 2014). These nuclei are distributed as follows: medulla oblongata (CN IX, X, XII), pons (CN V, VI, VII, VIII) and midbrain (CN III, IV) (Feldman et al., 2021).

Above the brainstem lies the forebrain, subdivided into the diencephalon and telencephalon. The diencephalon includes the thalamus, hypothalamus, and epithalamus (Puelles, 2019). The thalamus functions as an integration center for sensory and motor signals to the cerebral cortex (Fama and Sullivan, 2015), while the hypothalamus regulates endocrine and autonomic processes essential for homeostasis (Sawchenko and Swanson, 1981). The epithalamus, which includes the pineal gland, contributes to circadian rhythm regulation (Begemann et al., 2025).

The telencephalon represents the most evolutionarily advanced region of the brain and encompasses the cerebral cortex and subcortical structures such as the caudate nucleus, putamen and septal nuclei (Briscoe and Ragsdale, 2019). The cerebral cortex is anatomically divided into four lobes — frontal, parietal, temporal, and occipital — named according to the overlying cranial bones (Bruner et al., 2015) (Fig. 3B). Each lobe contains specialized subregions responsible for distinct motor, sensory, and cognitive functions.

The frontal lobe includes the primary motor cortex (M1), which initiates voluntary movement, and the secondary motor cortex, a broader functional region involved in motor planning, coordination, and integration of sensory input into motor output (Ohbayashi, 2021; Yoshida et al., 2025). The prefrontal cortex, encompassing the prelimbic, infralimbic, and orbitofrontal cortices (Mathiasen et al., 2023), plays a central role in executive functions, decision-making, and social behavior (Funahashi, 2017).

The parietal lobe houses the primary somatosensory cortex (S1), which processes tactile, proprioceptive, and nociceptive input (Borich et al., 2015). Posterior to S1 lies the secondary somatosensory cortex, which integrates bilateral sensory information and contributes to higher-order somatosensory perception, such as object recognition through touch and texture discrimination (Taub et al., 2024).

The temporal lobe contains the primary auditory cortex, responsible for processing acoustic input. Surrounding this area, the secondary auditory cortex contributes to the interpretation of complex sounds by integrating basic auditory features with memory and other sensory inputs (Angeloni and Geffen, 2018; Moerel et al., 2019). Deep within the temporal lobe lies the mesiotemporal region, which includes the hippocampus (Hpc), amygdala, subiculum, perirhinal and entorhinal cortices—structures essential for memory, spatial navigation, and emotional regulation (Squire and Zola-Morgan, 1991; Eichenbaum, 2000).

The occipital lobe is primarily dedicated to visual processing. It contains the primary visual cortex (V1), which receives input from the retina and encodes orientation, contrast, and motion. The secondary visual cortex (V2), adjacent to V1 contributes to higher-order visual functions including object recognition, color perception, and motion tracking (Uysal, 2023).

In addition to the classical lobes, the insular cortex — often referred to as the insular lobe — is a distinct cortical region located deep between the frontal and temporal cortex. The insula is involved in multimodal sensory integration, interoceptive awareness, emotional processing, and autonomic regulation (Evrard, 2019).

Cerebral cortex	Core functions
Frontal lobe	Motor control, executive functions (planning, decision-making), social behavior
Parietal lobe	Somatosensory perception, tactile and visuomotor integration
Temporal lobe	Auditory processing, memory formation, emotional processing
Occipital lobe	Visual perception, object and motion recognition, color discrimination
Insular cortex	Sensory integration, interoception, emotion, autonomic regulation

Table 1. *Overview of major cerebral lobes and their principal functions.*

Embedded within the CNS is the ventricular system, a series of interconnected cavities filled with CSF (Fig. 3C). CSF serves multiple essential functions, including mechanical protection, metabolic waste clearance, and the maintenance of intracranial pressure and ionic homeostasis (Brown *et al,* 2004). The entire CNS is enveloped by CSF and further protected by three meningeal layers: the dura mater, arachnoid mater, and pia mater (Schnell & Maher de Leon, 1998).

While anatomical organization delineates cortical regions and provides a useful map of specialization, the brain can also be understood in terms of functional systems that transcend lobe boundaries. Two of the most prominent among these are the limbic and olfactory systems.

2.1.3 The limbic system

The limbic system is a complex network of interconnected structures located between the cerebral cortex and brainstem, lateral to the thalamus. Its components derive from distinct embryological origins: mesencephalic regions process visual, auditory, and

somatosensory input; diencephalic structures include the hypothalamus, anterior thalamic nuclei, and habenular commissure; and telencephalic regions encompass cortical and subcortical areas such as the OB, Hpc, parahippocampal gyrus, fornix, mammillary bodies, septum pellucidum, nuclei septales, amygdala, cingulate gyrus, and entorhinal cortex (Catani et al., 2013) (Fig. 3D).

The limbic system is recognized as one component within a broader network regulating cognitive, autonomic and visceral functions. It plays a key role in spatial memory, learning, motivation, emotional processing, and social behavior (Hariri et al., 2000).

The hypothalamus, though primarily associated with homeostatic regulation, forms reciprocal connections with the nucleus accumbens, ventral tegmental area, hippocampus, and amygdala. This network — termed the “limbic-motor interface” — is essential for initiating behaviors such as feeding and fear responses, integrating emotional and cognitive signals to drive action (Mogenson et al., 1980).

The OBs transmit sensory input to the amygdala, orbitofrontal cortex, and Hpc, facilitating associative odor-taste learning (Schoenbaum et al., 1999; Royet and Plailly, 2004).

The amygdala, processes emotional responses, particularly fear, anxiety, and aggression, and contributes to memory formation and decision-making (Amunts et al., 2005).

The Hpc is an allocortical structure essential for memory consolidation (Squire, 1992). The parahippocampal gyrus, surrounding the Hpc, supports scene recognition and memory retrieval (Epstein and Kanwisher, 1998; McDonald et al., 2000).

The fornix serves as the Hpc’s primary efferent tract, terminating in the mammillary bodies, which are involved in episodic memory (Lövblad et al., 2014).

The cingulate gyrus, located above the corpus callosum, receives input from the thalamus and neocortex and is involved in emotion formation, learning, and motivation-linked behavior (Hadland et al., 2003; Hayden and Platt, 2010).

The entorhinal cortex, situated in the MTL, acts as the primary interface between the Hpc and neocortex. It is crucial for declarative and spatial memory, as well as memory formation and consolidation (Hargreaves et al., 2005; Jacobs et al., 2010).

Together, these structures form a dynamic system integrating sensory, emotional, and cognitive information, enabling adaptive behavior and complex memory processing. Notably, the limbic system is closely interconnected with the olfactory system, which provides direct input to limbic regions such as the amygdala, Hpc and entorhinal cortex. This anatomical and functional coupling underlies the profound influence of olfactory stimuli on emotional states and memory formation (Krusemark et al., 2013; Mena et al., 2025).

2.1.4 The olfactory system

The olfactory system is a highly specialized sensory network responsible for detecting and processing odorant molecules. It comprises interconnected neural structures that transform chemical stimuli into perceptual experiences (Fig. 4).

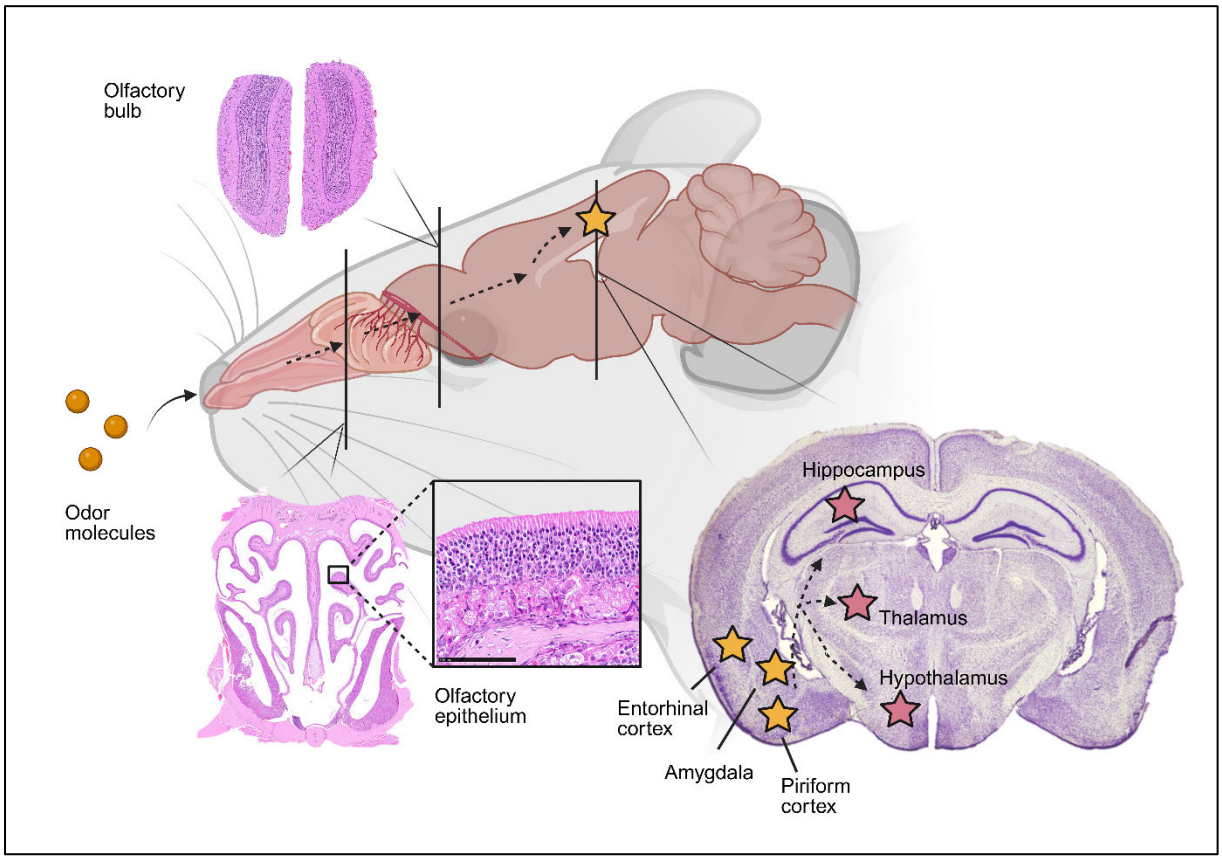

Fig. 4 Schematic overview of the murine olfactory pathway and associated cortical regions. *The scheme illustrates the pathway of odor detection and neural processing in the mouse, beginning with odorant molecules entering the nasal cavity and binding to receptors in the olfactory epithelium. Sensory input is transmitted via olfactory receptor neurons to the olfactory bulb, where initial signal processing occurs, and subsequently relayed to higher brain regions including the piriform cortex, amygdala, entorhinal cortex, hippocampus, thalamus, and hypothalamus. A coronal section of the telencephalon (modified from 'The Mouse Brain in Stereotaxic Coordinates' (Paxinos and Franklin, 2001)) illustrates the relative localization of olfactory projections within the forebrain. Scale bar: 100µm. Created with BioRender.com*

Odorant molecules bind to G-protein-coupled receptors located on the cilia of olfactory sensory neurons within the olfactory epithelium of the nasal cavity, initiating a transduction cascade that converts chemical signals into electrical activity transmitted via the olfactory nerve (Singletary and Hagerty, 2023). This nerve is formed by bundles of unmyelinated axons — collectively referred to as the *fila olfactoria* — which traverse the cribriform plate to terminate in the OB, located directly beneath the frontal lobe. Within the OB, these axons synapse onto mitral and tufted cells, initiating the central processing of olfactory input (Hintiryan et al., 2012; Durrant et al., 2016).

Mitral cells project broadly to nearly all regions of the olfactory cortex, integrating input from multiple glomeruli. Tufted cells, more numerous and highly excitable, project to more restricted cortical targets, supporting selective signal transmission (Nagayama et al., 2014; Cavarretta et al., 2018).

From the OB, olfactory information is transmitted via white matter tracts — including the uncinate fasciculus, inferior fronto-occipital fasciculus, and cingulum — to limbic structures such as the amygdala and entorhinal cortex, as well as to the piriform cortex (Pir) (Sosulski et al., 2011; Stenwall et al., 2025). The Pir, a key component of the primary olfactory cortex, is located between the insula and the MTL, and plays a central role in odor perception. Is also relays information to higher-order centers including the thalamus, hypothalamus, Hpc, and frontal cortex enabling integration of olfactory input with emotional and cognitive processing (Illig and Wilson, 2014; Yuan et al., 2014).

In parallel, the vomeronasal organ (VMO), situated bilaterally within the mucosa of the nasal septum, constitutes a distinct chemosensory subsystem specialized in detecting pheromonal cues. Sensory neurons within the VMO project to the accessory olfactory

bulb, forming a separate pathway that modulates instinctive social and reproductive behaviors (Hovis et al., 2012).

2.2 Innervation of the nasal, oral and nasopharyngeal region

The nasal, oral and nasopharyngeal region is innervated by a complex network of cranial nerves, including the olfactory nerve (CN I), trigeminal nerve (CN V), facial nerve (CN VII), glossopharyngeal nerve (CN IX), vagus nerve (CN X) and hypoglossal nerve (CN XII), each contributing distinct sensory, motor, and autonomic modalities (Fig. 5).

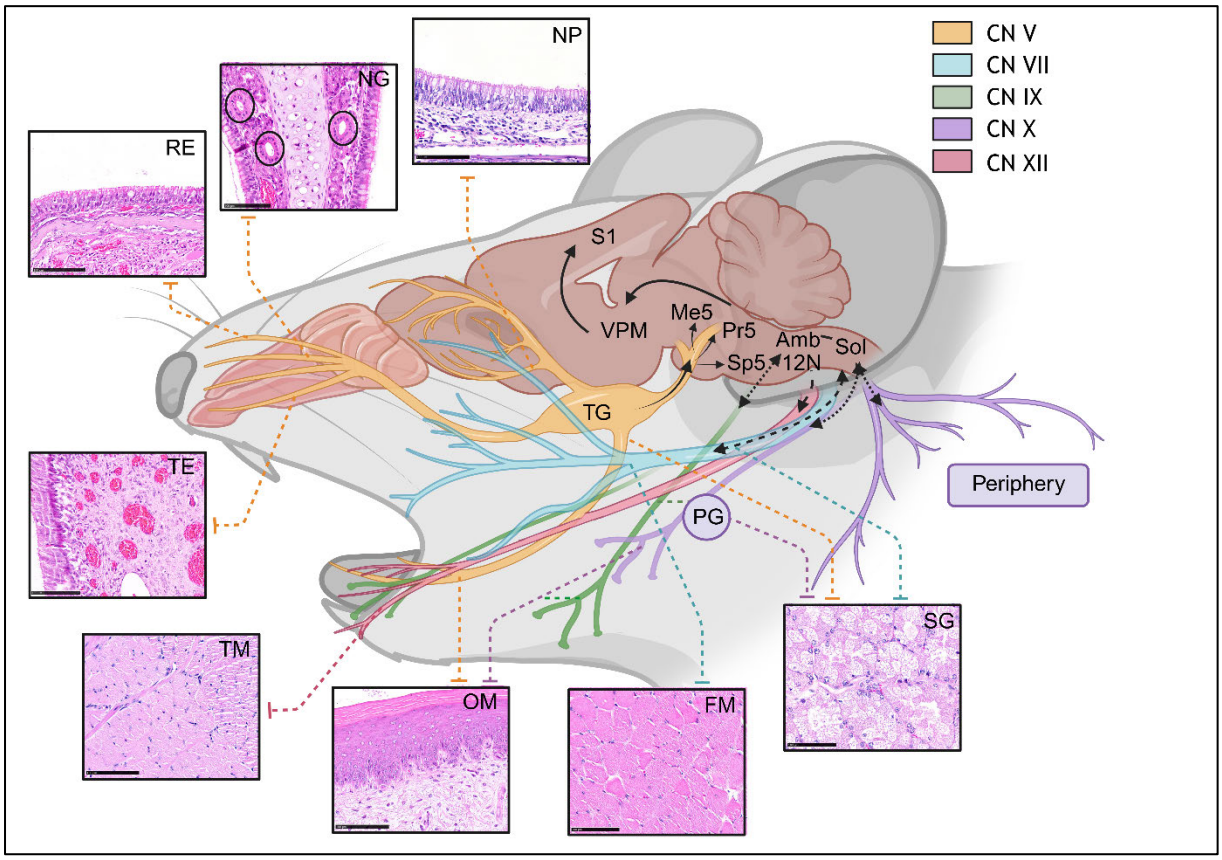

Fig. 5 Neuroanatomical and histological mapping of cranial nerve innervation in the murine nasal, oral and nasopharyngeal regions. *The schematic overview illustrates afferent and efferent projections of cranial nerves supplying the nasal cavity, oral cavity and nasopharynx. Color-coded tracts indicate individual nerves - CN V (trigeminal), CN VII (facial), CN IX (glossopharyngeal), CN X (vagus), and CN XII (hypoglossal) - and trace their connections from peripheral sensory and motor targets, including respiratory epithelium (RE), nasal glands (NG), nasopharynx (NP), salivary glands (SG), oral mucosa (OM), teeth (TE), tongue musculature (TM), and facial muscles (FM), to their respective brainstem nuclei and higher-order projections. Central nuclei are shown for each pathway: trigeminal ganglion (TG), principal sensory nucleus (Pr5), spinal trigeminal nucleus (Sp5), mesencephalic trigeminal nucleus (Me5), ventral posteromedial nucleus (VPM), nucleus of the solitary tract (Sol), nucleus ambiguus (Amb), hypoglossal nucleus (12N), and parasympathetic peripheral ganglia (PG). Representative histological micrographs highlight the cellular architecture of peripheral target tissues corresponding to each cranial nerve. Scale bar: 100µm. Created with BioRender.com.*

The olfactory nerve (CN I), is purely sensory and transmits afferent odor signals from the olfactory epithelium to the OB and to higher order olfactory centers, as described in the section: the olfactory system.

2.2.1 The trigeminal system

The trigeminal nerve (CN V), is the principal somatosensory nerve of the face and oral cavity. It innervates the face via three branches: the ophthalmic nerve (V1), the maxillary nerve (V2), and the mandibular nerve (V3). The ophthalmic and maxillary nerves are purely sensory, while the mandibular nerve carries both sensory and motor fibers (Fehrenbach, 2015). Collectively, these branches transmit tactile, thermal, vibratory, and proprioceptive information from facial dermatomes, the cornea, nasal and oral mucosa, and portions of the external ear (Baumel, 1974; Stewart, 1989).

The ophthalmic nerve exits the cranial cavity and gives rise to the frontal, lacrimal, and nasociliary nerves. Notably, the nasociliary branch innervates the olfactory mucosa in the dorsal nasal meatus and concha (Prendergast, 2013). The maxillary nerve leaves the cranial cavity and enters the pterygopalatine fossa, where it divides into the zygomatic, pterygopalatine, and infraorbital nerves. These branches supply the ventral and middle nasal meatuses, nasal conchae, hard and soft palate, and the upper jaw

including maxillary teeth. The mandibular nerve exits the skull and innervates the muscles of mastication (e.g. masseter and tensor veli palatini) and provides sensory input from lower jaw and anterior two-thirds of the tongue, including mandibular teeth (Glocker et al., 2006).

All three branches converge at the TG, located at the base of the rhombencephalon within the cranial cavity. The TG contains cell bodies of first-order sensory neurons, which are ensheathed by satellite glial cells (Messlinger et al., 2020). An exception is found in proprioceptive fibers, whose cell bodies reside in the mesencephalic trigeminal nucleus (Me5), bypassing the TG entirely (Kamel and Toland, 2001).

From the TG, afferent fibers enter the brainstem via the middle cerebellar peduncle and terminate in either the principal sensory nucleus (Pr5) or the spinal trigeminal nucleus (Sp5) within the hindbrain (Ezure et al., 2001). Pr5 is subdivided into dorsomedial and ventrolateral compartments, each receiving input from specific facial regions (Patestas and Gartner, 2016). Sp5, the largest of the trigeminal nuclei, is organized into three somatotopically arranged subnuclei: pars oralis, pars interpolaris, and pars caudalis, which process sensory input from the oral cavity, nasal passages and pharyngeal structures. Sp5 also receives convergent afferent input from other cranial nerves, including CN VII, CN IX, and CN X, facilitating multisensory integration within the oropharyngeal region (Patel et al., 2025). Together with the Me5 these nuclei represent the second-order neurons of the trigeminal system.

From the trigeminal nuclei, two major ascending tracts emerge: the spinal trigeminal tract and the trigeminothalamic tract. The former carries primary afferents to Sp5, while the latter transmits second-order fibers from Sp5 and Pr5 to the ventral posteromedial nucleus (VPM) of the thalamus (Nash et al., 2010; Wilcox et al., 2015). Third-order neurons in the VPM project to S1 in the parietal lobe, enabling conscious perception of facial and oral stimuli (Corkin et al., 1970). Additionally, VPM projections extend to the FR and are relayed to other thalamic and cortical regions, contributing to autonomic regulation and higher-order sensory integration (Arbuthnot et al., 1990).

2.2.2 The facial nerve

The facial nerve (CN VII) consists of a motor and a sensory-parasympathetic component (nervus intermedius). Originating from the medulla oblongata, it enters the facial canal, where the geniculate ganglion houses the cell bodies of pseudounipolar neurons transmitting gustatory input from the anterior two-thirds of the tongue via the chorda tympani, a branch of the nervus intermedius. The nervus intermedius also conveys parasympathetic fibers targeting glands of the head and neck (Ho et al., 2015). After exiting the skull, the facial nerve continues along its extracranial course, where it primarily innervates facial muscles (Martínez Pascual et al., 2019).

2.2.3 The vagus group

The glossopharyngeal nerve (CN IX), vagus (CN X) and accessory (CN XI) nerves — collectively referred to as the "vagus group" — originate from the medulla oblongata (Simon and Mertens, 2009). Sensory fibers of CN IX arise from the inferior (distal) glossopharyngeal ganglion, which contains afferent neuronal cell bodies. These fibers, together with afferents from CN VII, converge on the solitary tract and terminate in the nucleus tractus solitarii (Sol) and Sp5. Motor fibers arise from the nucleus ambiguus (Amb), while parasympathetic fibers originate from the parasympathetic nucleus of CN IX (Standring and Gray, 2005).

The vagus nerve (CN X) contains sensory fibers in the superior (proximal) and inferior (distal) vagal ganglia, which project to Sol and integrate glossopharyngeal inputs. Its motor fibers also emerge from the Amb (Thompson et al., 2019). Together, CN IX and CN X provide extensive innervation to the pharyngeal mucosa, palatine tonsils, and the posterior third of the tongue. They regulate secretory activity in the buccal, pharyngeal, and laryngopharyngeal glands, playing a critical role in swallowing, taste, and autonomic reflexes (Standring and Gray, 2005; Simon and Mertens, 2009).

2.2.4 The hypoglossal nerve

The hypoglossal nerve (CN XII) originates from the hypoglossal nucleus (12N) in the medulla oblongata. After exiting the cranial cavity, it functions as a purely somatic motor nerve, innervating both intrinsic and extrinsic tongue muscles. Its motor output is regulated by descending projections from the M1, which bilaterally synapse on

hypoglossal nucleus neurons, ensuring precise and coordinated tongue movement (Lin and Barkhaus, 2009).

The convergence of afferent fibers from CN V, VII, IX, and X within Sp5 and their integration into ascending thalamocortical pathways highlight the complex sensory interplay of the nasal, oral, and nasopharyngeal region (Henssen et al., 2019). Moreover, the presence of peripheral ganglia and direct central projections renders these cranial nerves susceptible to neuroinvasive pathogens (Dando et al., 2014; Hooi et al., 2025). The close anatomical continuity between peripheral sensory neurons, their associated ganglia (e.g., TG, Sol, Amb), and central nuclei establishes direct neuronal connections from mucosal surfaces to the CNS. These structural pathways, particularly the olfactory and trigeminal systems, are therefore key determinants of viral entry, dissemination, and subsequent neuropathology. Alphaherpesviruses, in particular, exploit these neuronal routes for entry into the CNS (Kramer and Enquist, 2013).

2.3 Alphaherpesviruses

2.3.1 Taxonomy and host diversity

Alphaherpesviruses are members of the order *Herpesvirales*, which comprises three distinct families: *Herpesviridae*, *Alloherpesviridae*, and *Malacoherpesviridae*. This viral order represents one of the most complex and widely distributed groups of viruses, with over 200 distinct species identified to date (Davison et al., 2009).

Herpesviruses infect an exceptionally broad range of hosts, from mollusks to mammals, and are a significant cause of morbidity and mortality across both human and animals (Sehrawat et al., 2018). Within the *Herpesviridae* family, viruses are further categorized into three subfamilies: *Alphaherpesvirinae*, *Betaherpesvirinae*, and *Gammaherpesvirinae* (Davison, 2002; Davison et al., 2009; Owens et al., 2012*)*. The *Alphaherpesvirinae* subfamily is pantropic and taxonomically subdivided into five genera: *Simplexvirus*, *Varicellovirus*, *Iltovirus*, *Mardivirus*, and *Scutavirus* (Mettenleiter et al., 2019).

The genus *Simplexvirus* includes several notable species such as Human alphaherpesvirus 1 (HSV-1) - commonly referred to as human herpes simplex virus 1, Human alphaherpesvirus 2 (HSV-2), and Bovine alphaherpesvirus 2 (BoHV-2), also known as bovine mammillitis virus (Mettenleiter et al., 2019). These viruses are primarily associated with mucocutaneous and neurotropic infections in humans and cattle (Lanave et al., 2020; Zhu and Viejo-Borbolla, 2021).

The genus *Varicellovirus* includes Human alphaherpesvirus 3 (VZV), the causative agent of varicella and herpes zoster (Ku et al., 2005). Animal-associated species within this genus include Bovine alphaherpesvirus 1 (BoHV-1), responsible for infectious bovine rhinotracheitis (Graham, 2013), and Bovine alphaherpesvirus 5 (BoHV-5), which causes bovine meningoencephalitis (Magyar et al., 1993). Equine herpesviruses, such as Equid alphaherpesvirus 1 (EHV-1), EHV-3, and EHV-4 also belong to this genus and cause respiratory disease, abortion, and coital exanthema in horses (Kapoor et al., 2014), together with Felid alphaherpesvirus 1 (FeHV-1), which causes feline viral rhinotracheitis in cats (Gaskell et al., 2007). Additionally, varicellovirus suid alpha1, Suid alphaherpesvirus 1 (SuHV-1), commonly referred to as pseudorabies virus (PrV), is the etiological agent of Aujeszky's disease in pigs and other mammals (Mettenleiter, 2000).

The genus *Iltovirus* is represented by Gallid alphaherpesvirus 1 (GaHV-1), the etiological agent of infectious laryngotracheitis in chickens (Gowthaman et al., 2020).

In contrast, genus *Mardivirus* includes Gallid alphaherpesvirus 2 (GaHV-2), known as Marek's disease virus (MDV) which induces T-cell lymphomas in poultry (Poonam et al., 2017), as well as other avian herpesviruses such as Anatid alphaherpesvirus 1 (AnHV-1) and Columbid alphaherpesvirus 1 (CoHV-1), infecting ducks and pigeons, respectively (Dhama et al., 2017; Gornatti-Churria et al., 2023).

Finally, the genus *Scutavirus* encompasses reptilian herpesviruses, with Chelonid alphaherpesvirus 5 (ChHV-5) and Testudinid alphaherpesvirus 3 (TeHV-3), both of which are associated with disease in turtles (Gandar et al., 2015; Whitmore et al., 2021).

2.3.2 Structural and genetic features

Herpesviruses share a set of conserved structural and genetic characteristics that form the basis of their replication strategy and ability to establish lifelong persistence in the host. Central to this conservation is a group of approximately 40 core genes present in all herpesvirus subfamilies (Albà et al., 2001; Arvin et al., 2007). These genes encode essential components of the viral nucleocapsid and proteins required for DNA replication, capsid assembly and viral egress.

The virion itself consists of a linear double-stranded DNA genome of approximately 125–290 kbp, enclosed within a T=16 icosahedral capsid, and surrounded by a protein-rich tegument layer. The tegument is organized into two zones: an inner layer adjacent to the capsid and an outer layer in close contact with the envelope (Mettenleiter et al., 2009). The envelope, derived from host cell membranes, contains virus-encoded glycosylated proteins that mediate attachment, entry, and cell-to-cell spread (Pilling et al., 1999; Davison et al., 2009) (Fig. 6).

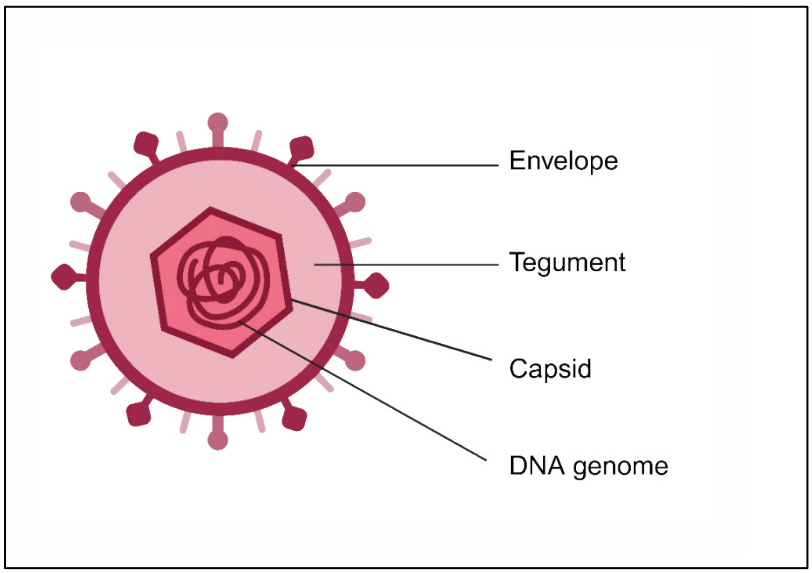

Fig. 6 Structure of a herpes virion. *Herpesvirions consist of a linear double-stranded DNA genome enclosed within an icosahedral capsid, surrounded by a protein-rich tegument layer and an outer lipid envelope embedded with viral glycoproteins. Created with BioRender.com.*

The genomes of alphaherpesviruses, such as HSV-1 and PrV, are organized into a unique long (U_L) and unique short (U_S) region. While HSV-1 contains inverted repeats flanking both regions, PrV possesses repeats only surrounding the US region, resulting

in four genomic isomers for HSV-1 but only two for PrV (Ben-Porat et al., 1983). The PrV genome spans ~143 kbp and encodes 72 ORFs, that give rise to about 70 proteins, showing a high degree of homology to HSV-1 (Klupp et al., 2004; Pomeranz et al., 2005). These include 11 glycoproteins, over 15 tegument proteins, six capsid proteins, and additional envelope-associated and non-structural components (Mettenleiter, 2002; Klupp et al., 2004).

2.3.3 Viral replication cycle

Herpesvirus replication is a highly coordinated multistep process involving distinct viral components and multiple cellular compartments (Fig. 7).

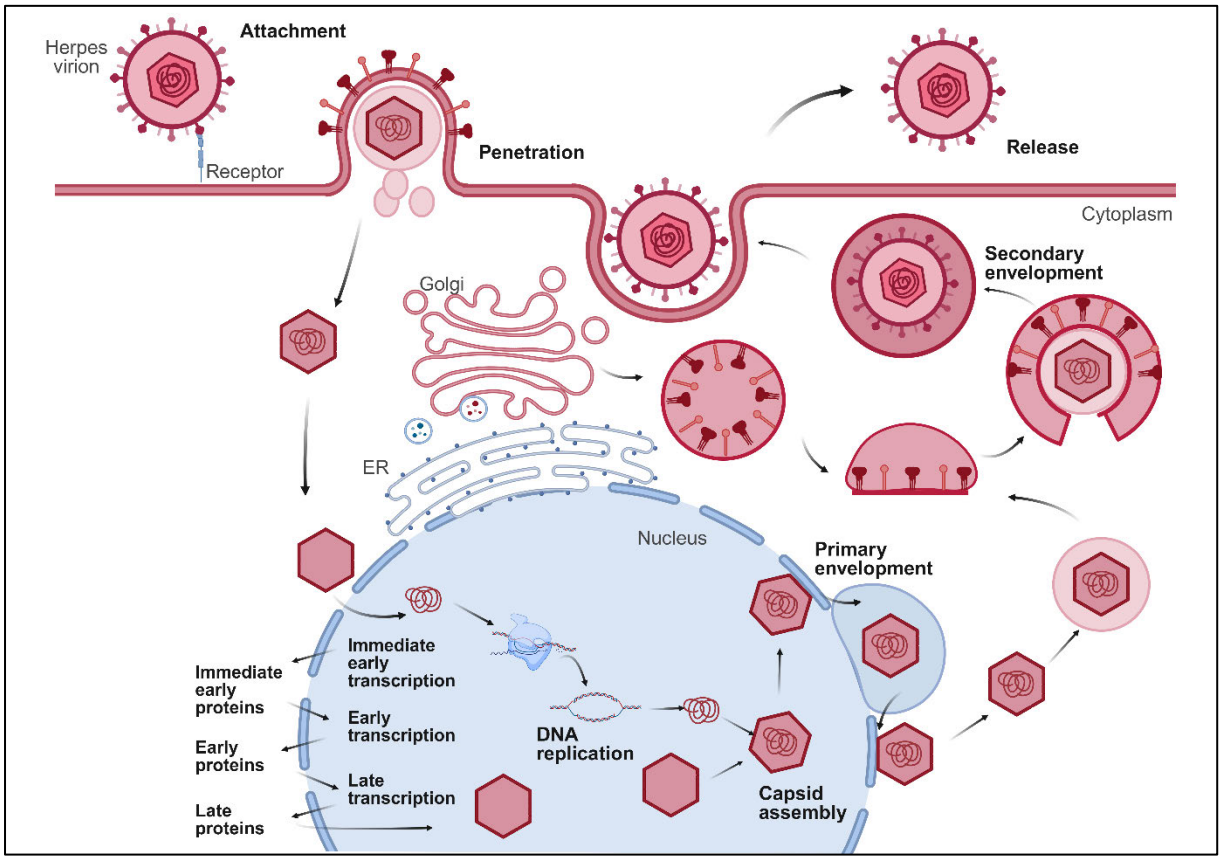

Fig. 7 Herpesviral replication cycle. *Entry is initiated by glycoprotein-mediated attachment and membrane fusion, followed by microtubule-guided transport of the nucleocapsid to the nuclear pore. After nuclear entry, the viral DNA circularizes, and gene expression follows the immediate-early (α), early (β), and late (γ) phases. Capsid assembly occurs in the nucleus, with primary envelopment at the inner nuclear membrane and subsequent release into the cytosol. Final maturation involves tegument acquisition and secondary envelopment via the trans-Golgi network. Mature virions are released through vesicular fusion with the plasma membrane. Modified from Mettenleiter (Mettenleiter, 2004). Created with BioRender.com.*

Infection is initiated with the attachment of viral glycoproteins to specific cell-surface receptors, triggering membrane fusion and delivery of the viral capsid and associated tegument proteins into the cytosol (Struyf et al., 2002; Krummenacher et al., 2004). This fusion typically occurs at the plasma membrane, but endocytic entry routes have also been described (Mettenleiter et al., 2019).

Once inside the host cell, most tegument proteins dissociate, while the capsid — still linked to an inner tegument layer — is actively transported along microtubules toward the nucleus (Sodeik et al., 1997). At the nuclear pore complex, the capsid docks with a vertex aligned to the pore, enabling genome release into the nucleus. There, the linear viral DNA circularizes, and gene expression proceed through a temporally regulated cascade of immediate-early (α), early (β), and late (γ) phases (Knipe, 1989; Schang et al., 1999; Shahin et al., 2006).

Specifically, viral transactivators initiate transcription of immediate early (IE) genes, whose products activate early (E) gene expression. Early proteins establish a cellular environment favorable for viral DNA replication, followed by transcription of late (L) genes encoding structural components of the virion. This transcriptional cascade ensures efficient replication and assembly of progeny virions (Honess and Roizman, 1974; Roizman and Whitley, 2013).

Capsid assembly occurs within the nucleus, and newly formed nucleocapsids exit via budding at the inner nuclear membrane, acquiring a primary envelope in the perinuclear space. This envelope then fuses with the outer nuclear membrane, releasing the de-enveloped capsids into the cytoplasm (Mettenleiter, 2002; Roller and Baines, 2017). In the cytosol, partial tegumentation occurs before the capsids undergo secondary envelopment by budding into trans-Golgi-derived vesicles. These vesicles contain the final envelope and complete tegument, forming mature virions (Turcotte et al., 2005; Mettenleiter et al., 2009; Hogue et al., 2014; Wild et al., 2018).

The final step involves transport to the plasma membrane, where fusion releases infectious virions into the extracellular space. In addition to extracellular release, herpesviruses can also spread directly between adjacent cells, though it remains unclear whether this transmission involves complete virions or subviral components such as nucleocapsids (Mettenleiter et al., 2009).

In alphaherpesviruses, fully assembled virions, naked capsids or viral glycoproteins can subsequently infect neighboring cells, including neurons of the peripheral nervous system. Alternatively, virions my undergo anterograde transport in vesicles along microtubule tracks to peripheral axons and terminals, where they are released (Miranda-Saksena et al., 2018).

2.3.4 Viral entry

Herpesviruses utilize a conserved set of envelope glycoproteins for entry, including the *bona fide* fusion protein gB and the heterodimeric complex gH/gL, collectively referred to as the "core fusion machinery." In addition, alphaherpesviruses require the subfamily-specific receptor-binding protein gD (Vallbracht et al., 2019). Glycoprotein gC enhances initial viral attachment to heparan sulfate, but is dispensable for entry when other glycoproteins are present. Membrane fusion is pH-independent and requires the coordinated engagement of multiple cell surface receptors (Spear and Longnecker, 2003).

Despite structural conservation, alphaherpesviruses such as HSV-1 and PrV display distinct functional requirements for glycoproteins and differential receptor usage (Fig. 8).

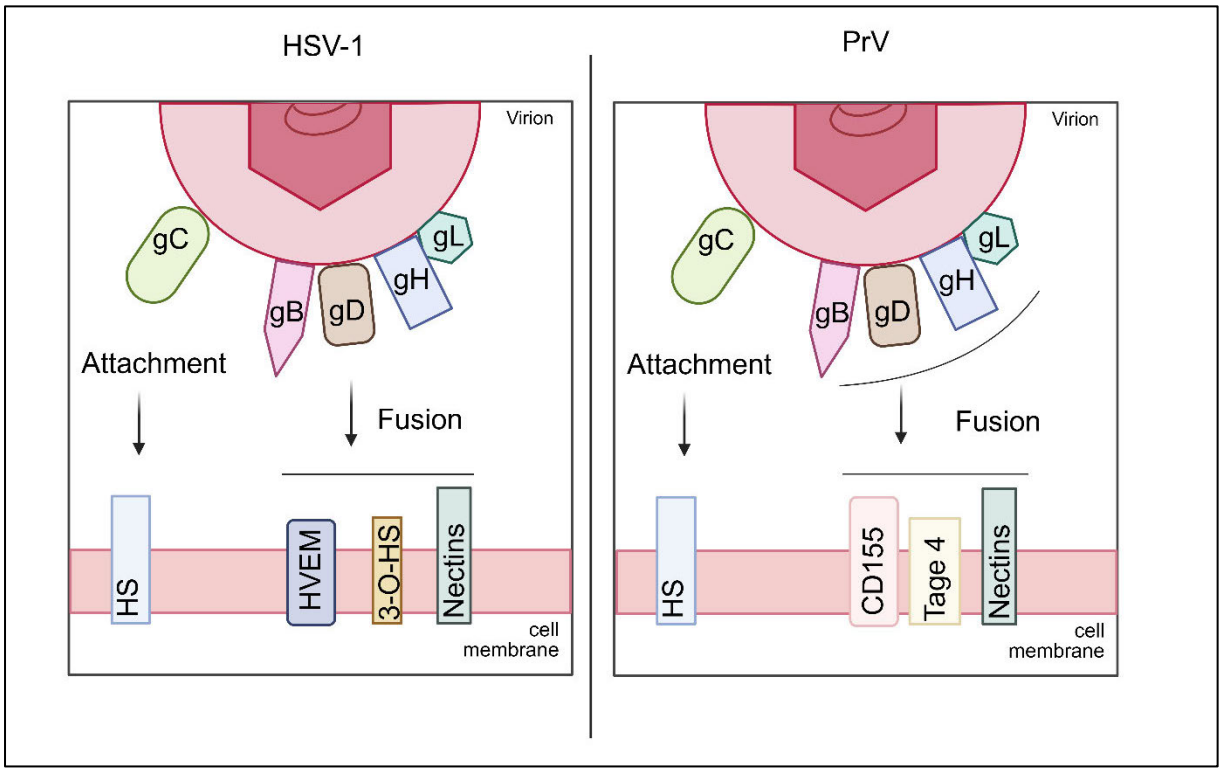

Fig. 8 Comparative mechanisms of viral entry for HSV-1 and PrV. *HSV-1 and PrV employ a coordinated cascade of glycoprotein-mediated interactions to attach to and fuse with host cell membranes. Initial attachment is mediated by glycoprotein gC binding to cell surface heparan sulfate (HS). Subsequent membrane fusion involves glycoprotein gD engaging specific cellular receptors — HVEM, 3-O-sulfated heparan sulfate (3-O-HS), and Nectins (nectin-1 and -2) for HSV-1; CD155, Tage4, and Nectins (multiple family members) for PrV — thereby activating the fusion complex of gB, gH, and gL. Unlike HSV-1, PrV can induce cell–cell fusion in certain cell types independently of gD, suggesting that gB or gH/gL complex can alternatively mediate receptor interaction. Created with BioRender.com.*

HSV-1 strictly requires gB, gD, gH, and gL for membrane fusion and entry, with gD playing a critical role in receptor engagement. In contrast, PrV, while employing the same glycoprotein repertoire, can mediate cell-cell fusion in some cell types (e.g., rabbit cells) even in the absence of gD, suggesting alternative receptor interactions via gB or gH/gL (Spear and Longnecker, 2003; Vallbracht et al., 2019).

HSV-1 engages three entry receptors classes via gD: HVEM, a member of the tumor necrosis factor receptor family, nectin-1 and nectin-2, belonging to the immunoglobulin superfamily localized at cadherin-based junctions, and 3-O-sulfated heparan sulfate, generated by specific glucosaminyl 3-O-sulfotransferases. Among these, HVEM and nectin-1 are the most efficient for HSV-1 entry, while nectin-2 is less active, and 3-O-sulfated heparan sulfate is uniquely utilized by HSV-1.

In contrast, PrV exhibits broader receptor tropism, engaging multiple nectin family members across species, as well as additional, yet unidentified receptors. Notably, PrV does not engage HVEM or 3-O-sulfated heparan sulfate. Instead, CD155 and its rodent homolog Tage4 serve as functional entry receptors for PrV but are inactive for HSV-1 (Spear et al., 2000; Spear and Longnecker, 2003).

2.3.5 Latency and Reactivation

A defining biological feature of all herpesviruses is their ability to establish latency. During this phase, viral gene expression is highly restricted, and no infectious particles are produced. This latent state enables the virus to persist for the lifetime of the host and allows for periodic reactivation, during which infectious virus is generated and transmitted to new hosts (Mettenleiter et al., 2019).

Unlike beta- and gammaherpesviruses, which establish latency in extraneural sites such as hematopoietic cells, alphaherpesviruses display a distinct tropism for the sensory ganglia of the PNS such as the TG or the dorsal root ganglia (DRG) (Koyuncu et al., 2018). However, several recent studies suggest that latency may also occur directly within the CNS (Yao et al., 2014; Sivasubramanian et al., 2022).

During latency, alphaherpesviruses persist in a transcriptionally repressed, non-productive state within neurons, effectively evading immune surveillance (Cao et al., 2024). At the molecular level, latent viral genomes persist as circularized episomes tightly associated with nucleosomes bearing repressive histone modifications thereby permitting transcription of only a small portion of the viral genome (Deshmane and Fraser, 1989; Kubat et al., 2004). Among the few transcripts expressed during latency, the LAT is the most abundant viral RNA in latently infected neurons (Mettenleiter et al., 2019). LATs are a set of co-linear RNAs transcribed from a locus located within the repeat regions flanking the unique long segment of the herpesviral genome. Transcription from this locus produces an initial 8.4 kb RNA, referred to as the ‘minor LAT’ or primary transcript, which undergoes rapid splicing to generate a highly stable 2.0 kb intron, further processed into an additional 1.5 kb intron. These two introns, owing to their abundance and stability, are collectively referred to as the ‘major LATs’ (Nicoll et al., 2012). In addition to LATs, several viral miRNAs are expressed during latency. These miRNAs act synergistically with LATs to suppress viral replication, inhibit apoptosis, and possibly facilitate controlled reactivation (Umbach et al., 2008; Brdovčak et al., 2018). Notably, LATs have also been implicated in promoting neuronal differentiation and modulating the host cellular environment (Hamza et al., 2007; Li et al., 2010).

The equilibrium between latency and reactivation can be disrupted by various physiological and environmental stimuli. Factors such as fever, emotional stress, hormonal fluctuations, ultraviolet radiation, physical trauma, and immunosuppression can trigger reactivation in latently infected tissue (Roizman et al., 2007). These stimuli may act directly on infected neurons or indirectly via non-neuronal cells, including satellite glial cells and $CD8^+$ T lymphocytes. Such interactions promote nuclear accumulation of host transcription factors and the viral transactivator VP16 within neurons (Wilson and Mohr, 2012), a critical step for initiating the reactivation cascade in HSV-1 (Thompson et al., 2009).

Reactivation typically culminates in the production of infectious virions that travel anterogradely to the site of infection, facilitating viral shedding and transmission to new hosts (Wilson and Mohr, 2012; Koyuncu et al., 2018).

Ultimately, the outcome of latency and reactivation depends on the dynamic interplay between host signaling pathways, particularly those regulating stress responses and neuronal survival, and viral transcriptional and replicative machinery (Smith, 2012).

2.3.6 Neuroinvasion

In addition to their broad host range, rapid lytic replication, and ability to establish latency — especially within peripheral ganglia — alphaherpesviruses are distinguished by their neuroinvasive potential, enabling entry, axonal transport, and spread within the nervous system (Card, 2001; Salinas et al., 2010; Taylor and Enquist, 2015). Neurovirulence, distinct from neuroinvasiveness, denotes the capacity of the virus to cause pathological damage within the nervous system (Card and Enquist, 1995).

Following productive replication in epithelial cells of the oronasal mucosa, alphaherpesviruses invade peripheral sensory nerve endings by binding to synaptic receptors. Fusion of the viral envelope with the neuronal plasma membrane (axolemma) enables entry of the nucleocapsid and tegument proteins into the neuronal cytoplasm, where viral replication may proceed (Spear et al., 2000; Mettenleiter, 2003).

To facilitate directed transport within neurons, alphaherpesviruses exploit host adaptor and motor proteins in the cytoplasm that mediate viral capsid trafficking along microtubules. These motor proteins operate in an ATP-dependent manner: dynein drives intraaxonal retrograde transport from synaptic terminals to the soma, while kinesins mediate anterograde transport from the soma to distal axons and synapses. During retrograde spread, virions reach the neuronal cell body of the presynaptic neuron; conversely, anterograde transport enables infection of postsynaptic targets (Taylor and Enquist, 2015). Although retrograde transport predominates during CNS invasion, anterograde spread plays a critical role in viral dissemination and pathogenesis (Kramer and Enquist, 2013).

Trigeminal invasion route

During primary infection or following reactivation from latency in the peripheral sensory ganglia, particularly the TG, newly assembled virions can travel anterogradely within pseudounipolar TG neurons. One axonal branch projects back to the primary site of infection, resulting in recurrent mucocutaneous lesions such as blisters, sores, or ulcers (Ramchandani et al., 2016). The central branch extends to trigeminal nuclei in the brainstem, facilitating transsynaptic spread to higher-order brain regions (Bearer, 2012; Smith, 2012). Specifically, virions may propagate from second-order neurons in the Sp5 and Pr5 via the trigeminothalamic tract, terminating in the VPM of the thalamus (Nash et al., 2010; Wilcox et al., 2015). From the VPM, third-order neurons can relay the infection to S1, the FR, and other cortical areas (Shigenaga et al., 1979; Arbuthnot et al., 1990; Donovan and McCasland, 2008). This pathway has been experimentally validated in HSV-1 infection models (Shukla et al., 2012; Mancini and Vidal, 2018; Doll et al., 2019), and further corroborated for PrV in mice, where PrV antigens were detected in the nasal respiratory epithelium, TG, Sp5, Pr5, VPM, and S1 (Babic et al., 1994; Klopfleisch et al., 2004; Klopfleisch et al., 2006; Sehl et al., 2020; Sehl and Teifke, 2020).

Emerging evidence indicates that, in addition to the trigeminal pathway, alternative entry routes such as the olfactory pathway also contribute to CNS dissemination (Held and Derfuss, 2011; Menendez and Carr, 2017a).

Olfactory invasion route

Following replication within the OE, virions may undergo anterograde axonal transport toward the OB (Hintiryan et al., 2012). From the OB, viral particles can spread to various brain regions, including the Pir, and components of the limbic system within the MTL (Sosulski et al., 2011; Illig and Wilson, 2014; Yuan et al., 2014). Evidence from human HSV-1 infections and experimental models indicate that alphaherpesviruses are capable of invading the CNS via the olfactory nerve, as viral antigen and nucleic acids have been detected in the OE and olfactory cortex (Twomey et al., 1979; Esiri, 1982; Shivkumar et al., 2013; Menendez and Carr, 2017b; Niemeyer et al., 2024). In PrV infection, olfactory transmission has been demonstrated in pigs of different ages, further supporting this route of neuroinvasion (Verpoest et al., 2017).

Alternative invasion routes

Beyond the classical trigeminal and olfactory pathways, additional cranial nerves have been implicated in alphaherpesviral neuroinvasion. Specifically, the glossopharyngeal (CN IX), vagus (CN X), and hypoglossal (CN XII) nerves have been associated with CNS entry.

HSV-1 antigen has been detected in brainstem nuclei connected to these nerves, indicating their potential role in facilitating viral spread (Niemeyer et al., 2024). Likewise, VZV has been shown to infect the vagus nerve, underscoring the broader neuroinvasive capacity of alphaherpesviruses (Chen et al., 2011; Seidel et al., 2015; Gershon et al., 2015).

The autonomic nervous system also contributes to viral dissemination. The pterygopalatine ganglion, part of the parasympathetic nervous system, has repeatedly tested positive for PrV antigen (Babic et al., 1994; Klopfleisch et al., 2006; Sehl et al., 2020). Similarly, the superior cervical ganglion (SCG), a key sympathetic ganglion, has shown viral antigen presence after infection (Babic et al., 1994; Sehl et al., 2020), further highlighting the involvement of both autonomic branches in neuroinvasion.

2.3.7 Herpes Simplex Encephalitis (HSE)

HSV-1 is the primary etiological agent responsible for labial, genital, and corneal herpes manifestations, clinically referred to as herpes labialis and herpes keratitis. In addition to these mucocutaneous infections, HSV-1 can cause life-threatening human HSE, for which it represents the predominant causative pathogen (Chentoufi et al., 2012; Gnann and Whitley, 2017).

HSE is associated with a mortality rate of up to 70%, if left untreated. Even with antiviral therapy, approximately 30% of patients succumb to the disease, and only around 9% achieve full recovery (Whitley and Lakeman, 1995; Tyler, 2009; Steiner and Benninger, 2013; Whitley and Baines, 2018).

Initial clinical signs are often nonspecific (fever, headache, neck pain), followed by neurological signs such as aphasia, disorientation, seizures, and altered mental status (Raschilas et al., 2002; Steiner and Benninger, 2013). Limbic involvement frequently leads to behavioral changes, including hypomania, memory deficits, and Kluver–Bucy

syndrome (Gnann and Whitley, 2017). The majority of survivors experience debilitating long-term sequelae, including persistent cognitive and memory impairments, epilepsy, and speech or behavioral disturbances (McGrath et al., 1997; Raschilas et al., 2002; Whitley and Baines, 2018). In rare cases, relapsing or chronic inflammation of the CNS may occur, affecting both immunocompetent and immunocompromised individuals (Yamada et al., 2003; Landau et al., 2005; Sköldenberg et al., 2006; Alsweed et al., 2018).

Due to its ability to invade neural tissue, HSV-1 can access the CNS via trigeminal and/or olfactory pathways, either during primary infection — predominantly observed in children and adolescents — or following reactivation in adults (Whitley and Lakeman, 1995; Steiner and Benninger, 2013; Whitley and Baines, 2018).

Supporting the role of primary infection, more than 50% of HSE cases involve viral strains distinct from those responsible for previous cold sores (Whitley et al., 1982; Steiner and Benninger, 2013). Nevertheless, reactivation remains a plausible mechanism, as HSV-1 can spread from latently infected TG to the forebrain (Koyuncu et al., 2018). The detection of viral DNA in postmortem brain tissue and observations in animal models further suggest that latency may be established not only in peripheral ganglia but also within the CNS, indicating the possibility of recurrent infection originating endogenously within the brain (Fraser et al., 1981; Baringer and Pisani, 1994; Yao et al., 2014; Menendez and Carr, 2017a; Sivasubramanian et al., 2022).

HSE predominantly affects the frontal and mesiotemporal lobes of the forebrain, including structures of the limbic system (Esiri, 1982; Nicoll et al., 1993). The infection typically manifests asymmetrically within these regions, while brainstem involvement is relatively rare (Bradshaw and Venkatesan, 2016). Viral antigen is most frequently detected in the amygdaloid nuclei, cortical regions, and the white matter of the lateral olfactory striae. Additional regions include the entorhinal cortex, subiculum, Hpc, insular cortex, and cingulate gyrus. In contrast, antigen presence is less commonly observed in the OBs and the pons (Esiri, 1982).

Histopathologically, HSE is characterized by extensive neuronal necrosis accompanied by mononuclear inflammatory infiltrates, composed predominantly of lymphocytes and histiocytes, distributed across the meninges, perivascular spaces, and brain parenchyma. Reactive astro- and microgliosis, neuronophagy (phagocytosis

of damaged neurons), satellitosis (accumulation of glial cells around neurons) and extensive cerebral edema are also typical features of the brain's response to viral injury (Booss and Kim, 1984; Kennedy et al., 1988; Wnęk et al., 2016).

2.3.8 The PrV-ΔUL21/US3Δkin mouse model for HSE

Due to the limited availability of mouse models that accurately replicate HSV-1 infection, recent studies have introduced an alternative approach using a mutant strain of PrV (Sehl et al., 2020; Sehl-Ewert et al., 2022).

Unlike HSV-1, PrV is generally non-pathogenic to humans, although rare human infections have been reported (Wang et al., 2019; Chen et al., 2025). PrV infection causes Aujeszky's disease, which affects a wide range of domestic mammals. Pigs are the primary host: in adult pigs, the virus typically leads to respiratory symptoms, abortion, or even subclinical infection, whereas piglets often develop severe neurological disease. While pigs may survive the infection, it is invariably fatal in other susceptible species such as dogs, cats, ruminants, and rodents, which exhibit severe neurological signs and intense pruritus, a condition known as "mad itch" syndrome (Mettenleiter, 2000).

Over the past decades, numerous studies have characterized PrV deletion mutants to investigate the roles of specific viral proteins in neuroinvasion and neurovirulence (Klopfleisch et al., 2004; Klopfleisch et al., 2006; Maresch, 2011). One mutant strain has emerged as particularly noteworthy: PrV-ΔUL21/US3Δkin, which combines a deletion of the tegument protein pUL21 with a non-functional kinase pUS3 (Maresch, 2011).

The viral gene products pUS3 and pUL21 are conserved across *Alphaherpesvirinae* and dispensable for viral replication in PrV and HSV-1 (Kimman et al., 1994; Baines et al., 1994; Klupp et al., 2001; Klupp et al., 2005). pUS3 modulates immune evasion, T cell activity, and interferon signaling, and contributes to virus-induced inhibition of apoptosis (Leopardi et al., 1997; Munger and Roizman, 2001; Cartier, Komai, Masucci, 2003; Benetti et al., 2003; Cartier, Broberg et al., 2003; Cartier and Masucci, 2004; Ogg et al., 2004; Geenen et al., 2005; Aubert et al., 2006; Benetti and Roizman, 2007; Wang et al., 2011; Imai et al., 2013; Yang et al., 2015; Xiong et al., 2015; Rao et al.,

2018). Despite its multifunctionality (Kato and Kawaguchi, 2018), the single deletion of pUS3 in PrV results in a wildtype-like phenotype in mice (Sehl et al., 2020).

In contrast, pUL21 affects multiple steps of the viral replication cycle and plays a critical role in neuroinvasion (Wind et al., 1992; Klupp et al., 1995; Wagenaar et al., 2001; Klupp et al., 2005; Michael et al., 2007; Mbong et al., 2012; Finnen and Banfield, 2018). Its absence impairs retrograde axonal transport, likely due to disrupted interaction with the dynein-associated protein Roadblock-1 (Curanović et al., 2009; Yan et al., 2019). UL21-deficient PrV displays delayed spread and extended survival in mice, although the infection remains fatal (Yan et al., 2019). The combined deletion of pUL21 and pUS3 kinase likely reflects additive effects or a functional interplay between the two proteins. Notably, absence of pUL21 reduces pUS3 incorporation into virions (Lyman et al., 2003; Michael et al., 2007), which may enhance the attenuation observed in the double mutant.

In female 6-8-week-old CD1 mice, the PrV-ΔUL21/US3Δkin mutant mirrors key features of HSE. Unlike wild-type PrV-Kaplan (PrV-Ka), which causes rapid, fatal brainstem-restricted disease around 2–3 dpi (Klopfleisch et al., 2004; Klopfleisch et al., 2006), mutant-infected mice survive longer despite productive infection and extensive neuroinvasion, particularly in the frontal and mesiotemporal cortices. Viral antigen and histopathological findings — including severe meningoencephalitis with neuronal necrosis, lymphohistiocytic infiltrates, and glial activation — were detected mainly unilaterally in MTL, Pir and Hpc (Esiri, 1982; Nahmias et al., 1982; Damasio and van Hoesen, 1985; Tyler, 2004; Wnęk et al., 2016). Apoptosis occurred predominantly in non-inflamed areas, suggesting virus-induced neuronal injury (Haanen and Vermes, 1995; Laval et al., 2018; Laval et al., 2019). Clinical signs including ruffled fur, hunching, pruritus, alopecic skin erosions and behavioral abnormalities such as stargazing appeared during acute inflammation.

Long-term studies revealed a biphasic disease course, with initial recovery followed by recurrence of clinical signs beyond 28 dpi in 74% of surviving mice, characterized by behavioral abnormalities and non-specific clinical signs including ruffled fur or hunching (Sehl-Ewert et al., 2022). Seizures occurred in a low number of animals approximately six months post-infection, potentially indicating relapsing encephalitis (Jay et al., 1995; Laohathai et al., 2016; Zhang et al., 2020). These clinical features

closely parallel long-term complications in human HSE, such as memory impairment, personality changes, and epilepsy (McGrath et al., 1997). Notably, viral antigen was detected at 49 and 84 dpi in individual animals, pointing to possible reactivation from latency, consistent with recurrent encephalitis observed in humans (Yamada et al., 2003; Landau et al., 2005). In these late stages, meningoencephalitis remained confined to the temporal and frontal lobes, with variable meningeal, perivascular, and neuroparenchymal inflammatory infiltrates and neuronal necrosis (Sehl-Ewert et al., 2022).

Overall, this study investigates how alphaherpesviruses invade, disseminate, and persist within the murine CNS. Using the PrV-ΔUL21/US3Δkin model, we integrate in vitro and in vivo analyses to define region- and cell type–specific susceptibility, to map early entry routes, and to characterize the neuropathological sequelae of long-term infection with respect to viral persistence, reactivation, and neuroinflammation.

3 Publications

Paper [I]

Neurotropism of alphaherpesviruses is most prominent in the mesiotemporal, piriform and prefrontal cortices in mice

Authors

Viktoria Korff, Issam El-Debs, Sonja Bröer, Barbara G. Klupp, Jens P. Teifke, Thomas C. Mettenleiter, Julia Sehl-Ewert

Journal

Neuroscience

Volume 584, pages 367-381

Print: 01.10.2025 (online first: 22.08.2025)

doi: https://doi.org/10.1016/j.neuroscience.2025.08.024

Erratum: https://doi.org/10.1016/j.neuroscience.2025.10.037

Neuroscience 584 (2025) 367–381

Contents lists available at ScienceDirect

Neuroscience

journal homepage: www.elsevier.com/locate/nsc

Research Article

Neurotropism of alphaherpesviruses is most prominent in the mesiotemporal, piriform and prefrontal cortices in mice

Viktoria Korff[a], Issam El-Debs[a], Barbara G. Klupp[b], Jens P. Teifke[a], Thomas C. Mettenleiter, Julia Sehl-Ewert[a,*]

[a] Department of Experimental Animal Facilities and Biorisk Management, Friedrich-Loeffler-Institut, Greifswald-Insel Riems, Germany
[b] Institute of Molecular Virology and Cell Biology, Friedrich-Loeffler-Institut, Greifswald-Insel Riems, Germany

ARTICLE INFO

Keywords:
Alphaherpesvirus
Herpes simplex encephalitis
Pseudorabies virus
Neurotropism
Mouse model
Nectin-1

ABSTRACT

Alphaherpesviruses, such as Herpes Simplex Virus 1 (HSV-1) and Pseudorabies Virus (PrV), exhibit pronounced neurotropism. HSV-1 can cause Herpes simplex encephalitis (HSE), primarily affecting the mesiotemporal lobe. CD1 mice inoculated with a PrV mutant (PrV-ΔUL21/US3Δkin) showed striking analogies to HSE, including comparable virus distribution and inflammatory patterns, providing a suitable model to analyze the specificity of the invasion route of alphaherpesviruses. Here, we investigated the strong preference for the mesiotemporal lobe by artificial targeted stereotactic inoculation of PrV-ΔUL21/US3Δkin and wildtype PrV-Kaplan into the temporal lobe or cerebellum in a kinetic approach. In the most severely affected brain areas viral antigen was quantified and correlated with the expression of the alphaherpesvirus entry receptor nectin-1. Temporal lobe inoculated mice showed viral antigen starting at 2dpi in this location. In contrast, only a low amount of viral antigen was found in the cerebellum after cerebellar inoculation but massive staining was observed in the mesiotemporal lobe at 7dpi. Correspondingly, cultured cerebral cortical neurons exhibited higher viral titers than cerebellar neurons, reflecting alphaherpesviral tropism for cerebral regions. Mice inoculated in the temporal lobe developed symptoms earlier than those inoculated into the cerebellum. PrV-Kaplan resulted in rapid lethality within 2 days, with antigen distribution mirroring that of PrV-ΔUL21/US3Δkin. High nectin-1 expression correlated strongly with viral antigen presence in the mesiotemporal lobe, piriform and prefrontal cortices. In summary, our studies demonstrate the high susceptibility of the mesiotemporal, piriform and prefrontal cortices upon artificial PrV inoculation, and highlight the suitability of this model for future investigations on HSE.

Introduction

The alphaherpesviruses Herpes Simplex Virus 1 (HSV-1) and Pseudorabies virus (PrV) are characterized by their potential to cause severe neurological diseases in their respective hosts (Stahl & Mailles, 2019). Viral entry into cells is mediated by the envelope glycoproteins gB, gD, gH, and gL. While gD is the receptor binding protein, gB and the gH/gL complex are essential for membrane fusion (Vallbracht et al., 2019). The

Abbreviations: 12N, hypoglossal nucleus; AI, agranular insular cortex; AO, anterior olfactory nucleus; BSA, bovine serum albumin; CeM, central amygdaloid nucleus; Cer, cerebellum; Cg, cingulate gyrus; CNS, central nervous system; CPu, caudate putamen; Cu, cuneate nucleus; d p. i., days post infection; DEn, dorsal endopiriform nucleus; DG, dentate gyrus; DpMe, deep mesencephalic nucleus; Ect, ecotorhinal cortex; FCS, fetal calf serum; FR, reticular formation; gfp, green fluorescent protein; HCMV, human cytomegalievirus; Hpc, hippocampus; HSE, Herpes Simplex Encephalitis; HSV-1, Herpes Simplex Virus 1; IFN, interferon; IL, infralimbic cortex; IO, inferior olive; LEnt, lateral entorhinal cortex; LH, lateral hypothalamic area; LS, lateral septal nucleus; M1, primary motor cortex; MEM, minimum essential medium; MO, medial orbital cortex; MOI, multiplicity of infection; MTL, mesiotemporal lobe; PBS, phosphate buffered saline; PFA, paraformaldehyde; PFU, plaque forming units; Pir, piriform cortex; Pn, pontine nucleus; PRh, perirhinal cortex; PrL, prelimbic cortex; PrV, Pseudorabies virus; PrV-Ka, PrV-Kaplan; PVA, paraventricular thalamic nucleus; Py, pyramidal cell layer of the hippocampus; Re, reuniens thalamic nucleus; RK13, rabbit kidney cells; ROI, region of interest; RT, room temperature; S1, primary somatosensory cortex; Sol, nucleus of the solitary tract; Sp5, spinal trigeminal nucleus; SpVe, spinal vestibular nucleus; SuM, supramammilary nucleus; TG, trigeminal ganglion; V1, primary visual cortex; V2, secondary visual cortex; VPL, ventral posteriolateral thalamic nucleus; VPM, ventral posteriomedial thalamic nucleus.

* Corresponding author at: Department of Experimental Animal Facilities and Biorisk Management, Friedrich-Loeffler-Institut, Südufer 10, Greifswald-Insel Riems 17493, Germany.
E-mail address: julia.sehl-ewert@fli.de (J. Sehl-Ewert).

https://doi.org/10.1016/j.neuroscience.2025.08.024
Received 11 April 2025; Accepted 15 August 2025
Available online 22 August 2025

human and murine nectin-1, located at junctions in epithelial cells and expressed on neuronal cells, reveal broad specificity for mediating alphaherpesvirus entry via interaction with gD (Geraghty et al., 1998; Shukla et al., 2000). Following productive infection of mucosal epithelial cells, alphaherpesviruses are able to invade peripheral nerve endings by binding to nectin-1 (Spear et al., 2000; Mettenleiter, 2003). In axons, viral particles travel retrogradely to ganglia of the peripheral nervous system including the trigeminal ganglion (TG), where either life-long-latency can be established or invasion of higher areas of the nervous system can take place (Smith, 2012; Koyuncu et al., 2018). Entry into the central nervous system (CNS) has been suggested to occur via two routes: the trigeminal tract which is connected to higher areas of the brain including cerebrocortical areas (Held & Derfuss, 2011) and the olfactory tract as HSV-1 has been found in the human and murine olfactory epithelium and synaptically connected cerebrocortical areas (Menendez & Carr, 2017; Shivkumar et al., 2013; Esiri, 1982; Twomey et al., 1979).

The inflammatory reaction in the brain elicited by HSV-1 is known as Herpes Simplex Encephalitis (HSE) (Gnann & Whitley, 2017). HSE primarily affects the frontal and mesiotemporal lobes (MTL) including the limbic system (Bradshaw & Venkatesan, 2016), and is characterized by asymmetric necrotizing inflammation (Taylor et al., 2005; Wnęk et al., 2016). Patients afflicted with HSE predominantly exhibit clinical signs such as fever, headache, lethargy, disorientations, and seizures (Steiner & Benninger, 2013; Raschilas et al., 2002) with serious long-term sequelae, including behavioral and cognitive abnormalities (Raschilas et al., 2002; Whitley & Baines, 2018; McGrath et al., 1997).

PrV, an alphaherpesvirus closely related to HSV-1, can cause neurological signs and severe pruritus in susceptible animals such as cats, dogs, cattle, sheep and rodents. Affected animals always succumb to death within a short time, while pigs as the natural host of PrV can survive productive infection (Mettenleiter, 2000). Laboratory animals such as mice are highly susceptible to PrV infection (Babic et al., 1994). Mice intranasally infected with the laboratory-adapted wildtype strain PrV-Kaplan (PrV-Ka) suffered within 3 days from severe clinical signs and showed hunching, pruritus and automutilation. PrV antigen was found in areas of the trigeminal pathway including the TG and the trigeminal brainstem nuclei (Klopfleisch et al., 2006).

A specific PrV mutant PrV-ΔUL21/US3Δkin carrying a deletion of the tegument protein pUL21 and a kinase-dead pUS3, demonstrated delayed neuroinvasion compared to PrV-Ka, and widespread CNS infection predominantly affecting the cerebral cortex of the frontal and mesiotemporal lobe including the insular cortex, lateral entorhinal cortex (LEnt) and hippocampus (Hpc) (Sehl et al., 2020). The animals were able to survive despite productive infection with concomitant predominantly unilateral severe lymphohistiocytic meningoencephalitis and showed behavioral abnormalities. Antigen distribution, histopathological inflammation patterns and clinical data showed striking analogies to human HSE suggesting suitability of this model to study herpesviral encephalitis (Sehl et al., 2020; Sehl-Ewert et al., 2022).

To date, the high vulnerability of the MTL to alphaherpesviral infection remains still unresolved. Differences in expression levels of viral entry receptors or neuroanatomical reasons were suggested as the predilection of alphaherpesviruses to the MTL (Boggian et al., 2000; Tyler, 2004; Damasio & van Hoesen, 1985). In this study we conducted *in-vitro* infection assays to elucidate region-dependent cell type-specific properties in cultivated cerebral and cerebellar primary neurons and applied artificial intracranial stereotactic inoculation of PrV to explore the specificities of viral spread within the CNS and to analyze differences in susceptibility of the MTL and the cerebellum (Cer). To characterize the dynamics of infection, we applied a kinetic approach by investigating PrV-infected CD1 mice at defined time points −2, 4, and 8 days post infection (d p.i). Furthermore, we examined the susceptibility of different brain regions to PrV-ΔUL21/US3Δkin infection by analyzing the nectin-1 receptor expression.

Experimental procedures

Viruses

PrV-ΔUL21/US3Δkin and recombinant green fluorescent protein (gfp) expressing PrV-Kaplan-ΔgGgfp with the non-essential gG gene deleted were derived from PrV wildtype strain Kaplan (Kaplan & Vatter, 1959) as described previously (Sehl et al., 2020; Fuchs et al., 2012). The viruses were propagated in rabbit kidney cells (RK13) and cultured at 37 °C in minimum essential medium (MEM) supplemented with 10 % fetal calf serum (FCS) (Invitrogen).

Generation of PrV-ΔUL21gfp/US3Δkin

PrV-ΔUL21gfp/US3Δkin expressing gfp was generated after co-transfection of PrV-ΔUL21/US3Δkin viral DNA (Sehl et al., 2020) with plasmid pBs-ΔUL21gfp into RK13 cells. Green fluorescing plaques were purified to homogeneity and absence of UL21 and presence of pUS3 was verified by Western blotting. The mutation in the catalytic domain of pUS3 was further confirmed by sequence analysis.

Cells

RK13 cells were cultured at 37 °C in MEM supplemented with 10 % FCS (Invitrogen).

Primary CD1 mouse neurons were provided by Lonza Walkersville, Inc. Each vial contained approximately 4 million of viable cells. Mouse CD1 cortical neurons (M−Cx−400, QBM Cell Science) and mouse CD1 cerebellar neurons (M−Cb−403, QBM Cell Science) were cultivated with primary neuron basal medium (PNBM Basal Medium, Lonza) added with NSF-1, L-glutamine and GA-1000 (PNGM BulletKit, Lonza) in a Poly-D-lysine coated culture plate at 37 °C according to manufacturer's instruction. Medium was changed after the first 2 h of incubation. After another medium change on day 7, 50 % of the media was renewed every 3 days. From day 4 onwards, cells began to organize themselves into a network of neurites. At day 7, the network was fully formed by extending across the entire well.

In vitro replication studies

For characterization of PrV-ΔUL21gfp/US3Δkin, multi-step replication kinetics were performed. RK13 cells were infected with PrV-Kaplan-ΔgGgfp, PrV-ΔUL21/US3Δkin and PrV-ΔUL21gfp/US3Δkin at a multiplicity of infection (MOI) of 0.5 and incubated for 1 h on ice. The inoculum was then replaced with prewarmed medium, and cells were incubated at 37 °C for 1 h, allowing the virus to penetrate. Thereafter, remaining extracellular virus was inactivated by low-pH treatment (Mettenleiter, 1989). Cells and supernatant were harvested immediately (0 h) and after 6, 8, 10, 24, 34 and 48 h. Virus titers were determined on RK13 cells. Average values and standard deviations from three independent experiments were calculated. In addition, plaque diameters of 20 plaques per virus in three independent assays were measured 48 h p.i. to determine characteristics of cell-to-cell spread of the respective virus mutants. Green fluorescing plaques of PrV-ΔUL21gfp/US3Δkin and PrV-Kaplan-ΔgGgfp were determined by immunofluorescence. Plaque diameter values of the PrV mutants were set in relation to those of PrV-Kaplan-ΔgGgfp (set as 100 %).

Multi-step replication kinetics were also performed with CD1 mouse primary neurons in comparison to RK13 as a control. RK13, mouse CD1 cortical and cerebellar neurons were infected with $5x10^4$ PFU/48well of PrV-Kaplan-ΔgGgfp and PrV-ΔUL21gfp/US3Δkin and incubated at 37 °C for 1 h, followed by low-pH treatment (1 min) as described above. Cells and supernatant were harvested after 0, 12, 24, 48 and 72 h and virus titers were determined on RK13 cells. Average values and standard deviations from three independent experiments were calculated.

Immunofluorescence

To visualize and characterize PrV-Kaplan-ΔgGgfp and PrV-ΔUL21gfp/US3Δkin-infected cells over time, we performed immunofluorescence on RK13 cells and primary murine neurons. For immunofluorescence, infected cells (cultivated on ø 10 mm cover-glasses (No. 1.5, MARIENFELD)) were washed in 0.1 M phosphate buffered saline (PBS, pH 7.4) for 5 min and then fixed in 4 % paraformaldehyde (PFA) for 30 min at room temperature (RT). Subsequently, the cells were washed and neutralized with PBS + NH_4Cl solution for 30 min at RT. Thereafter, the cells were washed with PBS for 5 min and permeabilized with 0.5 % Triton X-100 in PBS for 15 min at RT. The cells were then blocked in 0.25 % skim milk (Hobbybäcker-Versand) in PBS for 20 min at RT, followed by washing with PBS three times. For staining with the primary antibody, the antibody was diluted in PBS and incubated for at least 1.5 h at RT and then washed in PBS three times. After washing, the cells were treated with a secondary antibody for 1 h at RT, protected from light. Then, the cells were washed in PBS three times and stained with nuclear counterstain for 5 min at RT, protected from light. After washing, stained cover-glasses were mounted and covered on cut-edge frosted slides (VWR) using Kaisers glycerol gelantine (Merck).

Infection was visualized by autofluorescence of the gfp-tagged viruses. Neuronal cells were identified by immunostaining using a primary mouse anti-TUJ-1 antibody (β-III tubulin; 1:400, Invitrogen, MA1-118) and a primary guinea pig anti-NeuN antibody (1:200, Synaptic Systems, 266004). Corresponding secondary antibodies conjugated to fluorescent dyes included Alexa Fluor 568 goat anti-mouse IgG (1:1000, Abcam, ab175473) and Alexa Fluor 647 goat anti-guinea pig IgG (1:1000, Invitrogen, A21450). Astroglia was visualized using a primary chicken anti-GFAP antibody (1:1000, ThermoFisher, PA1-10004) and a Alexa Fluor 568 goat anti-chicken (1:1000, Invitrogen, A11041) secondary antibody. Nuclei were counterstained with 4‘,6-diamidino-2-phenylindole (DAPI) (1:1000 intermediate solution, Invitrogen).

Nectin-1 expression in neuronal cultures

To visualize nectin-1 expression, we performed immunofluorescence staining on primary murine neurons, following the same standard protocol previously used for the staining of infected neurons. Primary antibodies included a rabbit anti-nectin-1 antibody (1:250, Abcam, ab229464) and a mouse anti-TUJ-1 antibody targeting β-III tubulin (1:400, Invitrogen, MA1-118). For detection, secondary antibodies—goat anti-rabbit Alexa Fluor 568 (1:1000, Invitrogen, A11011) and goat anti-mouse Alexa Fluor 488 (1:1000, Invitrogen, A11001)—were applied.

Animal experiments

Six to eight week-old female CD1 mice, used as the standard model in our laboratory (Sehl et al., 2020), were purchased from Charles River Laboratory. The animals were housed in groups of maximal five in conventional cages type II L under BSL 2 conditions at the animal facilities of the Friedrich-Loeffler-Institut, Greifswald-Insel Riems. Mice were kept under a 12 h light–dark cycle (daylight intensity 60 %) and at a temperature of 20–24 °C with free access to food (ssniff Ratte/Maus-Haltung) and clean drinking water. Bedding (ssniff Spezialdiäten Abedd Espen CLASSIC), nesting (PLEXX sizzle nest), and enrichment material (PLEXX Aspen Bricks medium, mouse smart home, mouse tunnel) were provided.

Stereotactic surgeries

After one week of acclimatization, stereotactic intracranial inoculation was performed using a stereotactic device (Digital Compact Mouse Stereotaxic Frame-Single Manipulator Arm (504926), WPI). For analgesia, mice were premedicated with Carprofen (Rimadyl, Pfizer, 10 mg/kg, s.c.). After 20 min, mice were placed in an isoflurane chamber with a flow rate of 1–2 %. Deeply anesthetized mice were head shaved and the skin was disinfected with 70 % ethanol and topically anesthetized with 0.2 % lidocaine-solution (Xylocaine, AstraZeneca). Then mice were placed in a stereotactic device by fixing the right and left ear with ear fixation aids (Ear bars, 45°, Non-Rupture). The mouth was fixed in a fixation device with an inhalation mask that enabled continuous isoflurane anesthesia. Eyes were protected from dehydration with eye protection gel (Thilo-Tears Gel, Alcon). Following fixation, a 2 cm skin incision was made from the forehead to the nape of the neck. The skull was treated with 0.1 % hydrogen peroxide solution to visualize the cranial sutures and landmarks including lambda (posterior crossing point of the cranial sutures) and bregma (anterior crossing point of the cranial sutures) as reference points for stereotactic coordinates. At the level of bregma, the values of the 3 axes (x = mediolateral, y = anteroposterior, z = dorsoventral) were set to 0. After setting the coordinates the skull was perforated with a mains powered drill (OmniDrill35, 240 V (503599), WPI) using a ball mill with 1.6 mm diameter (Ball Mill, Carbide, #5, 0.063″ diameter (1.6 mm), WPI). After drilling, the coordinates for the injection were set followed by a slow injection of virus into the respective brain region using a 10 µl Hamilton syringe with a 35-gauge needle (NF35BV, WPI). A total volume of 10 µl PrV-ΔUL21gfp/US3Δkin or PrV-Ka was inoculated. The virus suspension containing $1x10^4$ PFU/ml was previously diluted in the lab and transported on ice to the animal facility. Mock mice were treated with cell culture supernatant from RK13 cells (MEM + 5 % FCS) accordingly. Afterwards, the scalp was closed with an intracutaneous suture (Ethicon, Monocryl, monofil, absorbable, 4–0). The animals were placed back in their home cages and exposed to red light during the awakening process. After surgery, mice were supplied with soaked food and water gel as well as Carprofen analgesia (Rimadyl, Pfizer, 10 mg/kg, s.c.) twice daily for the following 3 days.

Inoculation dose finding

A pre-trial was performed to determine the appropriate inoculation dose that would allow the development of a productive infection without having the animal to be euthanized too early (before day 4p.i.). Four different groups (n = 7 per group) were stereotactically inoculated either with 10 µl of $1x10^4$, $1x10^5$, $1x10^6$ PFU/ml of PrV-ΔUL21gfp/US3Δkin suspension or cell culture supernatant as mock control. Mice were inoculated directly into the temporal lobe at the level of the LEnt: posterior, −3.4; lateral, −3.75; and ventral, −4.5 (in mm relative to bregma according to the atlas of Paxinos & Franklin, 2001 (S5 Fig.). Inoculation into LEnt was selected as it has been identified as a highly vulnerable brain region to PrV infection (Sehl et al., 2020). The pre-trial was scheduled for 4 days.

For the main trial, six groups (n = 5 per group) were stereotactically inoculated with $1x10^4$ PFU/ml of PrV-ΔUL21gfp/US3Δkin into the temporal lobe (LEnt): posterior, −3.4; lateral, −3.75; and ventral, −4.5 mm or the Cer: posterior, −6.96; lateral, −1; and ventral, −3mm (S5 Fig.), followed by sequential euthanasia after 2, 4 and 8 days p.i. (kinetic approach). Another six groups (n = 5 per group) were stereotactically inoculated with cell culture supernatant (mock) into LEnt or Cer, followed by sequential euthanasia after 2, 4 and 8 days p.i. Two groups (n = 5 per group) were stereotactically inoculated with $1x10^4$ PFU/ml of PrV-Ka into LEnt or Cer, followed by sequential euthanasia as defined for the other groups.

Animals were monitored 24-hours over a period of maximal 8 days. Mice were evaluated based on a predefined scoring system with the following three categories: (I) external appearance, (II) behavior and activity and (III) body weight (S1 Table). For each category, a score ranging from 0 to 3 was determined. Score 3 in one category or score 2 in all three categories was defined as the humane endpoint which led to euthanasia of the animal. The animals were sacrificed under deep isoflurane anesthesia with prior Carprofen (Rimadyl, Pfizer, 10 mg/kg, s.c.) analgesia. Under deep anesthesia, the right atrium was incised and a 26-gauge needle was inserted into the left ventricle. Then mice were perfused with PBS, followed by 4 % PFA (Gage et al., 2012).

Immediately after perfusion, mice were decapitated by removing the head at the level of the first cervical vertebrae. The brain was removed from the skull and fixed in 4 % PFA for at least 1 week.

Tissue processing and immunolabeling for viral antigen detection

Fixed tissues were stored in PBS/0.02 % NaN3 at 4 °C. Brains were cut into twelve 50 μm coronal sections at the level of the brainstem/cerebellum, mesencephalon/diencephalon as well as caudal, medial and rostral regions of the telencephalon, using a vibratome (VT1200S, Leica Biosystems, Germany), and kept in PBS until use. For permeabilization, sections were transferred to 0,25 % Triton X-100/0,2% gelatin/PBS solution (permeabilization buffer) for 10 min. After permeabilization, the samples were blocked in 5 % bovine serum albumin (BSA) in permeabilization buffer, at RT for 1 h. For viral antigen detection, sections were incubated with a primary rabbit polyclonal anti-PrV gB antibody, diluted in 0.1 % BSA in permeabilization buffer (1:2000 (Kopp et al., 2003)) for 1 h at RT. After washing (two times for 2 min in PBS and 10 min in permeabilization buffer) the samples were treated with a secondary antibody goat anti-rabbit Alexa Fluor 568 (1:1000, Invitrogen, A11011) for 1 h at RT protected from light. Samples were washed (two times for 2 min in PBS) and stained with nuclear counterstain Hoechst 33,258 (1:20.000, Sigma-Aldrich, 94403) for 5 min at RT protected from light. Next, the samples were washed with PBS and transferred to a 10 mM Copper (II) sulfate ($CuSO_4$)/ 50 mM Ammonium chloride (NH_4Cl) (wash buffer 2) solution for 10 min at RT protected from light to avoid background signaling. Samples were then washed in deionized water for 2 min. The brain sections were mounted on Super-Frost-Plus-Slides (Carl Roth GmbH, Germany) with Mounting Medium (1 drop per sample, ibidi) and air-dried for 24 h.

Nectin-1 immunofluorescence

Fixed mock-infected brains were cut into 7–8 coronal pieces with 2.0 mm section slice intervals. Sections were embedded in paraffin wax and cut at 5 μm thick slices using a rotating microtome (Hyrax M55, Zeiss). Then, the sections were mounted on Super-Frost-Plus-Slides and dried for 2 h at 40 °C. The slides were stored at RT until staining.

For immunofluorescence, brain sections were dewaxed and rehydrated. Tissue sections were treated with 10 mM citrate buffer (pH 6.0, without detergent) and steamed with a pressure cooker (Sichler, Germany, NX-3213–675) for 20 min for antigen retrieval. Using a wet chamber, sections were washed two times for 2 min in PBS and 10 min in permeabilization buffer. The samples were blocked in 5 % BSA in permeabilization buffer at RT for 1 h, followed by staining with primary antibodies. The sections were treated with a guinea pig polyclonal anti-NeuN (1:200, synaptic systems, 266004) and a rabbit polyclonal anti-nectin-1 (1:250, abcam, 229464), diluted in 0.1 % BSA in permeabilization buffer for 1 h at RT. Thereafter the samples were washed two times for 2 min in PBS and 10 min in permeabilization buffer and incubated with secondary antibodies using a goat anti-guinea pig Alexa Fluor 647 (1:1000, Invitrogen, A21450) and a goat anti-rabbit Alexa Fluor 568 (1:1000, Invitrogen, A11011) for 1 h at RT, protected from light. Samples were washed two times for 2 min in PBS and stained with Hoechst 33,258 (1:20.000, Sigma-Aldrich, 94403) for 5 min at RT, protected from light followed by another washing step with PBS. Finally, sections were washed with washing-buffer 2 solution for 10 min at RT protected from light and stored shortly in deionized water. The brain sections were mounted and covered with Immu-Mount (epredia).

Quantitative image analysis

For quantitative image analysis of PrV gB and nectin-1 expression, the AI-powered pathology image analysis software Halo 4.0 (v4.0.5107.317-indica labs) was used. The regions of interest (ROI) (area of 521990 mm^2) were selected based on brain areas most affected after infection with PrV-ΔUL21/US3Δkin, including Hpc, LEnt, piriform cortex (Pir), agranular insular cortex (AI) and on areas with low antigen distribution such as Cer and secondary visual cortex (V2). The Highplex FL Module was used to measure the total cell count stained with Hoechst and the cells stained positive for PrV gB or nectin-1 antigen of the respective ROI. We compared the percentage of PrV gB or nectin-1 positive cells per ROI. Average values from three mice were calculated. A complete list of further ROIs can be found in the supplemented material (S8/9 Fig.).

Imaging

Images of cell culture experiments were acquired with a confocal laser scanning microscope (SP5; Leica, Germany). Brain tissue was analyzed with a THUNDER Imaging system (THUNDER Imager Tissue; Leica, Germany). Images were processed with arivis Vision4D (ZEISS).

Statistical analysis

GraphPad Prism 10.4.1 was used for statistical analysis and graphical presentation. Values from three independent experiments were analyzed. All values were calculated using the standard error of the mean (SEM). P-values with a significance limit of ≤ 0.05 were considered and indicated by an asterisk.

Replication kinetics of PrV-ΔUL21gfp/US3Δkin, PrV-ΔUL21/US3Δkin and PrV-Kaplan-ΔgGgfp in RK13 cells were analyzed using a Wilcoxon matched pairs signed rank test. For each virus mutant, the mean of the viral titer per time point was compared to those of PrV-Kaplan-ΔgGgfp as the control. Plaque assays were analyzed using an ordinary one-way analysis of variance (ANOVA) followed by corrected Dunnett's multiple comparison test. Twenty plaques each per virus mutant were measured and compared to plaque diameter of PrV-Kaplan-ΔgGgfp set as 100 %.

Statistical analysis of replication kinetics of PrV-ΔUL21gfp/US3Δkin and PrV-Kaplan-ΔgGgfp in CD1 mouse primary neurons and RK13 cells was performed using an ordinary two-way ANOVA. For each infected cell-line, the mean of the viral titer per time point was compared to the other infected cell-lines.

For animal experiments, a Kaplan-Meier curve was generated to demonstrate the relative survival rate after stereotactic inoculation with the respective viruses followed by survival analysis using the log rank test.

To analyze the quantification of the proportions of PrV gB and nectin-1 positive cells, we used ordinary one-way ANOVA followed by corrected Dunnett's multiple comparison test. Quantified values (mean) of each ROI were compared with each other. Correlation between the proportion of PrV gB positive cells and the proportion of nectin-1 positive cells per respective ROI has been tested by Spearman's coefficient analysis.

Results

In vitro characterization of a gfp-labeled reporter virus PrV-ΔUL21gfp/US3Δkin

For better imaging, we generated a reporter virus, PrV-ΔUL21gfp/US3Δkin, expressing gfp from the (deleted) UL21 gene locus under control of the human cytomegalovirus (HCMV) immediate early promotor/enhancer. PrV-ΔUL21gfp/US3Δkin revealed comparable growth properties in cell culture to the previously described "non-gfp" variant PrV-ΔUL21/US3Δkin (Sehl et al., 2020). As with PrV-ΔUL21/US3Δkin titers of PrV-ΔUL21gfp/US3Δkin were approx. 100- to 200-fold reduced compared to PrV-Kaplan-ΔgGgfp and plaque diameters reached only ca. 50 % of PrV-ΔgGgfp (S1 Fig.).

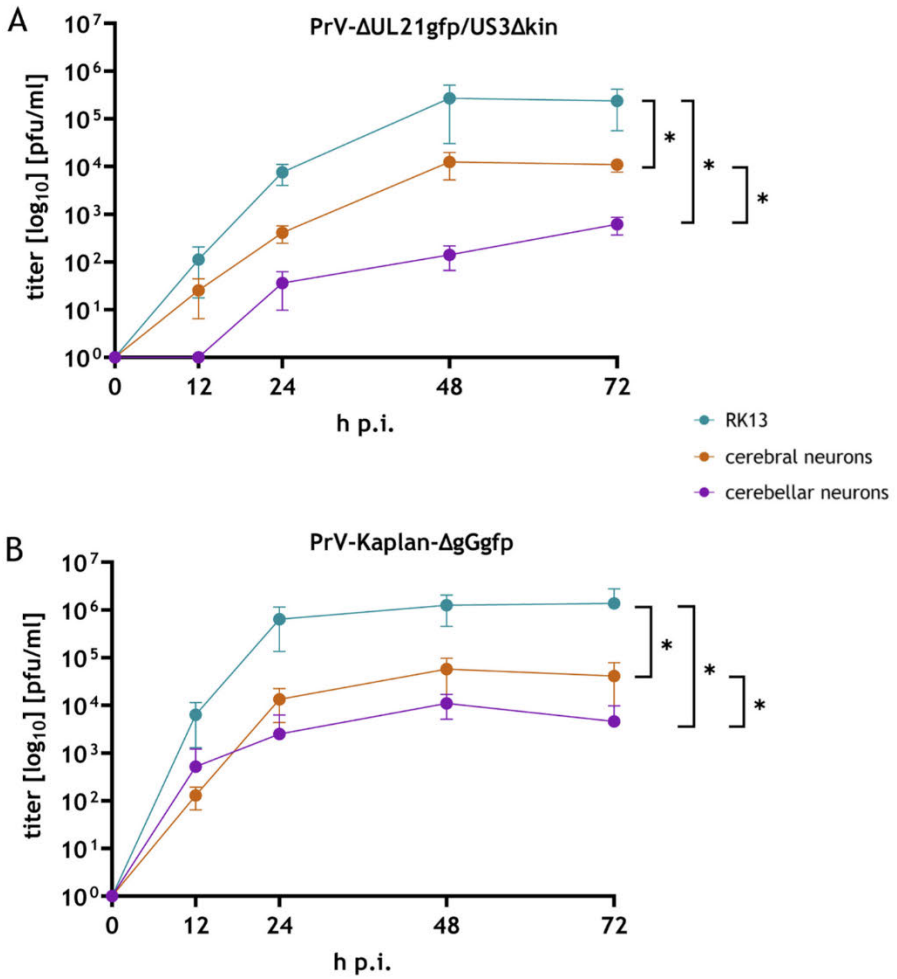

Fig. 1. In vitro replication kinetics of cerebral and cerebellar neurons infected with PrV. PrV-ΔUL21gfp/US3Δkin (A) and PrV-Kaplan-ΔgGgfp (B) were tested with $5x10^4$PFU/48well in primary cerebral and cerebellar neurons compared to rabbit kidney cells (RK13). Average values and standard deviations of three independent experiments are shown. Significant differences of virus replication in primary cerebral neurons compared to cerebellar neurons and to RK13 cells are indicated by an asterisk (*), two-way ANOVA test; $p \leq 0{,}01$.

Characterization and in vitro-susceptibility of murine primary neurons

For basic phenotypic characterization of cultured primary murine neurons, immunofluorescence staining was performed employing TUJ-1 and NeuN as neuronal markers. NeuN, which selectively labels neuronal nuclei and perinuclear regions, specifically stained neuronal soma, thereby enabling precise visualization of cell bodies. In contrast, TUJ-1, a neuron-specific antibody targeting βIII-tubulin, facilitated labeling of the entire neuronal morphology, including axonal and dendritic processes. Furthermore, GFAP (glial fibrillary acidic protein) was utilized as a marker for astroglial cells, reflecting the presence of glial populations within the cultures (S3 Fig.).

We further analyzed nectin-1 expression in primary cultured murine neurons. No significant differences were observed between the two neuronal populations (S4 Fig). To test whether there are differences in the susceptibility to infection at the cellular level, primary murine cerebral and cerebellar neurons were analyzed using multistep replication kinetics and immunofluorescence studies. Final titers of PrV-ΔUL21gfp/US3Δkin and PrV-Kaplan-ΔgGgfp were approx. 100-fold higher in cerebral neurons than in cerebellar neurons at different time points starting at 12 h post infection (p.i.) (Fig. 1). However, titers in RK13 cells, which served as positive control, were still approx. 100–200-fold higher than titers of cerebral neurons. Infection was visualized using gfp autofluorescence (S2 Fig.).

Analysis of the susceptibility difference of different brain regions in vivo

To visualize viral spread within the CNS and to analyze the susceptibility of different brain regions for infection, stereotactic inoculations (according to Bröer et al., 2012) were performed with PrV using 6–8-week-old female CD1 mice as our standard animal model for PrV infection (Sehl et al., 2020).

Determination of the inoculation dose

First, the optimal virus dose for stereotactic inoculation was determined. For this, four groups of seven animals each were inoculated either with 10 µl virus suspension containing $1x10^4$, $1x10^5$ or $1x10^6$ plaque forming units (PFU)/ml of PrV-ΔUL21gfp/US3Δkin or cell culture supernatant (mock) into the temporal lobe (LEnt) using coordinates: posterior, −3.4; lateral, −3.75; and ventral, −4.5 (in mm relative to bregma according to the atlas of Paxinos & Franklin, 2001 (S5 Fig.). Severity of clinical signs and mice affected differed substantially between the groups (S6 Fig.). Mice inoculated with $1x10^5$ or $1x10^6$ (PFU)/ml developed mild clinical signs already between days 1 and 2p.i. At day 4p.i. clinical signs increased and general condition worsened in all mice. The animals showed seizures, severe hunched posture and reduced spontaneous movement and three out of seven mice had to be sacrificed as they reached human endpoint criteria (S1 Table). However, mice inoculated with $1x10^4$PFU/ml showed no or only mild clinical

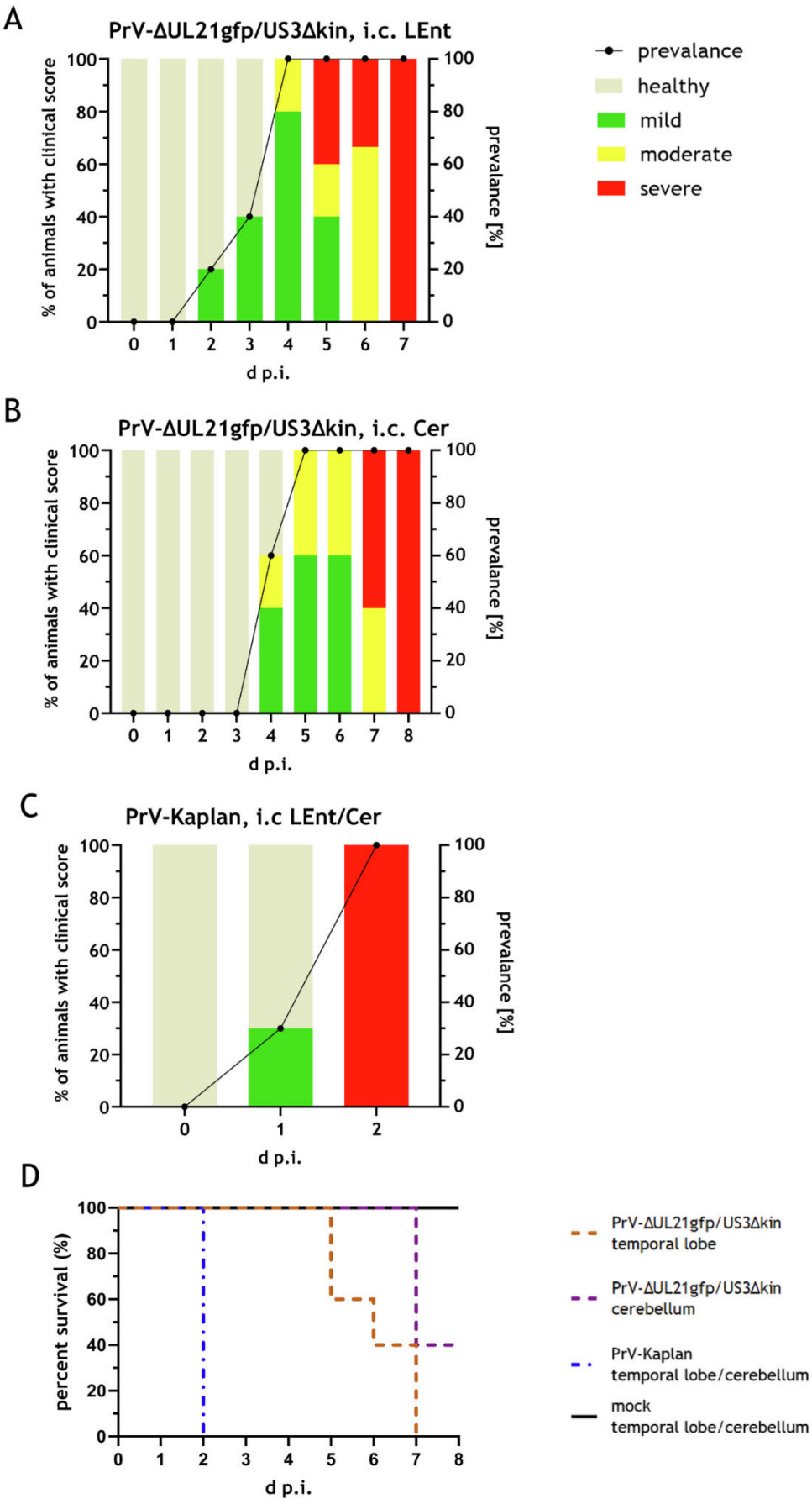

(caption on next page)

Fig. 2. Prevalence of diseased animals and Kaplan-Meier curve after stereotactic inoculation. The animals were inoculated with 10 µl $1x10^4$ PFU/ml of PrV-ΔUL21gfp/US3Δkin into the temporal lobe (LEnt) (A), cerebellum (Cer) (B) and with 10 µl $1x10^4$ PFU/ml of PrV-Kaplan into the temporal lobe or cerebellum (C). The frequency of sick animals per time is indicated by bars. Based on a scoring system (S1 Table) animals were categorized into either mildly (green), moderately (yellow) or severely affected (red). Prevalence is given by the black line on the right Y-axis. The Kaplan-Meier curve (D) showing the percent survival in comparison to mock-inoculated mice. The survival rates differ significantly (log-rank test, $p < 0{,}0001$) between the groups.

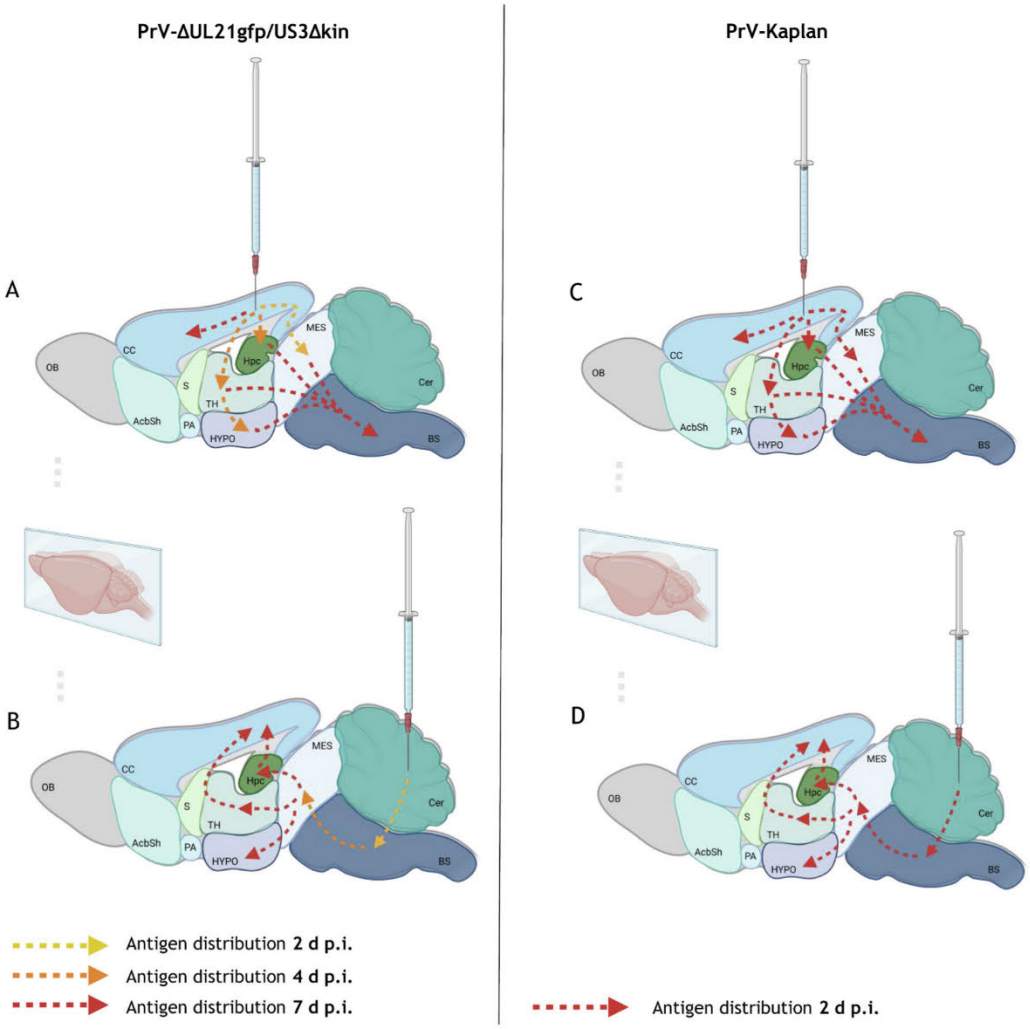

Fig. 3. Illustration of antigen distribution after stereotactic inoculation with PrV-ΔUL21gfp/US3Δkin and PrV-Kaplan into the temporal lobe (LEnt) (A, C) or cerebellum (Cer) (B, D). Viral antigen distribution is illustrated by different colors at 2, 4, 7 d p.i. Created in BioRender. Korff, V. (2025) https://BioRender.com/ak5wdv0.

signs starting at day 2p.i. and survived until the end of the experiment at day 4. Mice inoculated with cell culture supernatant remained healthy throughout the experiment. Thus, for further investigations a dose of $1x10^4$PFU/ml was applied.

Susceptibility of different brain areas

Mice (n = 5 per group and time point) were stereotactically inoculated with either 10 µl virus suspension containing $1x10^4$PFU/ml of PrV-ΔUL21gfp/US3Δkin, PrV-Ka or cell culture supernatant into the temporal lobe (LEnt): posterior, −3.4; lateral, −3.75; and ventral, −4.5 mm or Cer: posterior, −6.96; lateral, −1; and ventral, −3mm (S5 Fig.). After 2, 4, and 8 days p.i mice were sacrificed and further investigated (kinetic approach).

Clinical evaluation and relative survival rates

The development of clinical signs and relative survival rates differed depending on the virus and the inoculation site (Fig. 2). Details of clinical data are given in Table S2.

Mice inoculated with PrV-ΔUL21gfp/US3Δkin into the temporal lobe (Fig. 2A) developed clinical signs earlier than those inoculated into the Cer (Fig. 2B). Temporal lobe inoculated mice showed ruffled fur and reduced activity starting from day 2p.i. From day 4p.i., their clinical condition worsened and hunched posture, reduced reactions to external stimuli, mild pruritus and 'star gazing' were observed. After 5 days p.i. two out of five mice developed severe clinical signs including seizures, lacking spontaneous movement, severe hunched back and weight loss < 20 % which fulfilled humane endpoint criteria. Remaining mice had to be sacrificed at day 6 (n = 1) and 7 (n = 2) (Fig. 2D).

In comparison, in mice inoculated with PrV-ΔUL21gfp/US3Δkin into the Cer, mild to moderate clinical signs were first observed at day 4p.i. (Fig. 2B). At day 5p.i. two of five mice developed moderate clinical signs such as pruritus, ruffled fur, nasal bridge edema and reduced reactions

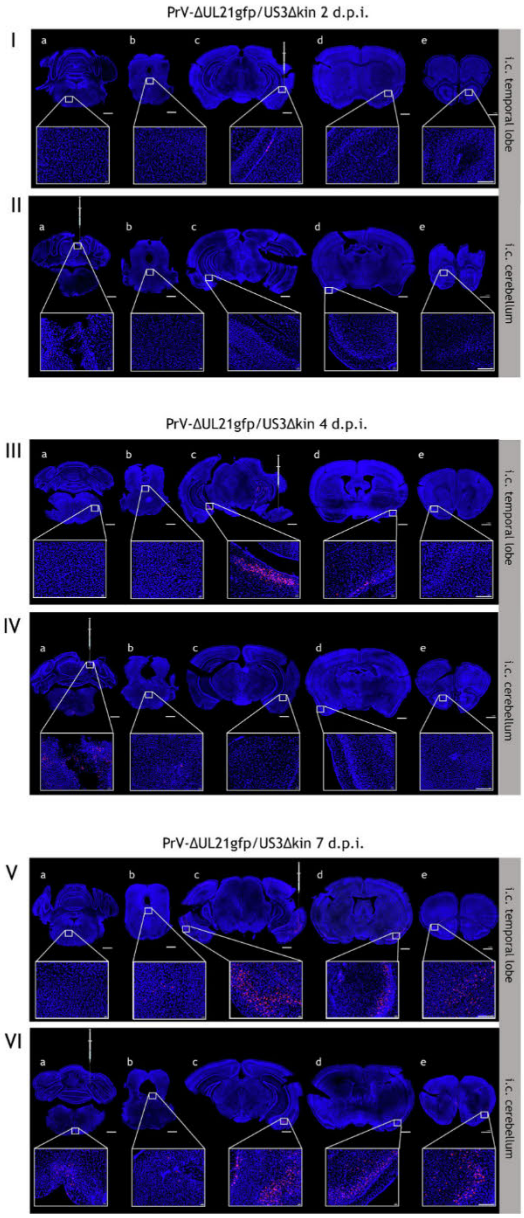

Fig. 4. Immunofluorescence showing viral antigen distribution after stereotactic inoculation with PrV-ΔUL21gfp/US3Δkin into the temporal lobe or cerebellum. Localization of viral antigen is shown after 2 (I + II), 4 (II + III) and 7 (VI + V) days p.i. For immunolabelling a rabbit polyclonal anti-PrV gB antibody and a goat anti-rabbit Alexa Fluor 568 antibody (red) was utilized, nuclei were visualized using Hoechst (blue). Coronal sections of five different brain areas were stained and analyzed (a = cerebellum and brainstem, b = mesencephalon and diencephalon, c = caudal regions of the telencephalon, d = medial regions of the telencephalon, e = rostral regions of the telencephalon). Scale bar = 1 mm (coronal sections); scale bar = 200 μm (magnification).

to external stimuli. At day 7 and 8p.i. severe clinical signs including severe hunching, severe pruritus, hemorrhagic skin erosions, lacking spontaneous movement, behavioral abnormalities including 'star gazing' and weight loss < 20 % were monitored which led to euthanasia of all mice (Fig. 2D).

PrV-Ka infected mice, inoculated either into the temporal lobe or cerebellum, reached humane endpoint criteria at 2 days p.i. (Fig. 2C, D) showing moderate pruritus, hunched posture, seizures, reduced spontaneous movement, dyspnea and apathy. In contrast, seizures were observed only in animals inoculated into the temporal lobe. Mock inoculated animals were always clinically inapparent.

Detection of viral antigen

To analyze viral spread upon stereotactic inoculation into the temporal lobe and Cer, five coronal brain sections obtained from the brainstem/cerebellum, mesencephalon/diencephalon as well as caudal, medial and rostral regions of the telencephalon were analyzed by immunofluorescence at different times p.i. A schematic summary of viral antigen distribution after stereotactic inoculation of PrV-ΔUL21gfp/US3Δkin or PrV-Ka is illustrated in Fig. 3. A detailed presentation of affected brain areas is shown in Fig. S7. Representative images from immunofluorescence staining are provided in Fig. 4 (PrV-ΔUL21gfp/US3Δkin) and in Fig. 5 (PrV-Ka).

After inoculation of PrV-ΔUL21gfp/US3Δkin into the temporal lobe, specifically into the lateral entorhinal cortex (LEnt), the virus spread rapidly within the temporal lobe which remained strongly positive until 7 days p.i. However, over time the virus spread from the inoculated temporal lobe and was found mostly bilaterally in areas of the telencephalon, the mesencephalon/diencephalon and brainstem (Fig. 3A). As shown in detail in Fig. S7, after 2 days p.i. temporal lobe inoculated mice showed antigen positive cells at the inoculation site (LEnt) as well as in other parts of the MTL (pyramidal cell layer of the hippocampus (Py)) and in the midbrain (caudate putamen (CPu)). At 4 days p.i. antigen was detected in the midbrain (CPu), hypothalamus (lateral hypothalamic area (LH)), Pir and in the MTL (central amygdaloid nucleus (CeM), Py, dentate gyrus (DG), perirhinal cortex (PRh), LEnt). From day 5p.i. on, signals were moreover detected in the brainstem (inferior olive (IO), spinal vestibular nucleus (SpVe)), reticular formation (FR), midbrain (CPu), thalamus (ventral posteriomedial thalamic nucleus (VPM), ventral posteriolateral thalamic nucleus (VPL)), hypothalamus (LH), primary somatosensory (S1), visual (V1), motor cortex (M1), piriform cortex (Pir, dorsal endopiriform nucleus (DEn)), MTL (lateral septal nucleus (LS), CeM, Py, cingulate gyrus (Cg), DG, PRh, ecotorhinal cortex (Ect), LEnt) and in the prefrontal cortex (AI, prelimbic cortex (PrL), medial orbital cortex (MO), infralimbic cortex (IL), anterior olfactory nucleus (AO)).

After inoculation of PrV-ΔUL21gfp/US3Δkin into the Cer, the infection spread from the Cer via the brainstem to the mesencephalon/diencephalon and finally to the cerebral cortex mainly involving the mesiotemporal lobe (Fig. 3B). Viral antigen was found mostly bilaterally in the affected areas. In more detail, after 2 days p.i. viral antigen was present in the Cer and FR. After 4 days p.i., antigen was detected also in the brainstem (spinal trigeminal nucleus (Sp5), IO) and midbrain (deep mesencephalic nucleus (DpMe)). After 7 days p.i. positive cells were found in Cer, FR, brainstem (nucleus of the solitary tract (Sol), Sp5, IO, SpVe), midbrain (DpMe, CPu), thalamus (paraventricular thalamic nucleus (PVA), reuniens thalamic nucleus (Re)), hypothalamus (LH), S1, Pir, MTL (LS, CeM, Py, Cg, DG, LEnt) and in the prefrontal cortex (AI, MO, AO).

As control, mice inoculated with PrV-Ka either into the temporal lobe or Cer, showed similar antigen distribution 2 days p.i., independent of the site of inoculation (Fig. 3C and D). In temporal lobe inoculated mice, viral antigen was detected in the brainstem (Sol, Sp5), FR, midbrain (CPu), hypothalamus (LH, supramammilary nucleus (SuM)), S1, M1, V1, piriform cortex (Pir, DEn), MTL (LS, Py, Cg, DG, PRh, Ect, LEnt) and in the prefrontal cortex (AI, PrL, MO, AO). In cerebellum inoculated mice, antigen was found at the inoculation site (Cer), in the brainstem (Sol, Sp5, IO, SpVe, hypoglossal nucleus (12 N), pontine (Pn) and cuneate nucleus (Cu)), FR, midbrain (DpMe), hypothalamus (LH, SuM), S1, Pir, MTL (Py, Cg) and in the prefrontal cortex (AO).

In essence, in temporal lobe inoculated mice starting at day 4p.i. high levels of viral antigen were found in areas especially of the telencephalon (MTL, Pir and prefrontal cortex) (Fig. 4 III c-e, V c-e) when compared to the brainstem (Fig. 4 III a, V a) and mesencephalon/diencephalon (Fig. 4 III b, V b) where antigen prevalence was considerably lower. Similarly, mice inoculated into the Cer also presented with

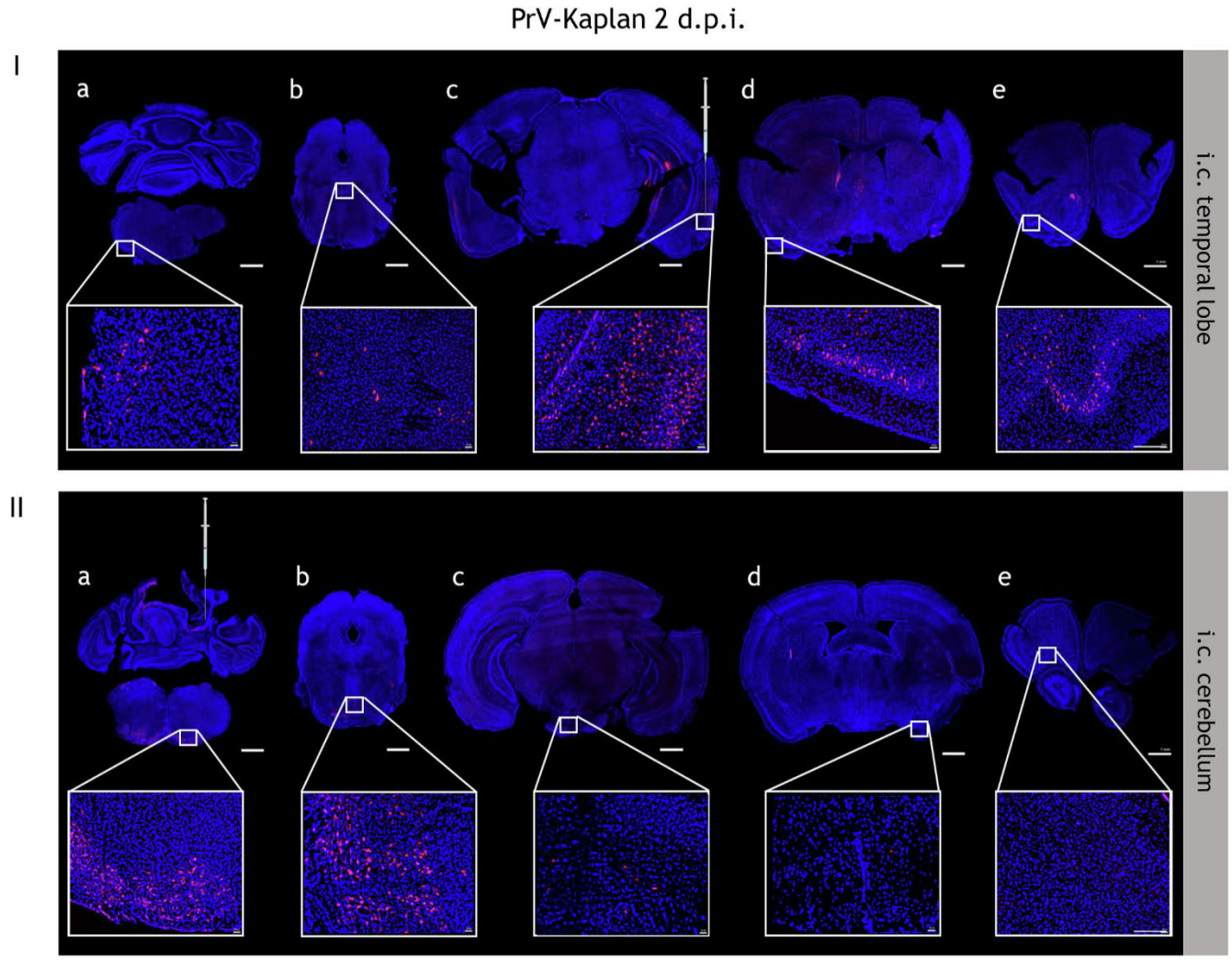

Fig. 5. Immunofluorescence showing viral antigen distribution after stereotactic inoculation with PrV-Kaplan into the temporal lobe (I) or cerebellum (II) 2 days p.i. Viral antigen was visualized using a rabbit polyclonal anti-PrV gB antibody and a goat anti-rabbit Alexa Fluor 568 antibody (red). Hoechst (blue) served as nuclear counterstain. Coronal sections of five different brain areas were stained and analyzed (a = cerebellum and brainstem, b = mesencephalon and diencephalon, c = caudal regions of the telencephalon, d = medial regions of the telencephalon, e = rostral regions of the telencephalon). Scale bar = 1 mm (coronal sections); scale bar = 200 μm (magnification).

comparable high amounts of viral antigen in MTL, Pir and prefrontal cortex, however slightly later at day 7p.i. (Fig. 4 VI c-e), while cerebellum, brainstem and mesencephalon/diencephalon were only sparsely positive at the investigated time points (Fig. 4 II a-b, IV a-b, VI a-b).In comparison to PrV-ΔUL21gfp/US3Δkin, PrV-Ka infection resulted in higher numbers of positive cells in the area of inoculation. In temporal lobe-infected animals, markedly positive areas were found in the regions of the telencephalon (MTL, Pir and prefrontal cortex) (Fig. 5 I c-e) and less in the brainstem (Fig. 5 I a) and mesencephalon/diencephalon (Fig. 5 I b). In Cer inoculated animals, strongly positive areas appeared in the brainstem (Fig. 5 II a) and mesencephalon (Fig. 5 II b). However, the virus also spread sparsely into telencephalic regions, including MTL, Pir and prefrontal cortex in Cer inoculated mice (Fig. 5 II c-e).

Quantitative image analysis

To measure the PrV gB specific antigen signal the stained sections were analyzed by quantitative image analysis, and ROIs with high or low antigen load were selected. Areas with high viral antigen amounts were selected from the MTL, Pir and prefrontal cortex and specifically included Hpc (Py), LEnt, Pir and AI. Cer and V2 were chosen as ROIs with low antigen detection, respectively (Fig. 6). Analysis of further ROIs are shown in the supplemented material (S8 Fig.). For analysis, stained brain tissue sections from mice stereotactically inoculated with PrV-ΔUL21gfp/US3Δkin into the cerebellum after 7 dpi (infection peak) were used.

PrV gB was sparsely detected in Cer and V2 (Fig. 6A), with a proportion of antigen-positive cells of 9 % in Cer and 2 % in V2 (mean, n = 3) (Fig. 6B). In contrast, antigen was massively detected and significantly higher in Hpc, LEnt, Pir and AI (Fig. 6A), with a proportion of antigen-positive cells of 47 % in Hpc, 63 % in LEnt, 70 % in Pir and 52 % in AI (mean, n = 3) (Fig. 6B).

Presence of alphaherpesvirus entry receptor nectin-1 in different brain areas

To investigate whether nectin-1 expression correlates with viral antigen found in specific brain areas, ROIs tested for viral antigen (see Fig. 6, S8 Fig.) were analyzed for nectin-1 positive neurons by quantitative image analysis. Results are represented in Fig. 7 and Fig. S9.

Nectin-1 was detected at significantly higher levels in Hpc, LEnt, Pir and AI (Fig. 7A), with a proportion of nectin-1-positive cells of 72 % in Hpc, 72 % in LEnt, 75 % in Pir and 60 % in AI (mean, n = 3) (Fig. 7B).

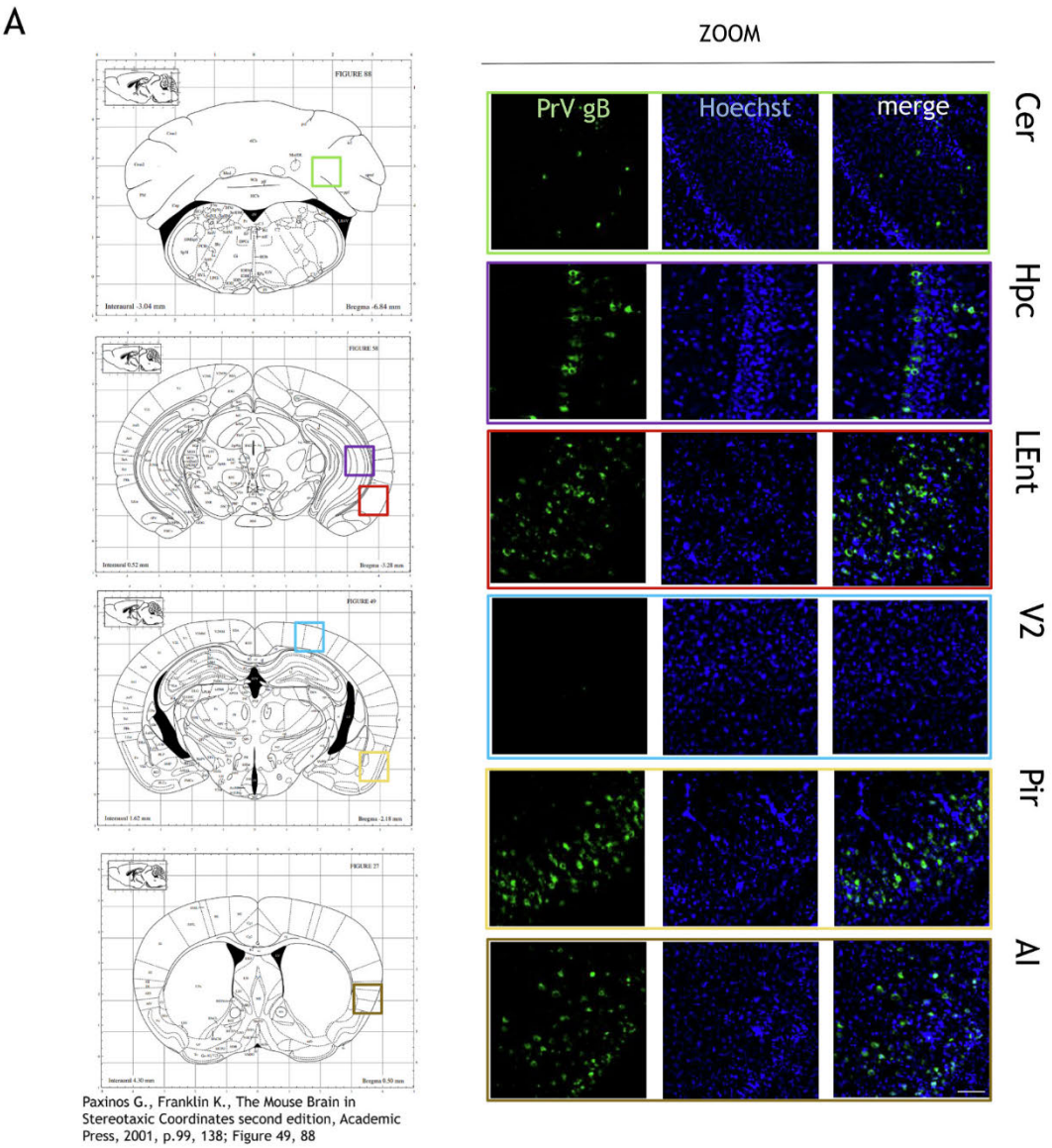

(caption on next page)

Fig. 6. Quantitative image analysis of PrV gB signals in different brain regions of CD1 mice stereotactically inoculated with PrV-ΔUL21gfp/US3Δkin into the cerebellum after 7 dpi. Immunofluorescence studies of PrV gB-antigen distribution in different brain regions defined as ROIs (green box = Cer, purple box = Hpc, red box = LEnt, blue box = V2, yellow box = Pir, brown box = AI) (A). For immunolabelling a polyclonal rabbit anti-PrV gB serum and a goat anti-rabbit Alexa Fluor 568 antibody (green) was utilized. Nuclei were visualized using Hoechst (blue). Different ROIs were analyzed by quantification of PrV gB positive cells compared to the total cell count of the respective ROI (B). Average values and standard deviations of three independent experiments are shown. Significant differences are indicated by an asterisk (*) one-way ANOVA test, followed by corrected Dunnett's multiple comparison test; $p < 0{,}0001$. Cer = cerebellum, V2 = secondary visual cortex, Hpc = hippocampus, LEnt = lateral entorhinal cortex, Pir = piriform cortex, AI = agranular insular cortex. Scale bar 100 μm.

Cer and V2, areas which revealed low antigen amounts showed also lower proportions of nectin-1 positive cells, with 6 % in Cer and 7 % in V2 (mean, n = 3).

A strong positive correlation (Spearman, $p \leq 0.05$) was found between the presence of viral antigen and nectin-1-positive cells in the respective ROIs. (Fig. 8, S10 Fig.).

No differences in nectin-1 receptor expression were observed between PrV-infected and mock-treated mice. The corresponding analysis is presented in Supplementary Fig. S11.

Discussion

In the present study, we investigated the high susceptibility of the MTL to alphaherpesviral infection. We performed artificial intracranial stereotactic injections into permissive (temporal lobe/LEnt) and non-permissive brain areas (cerebellum) to analyze viral spread to target regions after targeted infection.

We show that the MTL as well as Pir and the prefrontal cortices were primary targets of PrV infection, irrespective of whether the virus was inoculated into the temporal lobe or the cerebellum. Immunolabeling revealed strongly positive LEnt, Hpc, Pir, and AI cortices which have also been shown to be infected upon intranasal inoculation (Sehl et al., 2020) and which are known to be affected in HSE (Esiri, 1982; Taylor et al., 2005; Yong et al., 2021; Armien et al., 2010). However, when virus was intracranially inoculated into the temporal lobe, no antigen was detectable in the Cer, and only sparse detection was observed after inoculation into the Cer itself. This confirms previous observations that the cerebellum is not highly susceptible to infection with PrV (Sehl et al., 2020).

This could be also mirrored in cultured neuronal cells. Primary cortical neurons from the cerebrum and cerebellum derived from CD1 mice were infected with PrV. Higher PrV titers, independent of infection with PrV-ΔUL21gfp/US3Δkin or wild-type gfp expressing PrV-Ka (PrV-ΔgGgfp) were measured in cerebral cortical cells in contrast to those derived from the cerebellum showing that cerebral neurons are more susceptible. Similar results were obtained in a study with the neurotropic West Nile virus (WNV) (Cho et al., 2013). A unique innate immune response based on different basal levels of interferon-stimulated genes in WNV infected cerebral cortical and granule cell neurons has been assumed to impair successful infection. Other studies have also indicated that type I interferons (IFN) result in a neuron cell type-specific protective effect against viral infections as caused by HSV-1. Type I IFN-related immunity in neurons may play a key role in the brain region-specific control of viral infections (Zhang et al., 2021). Although the analysis of the immune response was not part of this study it provides a valuable future perspective to investigate susceptibility differences associated with alphaherpesvirus infection.

Temporal lobe and Cer inoculated mice were closely monitored, and clinical signs were found to correlate with the extent of viral spread. In an eight-day experiment, mice inoculated with PrV-ΔUL21gfp/US3Δkin into the temporal lobe suffered one to two days earlier from severe clinical signs than mice inoculated into the Cer. This is most likely due to the extended transport route of the virus from the cerebellum to the target regions such as MTL, Pir and prefrontal cortex, where a productive infection could be established. Temporal lobe inoculated mice primarily showed neurological deficits such as seizures and 'stargazing'. In comparison, itching was prevalent in mice inoculated into the cerebellum, while at the end of the experiment the animals also developed behavioral abnormalities including star gazing. In particular, seizures and behavioral disorders, which have also been observed after HSV-1 and Varicella Zoster Virus infection, have been related to damages in the limbic system which is a key structure in the MTL (Wu et al., 2003; Hokkanen et al., 1997; Chee et al., 2022). Moreover, disorders of Pir, located at the interface between the frontal and temporal lobes, have also been described as causative for temporal lobe seizures in rodents (Chee et al., 2022). PrV-Ka infected control mice either inoculated into the temporal lobe or Cer exhibited severe clinical signs including pruritus within 2 days p.i. Viral antigen distribution was comparable to mutant virus infected animals, indicating that viral spread after intracranial infection is independent of the deletions in PrV-ΔUL21gfp/US3Δkin. However, viral antigen was only detected to a limited extent in the MTL, Pir and prefrontal cortex in PrV-Ka infected mice. This is most likely due to the early onset of severe clinical condition prompting early euthanasia, which interrupts the spread of the virus to these regions.

Since high viral titers were employed in this study to investigate clinical symptom progression and to facilitate rapid dissemination into target areas, future studies using lower titers may provide valuable insights into delayed and potentially prolonged viral spread, as well as long-term outcomes influenced by the injection site.

In order to better understand the distinct tropism to MTL, Pir and prefrontal cortices, we next investigated viral spread via neuroanatomical structures that may have led the virus into the target areas. In a kinetic trial, antigen distribution in temporal lobe and cerebellar inoculated mice was analyzed at different time points p.i.

Following temporal lobe inoculation, viral antigen was found at the inoculation site (LEnt), in parts of the MTL and in the midbrain 2 days p.i. Later, after 4 days p.i., antigen was detected moreover in Pir and in the hypothalamus. From 5 days p.i. on, viral antigen was located in all target regions including MTL, piriform and prefrontal cortices, as well as in somatosensory and motor cortices, and in thalamic, hypothalamic and brainstem areas. Virtually identical results were obtained in Cer inoculated animals, in which the virus spread via the Cer, brainstem and midbrain into the target areas MTL, Pir and prefrontal cortices as well as somatosensory cortex, thalamic and hypothalamic areas slightly later at day 7p.i. These data show that despite artificial targeted inoculation into a less permissive brain area, PrV is transported to target regions where it causes a massive infection, as demonstrated for HSV-1 (Yong et al., 2021).

Irrespective of the inoculation site and the inoculated virus, viral antigen was found in large parts of the trigeminal pathway which is generally accepted as the main entry route of alphaherpesviruses into the brain (Held & Derfuss, 2011; Wang et al., 2020; Sehl & Teifke, 2020). The trigeminal system sends several projections which can be regarded as a transport network. Well known neuronal connections exist between Sp5, VPM (Shigenaga et al., 1979) and S1 (Hattox & Nelson, 2007; Donovan & McCasland, 2008). Trigeminal nerve branches have also been shown to project to nuclei of the FR, which were positive in our study and were also found infected by HSV-1 (Niemeyer et al., 2024). The FR appears to be important for alphaherpesviral invasion, as numerous areas of the cerebral cortex are associated with both the FR and areas which were positive for viral antigen as demonstrated for MTL (Hornung, 2003; Baker et al., 1990), trigeminal and hypoglossal nerve, hypothalamus, thalamus (Milsom et al., 2004; Wang, 2009), Sol (Ruggiero et al., 2000) and IO (Horn, 2006). MTL, Pir and prefrontal cortices were identified as main target areas in the present study, and are

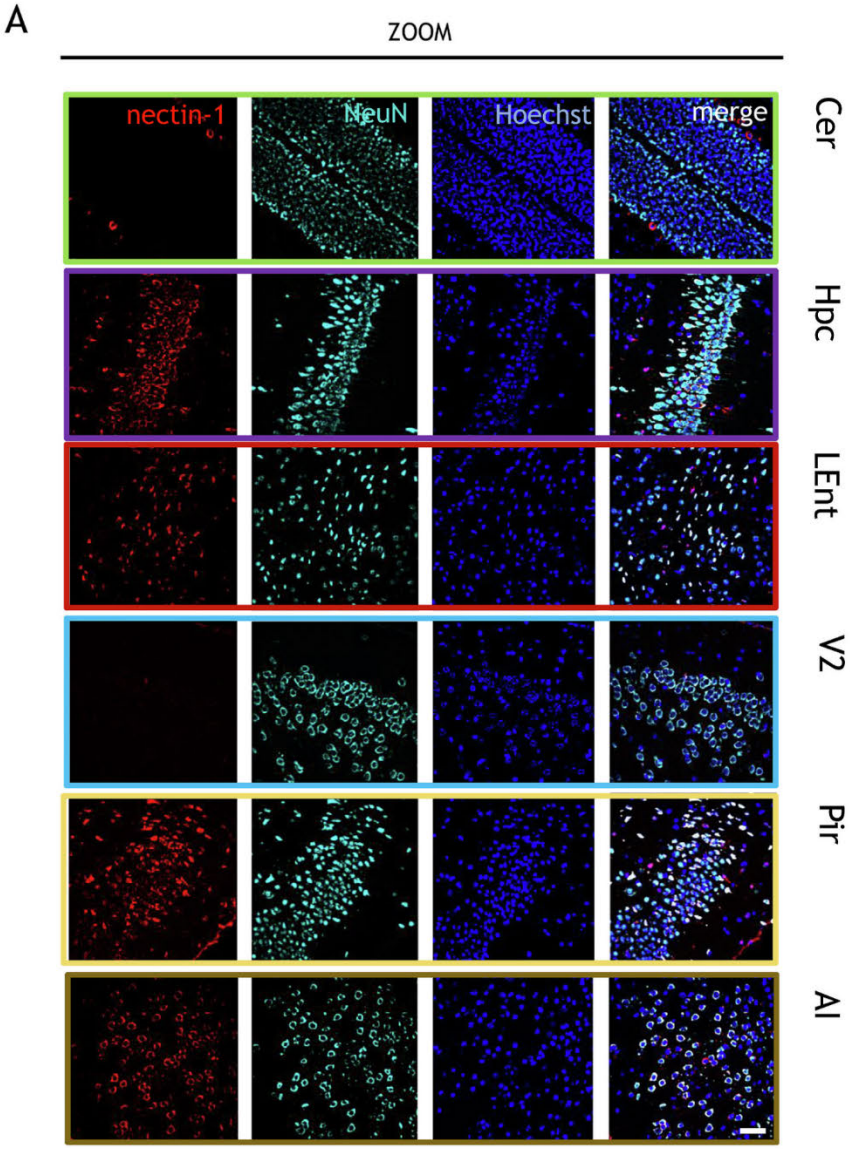

(caption on next page)

Fig. 7. Quantitative image analysis of nectin-1 expression in mock-infected brain tissue of CD1 mice. Labelling of nectin-1 positive neurons in different brain regions (green box = Cer, purple box = Hpc, red box = LEnt, blue box = V2, yellow box = Pir, brown box = AI) using a polyclonal rabbit anti-nectin-1 and a goat anti-rabbit Alexa Fluor 568 antibody (red) as well as a polyclonal guinea pig anti-NeuN and a goat anti-guinea pig Alexa Fluor 647 antibody (cyan) (A). Nuclei were visualized using Hoechst (blue). ROIs were analyzed by quantification of nectin-1 positive cells compared to the total cell count of the respective ROI (B). Average values and standard deviations of three independent experiments are shown. Significant differences are indicated by an asterisk (*), one-way ANOVA test, followed by corrected Dunnett's multiple comparison test; $p < 0{,}0001$. Cer = cerebellum, V2 = secondary visual cortex, Hpc = hippocampus, LEnt = lateral entorhinal cortex, Pir = piriform cortex, AI = agranular insular cortex. Scale bar 100 μm.

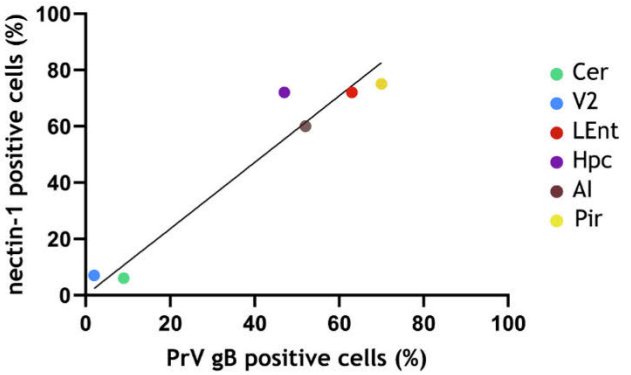

Fig. 8. Correlation and linear regression analysis of PrV gB and nectin-1 positive cells in different brain regions. Mean values (three replicates) of PrV gB positive cells are presented on the x-axis and of nectin-1 positive cells on the y-axis. Spearman's coefficient analysis; $p \leq 0.05$. Cer = cerebellum, V2 = secondary visual cortex, Hpc = hippocampus, LEnt = lateral entorhinal cortex, Pir = piriform cortex, AI = agranular insular cortex.

known to be connected to thalamic and hypothalamic areas and to S1 (Gehrlach et al., 2020; Qiu et al., 2024; O'Leary et al., 2022). It has been demonstrated that alphaherpesviruses preferentially target regions of the MTL that are involved in processing odor information (Menendez & Carr, 2017; Shivkumar et al., 2013; Boggian et al., 2000). MTL areas including Hpc and LEnt as well as the prefrontal cortical areas AI and MO are synaptically associated to the markedly positive Pir as shown in the present and previous studies (Neville & Haberly, 2004; Gehrlach et al., 2020; Qiu et al., 2024; Sehl et al., 2020). Pir as the largest primary olfactory cortical area receives direct projections from the olfactory bulb (Neville & Haberly, 2004; Kajiwara et al., 2007). Further, the caudate putamen, located to the midbrain, is connected to MTL and to the prefrontal cortex (Ghaziri et al., 2018; Alahmadi, 2023).

So far, our results provide detailed information on neuronal networks which are targeted by alphaherpesviruses in the brain. However, it remains unclear whether specific neuroanatomical structures are preferentially used, as the number of projections is extensive. Targeted stereotactic injections, the use of viral tracers or of transgenic mouse models to track the dynamics of viral infection could be useful for future investigations.

While stereotactic CNS injection allows precise and localized viral delivery, it bypasses natural entry routes and initial sites of alphaherpesvirus invasion, such as the olfactory and trigeminal pathways. As a result, it does not fully reflect the early infection dynamics seen in natural exposure. For example, direct injection into the temporal lobe circumvents the primary sites of infection, although subsequent viral spread to these areas can occur. While stereotactic inoculation remains useful for targeted investigations, it differs fundamentally from natural infection in terms of entry and early spatial progression. In contrast, intranasal inoculation better models initial viral entry and propagation via the olfactory system (Niemeyer et al., 2024). Natural infection may also involve additional structures such as the trigeminal ganglion (Sehl et al., 2020), which were not affected in the stereotactic model used here.

After investigating the viral spread in the brain and identifying the target areas upon alphaherpesviral infection, we analyzed the expression of nectin-1 in the affected areas. Nectin-1 as a key entry receptor for several alphaherpesviruses including PrV and HSV-1/-2 by interacting with the viral glycoprotein gD, and is widely expressed in brain tissue (Geraghty et al., 1998; Shukla et al., 2000; Spear et al., 2000). Our results extended previous studies confirming that nectin-1 shows different expression patterns in the brain (Haarr et al., 2001; Lathe & Haas, 2017; Horváth et al., 2006). Nectin-1 expression was abundant in regions of the MTL such as Hpc and LEnt, as well as in areas of Pir and prefrontal cortices where viral antigen was found in high amounts. In contrast, nectin-1 levels were lowest in Cer and V2 which are not or less targeted by alphaherpesvirus infection (Sehl et al., 2020; McFarland & Hotchin, 1987; Esiri, 1982). Low expression levels of nectin-1 in Cer and high expression levels in Hpc have also been shown in healthy human and murine brain tissue (Lathe & Haas, 2017; Prandovszky et al., 2008). In our study, viral antigen distribution and nectin-1 expression strongly correlated, suggesting that the high susceptibility of the MTL, Pir and prefrontal cortex may be related to the high expression of nectin-1 in these regions.

Studies on HSE showed that the cerebellum is rather resistant to alphaherpesviral infection (McFarland & Hotchin, 1987), which according to our results may be due to a lack of nectin-1. However, in the cerebellum alternative entry receptors are expressed, including PILRA (gB) (Lathe & Haas, 2017). In addition, cellular molecules interacting with nectin-1 may also play a role in contributing to the differences in susceptibility, such as human TMEFF1, a membrane protein preferentially expressed by cerebral neurons, which is able to interfere with HSV-1 entry by interacting with nectin-1 (Chan et al., 2024). In this respect, future research regarding nectin-1 expression would be beneficial, particularly in newborn mice since Horváth et al., 2006 indicated consistent changes in the distribution of nectin-1 with increasing age. Additionally, studies with HSV-1 demonstrated variations in expression levels of nectin-1 in infected compared to uninfected tissue. Here, apoptotic neurons showed minimal to no expression of nectin-1, in contrast to intact infected neurons, which showed stronger staining for nectin-1 compared to neurons in uninfected brain tissue (Shukla et al., 2006). In contrast, our analyses demonstrated no significant difference in nectin-1 distribution between PrV-infected and mock-treated mice, indicating stable receptor expression independent of infection status. These findings corroborate our hypothesis that regional nectin-1 expression constitutes a key determinant of susceptibility to viral targeting.

Furthermore, the regional variation observed in vivo may be influenced by factors such as tissue context, cytoarchitecture, and region-specific cellular composition. These elements are not fully preserved under culture conditions, which may explain the absence of detectable differences in vitro.

Future studies may yield further insights into viral neurotropism by investigating how anatomical targeting of the mesiotemporal lobe is modulated in genetically engineered mouse models with diminished or altered nectin-1 expression. Such models could elucidate whether alterations in nectin-1-mediated viral tropism correspond to distinct clinical phenotypes, modified cerebral viral spread, or even marked attenuation or abrogation of infection. Consistent with this concept, recent work has shown that nectin-1 knockout mice challenged intranasally with pseudorabies virus exhibit significantly enhanced survival compared to wild-type controls (Tomioka et al., 2024), thereby underscoring the critical role of nectin-1 in viral entry and pathogenicity.

In summary, we demonstrated that the alphaherpesvirus PrV

preferentially targets brain regions including MTL, Pir and prefrontal cortex despite artificial inoculation, specifically into the Cer which is generally not affected upon natural infection. Viral inoculation into the Cer and the temporal lobe revealed overlapping invasion pathways used by the virus, explicitly including the trigeminal route, which projects to target regions. The quantification of nectin-1 expression in highly and less susceptible brain regions suggested that the presence of this receptor plays an essential role in successful establishment of infection. In this respect, region-dependent cell type-specific characteristics further seem to play a major role in susceptibility, as in vitro experiments with primary neurons from the cerebral cortex and cerebellum have shown.

Funding statement

The project was funded by the Deutsche Forschungsgemeinschaft (DFG), grant number 466759708.

CRediT authorship contribution statement

Viktoria Korff: Writing – review & editing, Writing – original draft, Visualization, Validation, Methodology, Investigation, Formal analysis, Data curation. **Issam El-Debs:** Writing – review & editing, Methodology, Investigation. **Barbara G. Klupp:** Writing – review & editing, Supervision, Conceptualization. **Jens P. Teifke:** Writing – review & editing, Supervision, Conceptualization. **Thomas C. Mettenleiter:** Supervision, Conceptualization. **Julia Sehl-Ewert:** Writing – review & editing, Supervision, Resources, Project administration, Funding acquisition, Conceptualization.

Acknowledgements

The authors thank Silvia Schuparis, Robin Brandt, Cindy Krüper and Karla Günther for outstanding technical assistance. We especially thank Sonja Bröer for the training of stereotactic surgeries. Additionally, appreciation is extended to Angele Breithaupt, Tobias Britzke and Lukas Mathias Michaely for their invaluable scientific contributions.

Ethics statement

Animal experiments were approved by the State Office for Agriculture, Food Safety and Fishery in Mecklenburg-Western Pomerania (LALFF M-V) with reference number 7221.3-1-034/ 22.

Data availability statement

The data that support the findings of this study are available on request from the corresponding author.

Appendix A. Supplementary data

Supplementary data to this article can be found online at https://doi.org/10.1016/j.neuroscience.2025.08.024.

References

Alahmadi, A.A.S., 2023. Functional connectivity of sub-cortical brain regions: disparities and similarities. Neuroreport 34, 214–219.
Armien, A.G., Hu, S., Little, M.R., Robinson, N., Lokensgard, J.R., Low, W.C., Cheeran, M.-C.-J., 2010. Chronic cortical and subcortical pathology with associated neurological deficits ensuing experimental herpes encephalitis. Brain Pathol. 20, 738–750.
Babic, N., Mettenleiter, T.C., Ugolini, G., Flamand, A., Coulon, P., 1994. Propagation of Pseudorabies Virus in the nervous System of the Mouse after Intranasal Inoculation. Virology 204, 616–625.
Baker, K.G., Halliday, G.M., Törk, I., 1990. Cytoarchitecture of the human dorsal raphe nucleus. J. Comp. Neurol. 301, 147–161.
Boggian, I., Buzzacaro, E., Calistri, A., Calvi, P., Cavaggioni, A., Mucignat-Caretta, C., Palu, G., 2000. Asymptomatic herpes simplex type 1 virus infection of the mouse brain. J. Neurovirol. 6, 303–313.
Bradshaw, M.J., Venkatesan, A., 2016. Herpes simplex virus-1 encephalitis in adults: pathophysiology, diagnosis, and management. Neurotherapeutics 13, 493–508.
Bröer, S., Backofen-Wehrhahn, B., Bankstahl, M., Gey, L., Gernert, M., Löscher, W., 2012. Vigabatrin for focal drug delivery in epilepsy: bilateral microinfusion into the subthalamic nucleus is more effective than intranigral or systemic administration in a rat seizure model. Neurobiol. Dis. 46, 362–376.
Chan, Y.-H., Liu, Z., Bastard, P., Khobrekar, N., Hutchison, K.M., Yamazaki, Y., Fan, Q., Matuozzo, D., Harschnitz, O., Kerrouche, N., et al., 2024. Human TMEFF1 is a restriction factor for herpes simplex virus in the brain. Nature 632, 390–400.
Chee, K., Razmara, A., Geller, A.S., Harris, W.B., Restrepo, D., Thompson, J.A., Kramer, D.R., 2022. The role of the piriform cortex in temporal lobe epilepsy: a current literature review. Front. Neurol. 13, 1042887.
Cho, H., Proll, S.C., Szretter, K.J., Katze, M.G., Gale, M., Diamond, M.S., 2013. Differential innate immune response programs in neuronal subtypes determine susceptibility to infection in the brain by positive-stranded RNA viruses. Nat. Med. 19, 458–464.
Damasio, A.R., van Hoesen, G.W., 1985. The limbic system and the localisation of herpes simplex encephalitis. J. Neurol. Neurosurg. Psychiatry 48, 297.
Donovan, S.L., McCasland, J.S., 2008. GAP-43 is critical for normal targeting of thalamocortical and corticothalamic, but not trigeminothalamic axons in the whisker barrel system. Somatosens. Mot. Res. 25, 33–47.
Esiri, M., 1982. Herpes simplex encephalitis an immunohistological study of the distribution of viral antigen within the brain. J. Neurol. Sci. 54, 209–226.
Fuchs, W., Backovic, M., Klupp, B.G., Rey, F.A., Mettenleiter, T.C., 2012. Structure-based mutational analysis of the highly conserved domain IV of glycoprotein H of pseudorabies virus. J. Virol. 86, 8002–8013.
Gage, G.J., Kipke, D.R., Shain, W., 2012. Whole animal perfusion fixation for rodents. J. Vis. Exp.
Gehrlach, D.A., Weiand, C., Gaitanos, T.N., Cho, E., Klein, A.S., Hennrich, A.A., Conzelmann, K.-K., Gogolla, N., 2020. A whole-brain connectivity map of mouse insular cortex. Elife 9.
Geraghty, R.J., Krummenacher, C., Cohen, G.H., Eisenberg, R.J., Spear, P.G., 1998. Entry of alphaherpesviruses mediated by poliovirus receptor-related protein 1 and poliovirus receptor. Science 280, 1618–1620.
Ghaziri, J., Tucholka, A., Girard, G., Boucher, O., Houde, J.-C., Descoteaux, M., Obaid, S., Gilbert, G., Rouleau, I., Nguyen, D.K., 2018. Subcortical structural connectivity of insular subregions. Sci. Rep. 8, 8596.
Gnann, J.W., Whitley, R.J., 2017. Herpes simplex encephalitis: an update. Curr. Infect. Dis. Rep. 19, 13.
Haarr, L., Shukla, D., Rødahl, E., Dal Canto, M.C., Spear, P.G., 2001. Transcription from the gene encoding the herpesvirus entry receptor nectin-1 (HveC) in nervous tissue of adult mouse. Virology 287, 301–309.
Hattox, A.M., Nelson, S.B., 2007. Layer V neurons in mouse cortex projecting to different targets have distinct physiological properties. J. Neurophysiol. 98, 3330–3340.
Held, K., Derfuss, T., 2011. Control of HSV-1 latency in human trigeminal ganglia–current overview. J. Neurovirol. 17, 518–527.
Hokkanen, L., Launes, J., Poutiainen, E., Valanne, L., Salonen, O., Siren, J., Iivanainen, M., 1997. Subcortical type cognitive impairment in herpes zoster encephalitis. J. Neurol. 244, 239–245.
Horn, A.K., 2006. The reticular formation. In: Büttner-Ennever, J.A. (Ed.), *Progress in Brain Research : Neuroanatomy of the Oculomotor System*. Elsevier, pp. 127–155.
Hornung, J.-P., 2003. The human raphe nuclei and the serotonergic system. J. Chem. Neuroanat. 26, 331–343.
Horváth, S., Prandovszky, E., Kis, Z., Krummenacher, C., Eisenberg, R.J., Cohen, G.H., Janka, Z., Toldi, J., 2006. Spatiotemporal changes of the herpes simplex virus entry receptor nectin-1 in murine brain during postnatal development. J. Neurovirol. 12, 161–170.
Kajiwara, R., Tominaga, T., Takashima, I., 2007. Olfactory information converges in the amygdaloid cortex via the piriform and entorhinal cortices: observations in the guinea pig isolated whole-brain preparation. Eur. J. Neurosci. 25, 3648–3658.
Kaplan, A.S., Vatter, A.E., 1959. A comparison of herpes simplex and pseudorabies viruses. Virology 7, 394–407.
Klopfleisch, R., Klupp, B.G., Fuchs, W., Kopp, M., Teifke, J.P., Mettenleiter, T.C., 2006. Influence of pseudorabies virus proteins on neuroinvasion and neurovirulence in mice. J. Virol. 80, 5571–5576.
Kopp, M., Granzow, H., Fuchs, W., Klupp, B.G., Mundt, E., Karger, A., Mettenleiter, T.C., 2003. The pseudorabies virus UL11 protein is a virion component involved in secondary envelopment in the cytoplasm. J. Virol. 77, 5339–5351.
Koyuncu, O.O., MacGibeny, M.A., Enquist, L.W., 2018. Latent versus productive infection: the alpha herpesvirus switch. Future Virol 13, 431–443.
Lathe, R., Haas, J.G., 2017. Distribution of cellular HSV-1 receptor expression in human brain. J. Neurovirol. 23, 376–384.
McFarland, D.J., Hotchin, J., 1987. Contrasting patterns of virus spread and neuropathology following microinjection of herpes simplex virus into the hippocampus or cerebellum of mice. J. Neurol. Sci. 79, 255–265.
McGrath, N., Anderson, N.E., Croxson, C.M., Powell, K.F., 1997. Herpes simplex encephalitis treated with acyclovir: diagnosis and long term outcome. J. Neurol., Neurosurg., Psychiatry 63, 321–326.
Menendez, C.M., Carr, D.J.J., 2017. Herpes simplex virus-1 infects the olfactory bulb shortly following ocular infection and exhibits a long-term inflammatory profile in the form of effector and HSV-1-specific T cells. J. Neuroinflammation 14, 124.
Mettenleiter, T.C., 1989. Glycoprotein glll deletion mutants of pseudorabies virus are impaired in virus entry. Virology 171, 623–625.
Mettenleiter, T.C., 2000. Aujeszky's disease (pseudorabies) virus: the virus and molecular pathogenesis - State of the art, June 1999. Vet. Res. 31, 99–115.

Mettenleiter, T.C., 2003. Pathogenesis of neurotropic herpesviruses: role of viral glycoproteins in neuroinvasion and transneuronal spread. Virus Res. 92, 197–206.
Milsom, W.K., Chatburn, J., Zimmer, M.B., 2004. Pontine influences on respiratory control in ectothermic and heterothermic vertebrates. Respir. Physiol. Neurobiol. 143, 263–280.
Neville, K.R., Haberly, L.B., 2004. Olfactory Cortex. In: Shepherd, G.M. (Ed.), *The Synaptic Organization of the Brain*. Oxford University Press.
Niemeyer, C.S., Merle, L., Bubak, A.N., Baxter, B.D., Gentile Polese, A., Colon-Reyes, K., Vang, S., Hassell, J.E., Bruce, K.D., Nagel, M.A., et al., 2024. Olfactory and trigeminal routes of HSV-1 CNS infection with regional microglial heterogeneity. J. Virol. e0096824.
O'Leary, T.P., Kendrick, R.M., Bristow, B.N., Sullivan, K.E., Wang, L., Clements, J., Lemire, A.L., Cembrowski, M.S., 2022. Neuronal cell types, projections, and spatial organization of the central amygdala. iScience 25, 105497.
Paxinos, G., Franklin, K.B.J., 2001. *The Mouse Brain in Stereotaxic Coordinates*. Academic Press, San Diego.
Prandovszky, E., Horváth, S., Gellért, L., Kovács, S.K., Janka, Z., Toldi, J., Shukla, D., Vályi-Nagy, T., 2008. Nectin-1 (HveC) is expressed at high levels in neural subtypes that regulate radial migration of cortical and cerebellar neurons of the developing human and murine brain. J. Neurovirol. 14, 164–172.
Qiu, S., Hu, Y., Huang, Y., Gao, T., Wang, X., Wang, D., Ren, B., Shi, X., Chen, Y., Wang, X., et al., 2024. Whole-brain spatial organization of hippocampal single-neuron projectomes. Science 383, eadj9198.
Raschilas, F., Wolff, M., Delatour, F., Chaffaut, C., de Broucker, T., Chevret, S., Lebon, P., Canton, P., Rozenberg, F., 2002. Outcome of and prognostic factors for herpes simplex encephalitis in adult patients: results of a multicenter study. Clin. Infect. Dis. 35, 254–260.
Ruggiero, D.A., Underwood, M.D., Mann, J.J., Anwar, M., Arango, V., 2000. The human nucleus of the solitary tract: visceral pathways revealed with an "in vitro" postmortem tracing method. J. Auton. Nerv. Syst. 79, 181–190.
Sehl, J., Hölper, J.E., Klupp, B.G., Baumbach, C., Teifke, J.P., Mettenleiter, T.C., 2020. An improved animal model for herpesvirus encephalitis in humans. PLoS Pathog. 16, e1008445.
Sehl, J., Teifke, J.P., 2020. Comparative pathology of pseudorabies in different naturally and experimentally infected species-a review. Pathogens 9.
Sehl-Ewert, J., Schwaiger, T., Schäfer, A., Hölper, J.E., Klupp, B.G., Teifke, J.P., Blohm, U., Mettenleiter, T.C., 2022. Clinical, neuropathological, and immunological short- and long-term feature of a mouse model mimicking human herpes virus encephalitis. Brain Pathol. 32, e13031.
Shigenaga, Y., Takabatake, M., Sugimoto, T., Sakai, A., 1979. Neurons in marginal layer of trigeminal nucleus caudalis ventrobasal complex (VB) and posterior nuclear group (PO) by retrograde labeling with horseradish peroxidase Y. Brain Res. 166, 391–396.
Shivkumar, M., Milho, R., May, J.S., Nicoll, M.P., Efstathiou, S., Stevenson, P.G., 2013. Herpes simplex virus 1 targets the murine olfactory neuroepithelium for host entry. J. Virol. 87, 10477–10488.
Shukla, D., Dal Canto, M.C., Rowe, C.L., Spear, P.G., 2000. Striking similarity of murine nectin-1alpha to human nectin-1alpha (HveC) in sequence and activity as a glycoprotein D receptor for alphaherpesvirus entry. J. Virol. 74, 11773–11781.
Shukla, D., Scanlan, P.M., Tiwari, V., Sheth, V., Clement, C., Guzman-Hartman, G., Dermody, T.S., Valyi-Nagy, T., 2006. Expression of nectin-1 in normal and herpes simplex virus type 1-infected murine brain. Appl. Immunohistochem. Mol. Morphol. 14, 341–347.
Smith, G., 2012. Herpesvirus transport to the nervous system and back again. Annu. Rev. Microbiol. 66, 153–176.
Spear, P.G., Eisenberg, R.J., Cohen, G.H., 2000. Three classes of cell surface receptors for alphaherpesvirus entry. Virology 275, 1–8.
Stahl, J.P., Mailles, A., 2019. Herpes simplex virus encephalitis update. Curr. Opin. Infect. Dis. 32, 239–243.
Steiner, I., Benninger, F., 2013. Update on herpes virus infections of the nervous system. Curr. Neurol. Neurosci. Rep. 13, 414.
Taylor, S.W., Smith, R.M., Pari, G., Wobeser, W., Rossiter, J.P., Jackson, A.C., 2005. Herpes simplex encephalitis. Can. J. Neurol. Sci. 32, 246–247.
Tomioka, Y., Takeda, K., Ozaki, K., Inoue, H., Yamamoto, S., Takeuchi, T., Ono, E., 2024. Single amino acid mutation of nectin-1 provides remarkable resistance against lethal pseudorabies virus infection in mice. J. Vet. Med. Sci. 86, 120–127.
Twomey, J.A., Barker, C.M., Robinson, G., Howell, D.A., 1979. Olfactory mucosa in herpes simplex encephalitis. J. Neurol. Neurosurg. Psychiatry 42, 983–987.
Tyler, K.L., 2004. Update on herpes simplex encephalitis. Rev. Neurol. Dis. 1, 169–178.
Vallbracht, M., Backovic, M., Klupp, B.G., Rey, F.A., Mettenleiter, T.C., 2019. Chapter Seven - Common characteristics and unique features: a comparison of the fusion machinery of the alphaherpesviruses Pseudorabies virus and Herpes simplex virus. In: Kielian, M., Mettenleiter, T.C., Roossinck, M.J. (Eds.), *Advances in Virus Research : Virus Entry*. Academic Press, pp. 225–281.
Wang, D., 2009. Reticular formation and spinal cord injury. Spinal Cord 47.
Wang, Y., Wu, H., Wang, B., Qi, H., Jin, Z., Qiu, H.-J., Sun, Y., 2020. A NanoLuc luciferase reporter pseudorabies virus for live imaging and quantification of viral infection. Front. Vet. Sci. 7, 566446.
Whitley, R., Baines, J., 2018. Clinical management of herpes simplex virus infections: past, present, and future. F1000Research 7(F1000 Faculty Rev): 1726.
Wnęk, M., Ressel, L., Ricci, E., Rodriguez-Martinez, C., Guerrero, J.C.V., Ismail, Z., Smith, C., Kipar, A., Sodeik, B., Chinnery, P.F., et al., 2016. Herpes simplex encephalitis is linked with selective mitochondrial damage; a post-mortem and in vitro study. Acta Neuropathol. 132, 433–451.
Wu, H.-M., Huang, C.-C., Chen, S.-H., Liang, Y.-C., Tsai, J.-J., Hsieh, C.-L., Hsu, K.-S., 2003. Herpes simplex virus type 1 inoculation enhances hippocampal excitability and seizure susceptibility in mice. Eur. J. Neurosci. 18, 3294–3304.
Yong, S.J., Yong, M.H., Teoh, S.L., Soga, T., Parhar, I., Chew, J., Lim, W.L., 2021. The hippocampal vulnerability to herpes simplex virus type i infection: relevance to alzheimer's disease and memory impairment. Front. Cell. Neurosci. 15, 695738.
Zhang, S.-Y., Harschnitz, O., Studer, L., Casanova, J.-L., 2021. Neuron-intrinsic immunity to viruses in mice and humans. Curr. Opin. Immunol. 72, 309–317.

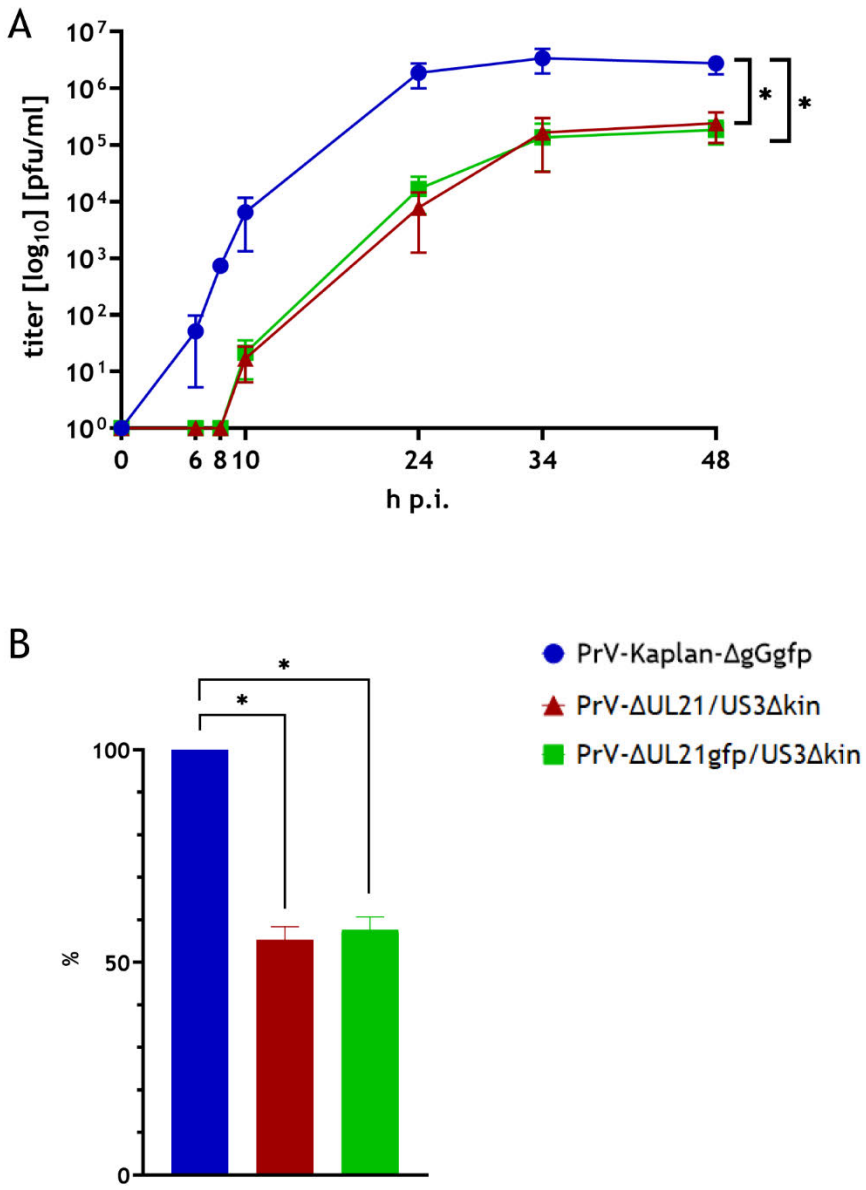

S1 Fig.: In vitro characterization of PrV-ΔUL21gfp/US3Δkin. (A) Multi-step replication kinetics of PrV-ΔUL21gfp/US3Δkin compared to PrV-Kaplan-ΔgGgfp and PrV-ΔUL21/US3Δkin at a MOI of 0.5. (B) Plaque diameters of the virus mutants were assessed on RK13 cells. 20 plaques each per virus mutant were measured and compared to the plaque diameter of PrV-Ka-ΔgGgfp set as 100%. Average values and standard deviations of three independent experiments are shown. Significant differences of virus mutants compared to PrV-Ka-ΔgGgfp are indicated by an asterisk (*), Wilcoxon matched pairs signed rank test (replication kinetics), $p < 0.05$ and one-way ANOVA test, followed by corrected Dunnett's multiple comparison test (plaque assay), $p < 0,01$.

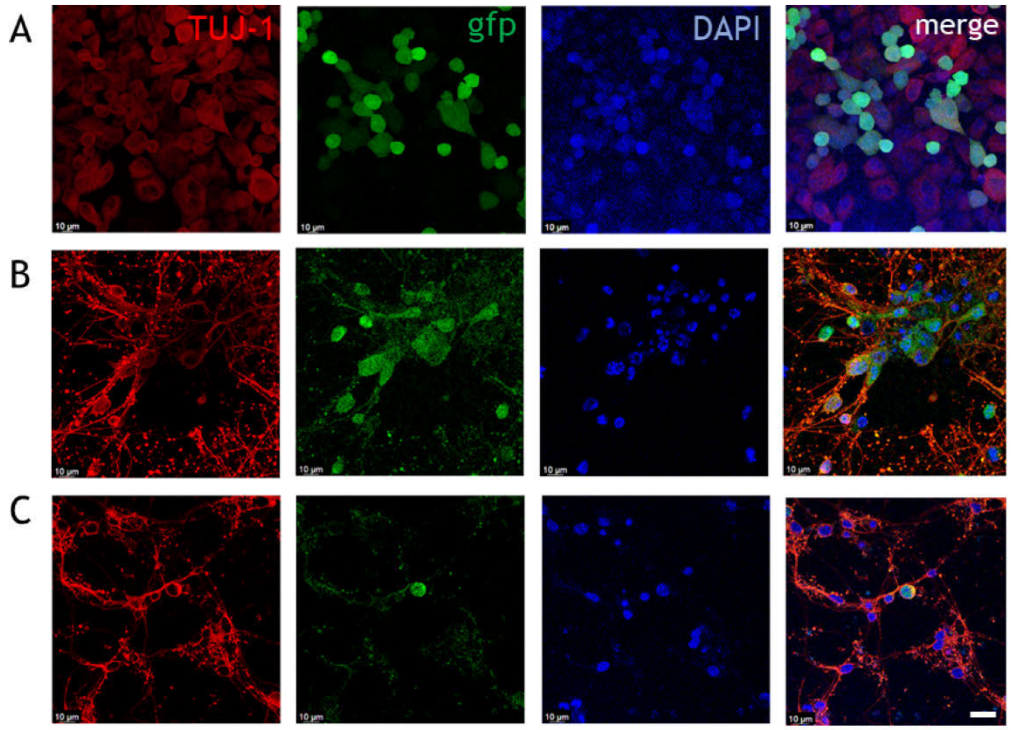

S2 Fig.: Auto- and immunofluorescence of PrV-ΔUL21gfp/US3Δkin infected cultivated primary mouse neurons. A) RK13 cells and B) primary neurons from the cerebral cortex and from C) the cerebellum from CD1 mice were infected with PrV-ΔUL21gfp/US3Δkin, 24hpi. Cells were stained with an anti-TUJ-1/ β-tubulin III antibody (red) and DAPI (blue). Scale bar = 10µm

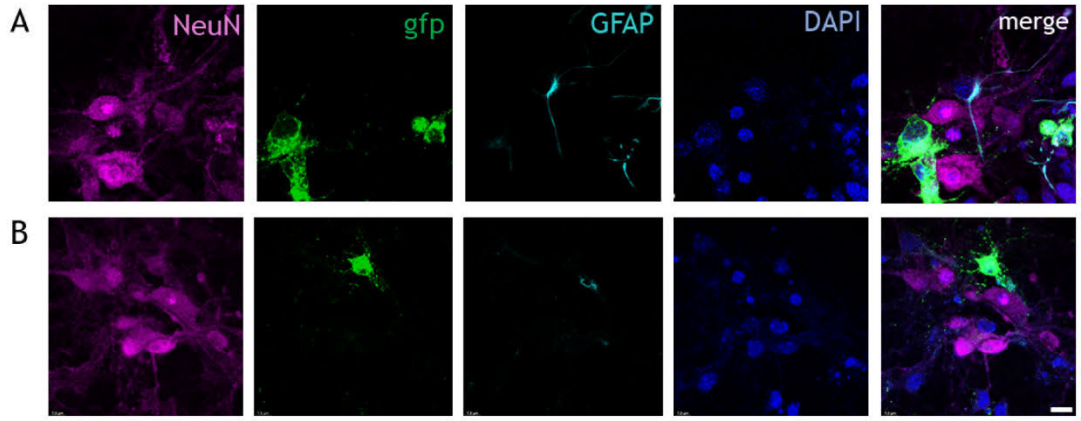

S3 Fig.: Immunofluorescence of PrV-ΔUL21gfp/US3Δkin infected cultivated CD1 primary mouse neurons. Primary neurons derived from (A) the cerebral cortex and (B) the cerebellum were infected with PrV-ΔUL21gfp/US3Δkin and examined 24 hours post-infection (hpi). Infection was visualized by virus-expressing gfp. Cells were stained with an anti-NeuN (purple) and anti-GFAP antibody (cyan). Nuclei were counterstained with DAPI (blue). Scale bar = 10µm

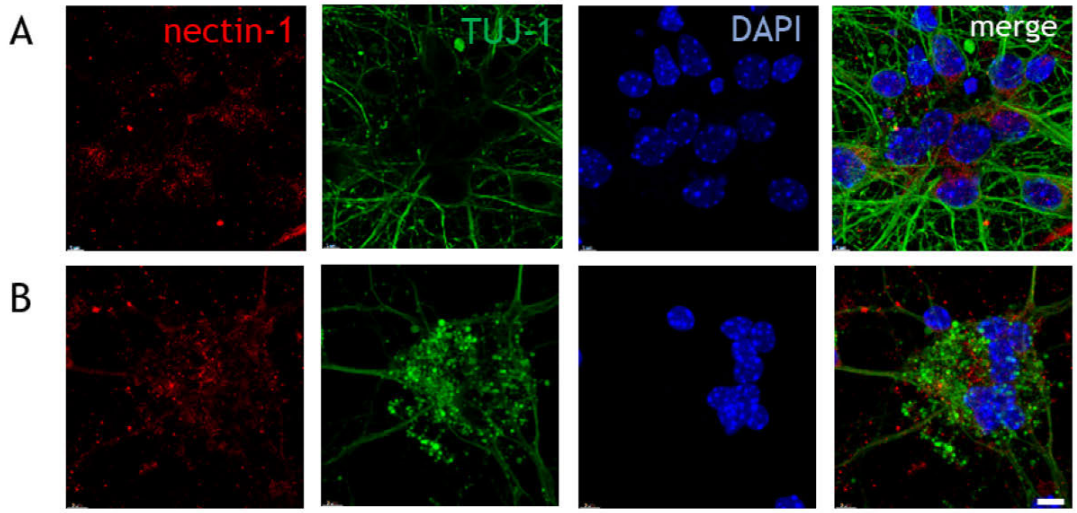

S4 Fig.: Nectin-1 expression in cultivated primary mouse neurons. A) RK13 cells and B) CD1 primary neurons from the cerebral cortex and from C) the cerebellum were stained with an anti-nectin-1 and anti-TUJ-1/ β-tubulin III antibody (green). Nuclei were counterstained with DAPI (blue). Scale bar = 5µm

A

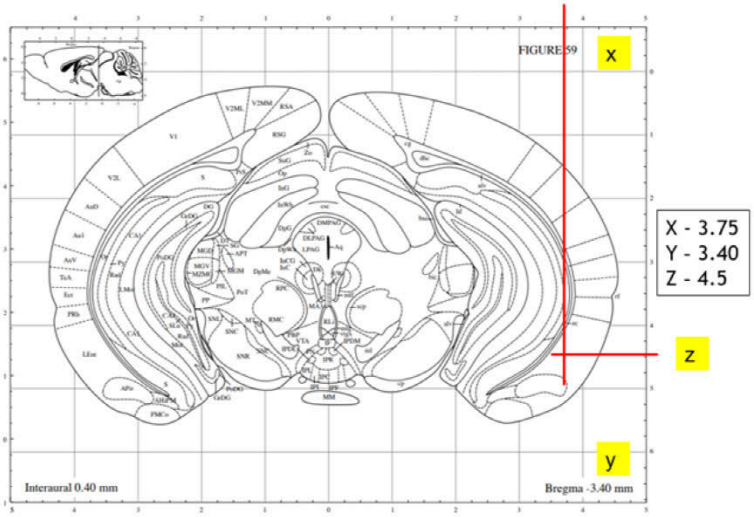

Paxinos G., Franklin K., The Mouse Brain in Stereotaxic Coordinates second edition, Academic Press, 2001, p.109, Figure 59

B

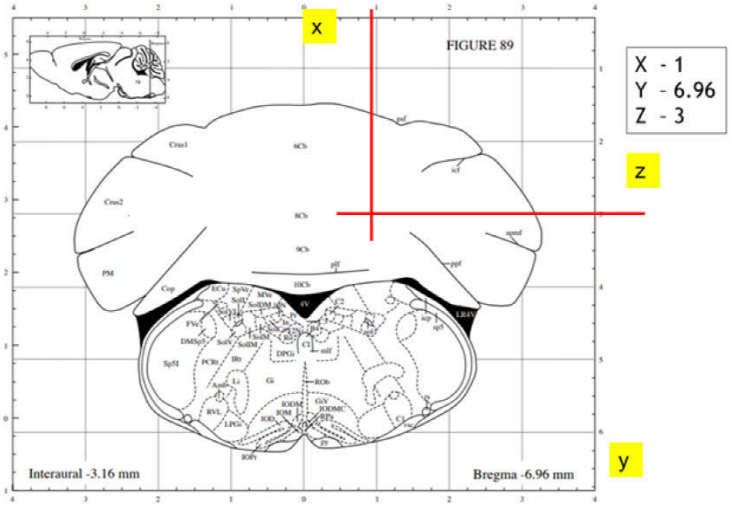

Paxinos G., Franklin K., The Mouse Brain in Stereotaxic Coordinates second edition, Academic Press, 2001, p.139, Figure 89

S5 Fig.: Schematic illustration of brain sections indicating the coordinates for stereotactic inoculation. A) For temporal lobe inoculation the coordinates of the lateral entorhinal cortex (LEnt) and B) the cerebellar coordinates are given (red lines, boxes) based on The Mouse Brain in Stereotaxic Coordinates by Paxinos and Franklin, 2001.

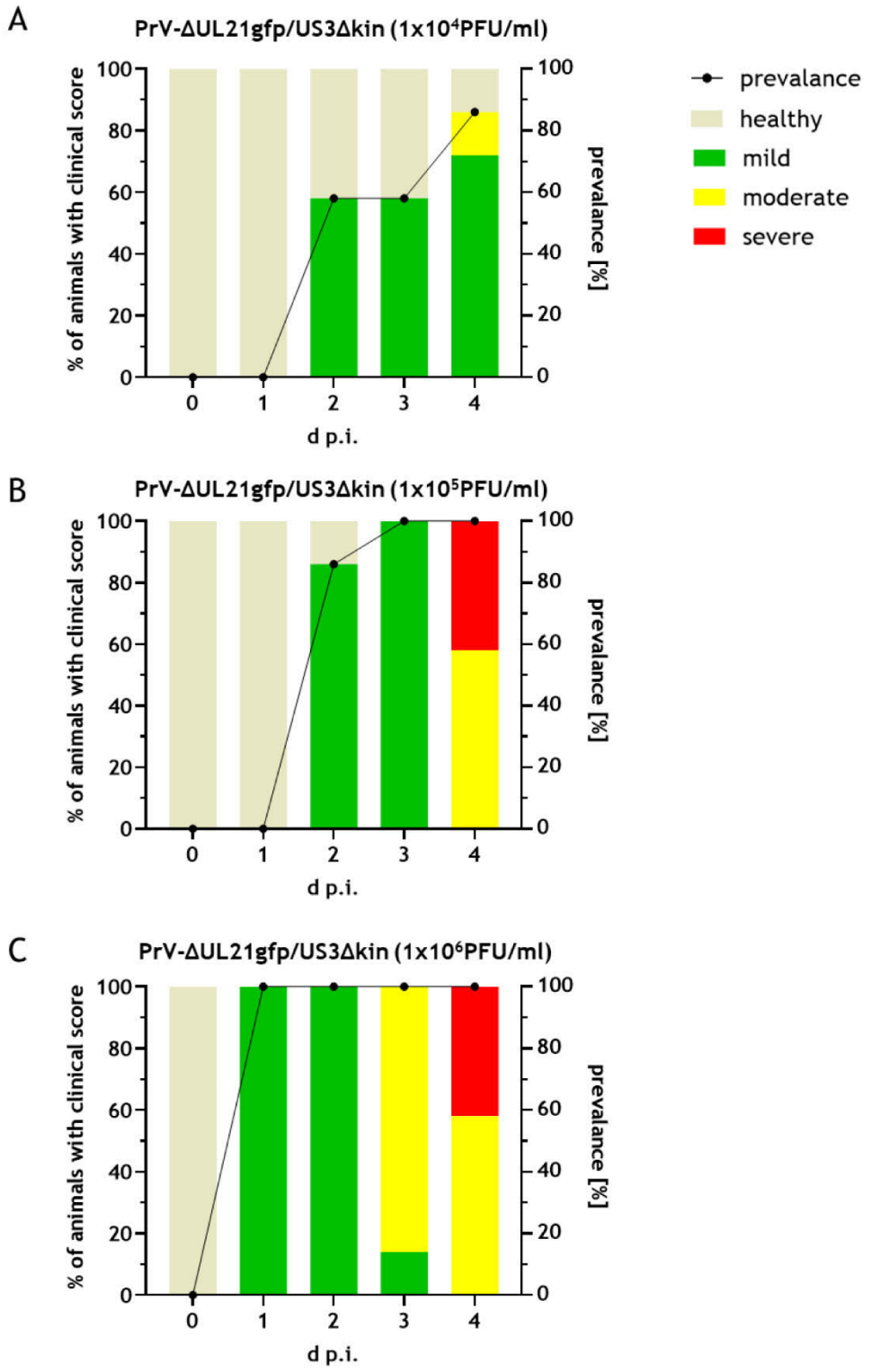

S6 Fig.: Prevalence of diseased animals in a dose finding experiment after stereotactic inoculation of different virus quantities of PrV-ΔUL21gfp/US3Δkin into the temporal lobe. The animals were either inoculated with a total volume of 10µl virus suspension containing: A) $1x10^4$PFU/ml, B) $1x10^5$ PFU/ml or C) $1x10^6$ PFU/ml. The frequency of sick animals per time is indicated by bars. Based on a scoring system (S1 Table) animals were categorized into either mildly (green), moderately (yellow) or severely affected (red). Prevalence is given by the black line on the right Y-axis.

category	clinical signs	score
external appearance (I)	normal posture, smooth and glossy fur, no pruritus	0
	normal posture, ruffled and dull fur, mild pruritus, nasal bridge edema, conjunctivitis, dermal erosions	1
	mild hunched back, ruffled fur, moderate itching, weeping skin erosions on various parts of the body	2
	severely hunched back, ruffled and dull fur, severe pruritus, automutilation with bloody skin erosions, dyspnea, seizure without recovery	3
behavior and activity (II)	intently and curious	0
	very calm, mild reduced spontaneous activity, no reduced induced activity	1
	paroxysmal hyperactivity, apathy, moderate reduced spontaneous activity, moderate reduced induced activity, fasciculations, seizure with recovery, 'star gazing' periods	2
	stupor, no spontaneous activity, lateral position	3
body weight (III)	no change: < 5% of the initial weight	0
	reduction of 5-10% from the initial weight	1
	reduction of 10-15% from the initial weight	2
	reduction of 20% from the initial weight	3

S1 Table: Standardized scoring system for mice infected with PrV. Three categories including (I) external appearance, (II) behavior and activity and (III) body weight were assessed daily and utilized to evaluate mice either as mildly (max. score 1 in three out of three categories), moderate (max. score 2 in two out of three categories) and severely affected (max. score 2 in all categories or max. score 3 in one out of three categories). The humane endpoint was defined as score 3 in one out of three categories or score 2 in all categories.

mouse nr	virus	inoculation site	clinical signs (humane endpoint)	humane endpoint
M1*	PrV-ΔUL21gfp/US3Δkin	LEnt	severely hunched back, ruffled and dull fur, mild pruritus, seizure with recovery, 'star gazing' periods, paroxysmal hyperactivity, reduction of 20% from the initial weight	5 d p.i.
M2*	PrV-ΔUL21gfp/US3Δkin	LEnt	severely hunched back, ruffled and dull fur, mild pruritus, seizure with recovery, 'star gazing' periods, moderate reduced spontaneous activity, apathy	7 d p.i.
M3*	PrV-ΔUL21gfp/US3Δkin	LEnt	severely hunched back, ruffled and dull fur, moderate pruritus, seizure with recovery, 'star gazing' periods, reduction of 12% from the initial weight	6 d p.i.
M4*	PrV-ΔUL21gfp/US3Δkin	LEnt	severely hunched back, ruffled and dull fur, mild pruritus, 'star gazing' periods, reduction of 12% from the initial weight	7 d p.i.
M5*	PrV-ΔUL21gfp/US3Δkin	LEnt	severely hunched back, ruffled and dull fur, mild pruritus, seizure with recovery, 'star gazing' periods	5 d p.i.
M6*	PrV-ΔUL21gfp/US3Δkin	Cer	severely hunched back, ruffled and dull fur, severe pruritus, automutilation with hemorrhagic skin erosions, 'star gazing' periods, reduction of 24% from the initial weight	7 d p.i.
M7*	PrV-ΔUL21gfp/US3Δkin	Cer	severely hunched back, ruffled and dull fur, moderate pruritus, dermal erosions, reduction of 8% from the initial weight	7 d p.i.
M8	PrV-ΔUL21gfp/US3Δkin	Cer	ruffled and dull fur, moderate pruritus, dermal erosions, 'star gazing' periods, reduction of 8% from the initial weight	8 d p.i.
M9*	PrV-ΔUL21gfp/US3Δkin	Cer	severely hunched back, ruffled and dull fur, severe pruritus, automutilation with hemorrhagic skin erosions	7 d p.i.
M10	PrV-ΔUL21gfp/US3Δkin	Cer	moderatly hunched back, ruffled and dull fur, mild pruritus, 'star gazing' periods, paroxysmal hyperactivity	8 d p.i.
M1*	PrV-Kaplan	LEnt	severely hunched back, ruffled and dull fur, moderate pruritus, moderate reduced spontaneous activity	2 d p.i.
M2*	PrV-Kaplan	LEnt	severely hunched back, ruffled and dull fur, moderate reduced spontaneous activity, apathy, dyspnea	2 d p.i.
M3*	PrV-Kaplan	LEnt	severely hunched back, ruffled and dull fur, moderate pruritus, seizure with recovery	2 d p.i.
M4*	PrV-Kaplan	LEnt	severely hunched back, ruffled and dull fur, moderate pruritus, dyspnea, seizure with recovery, moderate reduced spontaneous activity	2 d p.i.
M5*	PrV-Kaplan	LEnt	severely hunched back, ruffled and dull fur, moderate pruritus, seizure with recovery	2 d p.i.
M6*	PrV-Kaplan	Cer	severely hunched back, ruffled and dull fur, moderate pruritus, moderate reduced spontaneous activity, apathy	2 d p.i.
M7*	PrV-Kaplan	Cer	severely hunched back, ruffled and dull fur, moderate reduced spontaneous activity, dyspnea, apathy	2 d p.i.
M8*	PrV-Kaplan	Cer	severely hunched back, ruffled and dull fur, mild reduced spontaneous activity, dyspnea, apathy	2 d p.i.
M9*	PrV-Kaplan	Cer	severely hunched back, ruffled and dull fur, moderate pruritus, moderate reduced spontaneous activity	2 d p.i.
M10*	PrV-Kaplan	Cer	severely hunched back, ruffled and dull fur, moderate reduced spontaneous activity, dyspnea	2 d p.i.
-	mock	Cer/LEnt	-	-

S2 Table: Overview of the clinical signs shown by individual mice following stereotactic inoculation with either PrV-ΔUL21gfp/US3Δkin or PrV-Kaplan into the temporal lobe (LEnt) or cerebellum (Cer) at the day of euthanasia. Animals that reached humane endpoint criteria are highlighted with an asterisk (*).

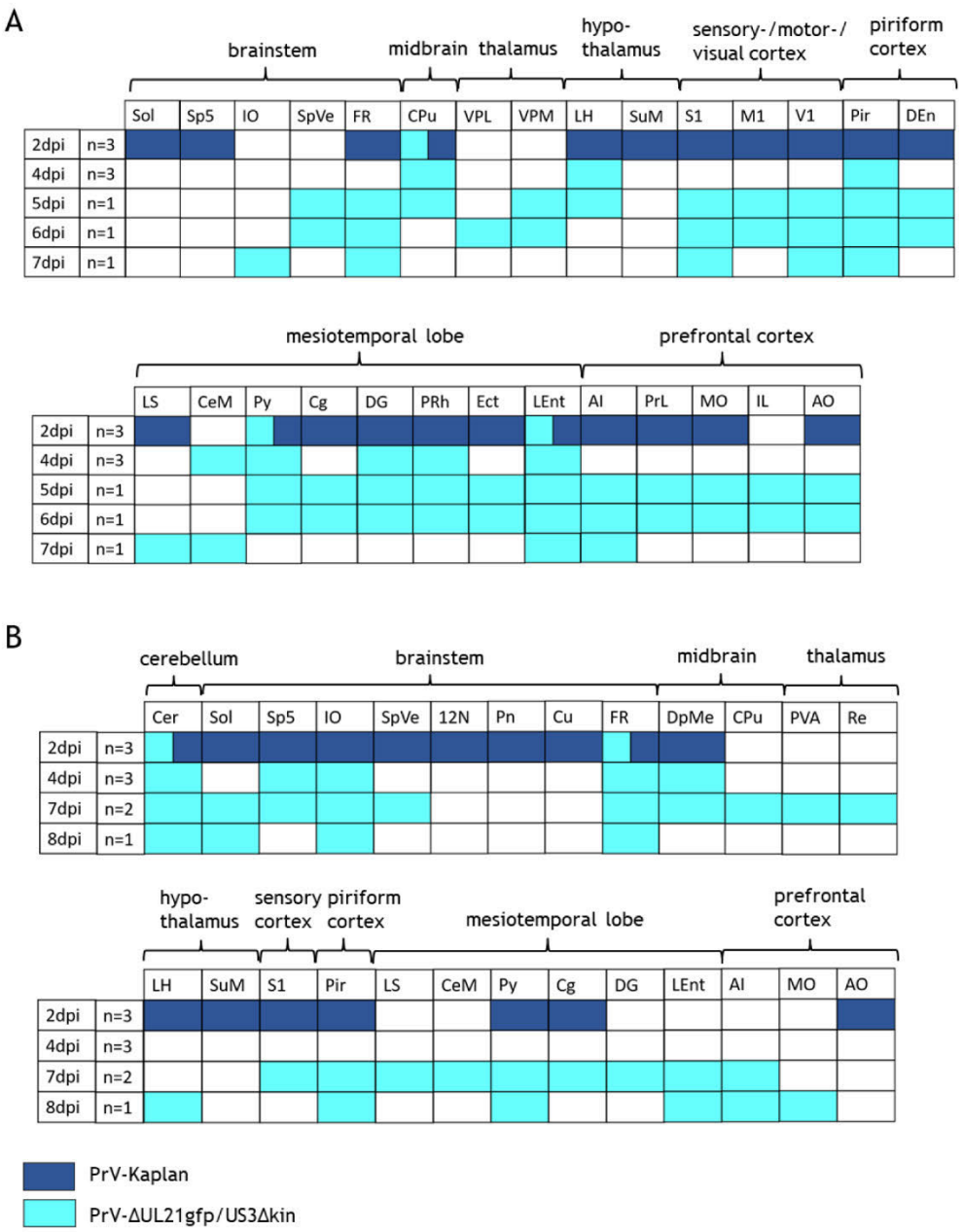

S7 Fig.: Summary presentation of viral antigen distribution in the brain. Colored boxes indicate viral antigen in the respective areas after inoculation with PrV-Kaplan (blue) and PrV-ΔUL21gfp/US3Δkin (cyan) into the temporal lobe (A) or into the cerebellum (B). Cer = cerebellum, Sol = nucleus of the solitary tract, Sp5 = spinal trigeminal nucleus, IO = inferior olive, SpVe = spinal vestibular nucleus, 12N = hypoglossal nucleus, , Pn = pontine nuclei, Cu = cuneate nucleus, FR = reticular formation, CPu = caudate putamen , DpMe = deep mesencephalic nucleus, VPM = ventral posteriomedial thalamic nucleus, VPL = ventral posteriolateral thalamic nucleus, PVA = paraventricular thalamic nucleus, Re = reuniens thalamic nucleus, LH = lateral hypothalamic area, SuM = supramammillary nucleus, S1 = primary somatosensory cortex, V1 = primary visual cortex, M1 = primary motor cortex, Pir = piriform cortex, DEn = dorsal endopiriform nucleus, LS = lateral septal nucleus, CeM = central amygdaloid nucleus, Py = pyramidal cell layer of the hippocampus, Cg = cingulate cortex, DG = dentate gyrus, PRh = perirhinal cortex, Ect = ectorhinal cortex, LEnt = lateral entorhinal cortex, AI = agranular insular cortex, PrL = prelimbic cortex, MO = medial orbital cortex, IL = infralimbic cortex, AO = anterior olfactory nucleus

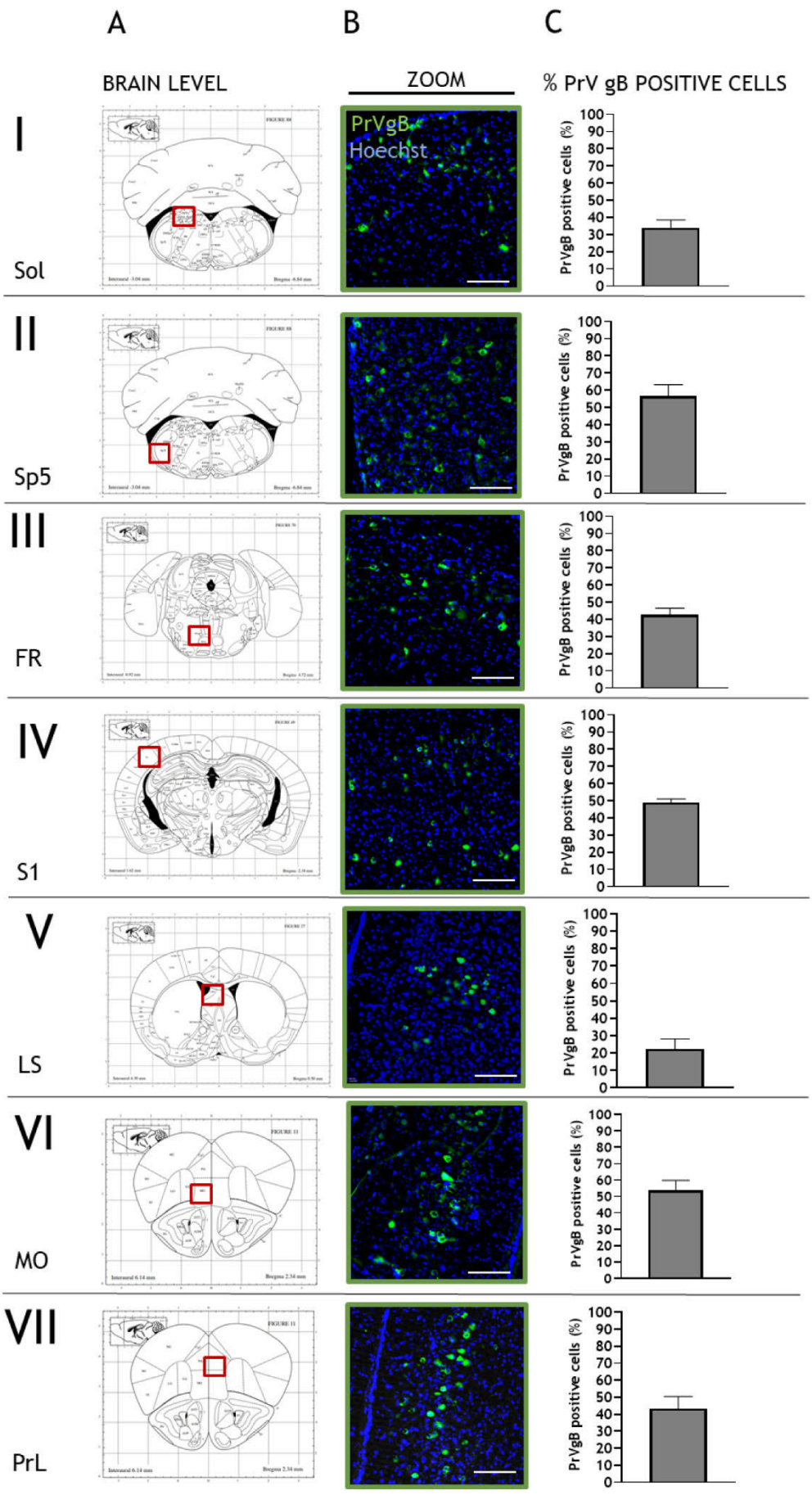
A
B
C
BRAIN LEVEL
ZOOM
% PrV gB POSITIVE CELLS
I
Sol
II
Sp5
III
FR
IV
S1
V
LS
VI
MO
VII
PrL
PrVgB
Hoechst
PrVgB positive cells (%)
0
10
20
30
40
50
60
70
80
90
100

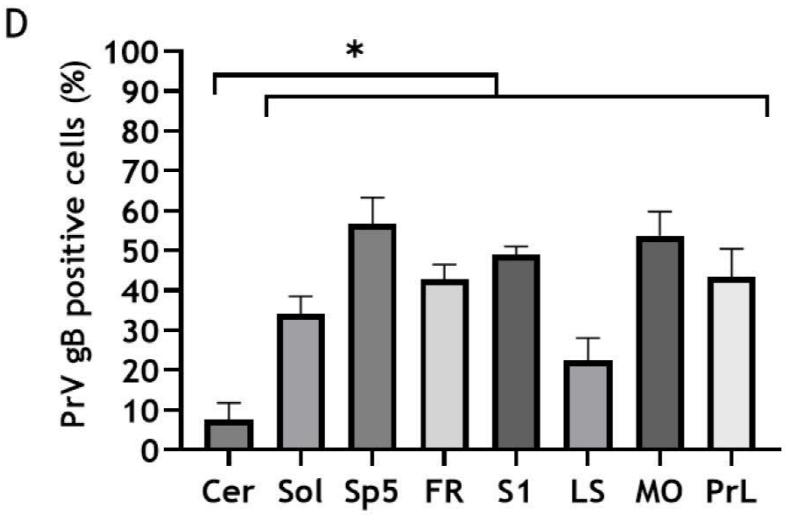

S8 Fig.: Summary of PrV gB expression and quantification. A) Different regions of interest (ROIs) (I-VII), are shown based on The Mouse Brain in Stereotaxic Coordinates by Paxinos and Franklin, 2001 B) Immunofluorescence of PrV gB expression in CD1 mouse PrV-ΔUL21gfp/US3Δkin-infected brain tissue after 7 dpi. For immunolabelling a rabbit polyclonal anti-PrV gB serum and a goat anti-rabbit Alexa Fluor 568 antibody (green) was utilized. Nuclei were visualized using Hoechst (blue). C) Quantification of PrV gB positive cells compared to the total cell count of the respective ROI. Average values and standard deviations of three independent experiments are shown. D) Statistical analysis of PrV gB positive cells of the cerebellum (Cer) in comparison to Sol, Sp5, FR, S1, LS, MO and PrL. Statistical significance is indicated by an asterisk (*), one-way ANOVA test, followed by corrected Dunnett's multiple comparison test; $p < 0,05$. Cer = cerebellum, Sol = nucleus of the solitary tract, Sp5 = spinal trigeminal nucleus, FR = reticular formation, S1 = primary somatosensory cortex, LS = lateral septal nucleus, MO = medial orbital cortex, PrL = prelimbic cortex. Scale bar 100 μm

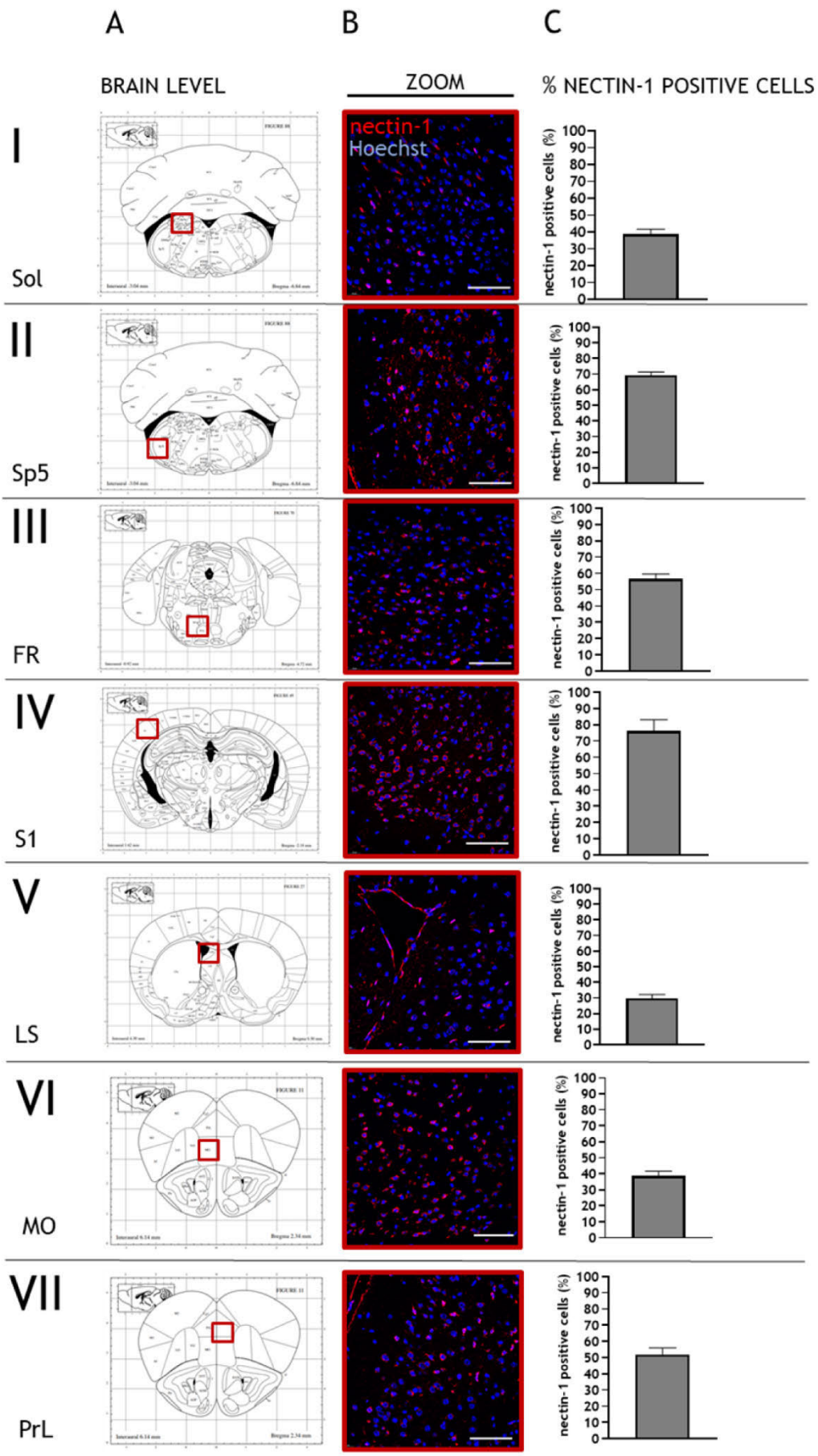
A
B
C
BRAIN LEVEL
ZOOM
% NECTIN-1 POSITIVE CELLS
I
Sol
II
Sp5
III
FR
IV
S1
V
LS
VI
MO
VII
PrL
nectin-1
Hoechst
nectin-1 positive cells (%)
0
10
20
30
40
50
60
70
80
90
100

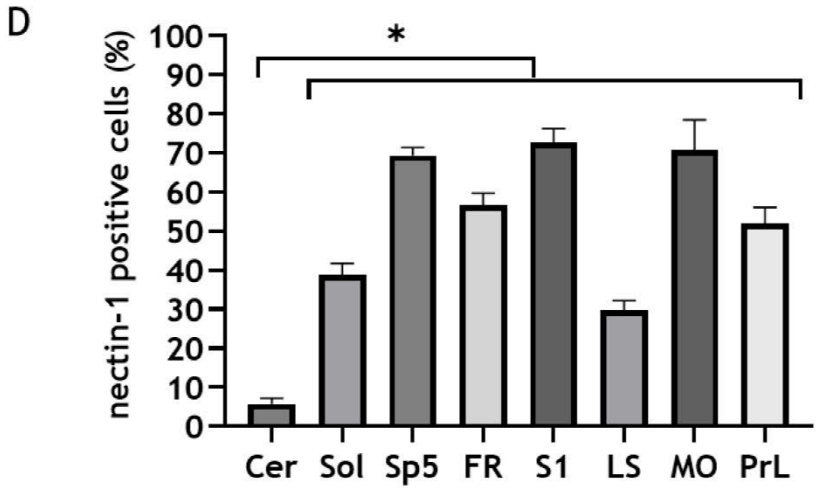

S9 Fig.: Summary of nectin-1 expression and quantification. A) Different regions of interest (ROIs) (I-VII), are shown based on The Mouse Brain in Stereotaxic Coordinates by Paxinos and Franklin, 2001 B) Immunofluorescence of nectin-1 receptor expression in CD1 mouse mock-infected brain tissue. For immunolabelling a rabbit anti-nectin-1 antibody and a goat anti-rabbit Alexa Fluor 568 antibody (red) was utilized. Nuclei were visualized using Hoechst (blue). C) Quantification of nectin-1 positive cells compared to the total cell count of the respective ROI. Average values and standard deviations of three independent experiments are shown. D) Statistical analysis of nectin-1 positive cells of the cerebellum (Cer) in comparison to Sol, Sp5, FR, S1, LS, MO and PrL. Statistical significance is indicated by an asterisk (*), one-way ANOVA test, followed by corrected Dunnett's multiple comparison test; $p < 0{,}0001$. Cer = cerebellum, Sol = nucleus of the solitary tract, Sp5 = spinal trigeminal nucleus, FR = reticular formation, S1 = primary somatosensory cortex, LS = lateral septal nucleus, MO = medial orbital cortex, PrL = prelimbic cortex. Scale bar 100 µm

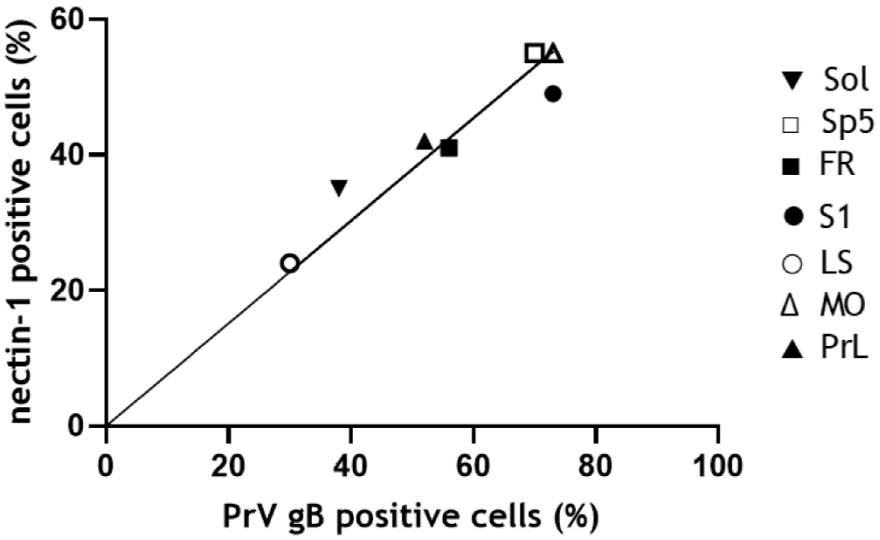

S10 Fig.: Correlation and linear regression analysis of PrV gB and nectin-1 positive cells in different brain regions. Mean values (three replicates) of PrV gB positive cells are presented on the x-axis and of nectin-1 positive cells on the y-axis. Spearman`s coefficient analysis; $p \leq 0.05$. Sol = nucleus of the solitary tract, Sp5 = spinal trigeminal nucleus, FR = reticular formation, S1 = primary somatosensory cortex, LS = lateral septal nucleus, AI = agranular insular cortex, PrL = prelimbic cortex.

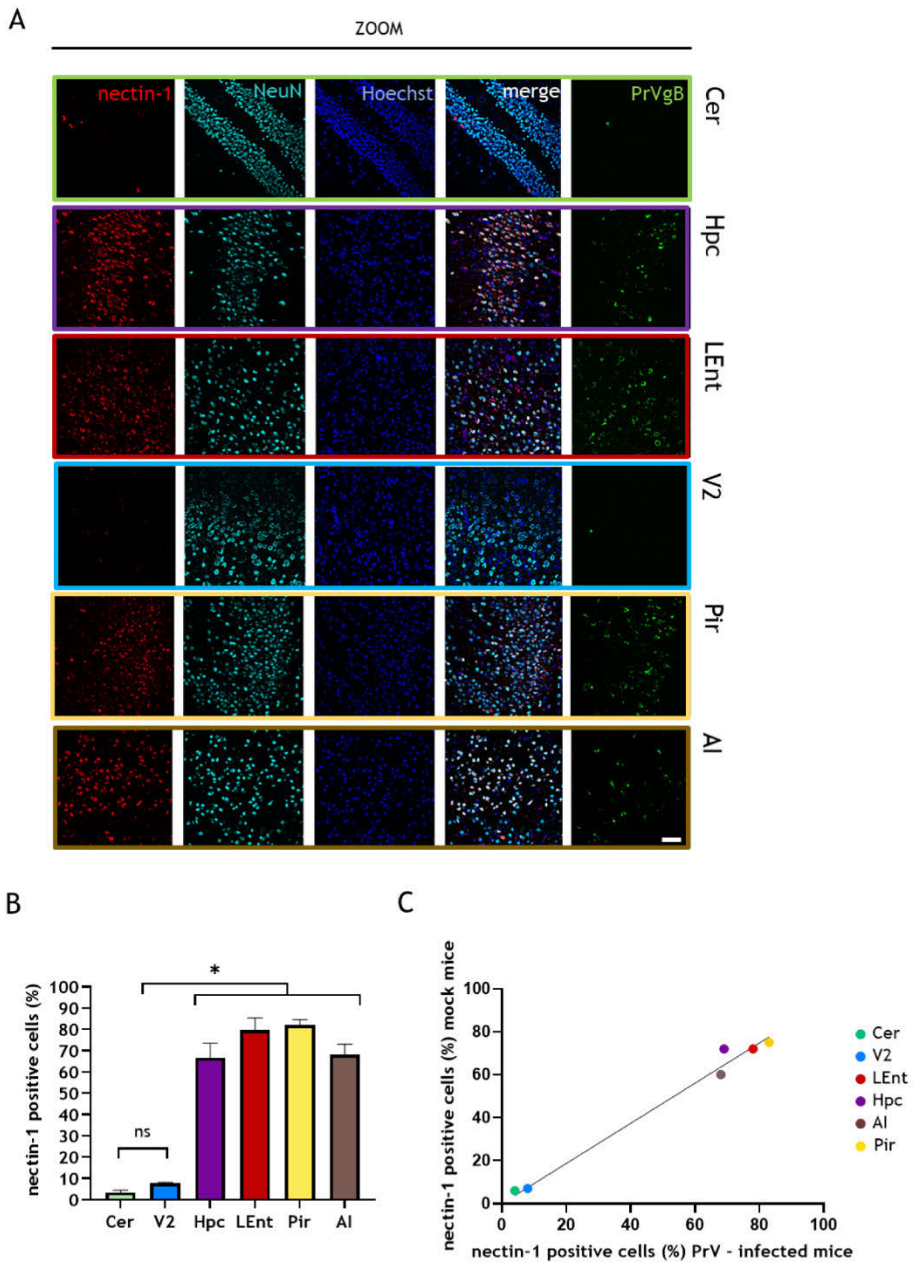

S11 Fig.: Quantitative image analysis of nectin-1 expression in PrV-infected brain tissue of CD1 mice. A) Labelling of nectin-1 positive neurons in different brain regions (green box = Cer, purple box = Hpc, red box = LEnt, blue box = V2, yellow box = Pir, brown box = AI) using a polyclonal rabbit anti-nectin-1 and a goat anti-rabbit Alexa Fluor 568 antibody (red) as well as a polyclonal guinea pig anti-NeuN and a goat anti-guinea pig Alexa Fluor 647 antibody (cyan). A polyclonal rabbit anti-PrV gB and a goat anti-rabbit Alexa Fluor 488 antibody (green) were used to visualize PrV-infected cells. Nuclei were counterstained with Hoechst (blue). Scale bar = 100µm. B) ROIs were analyzed by quantification of nectin-1 positive cells compared to the total cell count of the respective ROI. Average values and standard deviations of three independent experiments are shown. Significant differences are indicated by an asterisk (*), one-way ANOVA test, followed by corrected Dunnett's multiple comparison test; $p < 0{,}0001$. C) Correlation and linear regression analysis of nectin-1 positive cells of mock and PrV-infected mice in different brain regions. Mean values (three replicates) of nectin-1 positive cells in PrV-infected mice are presented on the x-axis and of nectin-1 positive cells of mock mice on the y-axis. Spearman`s coefficient analysis; $p \leq 0.001$. Cer = cerebellum, V2 = secondary visual cortex, Hpc = hippocampus, LEnt = lateral entorhinal cortex, Pir = piriform cortex, AI = agranular insular cortex.

Neuroscience 589 (2025) 194–194

Contents lists available at ScienceDirect

Neuroscience

journal homepage: www.elsevier.com/locate/nsc

Erratum

Erratum to "Neurotropism of alphaherpesviruses is most prominent in the mesiotemporal, piriform and prefrontal cortices in mice". [Neuroscience 584 (2025) 367–381]

Viktoria Korff [a], Issam El-Debs [a], Sonja Bröer [c], Barbara G. Klupp [b], Jens P. Teifke [a], Thomas C. Mettenleiter [b], Julia Sehl-Ewert [a,*]

[a] Department of Experimental Animal Facilities and Biorisk Management, Friedrich-Loeffler-Institut, Greifswald-Insel Riems, Germany
[b] Institute of Molecular Virology and Cell Biology, Friedrich-Loeffler-Institut, Greifswald-Insel Riems, Germany
[c] School of Veterinary Medicine, Institute of Pharmacology and Toxicology, Freie Universität Berlin, Berlin, Germany

The publisher regrets the omission of Sonja Bröer as co-author, and the subsequent omission of the following affiliation: School of Veterinary Medicine, Institute of Pharmacology and Toxicology, Freie Universität Berlin, Berlin, Germany.

The publisher would like to apologise for any inconvenience caused.

DOI of original article: https://doi.org/10.1016/j.neuroscience.2025.08.024.
* Corresponding author.
E-mail address: julia.sehl-ewert@fli.de (J. Sehl-Ewert).

https://doi.org/10.1016/j.neuroscience.2025.10.037

Available online 29 October 2025

Paper [II]

Spatial and temporal mapping of early alphaherpesvirus invasion routes into the mouse central nervous system

Authors

Viktoria Korff, Issam El-Debs, Julia Sehl-Ewert

Journal

Journal of NeuroVirology

online: 28.09.2025

doi: https://doi.org/10.1007/s13365-025-01278-3

Journal of NeuroVirology
https://doi.org/10.1007/s13365-025-01278-3

BRIEF REPORT

Spatial and temporal mapping of early alphaherpesvirus invasion routes into the mouse central nervous system

Viktoria Korff[1] · Issam El-Debs[1] · Julia Sehl-Ewert[1]

Received: 25 July 2025 / Revised: 18 August 2025 / Accepted: 21 August 2025

Abstract
Alphaherpesviruses such as Herpes Simplex Virus 1 (HSV-1) and Pseudorabies virus (PrV) invade the central nervous system (CNS) via peripheral nerves. While olfactory and trigeminal pathways are well-known, additional cranial routes remain underexplored. Using a PrV-ΔUL21gfp/US3Δkin mutant in CD1 mice, we mapped early neuroinvasion (4–96 hpi) by immunofluorescence and RNA in situ hybridization. Viral antigen and lytic viral gene expression (UL19 RNA) were detected in the olfactory epithelium, vomeronasal organ, incisors, palate, olfactory bulb, and brainstem. These results indicate multineural CNS access involving olfactory (I), trigeminal (V), glossopharyngeal (IX), and hypoglossal (XII) nerves, highlighting this model's value for studying early alphaherpesvirus spread.

Keywords Pseudorabies virus · Mouse model · Neuroinvasion · Trigeminal route · Olfactory route · Spatial mapping

Introduction

Alphaherpesviruses such as Herpes Simplex Virus 1 (HSV-1) and Pseudorabies Virus (PrV), are neurotropic, double-stranded DNA viruses. Following productive infection of the oral and nasal mucosa, viral particles enter peripheral sensory neurons (Spear et al 2000; Mettenleiter 2003) and travel retrogradely to the trigeminal ganglion (TG) and other peripheral sensory and autonomic ganglia, where they establish life-long latency (Smith 2012; Koyuncu et al 2018; Hill et al 2001, 1975; Duarte et al 2019). From there, they may reactivate followed by anterograde movement towards the periphery or continue to spread retrogradely, occasionally reaching the central nervous system (CNS) where they can establish life-threatening inflammation of the brain (Sivasubramanian et al 2022; Yao et al 2014).

Despite extensive research, the precise pathways of alphaherpesviral neuroinvasion remain incompletely defined. Two main invasion pathways to the CNS have been implicated: the trigeminal and olfactory nerve (Held and Derfuss 2011; Shivkumar et al 2013).

The trigeminal nerve provides direct monosynaptic input to brainstem nuclei such as the principal sensory (Pr5) and spinal trigeminal (Sp5) nuclei, which in turn project to higher brain regions (Ezure et al 2001; Arbuthnot et al 1990). Alternatively, the olfactory nerve, composed of axons from olfactory sensory neurons in the olfactory epithelium (OE), terminates in the olfactory bulb (OB), which connects to mesiotemporal areas including the piriform and entorhinal cortices (Menendez and Carr 2017; Esiri 1982; Twomey et al 1979; Niemeyer et al 2024; Sosulski et al 2011; Barrios et al 2014).

Beyond these classical routes, recent studies suggest that additional cranial nerves—including the glossopharyngeal (IX), vagus (X), and hypoglossal (XII) nerves—may contribute to CNS entry. HSV-1 has been detected in nervus vagus-associated brainstem nuclei (Niemeyer et al 2024). Furthermore, varicella-zoster virus, another alphaherpesvirus, has been shown to infect the vagus nerve (Chen et al 2011; Gershon et al 2015) supporting a model of multineural entry.

Once in the CNS, alphaherpesviruses can cause severe neurological disease (Stahl and Mailles 2019). HSV-1 is the primary cause of sporadic herpes simplex encephalitis (HSE) in humans (Bradshaw and Venkatesan 2016) with a tropism for mesiotemporal structures. PrV, a closely related

✉ Julia Sehl-Ewert
julia.sehl-ewert@fli.de

[1] Department of Experimental Animal Facilities and Biorisk Management, Friedrich-Loeffler-Institut, Südufer 10, 17493 Greifswald-Insel Riems, Germany

Published online: 28 September 2025

virus, induces fatal encephalitis in non-suid species, including mice, which are highly susceptible (Mettenleiter 2000; Babic et al 1994).

A specific PrV mutant, PrV-ΔUL21/US3Δkin—lacking the tegument protein pUL21 and encoding a kinase-deficient pUS3—exhibits pronounced neurotropism in CD1 mice, with early involvement of brainstem nuclei followed by the establishment of productive infection in mesiotemporal regions. Despite the characteristic pattern resembling HSE, the animals typically survive the infection although clinical signs may occur (Sehl et al 2020). This model provides a robust system for investigating alphaherpesviral neuroinvasion.

In this study, we used spatial–temporal mapping techniques to investigate early CNS entry routes of the gfp-tagged PrV mutant PrV-ΔUL21gfp/US3Δkin in mice following intranasal inoculation. By combining immunofluorescence and RNA in situ hybridization at defined time points, we identified viral spread through olfactory, trigeminal, and additional cranial nerve pathways, providing new insights into the mechanisms of alphaherpesviral CNS invasion.

Material and methods

Virus

PrV strain PrV-ΔUL21gfp/US3Δkin was kindly provided by B. G. Klupp, Friedrich-Loeffler-Institut Greifswald-Insel Riems. As previously described (Sehl et al 2020, Korff et al 2025), PrV-ΔUL21gfp/US3Δkin was derived from the PrV wildtype strain Kaplan (Kaplan and Vatter 1959). The virus was propagated in rabbit kidney (RK13) cells and cultured at 37 °C in minimum essential medium (MEM) with 10% fetal calf serum (FCS) (Invitrogen).

Animal experiments

We used six to eight-week-old female CD1 mice (Charles River Laboratory), as this strain serves as the standard infection model in our laboratory (Sehl et al 2020). The animals were housed in groups of four in conventional cages (type II L) under Biosafety Level 2 (BSL 2) conditions at the animal facility of the Friedrich-Loeffler-Institut, Greifswald-Insel Riems. Environmental conditions were kept constant, with a 12-h light–dark cycle (daylight intensity: 60%) and a temperature range of 20–24 °C. Mice had ad libitum access to a standardized diet (ssniff Ratte/Maus-Haltung) and fresh drinking water. To promote animal welfare, bedding (ssniff Spezialdiäten Abedd Espen CLASSIC), nesting material (PLEXX sizzle nest), and environmental enrichment (PLEXX Aspen Bricks medium, mouse smart home, mouse tunnel) were provided.

After a one-week acclimatization period, mice were deeply anesthetized by intraperitoneal injection of 200 µl of a ketamine-xylazine mixture (ketamine: 60 mg/kg; xylazine: 3 mg/kg) diluted in 0.9% sodium chloride. Following the onset of anesthesia, each nostril was inoculated with 5 µl of PrV-ΔUL21/US3Δkin suspension in cell culture medium, resulting in a total inoculation dose of 1×10^4 PFU/ml.

A total of nine groups of mice (n=4 per group) were included in the study, with scheduled euthanasia at defined time points post-infection: 4, 8, 16, 24, 36, 48, 60, 72, and 96 h post-infection (hpi). Animals were continuously monitored (24/7) throughout the experimental period. Clinical evaluation was based on a predefined scoring system (Sehl et al 2020) encompassing three categories: (I) external appearance, (II) behavior and activity, and (III) body weight. Each category was scored from 0 to 3. The humane endpoint for euthanasia was defined as either a score of 3 in one category or a score of 2 across all three categories.

Animals were euthanized under deep isoflurane anesthesia, preceded by Carprofen (Rimadyl, Pfizer, 10 mg/kg, subcutaneous) analgesia. Under deep anesthesia, the right atrium was incised, and a 26-gauge needle was inserted into the left ventricle to facilitate perfusion with phosphate-buffered saline (PBS), followed by fixation with 4% paraformaldehyde (PFA), as described by (Gage et al 2012). After perfusion, euthanasia was completed by decapitation, with the head removed at the level of the first cervical vertebra. Heads were fixed in 4% PFA for at least one week and then decalcified for seven days in Osteosoft ® (Merck).

Detection of viral antigen – immunolabeling

Three fixed and decalcified heads per time point were trimmed into six sections and cut into 50 µm thick coronal slices using a cryostat (CryoStar™ NX70, Epredia). Tissue sections were collected at defined anatomical landmarks following established protocols (Rao et al 2011; OECD 2010) including the posterior part of upper incisors (L1), incisive papilla (L2), second palatine crest/olfactory bulb (L3), midbrain (L4), cerebellum/pons (L5) and medulla (L6) (Fig. 1b). Tissue slices were transferred onto SuperFrost-Plus slides (Carl Roth GmbH, Germany) in a frozen state, air-dried at room-temperature (RT) for 5–10 min, and stored in PBS at 4 °C until further processing.

Prior to immunolabeling, slices were circumscribed using a grease pencil (Vector Laboratories, H-4000) to ensure precise application of reagents. In a humified chamber, tissue samples were permeabilized for 10 min using 0.25% Triton X-100 and 0.2% gelatin in PBS (permeabilization buffer). Blocking was performed with 5% bovine serum albumin

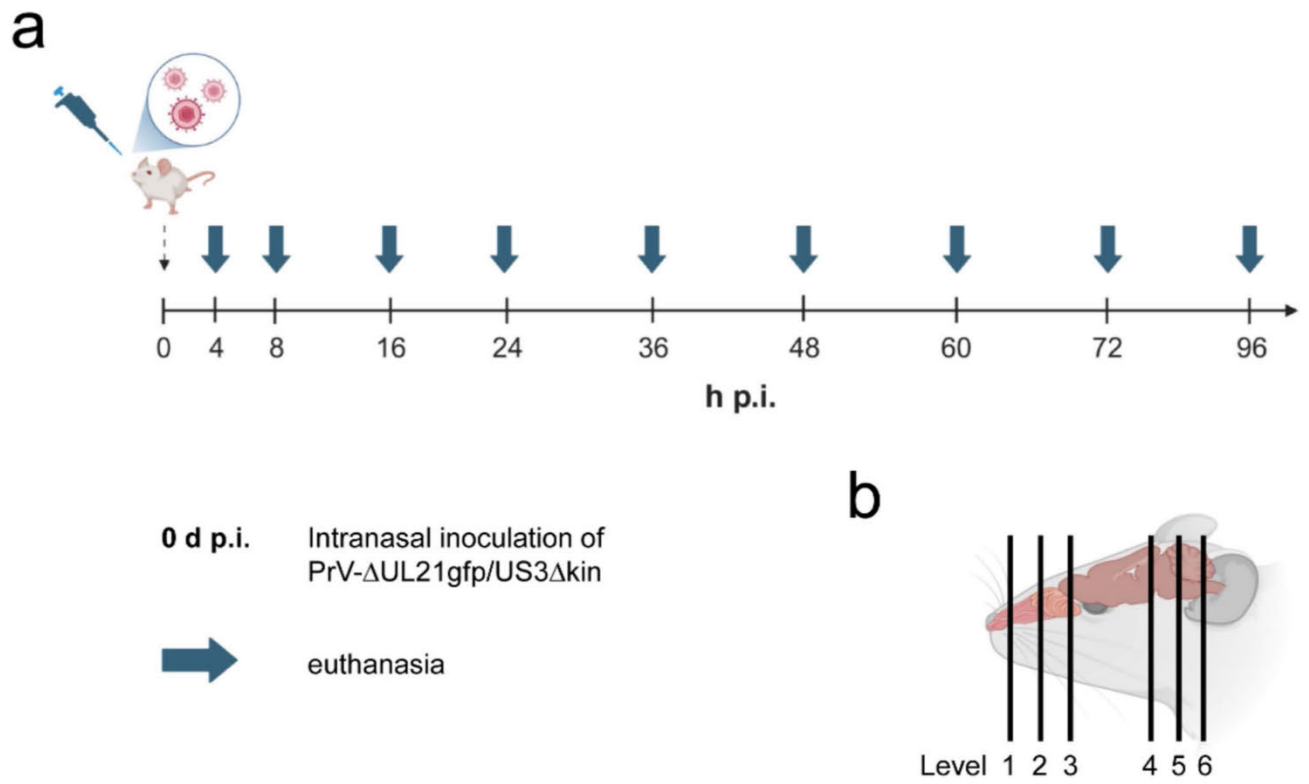

Fig. 1 (**a**) Sequential timeline of necropsies and tissue collection. Six- to eight-week-old CD1 mice were intranasally inoculated with PrV-ΔUL21gfp/US3Δkin (0 dpi) and sacrificed at the indicated time points. (**b**) Schematic illustration of analyzed head regions. Serial 50 µm coronal sections were collected at six defined rostrocaudal levels: L1 (posterior upper incisors), L2 (incisive papilla), L3 (second palatine crest/olfactory bulb), L4 (midbrain), L5 (cerebellum/pons), and L6 (medulla), for detailed analysis. Created in BioRender. Korff, V. (2025) https://BioRender.com/y01iyic

(BSA, Merck, A7979) in permeabilization buffer for 1 h at RT.

For primary antibody staining, samples were incubated for 1 h at RT with rabbit polyclonal anti-PrV glycoprotein B (gB) antibody (1:2000, (Kopp et al 2003)) and chicken polyclonal anti-neurofilament protein antibody (NEFM, 1:2000, ThermoFisher, PA1-16758), both diluted in 0.1% BSA in permeabilization buffer. After washing (twice for 2 min in PBS, followed by 10 min in permeabilization buffer), secondary antibodies were applied: goat anti-rabbit Alexa Fluor 488 (1:1000, Invitrogen, AB150077) and goat anti-chicken Alexa Fluor 568 (1:1000, Invitrogen, A11041). Incubation was performed for 1 h at RT under light-protected conditions.

Following secondary antibody incubation, samples were washed twice for 2 min in PBS and counterstained with Hoechst 33258 (1:20,000, Sigma-Aldrich, 94403) for 5 min at RT, protected from light. After two final washes in PBS (2 min each), samples were incubated for 10 min at RT in a light-protected 10 mM copper (II) sulfate ($CuSO_4$)/50 mM ammonium chloride (NH_4Cl) solution (wash buffer 2) to reduce background fluorescence. Finally, slices were rinsed in deionized water for 2 min, mounted with one drop of mounting medium (ibidi), and air-dried for 24 h.

Fluorescently labeled sections were analyzed with a THUNDER Imaging system (THUNDER Imager Tissue; Leica, Germany). Images were processed with arivis Vision4D (ZEISS).

In-Situ hybridization/RNA Scope™

One head per time point (24, 60, 72hpi) was trimmed into 6 sections as described in the section immunofluorescence (Fig. 1b), embedded in paraffin wax and cut at 3 µm thick slices using a rotating microtome (Hyrax M55, Zeiss). Sections were mounted on Super-Frost-Plus-Slides (Carl Roth GmbH, Germany) and dried for 2 h at 40 °C, and were stored at RT until staining.

To detect PrV mRNA, RNAscope™ in situ hybridization (Wang et al 2012) was performed on the formalin-fixed, paraffin-embedded (FFPE) head sections following the protocol for the RNAscope™ 2.5 HD Reagent Kit-RED (ACD Inc., Cat. No. 322350). A C1 probe was designed to target lytic viral gene expression with PrV UL19 mRNA (probe:

V-SHSV-UL19, specific to the 66973–68498 bp region of UL19; ACD Inc., Cat. No. 548251). Signal detection was based a chromogenic alkaline phosphatase (AP) reaction, producing red-colored punctate signals for each RNA transcript. As internal control, the murine housekeeping gene Mm-Ppib (ACD Inc., Cat. No. 313911, C1), encoding peptidyl-prolyl cis–trans isomerase B, was used. The negative control consisted of the Escherichia coli DapB transcript (RNAscope™ Negative Control Probe; ACD Inc., Cat. No. 310043) (S1 Fig.).

Before hybridization, slides were baked at 60 °C for 1 h deparaffinized in xylene (2 × 5 min) and rehydrated in 100% ethanol (2 × 1 min) at RT. After air-drying, sections were treated with hydrogen peroxide (H_2O_2; ACD Inc., Cat. No. 322330) for 10 min at RT. Target retrieval was carried out in boiling antigen retrieval buffer (ACD Inc., Cat. No. 322000) using a pressure cooker (Sichler, Germany, NX-3213–675) for 15 min, followed by washing in distilled water and dehydration in 100% ethanol. After air-drying, sections were circumscribed with a grease pencil (Vector Laboratories, H-4000) to confine reagent application to the tissue area. Slides were then treated with Protease Plus (ACD. Inc, Cat. No.322330) for 15 min at 40 °C in the ACD HybEZ™ II Hybridization System (ACD Inc., Cat. No. 321711) (HybEZ oven). Slides were rinsed in distilled water and incubated with the specific probe and controls for 2 h at 40 °C in the HybEZ oven, followed by two washes (2 min each) in the wash buffer provided (ACD Inc., Cat. No. 310091). Preamplification was performed by applying Amp 1 for 30 min at 40 °C. Amplification was continued with Amp 2 (15 min) and Amp 3 (30 min), both at 40 °C. These steps enable signal enhancement by sequential binding of amplification complexes. Chromogenic signal development for probe C1 was performed by incubating slides with Amp 4 enzyme solution for 15 min at 40 °C in the HybEZ oven, followed by chromogenic substrate Amp 5 for 30 min at RT, and the AP blocker Amp 6 for 15 min at RT. For visualization of the red signal, slides were treated with a 1:60 mixture of Red-B to Red-A for 10 min at RT. After signal detection, slides were then washed twice (2 min each) in wash buffer. All amplification and signal development reagents were included in the RNAscope™ 2.5 HD Reagent Kit-RED (ACD. Inc, Cat. No. 322350). Slides were counterstained with Mayer`s Hematoxylin staining solution for 30 s at RT and rinsed 5 min in tap water for bluing. After drying on a 60 °C heat plate (MEDITE, BD00575) for 15–30 min and cooling for 5 min, slides were immersed in fresh xylene for 5 min and mounted using EcoMount (Biocare Medical, BRR897L).

All slides were analyzed using a Zeiss Axio Scope. A1 microscope equipped with 5x, 10x, 20x, and 40 × N-ACHROPLAN objectives (Carl Zeiss Microscopy GmbH, Jena, Germany) and scanned with the NanoZoomer (Hamamatsu, S60) scanner.

Fig. 2 Viral antigen distribution in the murine head following intranasal inoculation with PrV-ΔUL21gfp/US3Δkin at different time points. (**a**) Viral antigen was detected in the olfactory epithelium (OE), vomeronasal organ (VMO), palate (Pal), incisor region (In) and brainstem (BS) at early time points (0–16 hpi), followed by signal in the olfactory bulb (OB) and reticular formation (FR) (24–60 hpi), and later in the lateral entorhinal cortex (LEnt) (72–96 hpi). The spatiotemporal distribution of viral antigen was visualized by immunofluorescence and is schematically indicated by arrows. Created in BioRender. Korff, V. (2025) https://BioRender.com/jtrk9ey (**b**) Schematic overview of viral antigen localization in brain regions of infected mice ($n = 3$) at different time points. Colored boxes (red) indicate the presence of viral antigen in the corresponding anatomical regions in at least 2 mice. Sol = nucleus of the solitary tract, Sp5 = spinal trigeminal nucleus, IO = inferior olive, 12 N = hypoglossal nucleus, Amb = nucleus ambiguus

Results

The primary objective of this study was to define cranial nerve-mediated entry of the PrV-ΔUL21gfp/US3Δkin mutant into the CNS using a standardized mouse intranasal infection model.

To achieve fine-scale spatial–temporal mapping of viral neuroinvasion, intranasally PrV-ΔUL21gfp/US3Δkin inoculated animals were sacrificed at defined time points post-infection (4, 8, 16, 24, 36, 48, 60, 72, and 96 hpi) and processed for subsequent histological and molecular analyses (Fig. 1a).

Clinical evaluation

No clinical signs were observed in any of the mice throughout the experimental period.

Mapping viral entry routes into the CNS

Spatial and temporal distribution of viral antigen

To define spatial dynamics of PrV-ΔUL21gfp/US3Δkin entry into the CNS, immunofluorescence analysis was conducted on six standardized coronal sections of the murine head, corresponding to defined anatomical landmarks: the posterior part of upper incisors (L1), incisive papilla (L2), second palatine crest/olfactory bulb (L3), midbrain (L4), cerebellum/pons (L5) and medulla (L6). These sections were analyzed at defined time points post-inoculation (p.i.) (Fig. 1b). An overview of early viral antigen distribution is provided in Fig. 2a with detailed regional data in Fig. 2b. Representative immunofluorescence images of viral antigen dissemination in nasal and brain regions are presented in Figs. 3 and 4, respectively.

a

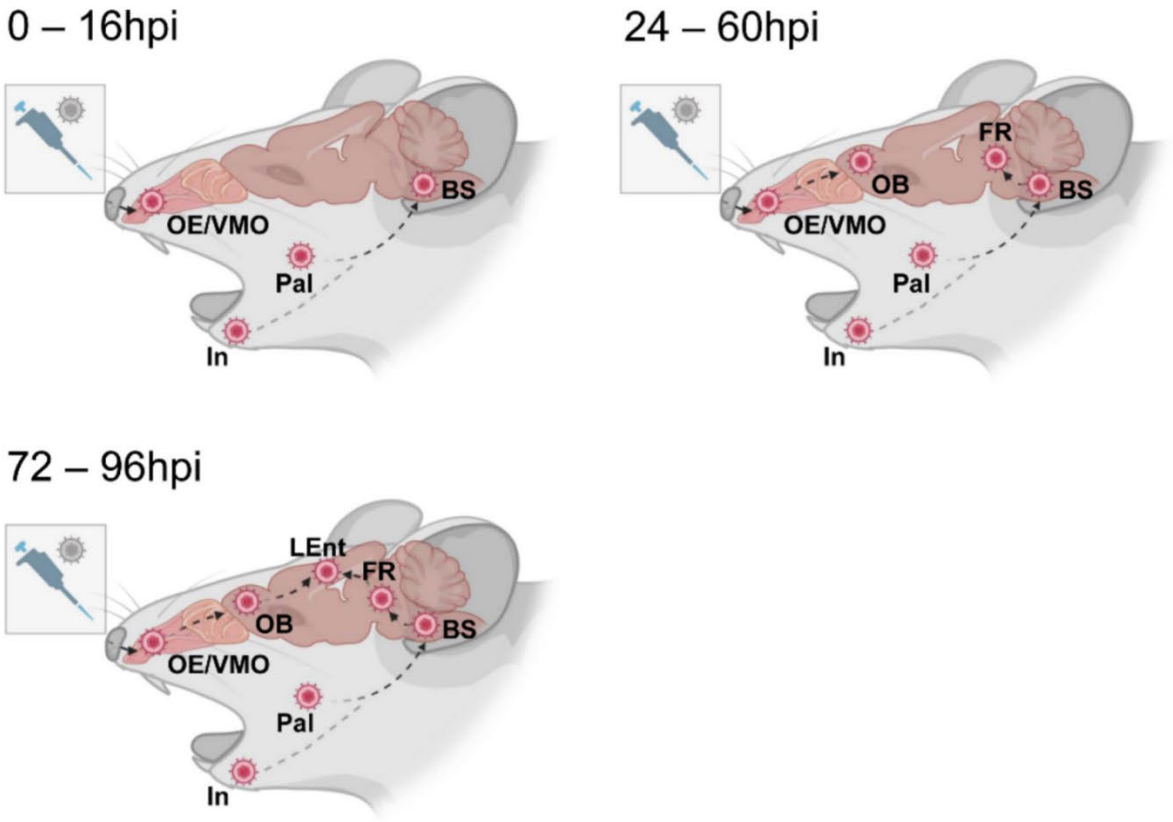

b

	OE	VMO	OB	LEnt	FR	BS: Sol	BS: Sp5	BS: IO	BS: 12N	BS: Amb	Pal	In
4hpi	■	■						■	■		■	■
8hpi	■	■					■	■	■		■	■
16hpi	■	■				■	■	■	■	■		■
24hpi	■	■	■			■	■	■	■	■		■
36hpi	■	■	■			■	■					■
48hpi	■	■	■		■	■	■					■
60hpi	■	■	■		■		■					■
72hpi	■	■	■	■	■		■					■
96hpi	■		■	■								

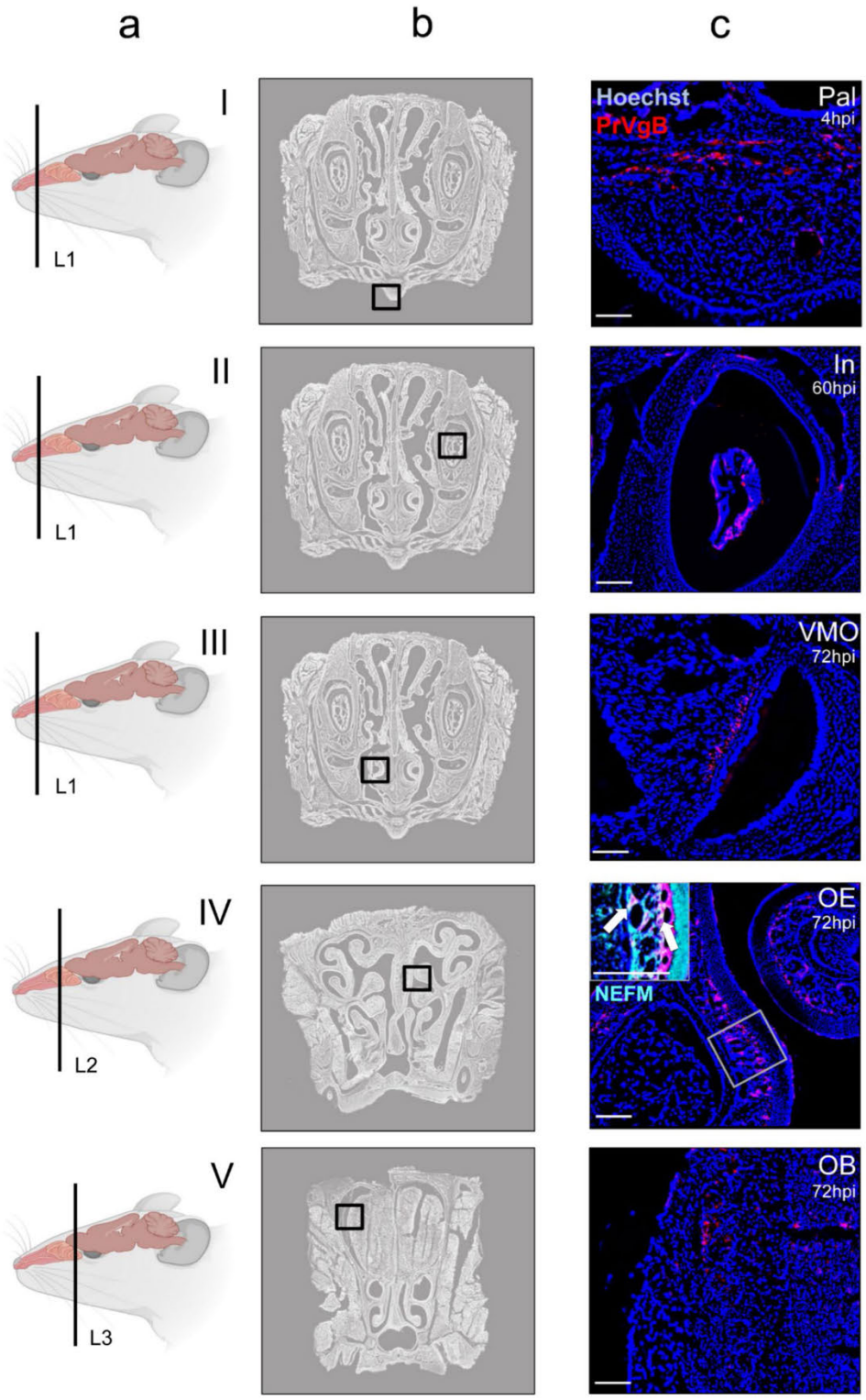

Fig. 3 Immunofluorescence analysis of viral antigen distribution in the CD1 mouse head following intranasal inoculation with PrV-ΔUL21gfp/US3Δkin. (**a**) Schematic illustration of coronal sections through the murine head (L1-3). Created in BioRender. Korff, V. (2025) https://BioRender.com/fjixhs4 (**b**) Overview of the anatomical regions analyzed in the coronal sections. (**c**) Representative immunofluorescence images showing PrV glycoprotein B (gB) expression in cranial sections from mice infected with PrV-ΔUL21gfp/US3Δkin. Immunolabeling was performed using a rabbit polyclonal anti-PrV gB serum and a goat anti-rabbit Alexa Fluor 488-conjugated secondary antibody (visualized in red). Neurofilament protein was labeled using a chicken polyclonal anti-NEFM antibody and a goat anti-chicken Alexa Fluor 568-conjugated secondary antibody (cyan). Double-labeling of NEFM and PrVgB is indicated by arrows. Cell nuclei were counterstained with Hoechst (blue). In = incisor, Pal = palate, VMO = vomeronasal organ, OE = olfactory epithelium, OB = olfactory bulb. Scale bar 100 µm

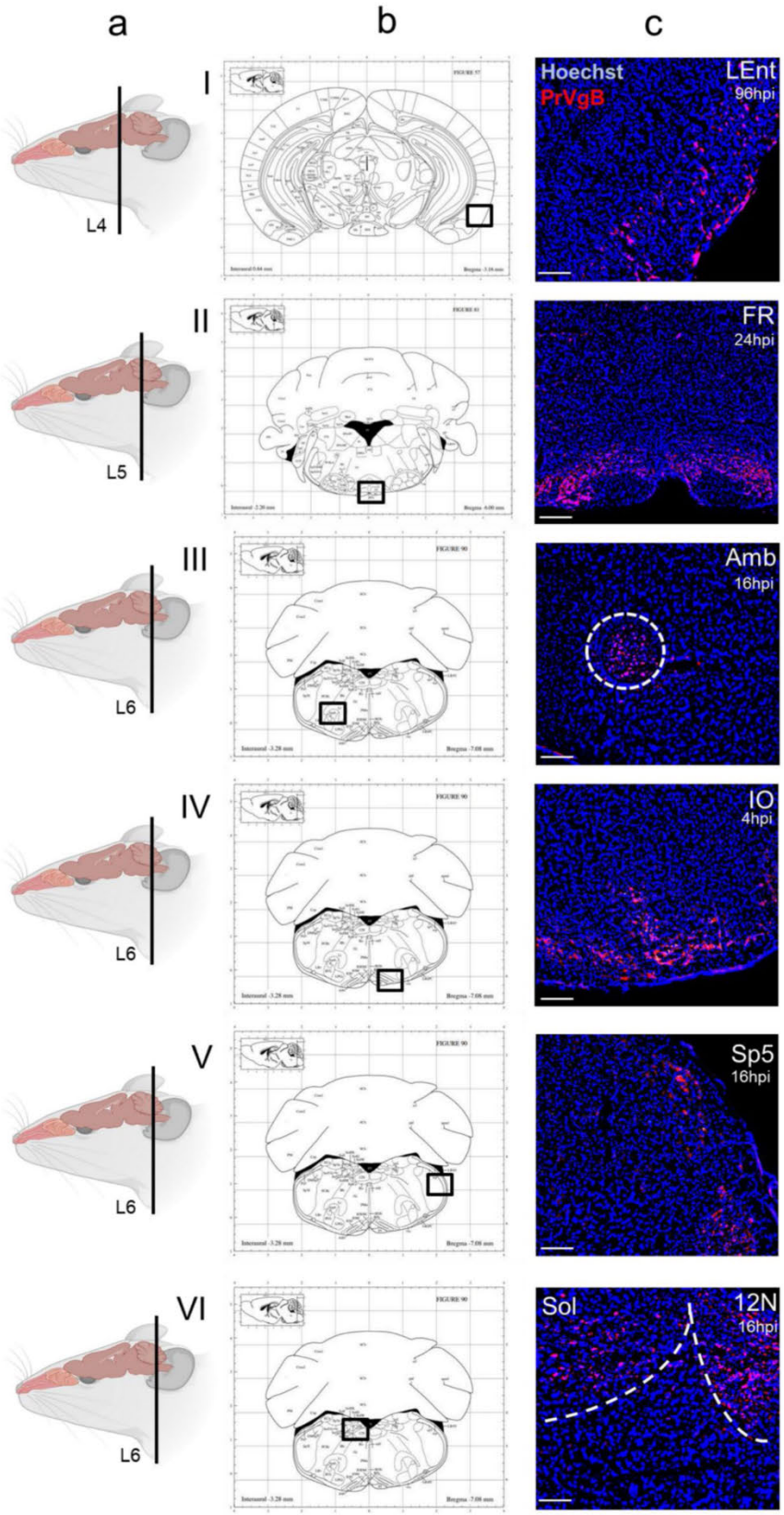

Fig. 4 Immunofluorescence analysis of viral antigen distribution in the murine brain following intranasal inoculation with PrV-ΔUL21gfp/US3Δkin. (**a**) Schematic illustration of coronal sections through the murine head (L4-6). Created in BioRender. Korff, V. (2025) https://BioRender.com/fjixhs4 (**b**) Schematic representation of the stained brain regions, shown in accordance with The Mouse Brain in Stereotaxic Coordinates (Paxinos and Franklin, 2001). (**c**) Representative immunofluorescence images showing PrV glycoprotein B (gB) expression in coronal brain sections from PrV-ΔUL21gfp/US3Δkin-infected CD1 mice. Immunolabeling was performed using a rabbit polyclonal anti-PrV gB serum and a goat anti-rabbit Alexa Fluor 488-conjugated secondary antibody (red). Nuclei were counterstained with Hoechst (blue). Sol = nucleus of the solitary tract, Sp5 = spinal trigeminal nucleus, IO = inferior olive, 12 N = hypoglossal nucleus, Amb = nucleus ambiguus, FR = reticular formation, LEnt = lateral entorhinal cortex. Scale bar: 100 µm

As early as 4–16 hpi, viral antigen was detected in the palate (Pal), incisors (In), vomeronasal organ (VMO), OE, and different brainstem (BS) regions. The virus progressively spread to the OB and reticular formation (FR), and by 72 hpi reached the temporal lobe, particularly the lateral entorhinal cortex (LEnt), where signal persisted until the termination of the experiment (96 hpi) (Fig. 2).

Region-specific analysis revealed transient signals in the Pal (Fig. 3I, ≤8 hpi), while antigen remained detectable in the In (Fig. 3II) and VMO (Fig. 3III) until 72 hpi. In the OE (Fig. 3IV), persistent viral labeling was observed from 4 to 96 hpi and was confirmed by co-localization with the neurofilament marker NEFM trough double immunolabeling. OB involvement (Fig. 3V) started at 24 hpi and was detectable until 96 hpi. In the BS, early infection of the inferior olive (IO) and hypoglossal nucleus (12N) was noted from 4 to 24 hpi (Fig. 4IV, VI), followed by Sp5 (8–72 hpi; Fig. 4V), nucleus ambiguus (Amb; 16–24 hpi; Fig. 4III), and nucleus of the solitary tract (Sol; 16–48 hpi; Fig. 4VI). FR involvement (Fig. 4II) was evident from 48 to 72 hpi, while viral antigen appeared in the LEnt of the temporal lobe (Fig. 4I) from 72 hpi onward.

Spatial detection of viral mRNA

To corroborate the distribution of viral antigen, in situ hybridization was performed using RNA Scope™ (Wang et al 2012) targeting the UL19 gene in one representative animal per time point (Fig. 5a). While in situ hybridization largely confirmed antigen distribution, notable temporal and spatial differences were observed: RNA signals in the VMO were transient and restricted to 24 hpi, while OB labeling appeared only from 60 hpi onward. Amb was no longer positive beyond 24 hpi, whereas the palate remained transcriptionally active up to 60 hpi despite declining antigen levels (Fig. 5b). Exemplary images of the OE (I) and OB (II) at 72hpi are shown in Fig. 5c.

Discussion

In the present study, we investigated the alphaherpesvirus neuroinvasive entry and characterized early viral spread using a murine intranasal inoculation model. By combining fine-scaled temporal and spatial analyses of viral antigen and mRNA expression, we defined the initial stages of CNS invasion.

Our data confirmed the established roles of the trigeminal and olfactory pathways for viral entry. Moreover, we detected viral antigen in brainstem nuclei linked to the glossopharyngeal and hypoglossal nerves. These findings indicate that these cranial nerves provide additional routes for CNS access.

Fig. 5 In situ hybridization-based detection of PrV UL19 RNA in the CD1 mouse head following intranasal inoculation with PrV-ΔUL21gfp/US3Δkin. (a) Schematic representation of the UL19-specific probe design (V-SHSV-UL19). V-SHSV-UL19 targets the 66973–68498 bp region of UL19 which is represented by the blue dots and connecting lines. (b) Schematic overview of viral mRNA detection in brain regions of infected mice (n = 1) at different time points. Colored boxes (red) indicate the presence of viral mRNA in the corresponding anatomical regions. (c) In situ hybridization of PrV UL19 RNA in murine coronal nose and brain Sects. 72hpi. Evidence of lytic viral replication is shown by RNA Scope™ detection of UL19 transcripts (red) in infected tissues. (I) RNA Scope™ signal for UL19 RNA in the olfactory epithelium. (II) RNA Scope™ signal for UL19 RNA in the olfactory bulb. Scale bar = 50 µm. Created in BioRender. Korff, V. (2025) https://BioRender.com/dzegatr

Throughout the study, mice remained clinically asymptomatic and survived the entire observation period, consistent with previous work using this model, where first mild clinical signs typically develop after 6 days post-infection (Sehl et al 2020).

Within the first 16 h post-infection, viral antigen was detected in the Pal, In, VMO, OE and brainstem nuclei: Sp5, Sol, Amb, IO and 12N. Later spread included the OB, FR, and by 72 hpi, the LEnt of the temporal lobe, a known target in herpesviral encephalitis (Esiri 1982; Taylor et al 2005; Yong et al 2021; Armien et al 2010, Korff et al 2025).

The present findings are consistent with recent reports of brainstem involvement following intranasal alphaherpesvirus infection; notably, however, those studies have been limited to analyses at later post-infection time points, in contrast to the current investigation, which encompasses earlier phases of infection (Sehl et al 2020; Niemeyer et al 2024; Klopfleisch et al 2006, 2004). Of note, infection of the OE following PrV infection has been so far solely detected in pigs (Verpoest et al 2017). However, we could show antigen signaling as early as 4 hpi in the murine OE alongside with a recent study showing HSV-1 signals 7 hpi (Niemeyer et al 2024).

Antigen detection findings were largely corroborated by RNA in situ hybridization; however, temporal and spatial discrepancies were noted. These likely reflect methodological differences: while immunohistochemistry detects accumulated viral proteins, in situ hybridization captures transcriptional activity. Notably, RNA analysis was performed on a single animal per time point and limited to one 3 µm section per anatomical level, in contrast to 50 µm sections used for antigen detection. This design—chosen to qualitatively confirm viral gene expression—offers only a limited snapshot rather than a comprehensive overview. Accordingly, the RNA-based data should be regarded as confirmatory and interpreted with caution in terms of spatial and temporal resolution.

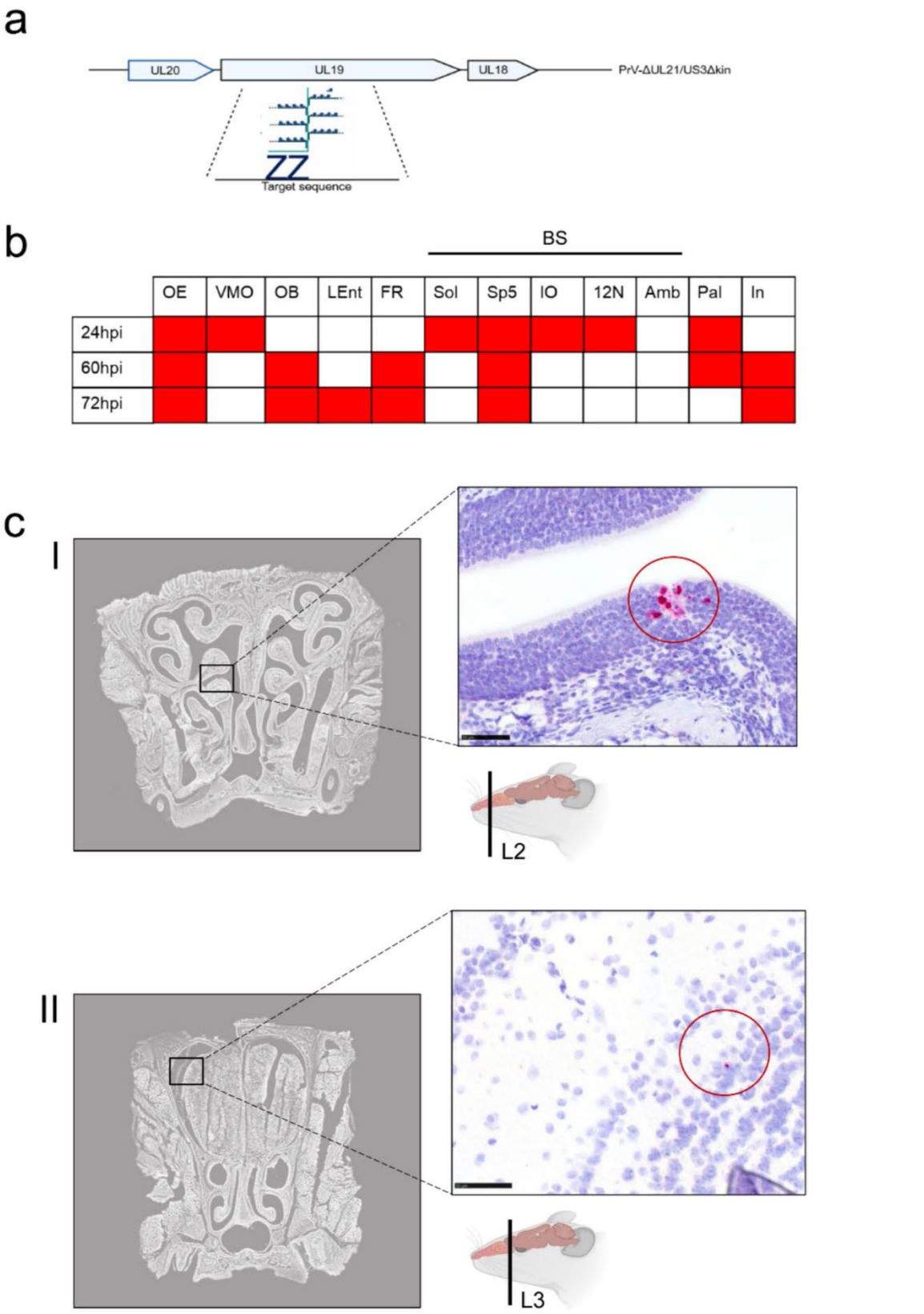
a
UL20
UL19
UL18
PrV-ΔUL21/US3Δkin
Target sequence
b
BS
OE
VMO
OB
LEnt
FR
Sol
Sp5
IO
12N
Amb
Pal
In
24hpi
60hpi
72hpi
c
I
L2
II
L3

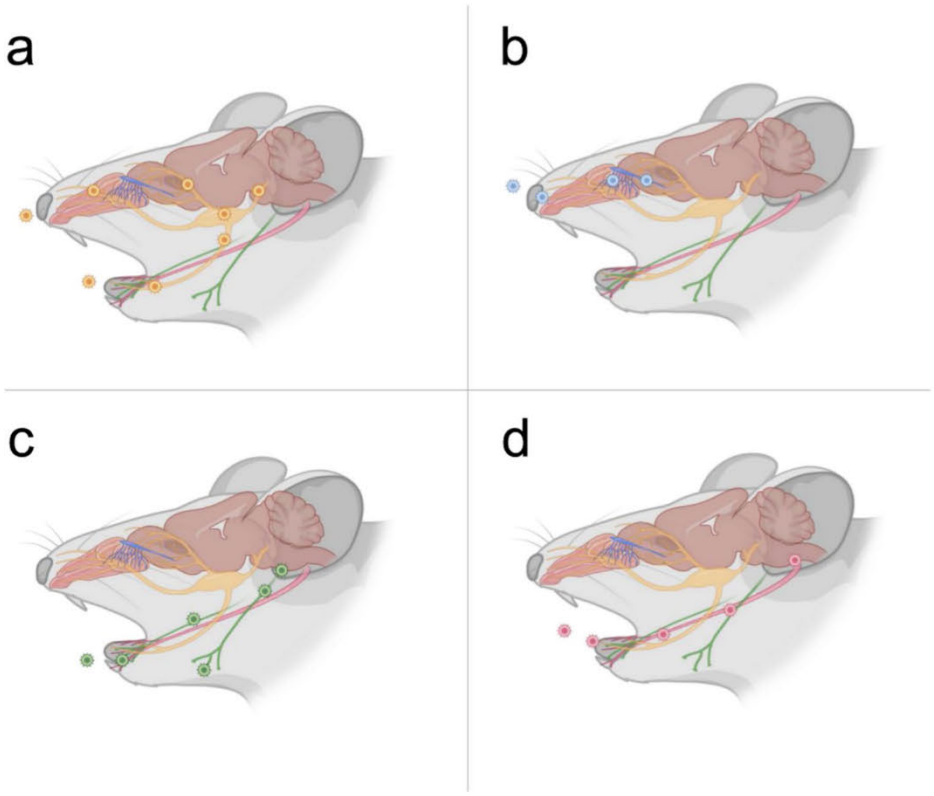

Fig. 6 Schematic presentation of experimentally supported infection routes of alphaherpesviruses via cranial nerves (CN). (a) Trigeminal nerve (CN V) route (yellow). (b) Olfactory nerve (CN I) route (blue). (c) Glossopharyngeal nerve (CN IX) route (green). (d) Hypoglossal nerve (CN XII) route (red). Created in BioRender. Korff, V. (2025) https://BioRender.com/vggf7zl

Our findings suggest that PrV exploits multiple neuroinvasive routes to enter the CNS. The trigeminal pathway emerges as a predominant route (Held and Derfuss 2011; Sehl and Teifke 2020; Wang et al 2020), supported by viral antigen detection in Sp5 (Fig. 6a) (García-Guillén et al 2021; Landisman and Connors 2007) and functionally connected regions (Amb, IO, FR) (Isokawa-Akesson and Komisaruk 1987; van Ham and Yeo 1992; Panneton and Gan 2014). In addition, viral signals were observed in peripheral sites innervated by the maxillary, mandibular and ophthalmic branches of the trigeminal nerve, including the palate (Shankland 2001), nasal mucosa (Grunditz et al 1994; Yun et al 2024; Prendergast 2013) and incisivi (Fried and Gibbs 2014; Naftel et al 1999).

The olfactory pathway (Niemeyer et al 2024; Mori 2015; Steiner and Benninger 2013) is likewise confirmed by the presence of viral antigen in the OE, OB, and LEnt (Fig. 6b), which are anatomically and functionally interconnected, and provide access to limbic brain structures (Gretenkord et al 2019; Stenwall et al 2025). Detection of viral antigen in the VMO, as similarly reported by Mori et al 2005 for HSV-1, reinforces its role in CNS entry.

Evidence for glossopharyngeal nerve involvement (Fig. 6c) includes viral antigen in the Pal (Mu et al 2021) and brainstem nuclei Sol and Amb, which serve as the primary afferent target (Mizuno and Nomura 1986) and motor fiber origin (Standring 2016), respectively. Close anatomical and functional connectivity between these nuclei (Forstenpointner et al 2022; Stuesse and Fish 1984) strengthen the plausibility of glossopharyngeal-mediated CNS entry.

The hypoglossal nerve is implicated by detection of antigen in its origin site (Yamaguchi 2021), the hypoglossal nucleus (12N) (Fig. 6d), consistent with infection patterns observed in related alphaherpesviruses such as HSV-1 (Niemeyer et al 2024).

Considering that Sol receives dense vagal input (Chen and Liu 2025), and Amb contains vagal motor neurons (Isabella and Moens 2024), and that these nuclei are functionally linked to the glossopharyngeal nerve and integrated within the FR (Ruggiero et al 2000; Nasse et al 2008), it is reasonable to propose that the vagus nerve indirectly contributes to CNS invasion.

The dense anatomical and functional interconnections among brainstem nuclei innervated by different cranial nerves likely facilitate cross-communication and redistribution of viral particles between neuroinvasive pathways. For example, Sol is connected to both the trigeminal Sp5 (Okada et al 2019; Guan et al 1998) and 12 N (Guo et al 2020; Borke et al 1983). Further synaptic connections exist likewise between 12 N and Sp5 (Sousa Costa et al 2023; Streppel et al 2000) as well as between 12 N and FR (Holstege and Kuypers 1982; Streppel et al 2000; Borke et al

1983). Detection of viral antigen in the FR and associated nuclei involved in respiratory control and swallowing (Milsom et al 2004; Jean 2001) raises the possibility of an ingestion-related route of neuroinvasion. Although mice were intranasally inoculated, incidental ingestion of viral particles during application cannot be excluded. This may explain viral entry via glossopharyngeal and hypoglossal pathways, indicating that ingestion-associated mechanisms could complement direct neural invasion routes.

Summary

This study identifies multiple early alphaherpesvirus neuroinvasion routes in a murine intranasal infection model (Fig. 6). The trigeminal and olfactory pathways are confirmed as primary entry points, alongside infection of the nasal mucosa. Furthermore, we demonstrate the involvement of the glossopharyngeal and hypoglossal nerves, showing that these cranial nerves also serve as important routes for CNS invasion. Given the extensive interconnectivity of brainstem nuclei associated with these nerves, including vagal inputs, the vagus nerve likely contributes as well. Viral spread into brainstem regions involved in respiratory and swallowing functions suggests a possible ingestion-associated entry route. These findings reveal a complex network of cranial nerve pathways facilitating early alphaherpesvirus neuroinvasion.

Supplementary Information The online version contains supplementary material available at https://doi.org/10.1007/s13365-025-01278-3 .

Acknowledgements The authors thank Silvia Schuparis and Robin Brandt for their excellent technical assistance. We further express our gratitude to Angele Breithaupt, Tobias Britzke and Lukas M. Michaely for their valuable scientific input, and to Thomas C. Mettenleiter for his critical review of the manuscript.

Author contributions The study was conceptualized and designed by J.SE. Material preparation, data collection, and analysis were performed by V.K., I.ED., and J.SE. The first draft of the manuscript was written by V.K. and J.SE. All authors critically revised previous versions of the manuscript and approved the final version for submission.

Funding Open Access funding enabled and organized by Projekt DEAL. The project was funded by the Deutsche Forschungsgemeinschaft (DFG), grant number 466759708.

Data availability No datasets were generated or analysed during the current study.

Declarations

Ethics statement Animal experiments were approved by the State Office for Agriculture, Food Safety and Fishery in Mecklenburg-Western Pomerania (LALFF M-V) with reference number 7221.3–1-034/22.

Competing interest The authors declare no competing interests.

References

Arbuthnot W, MacLeod NK, Maxwell DJ, Wright AK (1990) istribution and synaptic contacts of the cortical terminals arising from neurons in the rat ventromedial thalamic nucleus. Neuroscience 38:47–60

Armien AG, Hu S, Little MR, Robinson N, Lokensgard JR, Low WC, Cheeran MC-J (2010) Chronic cortical and subcortical pathology with associated neurological deficits ensuing experimental herpes encephalitis. Brain Pathol 20:738–750

Babic N, Mettenleiter TC, Ugolini G, Flamand A, Coulon P (1994) Propagation of pseudorabies virus in the nervous system of the mouse after intranasal inoculation. Virology 204:616–625

Barrios AW, Núñez G, Sánchez Quinteiro P, Salazar I (2014) Anatomy, histochemistry, and immunohistochemistry of the olfactory subsystems in mice. Front Neuroanat 8:63

Borke RC, Nau ME, Ringler RL Jr (1983) Brain stem afferents of hypoglossal neurons in the rat. Brain Res 269:47–55

Bradshaw MJ, Venkatesan A (2016) Herpes simplex virus-1 encephalitis in adults: pathophysiology, diagnosis, and management. Neurotherapeutics 13:493–508

Chen Z, Liu K (2025) Mechanism and applications of vagus nerve stimulation. Curr Issues Mol Biol 47(2):122

Chen JJ, Gershon AA, Li Z, Cowles RA, Gershon MD (2011) Varicella zoster virus (VZV) infects and establishes latency in enteric neurons. J Neurovirol 17:578–589

de Sousa Costa R, Ventura N, de Andrade Lourenção Freddi T, Da Cruz LCH, Corrêa DG (2023) The hypoglossal nerve. Semin Ultrasound CT MR 44:104–114

Duarte LF, Farías MA, Álvarez DM, Bueno SM, Riedel CA, González PA (2019) Herpes simplex virus type 1 infection of the central nervous system: insights into proposed interrelationships with neurodegenerative disorders. Front Cell Neurosci 13:46

Esiri M (1982) Herpes simplex encephalitis an immunohistological study of the distribution of viral antigen within the brain. J Neurol Sci 54:209–226

Ezure H, Goto N, Nonaka N, Goto J, Tani H (2001) Morphometric analysis of the human trigeminal nerve. Okajimas Folia Anat Jpn 78:49–53

Forstenpointner J, Maallo AMS, Elman I, Holmes S, Freeman R, Baron R, Borsook D (2022) The solitary nucleus connectivity to key autonomic regions in humans. Eur J Neurosci 56:3938–3966

Fried K, Gibbs JL (2014) Dental pulp innervation. In: Goldberg M (ed) The dental pulp: biology, pathology, and regenerative therapies. Springer Berlin Heidelberg, Berlin, Heidelberg, pp 75–95

Gage GJ, Kipke DR, Shain W (2012) Whole animal perfusion fixation for rodents. J Vis Exp 30(65):3564

García-Guillén IM, Martínez-de-la-Torre M, Puelles L, Aroca P, Marín F (2021) Molecular segmentation of the spinal trigeminal nucleus in the adult mouse brain. Front Neuroanat 15:785840

Gershon AA, Chen J, Gershon MD (2015) Use of saliva to identify Varicella zoster virus infection of the gut. Clin Infect Dis 61:536–544

Gretenkord S, Kostka JK, Hartung H, Watznauer K, Fleck D, Minier-Toribio A, Spehr M, Hanganu-Opatz IL (2019) Coordinated electrical activity in the olfactory bulb gates the oscillatory entrainment of entorhinal networks in neonatal mice. PLoS Biol 17:e2006994

Grunditz T, Uddman R, Sundler F (1994) Origin and peptide content of nerve fibers in the nasal mucosa of rats. Anat Embryol 189:327–337

Guan Z-L, Ding Y-Q, Li J-L, Lü B-Z (1998) Substance P receptor-expressing neurons in the medullary and spinal dorsal horns projecting to the nucleus of the solitary tract in the rat. Neurosci Res 30:213–218

Guo H, Yuan X-S, Zhou J-C, Chen H, Li S-Q, Qu W-M, Huang Z-L (2020) Whole-brain monosynaptic inputs to hypoglossal motor neurons in mice. Neurosci Bull 36:585–597

Held K, Derfuss T (2011) Control of HSV-1 latency in human trigeminal ganglia–current overview. J Neurovirol 17:518–527

Hill TJ, Field HJ, Blyth WA (1975) Acute and recurrent infection with Herpes simplex virus in the mouse: a model for studying latency and recurrent disease. J Gen ViroL 28:341–353

Hill JM, Lukiw WJ, Gebhardt BM, Higaki S, Loutsch JM, Myles ME, Thompson HW, Kwon BS, Bazan NG, Kaufman HE (2001) Gene expression analyzed by microarrays in HSV-1 latent mouse trigeminal ganglion following heat stress. Virus Genes 23:273–280

Holstege G, Kuypers HG (1982) The anatomy of brain stem pathways to the spinal cord in cat. A labeled amino acid tracing study. In: Kuypers H, Martin GF (eds) Progress in brain research, Elsevier, pp 145–175

Isabella AJ, Moens CB (2024) Development and regeneration of the vagus nerve. Semin Cell Dev Biol 156:219–227

Isokawa-Akesson M, Komisaruk BR (1987) Difference in projections to the lateral and medial facial nucleus: anatomically separate pathways for rhythmical vibrissa movement in rats. Exp Brain Res 65:385–398

Jean A (2001) Brain stem control of swallowing: neuronal network and cellular mechanisms. Physiol Rev 81:929–969

Kaplan AS, Vatter AE (1959) A comparison of herpes simplex and pseudorabies viruses. Virology 7:394–407

Klopfleisch R, Teifke JP, Fuchs W, Kopp M, Klupp BG, Mettenleiter TC (2004) Influence of tegument proteins of pseudorabies virus on neuroinvasion and transneuronal spread in the nervous system of adult mice after intranasal inoculation. J Virol 78:2956–2966

Klopfleisch R, Klupp BG, Fuchs W, Kopp M, Teifke JP, Mettenleiter TC (2006) Influence of pseudorabies virus proteins on neuroinvasion and neurovirulence in mice. J Virol 80:5571–5576

Kopp M, Granzow H, Fuchs W, Klupp BG, Mundt E, Karger A, Mettenleiter TC (2003) The pseudorabies virus UL11 protein is a virion component involved in secondary envelopment in the cytoplasm. J Virol 77:5339–5351

Korff V, El-Debs I, Klupp BG, Teifke JP, Mettenleiter TC, Sehl-Ewert J (2025) Neurotropism of alphaherpesviruses is most prominent in the mesiotemporal, piriform and prefrontal cortices in mice. Neurosci 584:367–381

Koyuncu OO, MacGibeny MA, Enquist LW (2018) Latent versus productive infection: the alpha herpesvirus switch. Future Virol 13:431–443

Landisman CE, Connors BW (2007) VPM and PoM nuclei of the rat somatosensory thalamus: intrinsic neuronal properties and corticothalamic feedback. Cereb Cortex 17:2853–2865

Menendez CM, Carr DJJ (2017) Herpes simplex virus-1 infects the olfactory bulb shortly following ocular infection and exhibits a long-term inflammatory profile in the form of effector and HSV-1-specific T cells. J Neuroinflammation 14:124

Mettenleiter TC (2000) Aujeszky's disease (pseudorabies) virus: the virus and molecular pathogenesis - state of the art, June 1999. Vet Res 31:99–115

Mettenleiter TC (2003) Pathogenesis of neurotropic herpesviruses: role of viral glycoproteins in neuroinvasion and transneuronal spread. Virus Res 92:197–206

Milsom WK, Chatburn J, Zimmer MB (2004) Pontine influences on respiratory control in ectothermic and heterothermic vertebrates. Respir Physiol Neurobiol 143:263–280

Mizuno N, Nomura S (1986) Primary afferent fibers in the glossopharyngeal nerve terminate in the dorsal division of the principal sensory trigeminal nucleus: an HRP study in the cat. Neurosci Lett 66:338–340

Mori I (2015) Transolfactory neuroinvasion by viruses threatens the human brain. Acta Virol 59:338–349

Mori I, Goshima F, Ito H, Koide N, Yoshida T, Yokochi T, Kimura Y, Nishiyama Y (2005) The vomeronasal chemosensory system as a route of neuroinvasion by herpes simplex virus. Virology 334:51–58

Mu L, Chen J, Li J, Fowkes M, Benson B, Nyirenda T, Sobotka S, Christopherson M, Sanders I (2021) Innervation of human soft palate muscles. Anat Rec (Hoboken) 304:1054–1070

Naftel JP, Richards LP, Pan M, Bernanke JM (1999) Course and composition of the nerves that supply the mandibular teeth of the rat. Anat Rec 256:433–447

Nasse J, Terman D, Venugopal S, Hermann G, Rogers R, Travers JB (2008) Local circuit input to the medullary reticular formation from the rostral nucleus of the solitary tract. Am J Physiol Regul Integr Comp Physiol 295:R1391–R1408

Niemeyer CS, Merle L, Bubak AN, Baxter BD, Gentile Polese A, Colon-Reyes K, Vang S, Hassell JE, Bruce KD, Nagel MA et al (2024) Olfactory and trigeminal routes of HSV-1 CNS infection with regional microglial heterogeneity. J Virol 98(11):e00968-24

OECD (2010) OECD guidance document 125: histopathology for subacute and subchronic inhalation toxicity studies

Okada S, Katagiri A, Saito H, Lee J, Ohara K, Iinuma T, Iwata K (2019) Functional involvement of nucleus tractus solitarii neurons projecting to the parabrachial nucleus in trigeminal neuropathic pain. J Oral Sci 61:370–378

Panneton WM, Gan Q (2014) Direct reticular projections of trigeminal sensory fibers immunoreactive to CGRP: potential monosynaptic somatoautonomic projections. Front Neurosci 8:136

Paxinos G, Franklin KBJ (2001) The Mouse Brain in Stereotaxic Coordinates. San Diego: Academic Press

Prendergast PM (2013) Neurologic anatomy of the nose. In: Shiffman MA, Di Giuseppe A (eds) Advanced aesthetic rhinoplasty: art, science, and new clinical techniques. Springer Berlin Heidelberg, Berlin, Heidelberg, pp 17–23

Rao DB, Little PB, Malarkey DE, Herbert RA, Sills RC (2011) Histopathological evaluation of the nervous system in national toxicology program rodent studies: a modified approach. Toxicol Pathol 39:463–470

Ruggiero DA, Underwood MD, Mann JJ, Anwar M, Arango V (2000) The human nucleus of the solitary tract: visceral pathways revealed with an "'in vitro"' postmortem tracing method. J Auton Nerv Syst 79:181–190

Sehl J, Teifke JP (2020) Comparative pathology of pseudorabies in different naturally and experimentally infected species-a review. Pathogens 9(8):633

Sehl J, Hölper JE, Klupp BG, Baumbach C, Teifke JP, Mettenleiter TC (2020) An improved animal model for herpesvirus encephalitis in humans. PLoS Pathog 16:e1008445

Shankland WE (2001) The trigeminal nerve. Part III: the maxillary division. Cranio 19:78–83

Shivkumar M, Milho R, May JS, Nicoll MP, Efstathiou S, Stevenson PG (2013) Herpes simplex virus 1 targets the murine olfactory neuroepithelium for host entry. J Virol 87:10477–10488

Sivasubramanian MK, Monteiro R, Harrison KS, Plakkot B, Subramanian M, Jones C (2022) Herpes simplex virus type 1 preferentially enhances neuro-inflammation and senescence in brainstem of female mice. J Virol 96:e0108122

Smith G (2012) Herpesvirus transport to the nervous system and back again. Annu Rev Microbiol 66:153–176

Sosulski DL, Bloom ML, Cutforth T, Axel R, Datta SR (2011) Distinct representations of olfactory information in different cortical centres. Nature 472:213–216

Spear PG, Eisenberg RJ, Cohen GH (2000) Three classes of cell surface receptors for alphaherpesvirus entry. Virology 275:1–8

Stahl JP, Mailles A (2019) Herpes simplex virus encephalitis update. Curr Opin Infect Dis 32:239–243

Standring S (2016) Gray's anatomy: the anatomical basis of clinical practice. 41st Edition.: cranial nerves: functional components and nuclei. Elsevier, pp 806–807

Steiner I, Benninger F (2013) Update on herpes virus infections of the nervous system. Curr Neurol Neurosci Rep 13:414

Stenwall A, Uggla A-L, Weibust D, Fahlström M, Ryttlefors M, Latini F (2025) The bulb, the brain and the being: new insights into olfactory system anatomy, organization and connectivity. Brain Sci 15(4):368

Streppel M, Popratiloff A, Gruart A, Angelov DN, Guntinas-Lichius O, Delgado-Garcia JM, Neiss WF, Stennert E (2000) Morphologische Verbindungen zwischen N.hypoglossus und N.facialis im Hirnstamm der Ratte. HNO 48:911–916

Stuesse SL, Fish SE (1984) Projections to the cardioinhibitory region of the nucleus ambiguus of rat. J Comp Neurol 229:271–278

Taylor SW, Smith RM, Pari G, Wobeser W, Rossiter JP, Jackson AC (2005) Herpes simplex encephalitis. Can J Neurol Sci 32:246–247

Twomey JA, Barker CM, Robinson G, Howell DA (1979) Olfactory mucosa in herpes simplex encephalitis. J Neurol Neurosurg Psychiatry 42:983–987

van Ham JJ, Yeo CH (1992) Somatosensory trigeminal projections to the inferior olive, cerebellum and other precerebellar nuclei in rabbits. Eur J Neurosci 4:302–317

Verpoest S, Cay B, Favoreel H, de Regge N (2017) Age-dependent differences in pseudorabies virus neuropathogenesis and associated cytokine expression. J Virol 91(2):10–128

Wang F, Flanagan J, Su N, Wang L-C, Bui S, Nielson A, Wu X, Vo H-T, Ma X-J, Luo Y (2012) RNAscope: a novel in situ RNA analysis platform for formalin-fixed, paraffin-embedded tissues. J Mol Diagn 14:22–29

Wang Y, Wu H, Wang B, Qi H, Jin Z, Qiu H-J, Sun Y (2020) A nanoluc luciferase reporter pseudorabies virus for live imaging and quantification of viral infection. Front Vet Sci 7:566446

Yamaguchi K (2021) Development of the human hypoglossal nucleus from mid-gestation to the perinatal period: a morphological study. Neurosci Lett 762:136154

Yao H-W, Ling P, Tung Y-Y, Hsu S-M, Chen S-H (2014) In vivo reactivation of latent herpes simplex virus 1 in mice can occur in the brain before occurring in the trigeminal ganglion. J Virol 88:11264–11270

Yong SJ, Yong MH, Teoh SL, Soga T, Parhar I, Chew J, Lim WL (2021) The hippocampal vulnerability to herpes simplex virus type I infection: relevance to Alzheimer's disease and memory impairment. Front Cell Neurosci 15:695738

Yun H, Gerges PH, Moghbeli K, Das J, Singh H, Davis BM, St. Leger A (2024) Dissecting mouse trigeminal ganglia: a comprehensive analysis through anatomical, immunohistochemical, and transcriptomic approaches. Invest Ophthalmol Vis Sci 65:3880

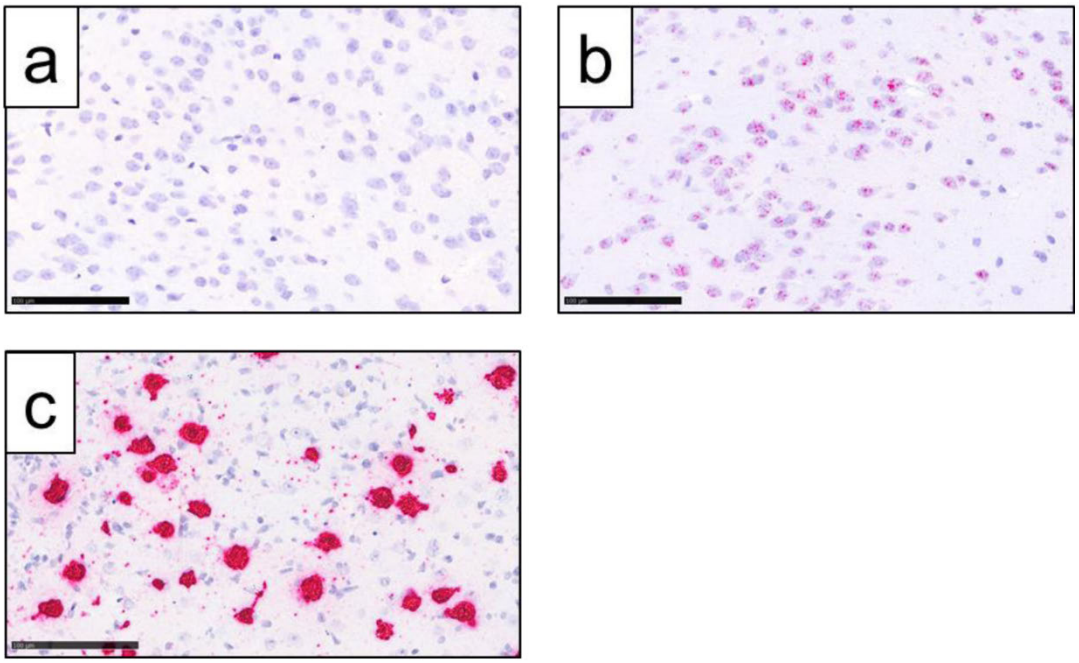

S1 Fig.: Representative images of RNA Scope™ control probe detection in the murine brain. (a) The Escherichia coli DapB probe served as a negative control probe and showed no specific signal. (b) The positive control probe Mm-Ppib (C1, red), demonstrated robust expression in neuronal tissue. (c) A brain section from a PrV-infected mouse at 14 days post-infection (dpi) was used as a positive control for UL19 probe detection during the acute phase of infection. Scale bar = 100 µm.

Paper [III]

Spatiotemporal dynamics of alphaherpesviral latency and reactivation in the murine central nervous system

Authors

Viktoria Korff, Issam El-Debs, Barbara G. Klupp, Thomas C. Mettenleiter, Julia Sehl-Ewert

Preprint: bioRxiv

online :16.09.2025

doi: https://doi.org/10.1101/2025.09.11.675502

Spatiotemporal dynamics of alphaherpesviral latency and reactivation in the murine central nervous system

Herpesvirus latency in the murine central nervous system

Viktoria Korff[1], Issam El-Debs[1], Barbara G. Klupp[2], Jens P. Teifke[1], Thomas C. Mettenleiter[2], Julia Sehl-Ewert[1*]

[1] Department of Experimental Animal Facilities and Biorisk Management, Friedrich-Loeffler-Institut, Greifswald-Insel Riems, Germany

[2] Institute of Molecular Virology and Cell Biology, Friedrich-Loeffler-Institut, Greifswald-Insel Riems, Germany

*Corresponding author
E-mail: julia.sehl-ewert@fli.de (JSE)

Abstract

Alphaherpesviruses, including Herpes Simplex Virus 1 (HSV-1) and Pseudorabies Virus (PrV), establish lifelong latency in the nervous system and can cause recurrent disease. While latency has classically been attributed to peripheral sensory ganglia, accumulating evidence indicates that the central nervous system (CNS) also act as a relevant reservoir for viral latency and reactivation. Here, we investigated the CNS as a site of latency using the attenuated mutant PrV-ΔUL21/US3Δkin which reproduces key features of herpes simplex encephalitis (HSE) in female CD1 mice. We mapped brain regions permissive to alphaherpesviral latency and analyzed the temporal dynamics of viral transcription, histopathology, and host clinical and immune responses. Following intranasal inoculation, mice were analyzed at 11 to 14, 21, 28, 42, 105, and 190 days post infection (dpi). To assess the potential of reactivation, a subset received cyclophosphamide/dexamethasone at 170 dpi. Viral transcripts were detected by RNAscope™ in situ hybridization and RT-qPCR targeting the lytic gene UL19 and the latency-associated transcript (LAT). Histopathological analyses included hematoxylin and eosin (H&E) staining and immunohistochemistry for CD3, Iba1, GFAP, and cleaved caspase-3. Major capsid protein (UL19) expression displayed marked regional and temporal heterogeneity, with prominent signals in mesiotemporal structures (piriform cortex, hippocampus, entorhinal cortex), coinciding with pronounced T-cell infiltration. LAT expression remained overall low, with a transient peak during the acute infection (11–14 dpi). RT-qPCR confirmed high viral transcript levels for both UL19 and LAT in mesiotemporal regions during early infection, while LAT expression returned to baseline levels thereafter. Histopathology demonstrated a transition from acute necrotizing meningoencephalitis to prolonged or recurrent low-grade inflammation, accompanied by glial activation and localized apoptosis. Notably, UL19 expression strongly correlated with $CD3^+$ T-cell infiltration, particularly at 42 dpi. These findings define the spatiotemporal interplay between viral transcriptional activity and neuroinflammation and identify selected CNS regions as reservoirs for latent or recurrent alphaherpesvirus infection.

Keywords: alphaherpesvirus, pseudorabies virus, mouse model, latency, In-situ hybridization, brain pathology

Author Summary

Alphaherpesviruses are pathogens that not only cause acute disease but also establish lifelong latency in the nervous system. Under certain conditions, they can reactivate and trigger recurrent disease. Using a genetically modified pseudorabies virus in mice, we mapped how latent and lytic phases occur within the brain over several months. By combining molecular, histological, and clinical analyses, we show that specific brain regions act as long-term viral reservoirs, where signs of inflammation and viral activity can reappear long after the initial infection. These findings provide new insights into how alphaherpesviruses persist in the central nervous system and suggest that recurrent or subclinical reactivation may

contribute to long-term neurological complications, including those resembling human herpes simplex encephalitis.

Introduction

Alphaherpesviruses such as Herpes Simplex Virus Type 1 (HSV-1) and Pseudorabies Virus (PrV) are neurotropic DNA viruses capable of establishing lifelong latency within the nervous system (1). Following primary mucosal infection, virions enter peripheral sensory neurons and undergo retrograde axonal transport to peripheral and autonomic ganglia, particularly the trigeminal ganglion (TG) (2, 3). Here, the viral genome persists in a latent, transcriptionally restricted state (4, 1, 5–8).

Productive infection is characterized by a temporally regulated cascade of immediate-early, early, and late gene expression (9, 10). In contrast, latency is defined by episomal genome maintenance in the absence of infectious virus production, with transcription largely restricted to the latency-associated transcripts (LATs). In PrV, these include an unstable 8.4 kb transcript, the large-latency transcript (LLT), a stable intron, eleven micro-RNAs, two small noncoding RNAs, and three transcripts antisense to the major LAT (10–12). LAT and their encoded micro RNAs synergistically inhibit apoptosis (13, 14), and suppress viral replication (15, 16). Establishment of latency is thought to depend on complex interactions between the viral genome, the host neuronal environment, and immune surveillance mechanisms (17).

Reactivation from latency can be triggered by physiological or environmental stressors leading to renewed viral replication and spread, either peripherally or towards the central nervous system (CNS) (18). While clinically apparent reactivation typically manifests peripherally (19), increasing evidence suggests that alphaherpesviruses may also establish latency within the CNS (20, 21). Such CNS latency may result in primary or recurrent encephalitis, or in subclinical reactivation events (22).

HSV-1 is the leading cause of herpes simplex encephalitis (HSE), a severe and often fatal condition with a predilection for mesiotemporal brain regions (23, 24). Beyond encephalitis, HSV-1 has been implicated as a potential co-factor in the pathogenesis of neurodegenerative disorders such as Alzheimer's disease (AD) (25, 26).

Although HSV-1 remains the most clinically relevant alphaherpesvirus in humans, PrV provides a valuable experimental model due to its close genetic and pathogenic relationship to HSV-1 (27, 28). In particular the attenuated mutant PrV-ΔUL21/US3Δkin, which lacks the functional tegument protein pUL21 and express a kinase-deficient pUS3, induces non-lethal encephalitis in female CD1 mice after intranasal inoculation (29). Infected animals develop severe lymphohistiocytic meningoencephalitis in mesiotemporal regions and neurological deficits reminiscent of HSE, yet most survive the acute phase, enabling long-term observation (30).

Our previous long-term studies demonstrated that infection with PrV-ΔUL21/US3Δkin results in a multiphasic disease course, with histopathological evidence of neuroinflammation, including mild

meningoencephalitis and gliosis, detectable up to 168 days post-infection (dpi) (30). These findings raised key questions regarding the underlying mechanisms: whether they reflect intermittent reactivation, persistent low-level infection, chronic inflammation, or even autoimmune responses, as suggested by previous murine models and human case reports (31–33).

To address these questions, we conducted a comprehensive long-term study extending to 105 days pi. Using molecular (RNAscope™ in situ hybridization and quantitative real-time PCR (RT-qPCR)) and histopathological approaches, we systematically assessed viral gene expression, immune cell infiltration, and lesion development across defined brain regions. Given the limited number of in vivo models for PrV latency (34), we specifically evaluated the potential for CNS latency beyond the TG, with a focus on mesiotemporal structures as candidate sites of long-term viral activity.

This study integrates spatially resolved molecular and histopathological analyses to elucidate mechanisms of alphaherpesvirus persistence in the CNS and its contribution to long-term neuropathology.

Results

The aim of this study was to identify brain regions that serve as sites for alphaherpesvirus latency and to investigate the temporal dynamics of latency and reactivation during long-term infection.

Female CD1 mice (6-8 weeks old) were intranasally inoculated and sacrificed at 21, 42 and 105 dpi for RT-qPCR, RNA in situ hybridization, and histopathological analyses (study 1). Archived brain sections from a previous long-term study (study 2) using the same model (30) were reanalyzed to investigate the post-acute phase at 28 dpi. In that study, a subset of animals received cyclophosphamide/dexamethasone at 170 dpi and were sacrificed 20 days later. These tissues were included for RNA in situ hybridization and histopathology. An overview of the experimental design is shown in Fig 1.

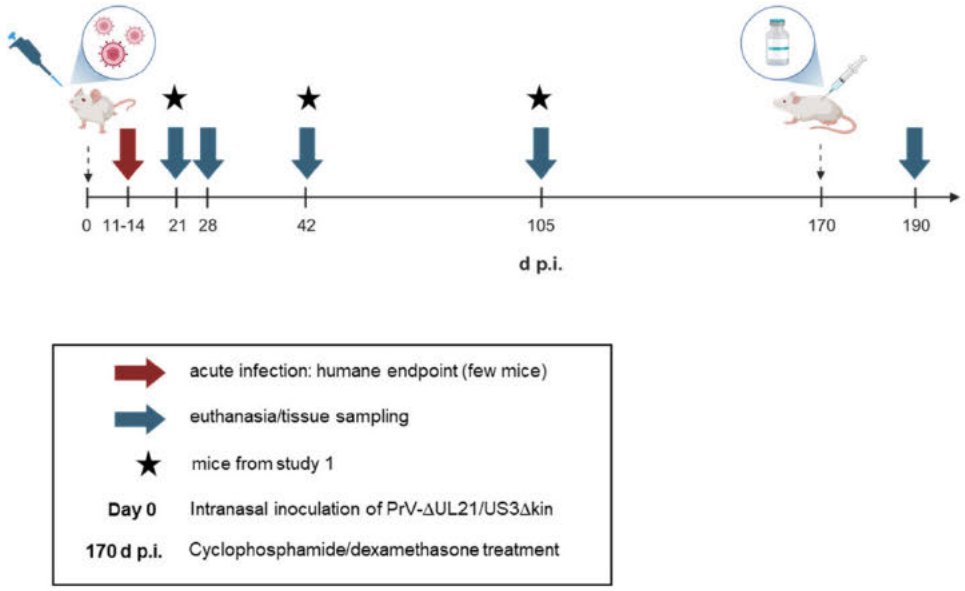

Fig 1. Experimental timeline of necropsies and tissue collection. Six- to eight-week-old CD1 mice were intranasally inoculated with PrV-ΔUL21/US3Δkin (day 0) in two independent studies. In study 1, tissue samples were collected at 21, 42, and 105 dpi (indicated by stars). In study 2, mice received an immunosuppressive treatment (cyclophosphamide/dexamethasone) at 170 dpi, and tissue was collected at 28 dpi and 190 dpi. During the acute infection phase (11–14 dpi), mice that reached the humane endpoint were euthanized, and tissues were collected for analysis. Created with BioRender.com

Clinical evaluation

As previously reported in mice from study 2 (0-168 dpi) (30), infection with PrV-ΔUL21/US3Δkin in study 1 followed a multiphasic disease course. From day 5 post-infection, mice developed mild clinical signs including ruffled fur and reduced activity. Disease symptoms peaked between 10-15 dpi, with incidence rates approaching 90%. During this acute phase, mice displayed alopecic skin erosions, nasal bridge edema, mild pruritus, and behavioral abnormalities such as hyperactivity and "star gazing". Approximately 10% of animals reached humane endpoint criteria due to severe manifestations including seizures and hyperexcitability.

By 30 dpi, predominantly mild clinical signs persisted in ~50% of mice. Between 45 and 105 dpi, incidence declined further to 20–30%, with fluctuating low-grade signs such as ruffled fur and subtle behavioral alterations (Fig 2A).

Following cyclophosphamide/dexamethasone treatment at 170 dpi in study 2, approx. 80% of animals developed mild clinical signs (ruffled fur, reduced activity) within the first 5 days post treatment (dpt). Between 5 and 10 dpt, the disease severity increased, and all animals exhibited signs of reactivation. Approximately 50% developed moderate symptoms including "star gazing," pruritus, and mild hunching. By 20 dpt, both incidence and severity steadily declined, with approx. 10% of animals were still symptomatic at the end of the observation period (Fig 2B).

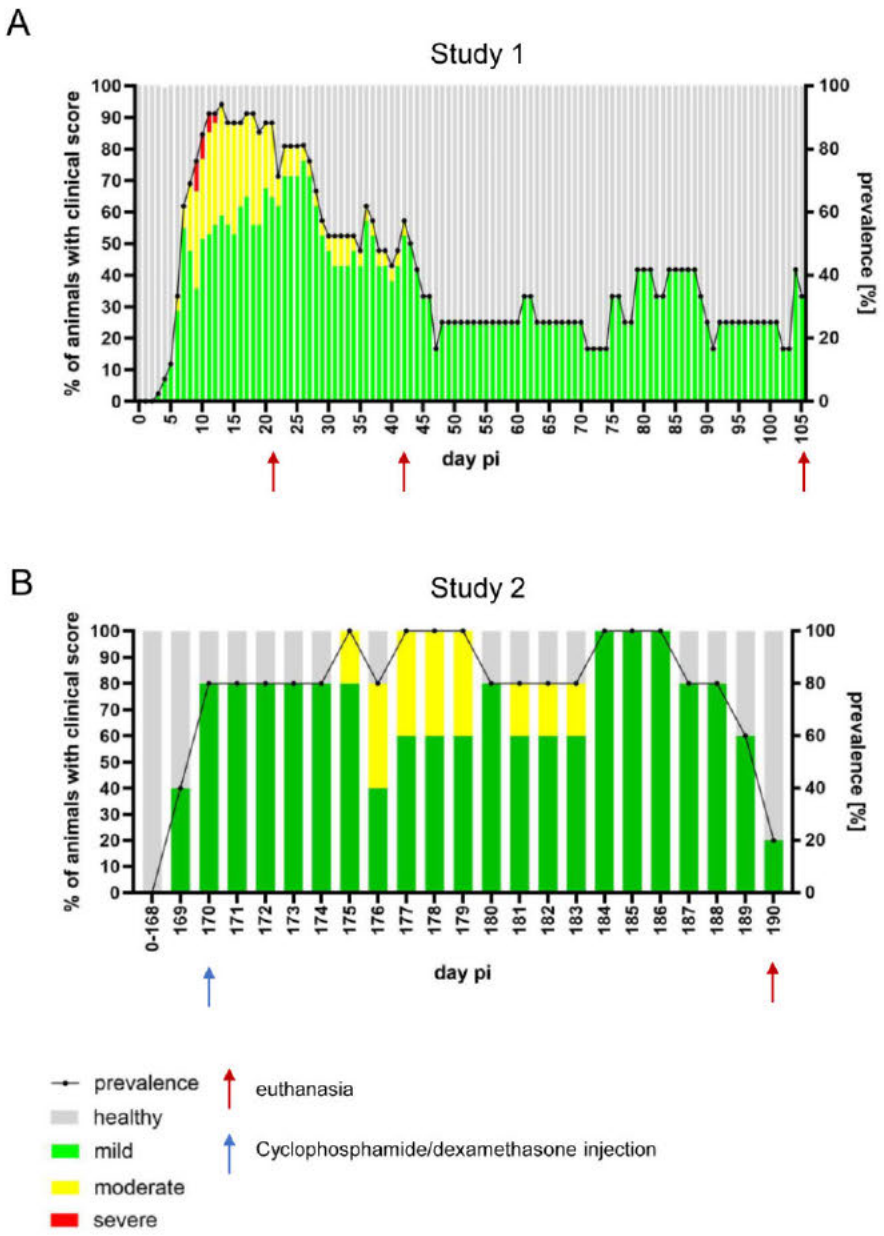

Fig 2. Longitudinal assessment of disease severity and incidence in PrV-ΔUL21/US3Δkin-infected mice. The proportion of clinically affected animals is shown as a percentage of the total number of infected mice. Disease severity is color-coded as follows: healthy (grey), mildly affected (green), moderately affected (yellow), and severely affected (red). Percentages are plotted on the left y-axis, while the overall incidence of clinical signs is indicated by a dotted line and shown on the right y-axis. Red arrows indicate necropsy time points. (A) Study 1: PrV-ΔUL21/US3Δkin or mock-inoculated mice (n=7) were sacrificed at 21, 42, and 105 dpi. (B) Study 2: Mice (n=5) were inoculated, monitored, and evaluated as in study 1, but received immunosuppressive treatment with cyclophosphamide/dexamethasone at 170 dpi (blue arrow), and were euthanized at 190 dpi.

Expression patterns of lytic and latency-associated transcripts

To characterize spatial and temporal expression of viral transcripts, brains from mice sacrificed at 11–14 dpi (reached humane endpoint), 28, 42, 105, and 190 dpi were analyzed. In situ RNA hybridization was performed on six standardized coronal brain sections per animal (Fig 3A, L1–L6), using the RNAscope™ method (35) with probes targeting the lytic gene UL19 and the latency-associated transcript LAT (Fig 3B).

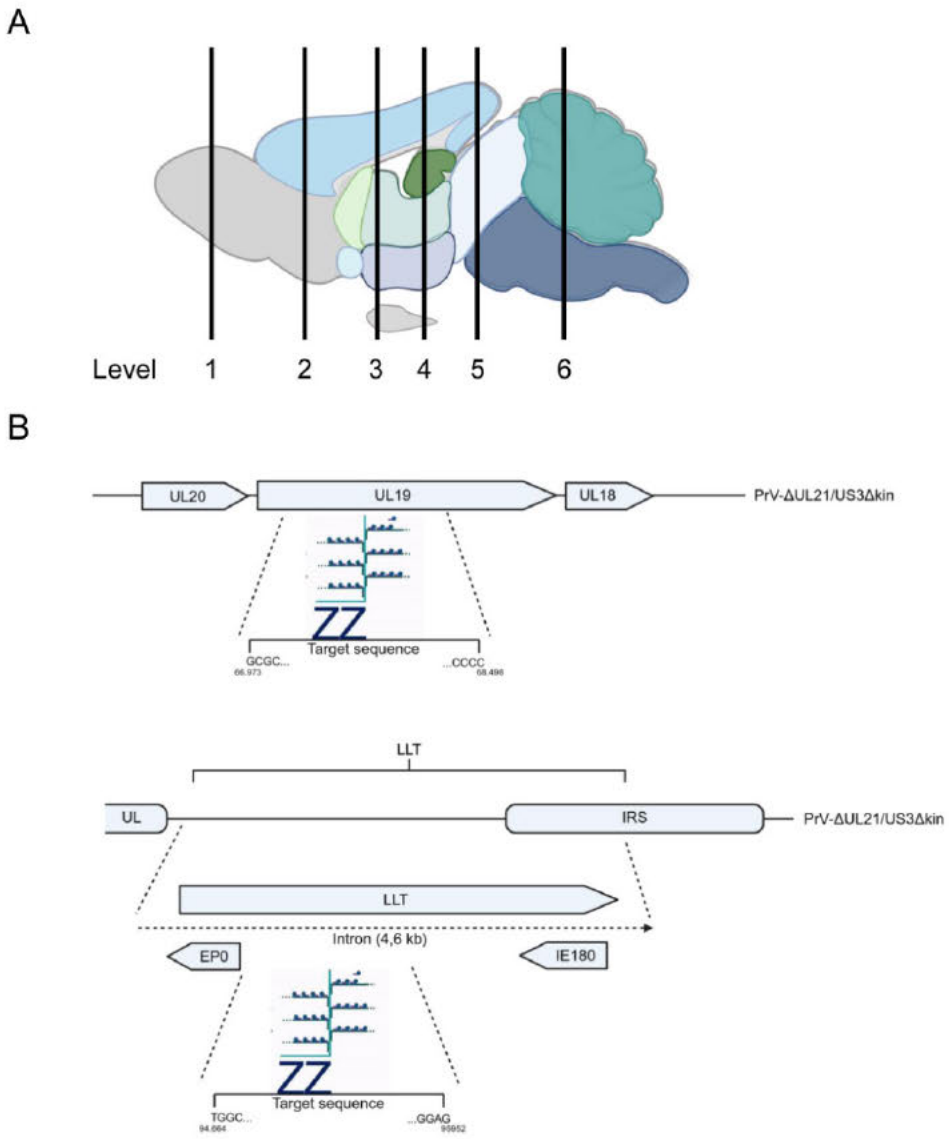

Fig 3. Experimental setup for RNAscope™ analysis. (A) Schematic overview of analyzed brain regions. Serial 3 µm coronal sections were collected for detailed analysis at six defined anatomical levels: L1 (olfactory bulb), L2 (prefrontal cortex), L3 (frontoparietal cortex, basal ganglia), L4 (parietal cortex, thalamus, hypothalamus, hippocampus), L5 (midbrain), and L6 (cerebellum/pons). (B) Design of UL19 (V-SHSV-UL19-C1) and LLT (V-SuHV1-LLT-O2-C2) probes used for detection of lytic and latency-associated (LAT) viral mRNA. V-SHSV-UL19-C1 targets the UL19 and V-SuHV1-LLT-O2-C2 the LAT region, which is represented by the blue dots and connecting lines. Location of the probes corresponds to nucleotide positions: 66973–68498 base pairs (UL19), 94664-95952 base pairs (LLT). Created with BioRender.com.

CNS sites of LAT expression

LAT signal was detected on multiple CNS structures across time points (Fig 4). In the hindbrain, expression was observed in the cerebellum (Cb) and brainstem (BS) nuclei including the nucleus of the solitary tract (Sol), inferior olive (IO), spinal trigeminal nucleus (Sp5), spinal vestibular nucleus (SpVe), facial nucleus (7N), and the reticular formation (FR).

In the midbrain, LAT-positive signals were found in the substantia nigra (SNR), caudate putamen (CPu), deep mesencephalic nucleus (DpMe), and central nucleus of the inferior colliculus (CIC). Thalamic and hypothalamic areas such as the ventral posteromedial nucleus (VPM) and lateral hypothalamus (LH) showed expression.

In the telencephalon, signals were consistently detected in mesiotemporal regions including the hippocampus (Hpc), lateral septal nucleus (LS), and lateral entorhinal cortex (LEnt). Additional expression was observed in the piriform cortex (Pir), agranular insular cortex (AI), prelimbic cortex (PrL), anterior olfactory nucleus (AO)), as well as in primary sensory (S1), visual (V1), and motor cortices (M1), and in the olfactory bulb (OB).

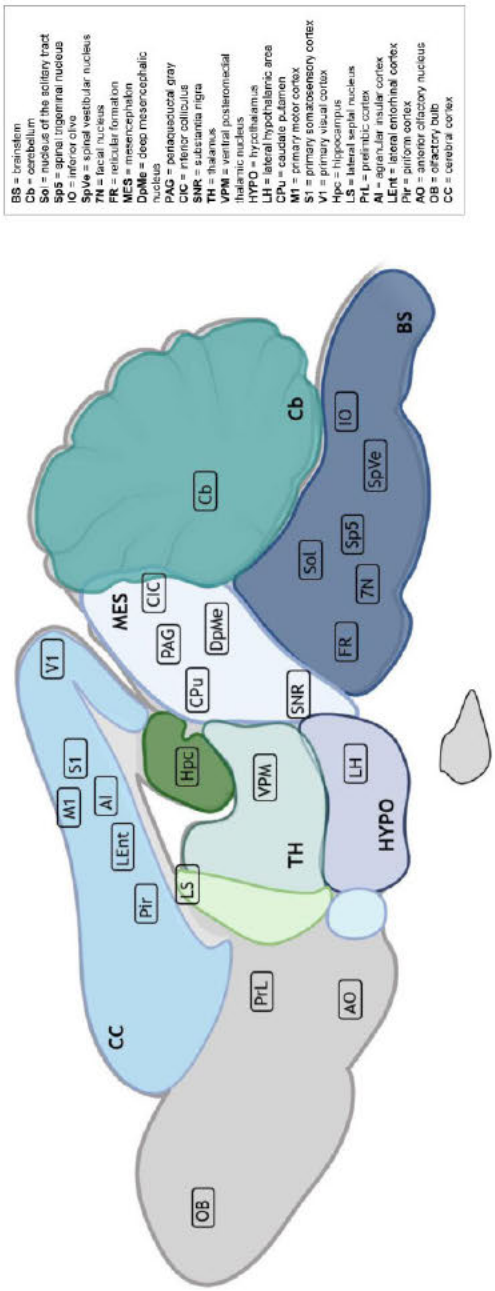

184

185 **Fig 4. Widespread detection of latency-associated transcript (LAT) expression in the murine**
186 **brain following intranasal PrV-ΔUL21gfp/US3Δkin infection**. LAT RNA was detected by
187 RNAscope™ in all analyzed anatomical regions across functional brain systems (brainstem,
188 mesencephalon, diencephalon, telencephalon, and cerebellum) at 11–14, 28, 42, 105, and 190 dpi. The
189 distribution of LAT-positive regions are illustrated on a schematic sagittal brain section. Created with
190 BioRender.com.

Semi-quantitative analysis of UL19 and LAT expression

To assess expression dynamics, nine brain regions were selected for semi-quantitative analysis at defined post-infection timepoints. Selected regions included known alphaherpesvirus target areas such as Pir, AI, LEnt, Hpc, S1, Sp5 and OB (36, 29). The Cb served as a reference region due to its low susceptibility to alphaherpesviral infection (37). The TG was included as a canonical latency site (1) (Fig 5A).

Signals were scored on a 0-5 scale (Fig 5B), distinguishing discrete puncta (Fig 5C) from clustered signal patterns (Fig 5D). Results are summarized in Fig 6 and detailed per animal in S1 Table. Representative RNAscope™ images are shown in Fig 7 and Fig 8.

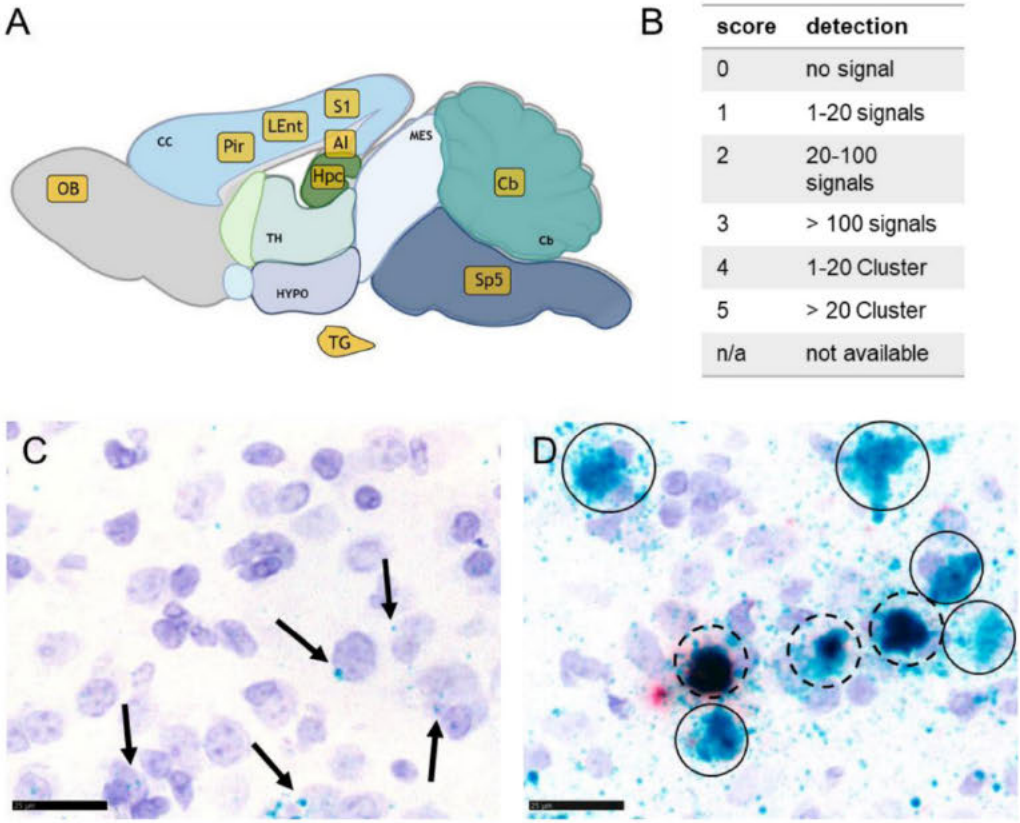

score	detection
0	no signal
1	1-20 signals
2	20-100 signals
3	> 100 signals
4	1-20 Cluster
5	> 20 Cluster
n/a	not available

Fig 5. Detection of UL19 and LAT RNA transcripts in murine brain tissue using RNAScope™ in situ hybridization. (A) Overview of the selected brain regions analyzed (yellow-shaded boxes). (B) Scoring criteria for positive signal detection based on the number and clustering of signals within these regions. Coronal brain sections representing six anatomical levels were examined by light microscopy. If multiple levels were available, the highest score per anatomical region was recorded. (C) Individual RNA transcripts appear as distinct chromogenic dots (arrow); green dots represent UL19 RNA

transcripts. (D) Accumulation of transcripts may result in clusters (solid circles), which can comprise different transcripts, indicated by a mixed red (LAT) and green (UL19) signals (dashed circles). TG = trigeminal ganglion, Cb = cerebellum, Sp5 = spinal trigeminal nucleus, S1 = primary somatosensory cortex, Hpc = hippocampus, LEnt = lateral entorhinal cortex, Pir = piriform cortex, AI = agranular insular cortex, OB = olfactory bulb. Scale bar = 25 µm. Created with BioRender.com.

11-14 dpi:

Both, UL19 and LAT transcripts were highly expressed (Fig 6A), particularly in temporal and frontoparietal regions (Fig 7A). Strong signals (Score 4–5) were observed in the LEnt; (Fig 7B), Hpc (Fig. 7C), Pir (Fig. 7D), AI, and S1. Sp5 and OB showed only few signals (Score 1). In the Cb only minimal or no signals (Score 0–1) were present, and no transcripts were detected in the TG (Fig 6A).

28 dpi:

LAT expression was at baseline across all regions (Score 0-1), with no signal in the TG. UL19 expression remained low in OB, Sp5, TG, and Cb, but was modestly elevated in the LEnt, Pir, AI, S1, and Hpc (Score 1-2) (Fig 6B).

42 dpi:

LAT largely remained at baseline, except in one animal showing increased signals (AI, Pir, S1: score 2; Hpc: score 3; Sp5: score 4). UL19 expression was very heterogenous. Cb, TG, and OB remained low (score 0–1), whereas AI, Pir, Hpc, LEnt, S1 and Sp5 varied widely (1-5) (Fig 6C). Representative animals illustrate this: Mouse M8 displayed UL19 clusters across regions, consistent with reactivation (Fig 8B), while mouse M7 showed LAT clusters in Sp5 and increased signal frequency in AI, Pir, Hpc, and S1, with low UL19 expression, suggestive for latency (Fig 8C). Representative RNAscope™ images of clustered transcript signals in M8 (S1) and M7 (Sp5) are provided in Fig 8D and Fig 8E, respectively.

105 dpi:

LAT remained at baseline, except consistently elevated signals in Sp5 (Score 4). UL19 again showed heterogeneity, with OB and Cb low (score 0 and 1), and highest variability in Sp5 (score 1–4), AI (1–3), Pir/Hpc (2–4), and LEnt/S1 (3–4) (Fig 6D). No TG samples were available for this time point.

190 dpi (post-immunosuppression):

LAT remained mostly at basal levels with isolated increases in S1, Hpc, Pir, and OB (score up to 2). UL19 was generally low (score 0-1), with isolated signals in Pir, Hpc, and Lent (up to score 2). (Fig 6E).

A shift in the intracellular distribution of viral transcripts was observed. During the acute phase, UL19 and LAT were frequently detected within the same neuron or in immediately adjacent neurons. From 28

238 dpi onward and persisting through the end of the observation period, this pattern changed and both
239 UL19 and LAT were detected in different cells with no co-localization in defined neurons.

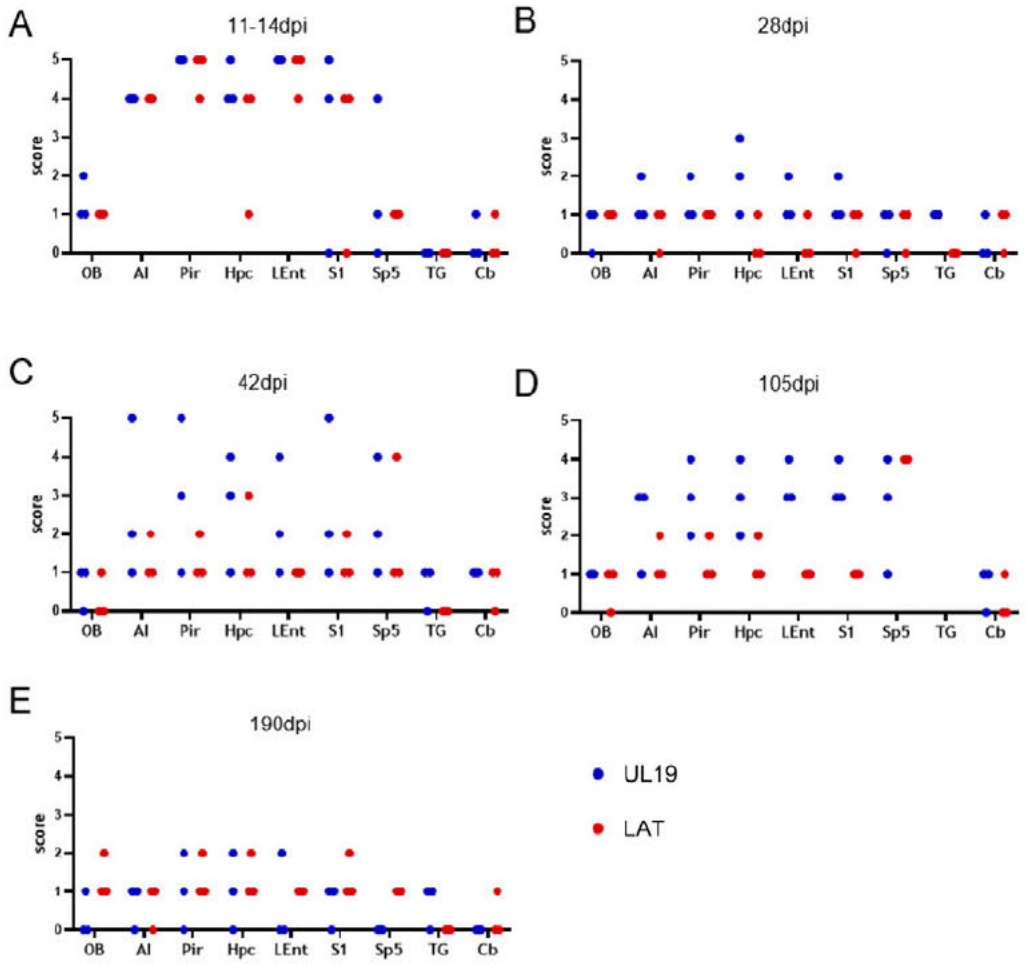

240

241 **Fig 6. Semi quantitative analysis of RNAScope™ signal detection in PrV-infected murine brain**
242 **tissue.** Positive signals for UL19 (blue) and LAT (red) RNA transcripts were scored at 11-14 dpi (A), 28
243 dpi (B), 42 dpi (C), 105 dpi (D) and 190 dpi (E). Scores represent data from three mice per time point
244 and brain region. TG = trigeminal ganglion, Cb = cerebellum, Sp5 = spinal trigeminal nucleus, S1 =
245 primary somatosensory cortex, Hpc = hippocampus, LEnt = lateral entorhinal cortex, Pir = piriform
246 cortex, AI = agranular insular cortex, OB = olfactory bulb.

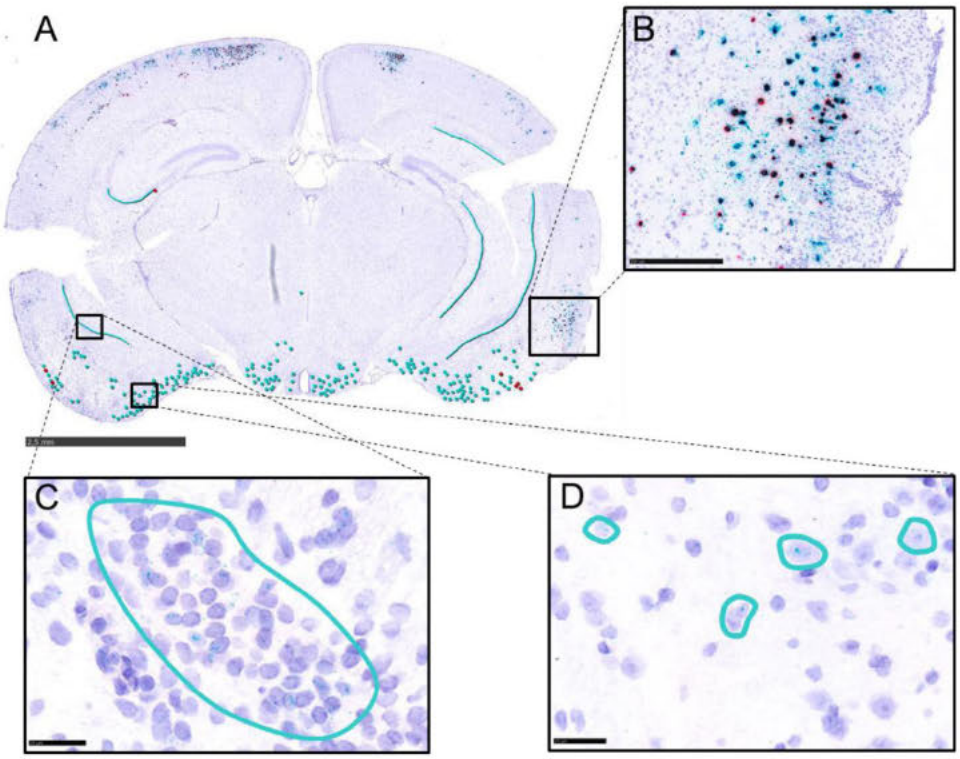

247

248 **Fig 7. Detection of UL19 and LAT RNA transcripts during the acute phase of PrV-ΔUL21/US3Δkin**
249 **infection using RNAscope™ in situ hybridization.** (A) Coronal section of a murine brain at the level
250 of the temporal lobe showing UL19 (green dots) and LLT (red dots) RNA signals at 14 dpi with PrV-
251 ΔUL21/US3Δkin. Scale bar = 2,5mm (B) Higher magnification of UL19 and LAT signals in LEnt. Scale
252 bar = 250 µm. (C) Higher magnification of scattered UL19 signals in Hpc (cyan outline). Scale bar =
253 25µm. (D) Higher magnification of UL19 signals in Pir (cyan circles). Scale bar = 25µm. Hpc =
254 hippocampus, LEnt = lateral entorhinal cortex, Pir = piriform cortex.

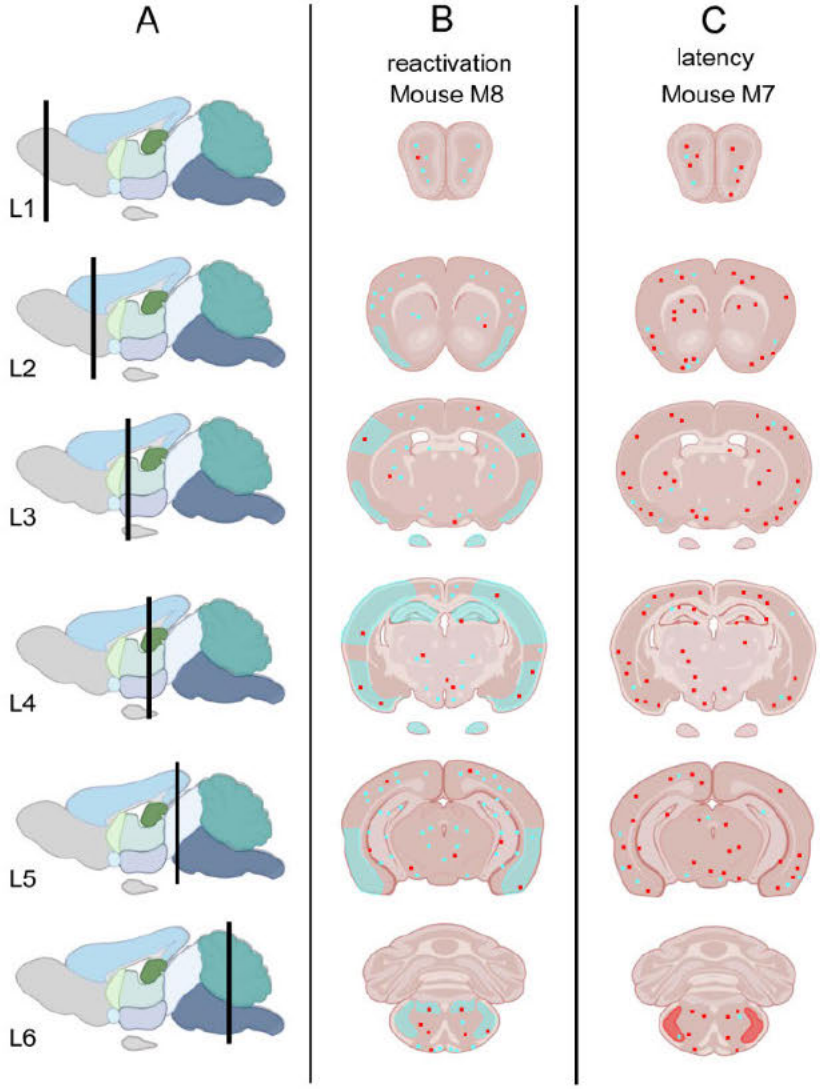

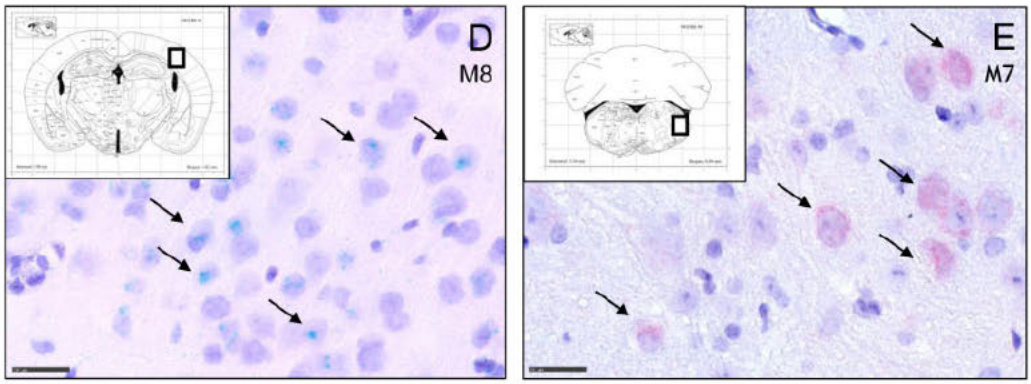

255

Fig 8. Distribution patterns of UL19 and LAT RNA signals across defined anatomical brain regions in selected mice at 42 dpi. (A) Sagittal view of the murine brain indicating the coronal section levels analyzed (L1-6). (B) Schematic coronal sections of mouse M8 during viral reactivation, depicting UL19 and LAT distribution. (C) Schematic coronal sections of mouse M7 during latency, depicting UL19 and LAT distribution. In panels B and C, dots indicate single RNA transcripts, while shaded areas represent clusters (red = LAT, cyan = UL19). (D) Higher magnification of the primary somatosensory cortex (S1) in mouse M8 showing intense intraneuronal UL19 signals, with clusters indicated by arrows. (E) Higher magnification of the spinal trigeminal nucleus (Sp5) in mouse M7, showing intense neuronal LAT signals, with clusters indicated by arrows. Sp5 = spinal trigeminal nucleus, S1 = primary somatosensory cortex. Scale bar = 25 µm. Coronal brain sections shown with *The Mouse Brain in Stereotaxic Coordinates* by Paxinos and Franklin, 2001. Created with BioRender.com.

Quantification of viral DNA by RT-qPCR

To complement RNAscope™ findings, RT-qPCR was performed on six brain regions (OB, Pir, temporal lobe (TL), TG, Cb, BS) from mice sacrificed at 9-10 (humane endpoint), 21, 42 and 105dpi. Ct values for UL19 and LAT are shown in Fig 9. Clinical correlations per mouse are detailed in S1 Fig.

9-10 dpi:

Animals reaching the humane endpoint exhibited severe signs (hunching, seizures, >20% weight loss) (S1 Fig). High expression levels of both UL19 and LAT were detected in the OB, TL, and Pir, as indicated by low Ct values, reaching values below 25. In contrast, the TG, Cb, and BS showed higher Ct (> 30), indicating lower abundance (Fig 9A).

21 dpi:

Both transcripts were near the detection threshold (Ct > 35). UL19 signals tended to be slightly more abundant than LAT, though not significant. Two mice (M25 and M24) showed lower LAT Ct values; but only one (M25) displayed seizures and localized alopecia (Fig. 9B, S1 Fig).

42 dpi:

UL19 expression was modestly elevated in OB, TL, Pir, and BS (Ct > 30), but undetectable in Cb and TG. LAT was absent except in one mouse (M29), which displayed low-level expression in all regions except Cb (Fig 9C).

105 dpi:

UL19 remained detectable in all regions except Cb (Ct 28-35). LAT was largely absent, except in two animals (M36, M37) with low-level expression in BS and Pir (Ct 32) (Fig 9D). Both showed only mild clinical signs (ruffled fur) (S1 Fig).

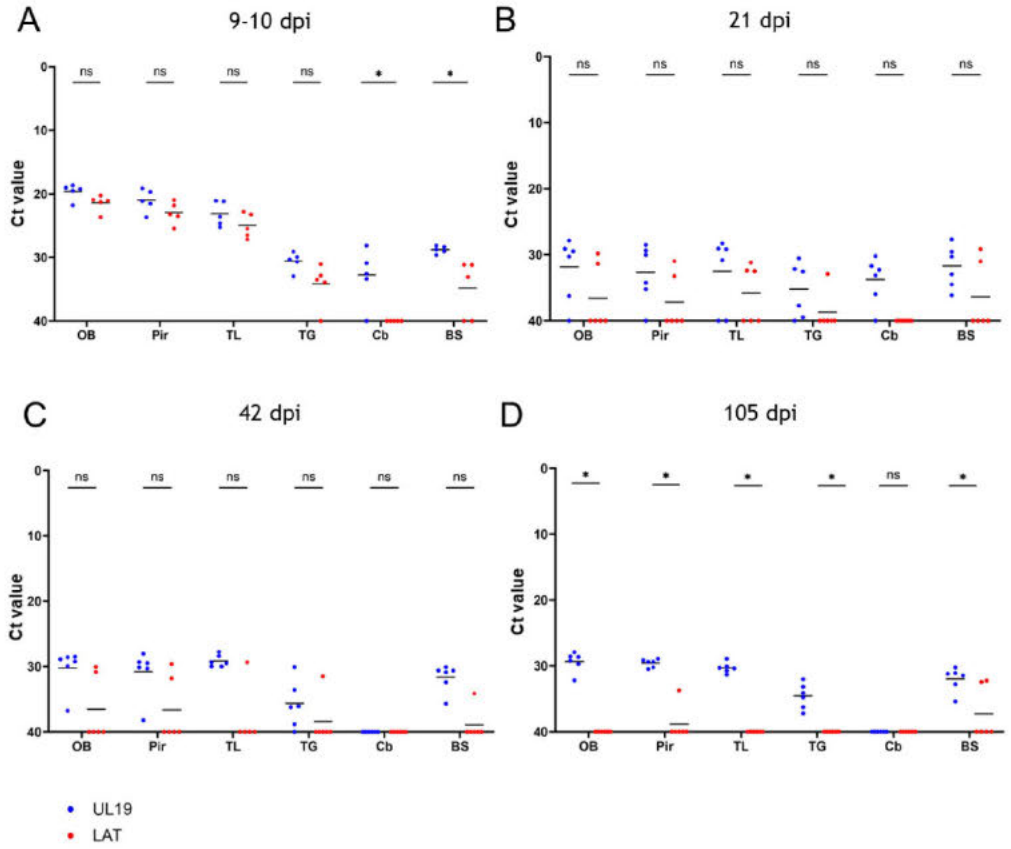

Fig 9. Quantification of UL19 and LAT genomic DNA in selected brain regions using RT-qPCR. cDNA levels of the lytic gene UL19 and the latency-associated transcript (LAT) were quantified by RT-qPCR in brain tissue from six mice per time point. Tissue was collected at four time points: (A) 9-10 dpi (five animals euthanized at the humane endpoint), (B) 21 dpi, (C) 42 dpi, and (D) 105 dpi. Dissected brain regions included the olfactory bulb (OB), piriform cortex (Pir), temporal lobe (TL), trigeminal ganglion (TG), cerebellum (Cb) and brainstem (BS). Ct values are shown for each region. Bars represent the geometric mean per group. *p<0,001.

Histopathological temporal profiling

Histopathology was performed on the same brain tissue analyzed by RNAscope™.

Long-term histomorphological alterations in the CNS

Histomorphological changes were consistently observed throughout the entire observation period across the analyzed brain regions (Fig 10).

H&E staining revealed severe necrotizing meningoencephalitis during the acute phase, predominantly affecting mesiotemporal regions (piriform and prefrontal cortices). Lesions were associated with dense T-cell and macrophage infiltrates, neuronal necrosis, and marked gliosis. Between 28 and 190 dpi, pathology shifted to a milder phenotype. Low-grade meningoencephalitis persisted with scattered single-cell necrosis in mesiotemporal and frontal regions. Perivascular and meningeal T-cell/histiocyte infiltrates remained detectable, alongside ongoing glial activation (S1 Table).

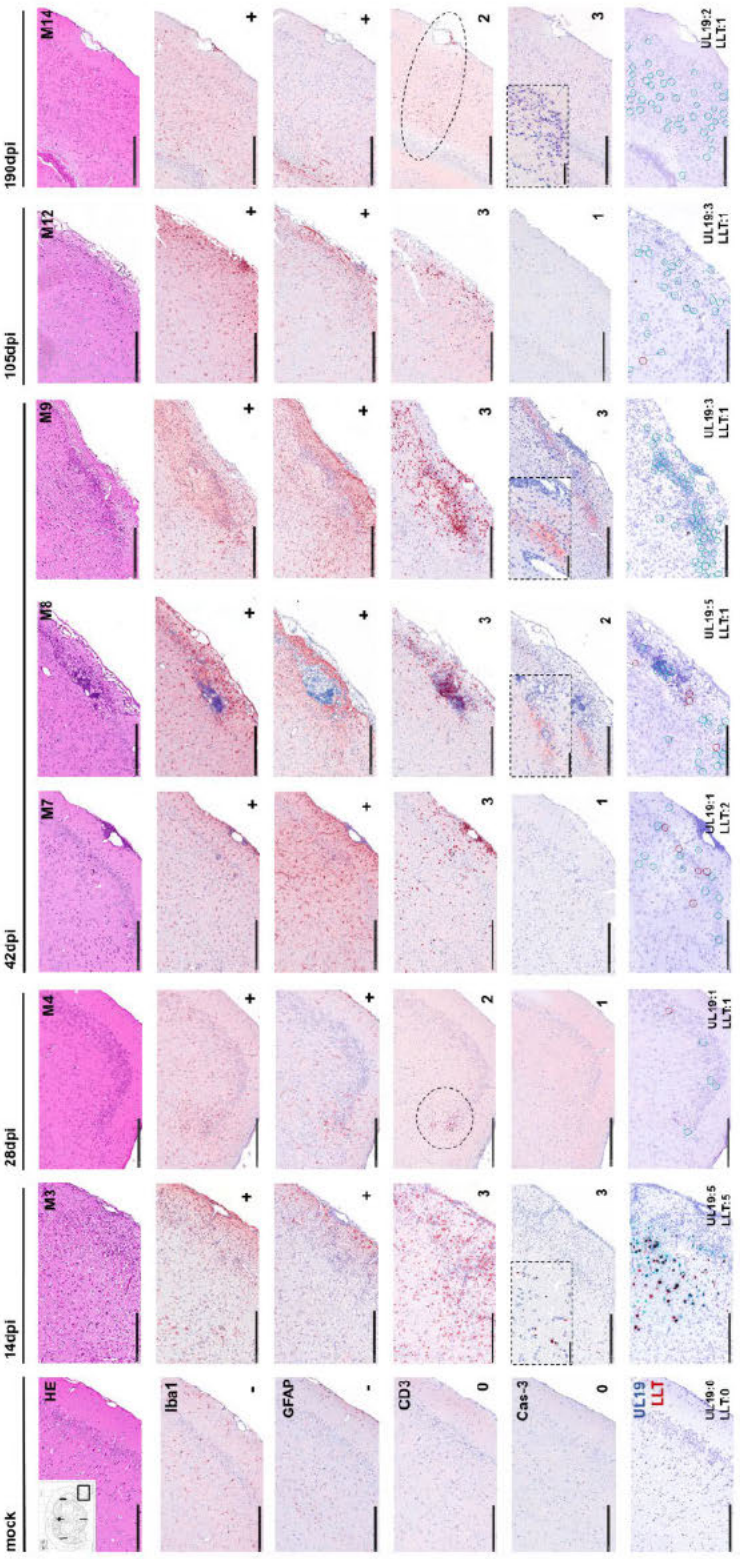

307

Fig 10. Representative images of long-term lesions in the temporal lobe (piriform cortex) from 14 to 190 dpi in PrV-ΔUL21/US3Δkin-infected mice. Temporal progression of infection-associated neuropathology was assessed by histopathology (H&E), immunohistochemistry (Iba1, GFAP, CD3, cleaved caspase-3 (Cas-3), and RNAscope™ in situ hybridization targeting UL19 (lytic) and LAT (latency-associated) transcripts. Representative brain sections are shown for mice sacrificed 14, 28, 105, and 190 dpi; three animals are shown for 42 dpi to illustrate interindividual variability histopathological and molecular findings. At 14 dpi, severe necrotizing meningoencephalitis was evident in the temporal lobe, accompanied by dense infiltrates of $CD3^+$ T-cells, $Iba1^+$ microglia/infiltrating macrophages, reactive $GFAP^+$ astrocytes, and abundant $Cas\text{-}3^+$ apoptotic cells. From 28 to 105dpi, mild meningoencephalitis was detected, characterized primarily by CD3+ and Iba1+ immune cells. A gradual increase in GFAP expression indicated ongoing astrogliosis, while only a few $Cas\text{-}3^+$ cells were detected, suggesting reduced apoptotic activity. At 42dpi, mild to moderate meningoencephalitis was present, with pronounced $CD3^+$ T-cell infiltration and interindividual variability in $Cas\text{-}3^+$ cell density ranging from low to high. At 190dpi, mild meningoencephalitis was still evident, characterized by ongoing $CD3^+$, $Iba1^+$ and $GFAP^+$ immune cell infiltration together with a high number of $Cas\text{-}3^+$ cells. Semi-quantitative scores from IHC and in situ hybridization analyses of the piriform cortex (ROI) are shown in the lower right corner of each panel. Scale bar = 250 µm.

Spatiotemporal T cells dynamics and correlation with lytic transcription

Region-specific patterns of T-cell infiltration detected by CD3 staining were observed (Fig 11A). In Pir and LEnt, T-cell scores remained high (2–3) through 105 dpi, declining slightly (1–2) at 190 dpi. AI showed a similar trajectory with earlier decline. Hpc infiltration remained at score 2–3 at most time points, peaking at 190 dpi. S1 fluctuated, with high scores at 11–14, 42, and 105 dpi. Sp5 was largely unaffected, except for a transient peak at 11–14 dpi. TG, Cb, and OB consistently showed minimal infiltration. Correlation analysis demonstrated a strong positive association between $CD3^+$ T-cell density and UL19 expression, particularly at 11–14 dpi ($p \leq 0.05$) and 42 dpi ($p \leq 0.01$) (Fig 11B).

A

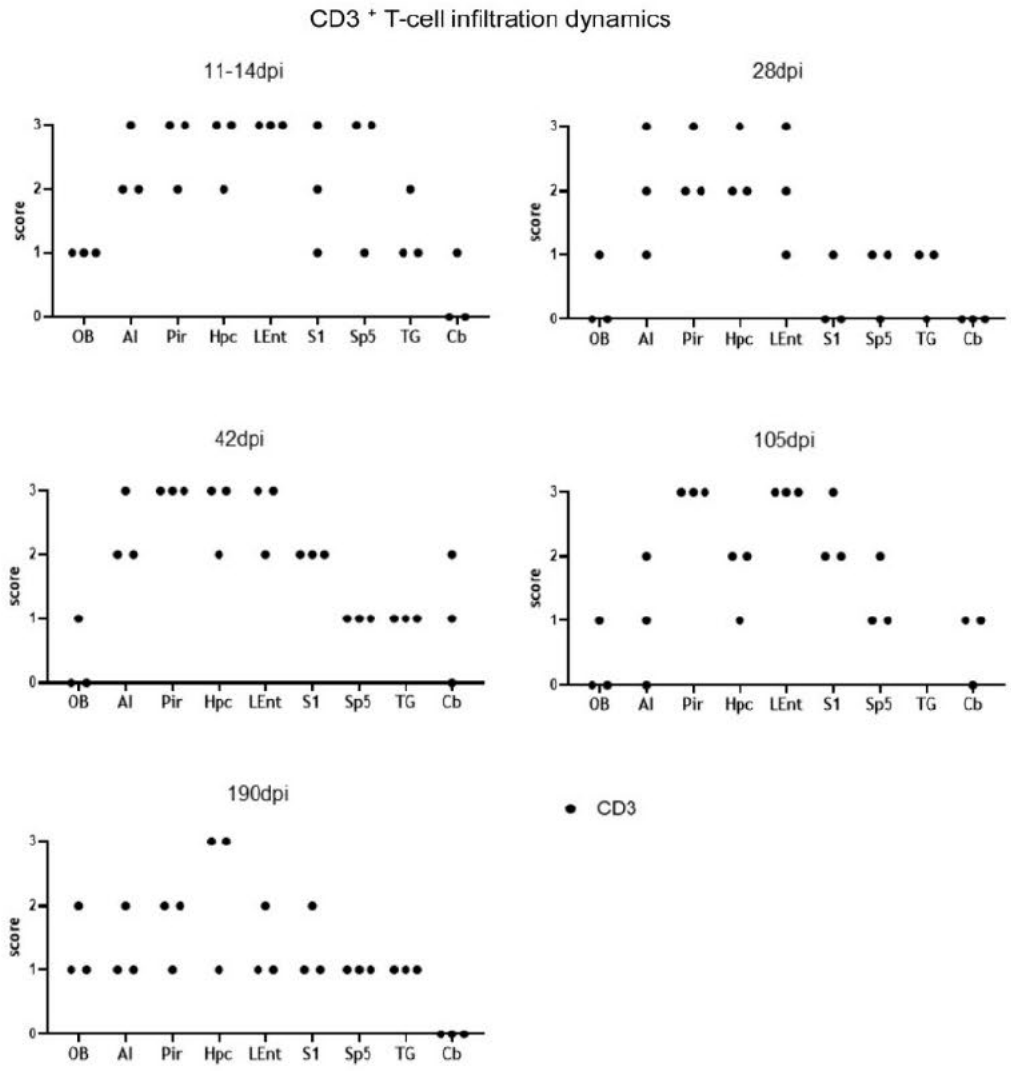

B

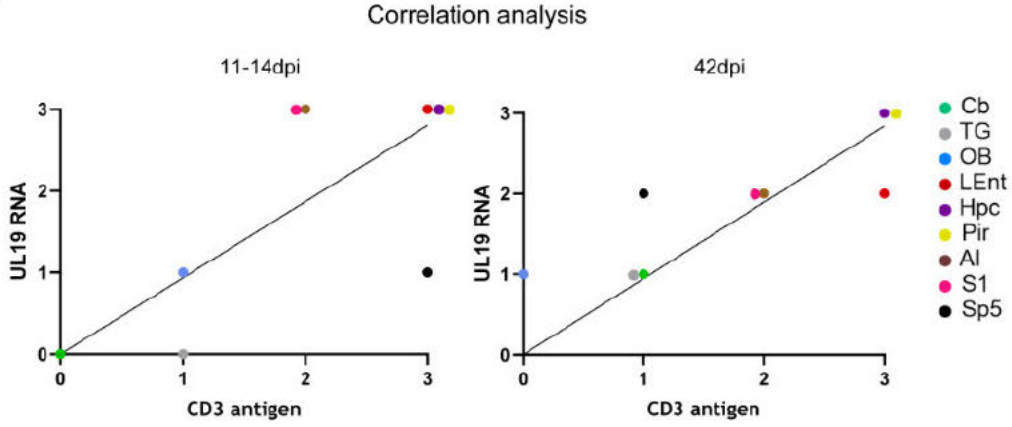

334

Fig 11. Semiquantitative analysis of CD3⁺ T-cell infiltration and correlation with UL19 RNA in PrV-ΔUL21/US3Δkin-infected murine brain tissue. (A) Semiquantitative scoring of CD3⁺ T-cell infiltration in selected brain regions at 11-14, 28, 42, 105 and 190 dpi. Scores from three mice per time point are shown. (B) Correlation analysis between CD3⁺ T-cell infiltration and UL19 RNA transcript detection. Mean CD3 antigen scores (x-axis) and mean UL19 RNA scores (y-axis) from three replicates per region were subjected to linear regression and Spearman's correlation analysis. A significant positive correlation was observed at 11–14 dpi ($p \leq 0.05$) and 42 dpi ($p \leq 0.01$). TG = trigeminal ganglion, Cb = cerebellum, Sp5 = spinal trigeminal nucleus, S1 = primary somatosensory cortex, Hpc = hippocampus, LEnt = lateral entorhinal cortex, Pir = piriform cortex, AI = agranular insular cortex, OB = olfactory bulb.

Integrated spatiotemporal profiling of viral transcripts, neuroinflammation, and clinical outcome

Representative images from the piriform cortex are shown in Fig 10.

During the acute phase (11–14 dpi), animals developed severe meningoencephalitis characterized by dense T-cell infiltrates (score 3), marked gliosis, and abundant apoptotic cells (cleaved caspase-3 (Cas-3) score 3). Strong signals for both UL19 and LAT transcripts (score 5) were detected, coinciding with severe clinical manifestations.

At 28 dpi, inflammation had subsided to a mild meningoencephalitis, accompanied by ongoing gliosis. T-cell infiltration (score 2) and apoptotic activity (Cas-3 score 1) were reduced, and viral transcript levels were low (score 1). Correspondingly, only minimal clinical signs were observed.

At 42 dpi, interindividual variability became apparent. In mouse M7, UL19 expression was low (score 1), LAT moderately increased (score 2), and apoptotic activity minimal. In contrast, M8 exhibited strong UL19 expression (score 5), moderate apoptosis (Cas-3 score 2), and low LAT, consistent with viral reactivation. Mouse M9 showed moderate UL19 levels (score 3), pronounced apoptosis (Cas-3 score 3), and behavioral abnormalities such as stargazing.

At 105 dpi, mild meningoencephalitis persisted, with high T-cell infiltration (score 3), moderate UL19 expression (score 3), and low LAT (score 1). Apoptosis remained minimal (Cas-3 score 1), while overt clinical signs were still present.

By 190 dpi, inflammation was mild, with ongoing T-cell infiltration (score 2) and low expression of UL19 (score 2) and LAT (score 1). Notably, apoptotic activity was elevated (Cas-3 score 3), despite the absence of clinical signs.

Mock-infected mice showed no abnormalities. An immunosuppressed mock control, however, exhibited increased apoptosis (Cas-3 score 3). A full summary of findings is provided in S1 Table.

Discussion

In this study, we examined the long-term dynamics of alphaherpesvirus infection in the murine CNS after intranasal inoculation with PrV-ΔUL21/US3Δkin. By integrating molecular, histopathological, and clinical analyses, we identified distinct spatiotemporal patterns of lytic and latent viral transcription and linked them to neuroinflammation and clinical outcome. In addition, an immunosuppressed cohort allowed us to assess the potential for viral reactivation.

The infected mice followed a multiphasic disease trajectory consistent with previous observations (30). During the acute phase, severe clinical signs including seizures, hyperactivity, and “stargazing” were observed, reflecting neuronal dysfunction particularly in mesiotemporal regions (38, 39). Mild to moderate signs persisted in a subset of animals during later time points, and immunosuppression at 170 dpi induced transient disease recurrence. These manifestations closely resemble the clinical signs reported in human herpes simplex encephalitis (HSE), where hippocampal and entorhinal involvement underlies cognitive deficits, memory impairment, and seizures (22, 40, 41).

RNAscope™ analysis demonstrated widespread neuronal permissiveness to latency, with LAT signals present across hindbrain, midbrain, diencephalon, and telencephalon including mesiotemporal, olfactory, and neocortical regions. Semi-quantitative analysis revealed distinct temporal patterns: during the acute phase (11–14 dpi), both LAT and UL19 were abundant in mesiotemporal and frontoparietal areas, by 28 dpi both signals had declined; and from 42 dpi onward, LAT remained at baseline, whereas UL19 displayed interindividual heterogeneity, with some animals showing strong signals suggestive of reactivation. Following immunosuppression (190 dpi), LAT remained low, while UL19 expression showed modest increases in selected regions.

RT-qPCR confirmed these dynamics, showing highest viral loads in the olfactory bulb, temporal lobe, and piriform cortex during the acute phase, with lower but persistent UL19 detection at later stages. Discrepancies between RNAscope™ and RT-qPCR, particularly in the OB, likely reflect methodological differences: whole-tissue qPCR versus single-section histological analysis.

A notable finding was the absence of detectable LAT signals in the TG, despite its canonical role as the primary latency reservoir (1, 42, 10). Instead, brainstem regions, especially the Sp5, consistently exhibited LAT expression at later time points. This aligns with reports suggesting that reactivation may occur more readily in brainstem neurons than in the TG (43, 20).

During the acute phase, LAT and UL19 were often detected within the same neuron, suggesting transient overlap of lytic and latent transcription. From 28 dpi onward, however, transcripts were strictly segregated to distinct cells, with no further co-localization. This shift suggests an early overshooting response that subsequently resolves into mutually exclusive transcriptional programs at the single-cell level. A similar phenomenon has also been described by Zhang ((44)), and is consistent with evidence that lytic and latent gene expression can transiently coexist (45–48).

UL19 expression showed pronounced inter-individual variability at 42 and 105 dpi. Some animals displayed strong UL19 signals across multiple regions, consistent with reactivation paralleling findings from Menendez ((49)), where lytic HSV-1 activity was detected post-60 dpi, while others exhibited primarily LAT signals with sparse UL19 expression, suggestive of latent infection. Such variability may reflect differences in latent genome copy numbers, which correlate with reactivation frequency (50, 51).

Histopathological analysis confirmed persistent CNS inflammation. During the acute phase, severe necrotizing meningoencephalitis was observed in mesiotemporal, piriform, and prefrontal regions. Thereafter, mild but sustained lymphohistiocytic meningoencephalitis, gliosis, and focal neuronal necrosis was present up to end of the experiment (190 dpi). Strong T-cell infiltration followed region-specific patterns and correlated with UL19 expression, particularly at 11–14 and 42 dpi, supporting the concept that T-cell clusters mark localized reactivation sites (42). $CD8^+$ T cells are known to suppress reactivation in an antigen-specific manner (47), and LAT transcripts may counteract this by inhibiting apoptosis through caspase-3 regulation (52). In our study, cleaved caspase-3 was frequently detected in regions with high UL19 expression and strong T-cell infiltration, further supporting the link between lytic activity, immune surveillance, and apoptosis.

Together these findings support two non-exclusive interpretations: (i) episodic, often subclinical reactivation, reflected by interindividual peaks of UL19 expression and clustered T-cell infiltrates, and (ii) chronic low-grade infection, indicated by persistent inflammation and ongoing UL19 detection across most animals and time points. This duality is consistent with reports of both spontaneous reactivation and chronic neuroinflammation during HSV-1 latency (20, 53, 31, 32, 54).

Beyond direct viral activity, secondary mechanisms may also contribute to long-term pathology. HSE can trigger autoimmune encephalitis, particularly anti-NMDAR encephalitis, which manifests with neuropsychiatric and cognitive symptoms resembling AD and amnestic mild cognitive impairment (aMCI) (55). Thus, recurrent viral activity and post-infectious autoimmunity may act in concert to drive progressive neurological dysfunction.

The immunosuppressed cohort provided further insights. Cyclophosphamide/dexamethasone-induced moderate clinical signs emerged within days, but by 20 dpi only low-level UL19 signals were detectable, while caspase-3 activity was elevated in both infected and control animals. This suggests that reactivation likely occurred shortly after treatment but was missed due to the timing of euthanasia. Glucocorticoid-induced depletion of T cells (56, 22) may have further obscured detection. These limitations highlight the need for shorter treatment-to-sampling intervals in future studies to better capture reactivation events.

In summary, our long-term study demonstrates that alphaherpesvirus latency is not confined to the TG but can be established in multiple CNS regions, with potential for sporadic reactivation and chronic low-grade inflammation. By integrating molecular, histopathological, and clinical readouts, we show how lytic activity and immune surveillance may contribute to long-term neuropathology. This model provides a

platform for addressing unresolved questions, including whether episodic reactivation or chronic infection is the primary driver of CNS disease progression.

Material and methods

Virus

The attenuated PrV mutant PrV-ΔUL21/US3Δkin, derived from the PrV wildtype strain Kaplan (57) was previously described (29, 58). Virus stocks were propagated in rabbit kidney (RK13) cells maintained at 37°C in minimum essential medium (MEM) supplemented with 10% fetal calf serum (FCS) (Invitrogen).

Animal experiments

Female CD1 mice (6-8 weeks old, Charles River Laboratories) were used as the standard infection model (29). Animals were housed in groups up to five in conventional cages (type II L) under Biosafety Level 2 (BSL 2) conditions at the experimental animal facility of the Friedrich-Loeffler-Institut, Greifswald-Insel Riems. Housing conditions included a 12h light/dark cycle (light intensity 60%), a temperature of 20-24°C, and ad libitum access to a standardized diet (ssniff Ratte/Maus-Haltung) and fresh drinking water. Bedding (ssniff Spezialdiäten Abedd Espen CLASSIC), nesting material (PLEXX sizzle nest), and environmental enrichment (PLEXX Aspen Bricks medium, mouse smart home, mouse tunnel) were provided.

After a 7-day acclimatization period, mice were deeply anesthetized by intraperitoneal injection of 200µl ketamine/xylazine (ketamine: 60 mg/kg; xylazine: 3 mg/kg, diluted in 0.9% NaCl). A total of 5 µl of virus suspension containing 1 × 10^4 plaque forming units (PFU)/ml of PrV-ΔUL21/US3Δkin were administered intranasally per nostril. Mock-infected mice received cell culture supernatant from uninfected RK13 cells.

Study 1: Twelve groups (n = 7 per group) were inoculated either with PrV-ΔUL21/US3Δkin or mock solution. Animals were euthanized at 21, 42, and 105 dpi. Groups 1–6 were analyzed by RNAscope™ and histopathology; groups 7–12 were analyzed by RT-qPCR.

Study 2: As described previously (30), six groups (n=6 per group) infected with PrV-ΔUL21/US3Δkin and one group mock treated, were euthanized at 28, 35, 42, 49, 84 and 168 dpi. An additional group (n= 10), 5 animals infected with PrV-ΔUL21/US3Δkin and 5 mock treated, received an immunosuppression at 170 dpi via intravenous injection of 5 mg cyclophosphamide and 0.2 mg dexamethasone in 250 µL phosphate-buffered saline (PBS). These mice were sacrificed 20 days later for histopathological and RNAScope™ analyses.

Randomization was performed prior to the experiment to assign animals to treatment groups and time points. Clinical evaluation was continuously monitored (24/7) using a standardized scoring system (29) encompassing three categories: (I) external appearance, (II) behavior and activity, and (III) body weight.

Scores ranged from 0 to 3; animals reaching a score of 3 in any category or 2 across all three were euthanized to meet humane endpoint criteria. For euthanasia, animals were pre-treated with Carprofen (Rimadyl, Pfizer, 10 mg/kg, subcutaneous) analgesia, followed by deep isoflurane anesthesia. Transcardial perfusion was performed via the left ventricle with PBS and subsequently 4% paraformaldehyde (PFA) as described by (59). Mice were euthanized by decapitation at the level of the first cervical vertebra.

In study 1, brains from groups 1-6 were post-fixed in 4% PFA for at least one week, brains from groups 7-12 were sectioned into six regions (see section RT-qPCR) and stored in PBS for molecular analysis. In study 2, entire heads were fixed in 4% neutral-buffered formalin and decalcified in Formical 2000 (Decal, Tallman, N.Y.) for at least three days.

Histopathological analysis

Brains from three PrV-ΔUL21/US3Δkin inoculated mice euthanized at 11-14 dpi (humane endpoint), 42 dpi, and 105 dpi (study 1), as well as heads from three infected mice euthanized at 28 dpi and from the cyclophosphamide/dexamethasone group (study 2) were processed for histopathology. Additionally, brains/heads from one mock-inoculated animal (study 1) and one mock-inoculated, immunosuppressed animal (study 2) served as controls.

Each brain/head was sectioned into six coronal levels from rostral to caudal, embedded in paraffin wax, and cut at 3 µm thick sections using a rotating microtome (Hyrax M55, Zeiss). Anatomical landmarks were defined according to Rao (60), resulting in six standardized levels: olfactory bulb (L1), prefrontal cortex (L2), frontoparietal cortex and basal ganglia (L3), parietal cortex, thalamus, hypothalamus, and hippocampus (L4), midbrain (L5), and cerebellum/pons (L6) (Fig. 3A, L1–L6). For light microscopy, sections were mounted on Super-Frost-Plus-Slides (Carl Roth GmbH, Germany) and stained with hematoxylin and eosin (H&E). Neuropathological analysis focused on CNS inflammation, neuronal necrosis and reactive gliosis.

Slides were examined using a Zeiss Axio Scope.A1 microscope equipped with 5x, 10x, 20x, and 40x N-ACHROPLAN objectives (Carl Zeiss Microscopy GmbH, Jena, Germany). Whole slide-scans were obtained with a NanoZoomer digital slide scanner (Hamamatsu, S60).

Immunohistochemistry

Immunohistochemistry was performed to identify infiltrating immune cells and apoptotic processes in relation to histopathological changes. Primary antibodies used are listed in Table 1.

Table 1: Primary antibodies used for immunohistochemistry.

antigen	target	manufacturer	clonality/host species	working dilution
Iba 1	microglia/ macrophages	FUJIFILM Wako, 01-19741	polyclonal rabbit	1:500
GFAP	astrocytes	Abcam, ab16997	polyclonal rabbit	1:400
CD3	t-cells	DAKO, A0452	polyclonal rabbit	1:100
cleaved caspase-3	apoptosis	Cell Signaling Technology, 9661	polyclonal rabbit	1:800

Paraffin-embedded tissue sections were dewaxed and rehydrated. Endogenous peroxidase activity was blocked with 3% hydrogen peroxide (Merck, Germany) for 10 min. Antigen retrieval was performed in 10mM citrate buffer (pH 6.0, without detergent) for Iba1, GFAP and Cas-3, or in 10mM Tris-EDTA buffer (10mM Tris base, 1mM EDTA solution, pH 9.0) for CD3. Sections were heated for 20 min in a pressure cooker (Sichler, Germany, NX-3213-675) for epitope demasking. After rinsing in Tris-buffered saline (TBS), nonspecific binding was blocked using normal goat serum (diluted 1:2 in TBS, 30min). Sections were incubated overnight at 4°C with primary antibodies diluted in TBS. The following day, slides were washed with TBS and incubated with biotinylated goat anti-rabbit IgG (Vector Laboratories, BA 1000, 1:200) for 30min at room temperature. For Iba1 and Cas-3 staining, detection used avidin-biotin-peroxidase (ABC) complex (Vectastain Elite, PK 6100), for 30 min at RT. For CD3 and GFAP, Polymere ImmPress®+ System (DAKO, MP-7451) was applied. Antigen-antibody complexes were visualized using AEC-substrate (abcam, ab64252), yielding red signal deposition. Slides were rinsed with deionized water, counterstained with Mayer's Hematoxylin for 10 min, and coverslipped using Aquatex (Merck).

Scoring of inflammatory cells

Inflammatory responses were assessed at 11–14, 28, 42, 105, and 190 dpi in eight anatomically defined brain regions: OB, AI, Pir, LEnt, S1, Sp5, TG and Cb. Regions of interest (ROIs) were defined according to *The Mouse Brain in Stereotaxic Coordinates* (61). Each region was systematically evaluated in standardized coronal brain sections : OB (L1), AI (L2/3), Pir (L2/3/4), LEnt (L5), S1 (L2/3/4), Sp5 (L6), Cb (L6), TG (L3/4) (S2 Fig). For regions analyzed at multiple levels, the highest score per region was recorded.

$CD3^+$ T-cell infiltration was semiquantitatively scored according to a published system (Table 2 (30)). Cas-3 was scored using the same criteria. $Iba1^+$ microglia/macrophages and $GFAP^+$ astrocytes were qualitatively assessed as present or absent (Table 3), based on glial activation regions with $CD3^+$ infiltration. All evaluations were perfomed at high-power (20x or 40x).

Table 2: Semiquantitative scoring of CD3 and cleaved caspase-3 immunoreactivity in murine brain sections.

score	CD3/ cleaved caspase-3
0	absent
1	<10 cells
2	11-20 cells
3	> 20 cells

The scoring system was applied to assess $CD3^+$ T cell infiltration and cleaved $caspase\text{-}3^+$ apoptotic cells across brain regions. Immunostaining for CD3 and cleaved caspase-3 was performed on coronal brain sections representing six anatomical levels. Selected regions of interest (ROIs) were evaluated; if multiple levels were available, the highest score per region was used. Scores ranged from 0 to 3 and were assigned according to the number of positive cells detected by light microscopy.

Table 3: Qualitative assessment of Iba1 and GFAP immunoreactivity in murine brain sections.

score	Iba- 1/ GFAP
-	absence of glial activation
+	glial activation/ cluster

Immunostaining for Iba1 and GFAP was performed on coronal brain sections representing six anatomical levels. Regions of interest (ROIs) were analyzed at these levels; if multiple levels were available, the highest score per region was recorded. Glial activation was assessed qualitatively and categorized as present (+) or absent (–), based on the presence of immunoreactive cells with reactive morphology.

In situ Hybridization (RNAscope™)

Detection of PrV mRNA transcripts was performed on FFPE sections (Fig 3A) using the RNAscope™ 2.5 HD Duplex Reagent Kit (ACD. Inc, Cat. No. 322430) (35).

A C1 probe targeting the lytic viral transcript UL19 (V-SHSV-UL19, 66973–68498 base pairs; ACD Inc., Cat. No. 548251) was detected as green punctate signals via horseradish peroxidase (HRP)-mediated chromogenic reaction.

A C2 probe targeting the large-latency transcript (LLT) region of the latency-associated transcript (LAT) (V-SuHV1-LLT-O2-C2, 94664-95952 base pairs, ACD. Inc, Cat. No. 1808611) was detected as red punctate signals by alkaline phosphatase (AP)-mediated chromogenic reaction (Fig 3B). Probes were mixed at a dilution of 1:50 (C2 in C1).

As technical control, the murine housekeeping gene - Ppib (Mm-Ppib, ACD Inc., Cat. No. 313911, C1), encoding the peptidyl-prolyl cis-trans isomerase B, was combined with ubiquitin C (Mm-Ubc, ACD. Inc, Cat. No. 310779, C2) at a dilution of 1:50 (C2 in C1). An Escherichia coli DapB probe (Duplex Negative Control Probe, ACD. Inc, Cat. No. 320759) served as negative control (S3 Fig).

Pre-treatment and hybridization:

Slides were baked at 60°C for 1 hour, deparaffinized in xylene (2x5 min), and rehydrated in 100% ethanol (2x1 min) at RT. After air-drying, endogenous peroxidase activity was quenched using hydrogen peroxide (H_2O_2; ACD Inc., Cat. No. 322330) for 10 min at RT. Target retrieval was performed by boiling slides in antigen retrieval buffer (ACD Inc., Cat. No. 322000) using a pressure cooker (Sichler, Germany, NX-3213-675) for 15 minutes. Slides were washed in distilled water, and dehydrated in 100% ethanol. After air-drying, sections were circumscribed with a hydrophobic barrier pen (Vector Laboratories, H-4000) to confine reagent application to the tissue area. Slides were then treated with Protease Plus (ACD Inc., Cat. No.322330) for 15 minutes at 40°C in the ACD HybEZ™ II Hybridization System (ACD Inc., Cat. No. 321711) (HybEZ oven). Slides were rinsed in distilled water and incubated with the specific probes and controls for 2 hours at 40 °C in the HybEZ oven, followed by two washes (2 minutes each) in the wash buffer (ACD Inc., Cat. No. 310091). Afterwards, the slides were stored overnight at RT in a 5X saline-sodium citrate buffer (SSC) (20X SSC, 1:4, diluted in distilled water; 20x SSC: 175 g of NaCl and 88 g of sodium citrate in 1 L distilled water, pH= 7.0).

Signal amplification and detection:

On the following day, slides were washed twice in wash buffer and preamplification was performed by applying amplicon (Amp) 1 for 30 minutes at 40 °C. Further amplification steps were carried out sequentially with Amp 2 (15 min) and Amp 3 (30 min), both at 40 °C. Detection of C2 (LAT) was achieved with Amp 4 (15 min at 40°C) in the HybEZ oven, followed by Amp 5 (30 min at RT), and the AP blocker Amp 6 (15 min at RT). For visualization of the red signal, slides were treated with a 1:60 mix of Red-B and Red-A (10min at RT). Detection of C1 (UL19) signal was performed using Amp 7-10 (Amp 7: 15mins, 40°C; Amp 8: 30mins, 40°C: HRP enzyme-solution; Amp 9: 30mins, RT; Amp 10: 15mins, RT), followed by green chromogenic development using a 1:50 mix of Green-B to Green-A (1:50) (10mins at RT). Between each step (Amp: 1-10 and chromogen development) slides were washed twice in wash buffer for 2 mins. Slides were counterstained with Mayer`s Hematoxylin (30 s at RT), blued in tap water (5min), dried at 60°C (15-30min) on a heat plate (MEDITE, BD00575) and cooled for 5 min. Finally,

586 slides were immersed in fresh xylene (5 min) and coverslipped using EcoMount (Biocare Medical,
587 BRR897L).

588 Semi quantitative analysis of *In-Situ* Hybridization

589 For the semi-quantitative analysis of PrV mRNA expression, eight anatomically defined brain regions
590 were analyzed as described in the section scoring of inflammatory cells. Each RNA transcript appeared
591 as a discrete chromogenic dot within the tissue section (LAT: red; Ul19: green). Signals were assessed
592 separately for UL19 and LAT in each predefined brain region. Scoring of positive cells was carried out
593 as illustrated in Fig 5, based on the number and distribution of RNA-positive signals within the ROI.
594 Briefly, punctate signals were scored on a scale from 0 to 3: score 0 represented no detectable signal,
595 score 1 corresponded to 1–20 signals, score 2 to 20–100 signals, and score 3 indicated more than 100
596 signals. Clustered signals were evaluated separately using scores 4 and 5, with score 4 assigned to 1–
597 20 clusters and score 5 to more than 20 clusters.

598 Real-time quantitative PCR (RT-qPCR)

599 Brains from six PrV-ΔUL21/US3Δkin- or mock-inoculated mice per time point (9-10, 21, 42, and 105 dpi,
600 study 1) were dissected into six regions: OB, Pir, TL, Cb, BS and TG. Tissues were homogenized in
601 PBS with 5mm steel-beads (Fabrikat Martin) using a bead beater (Retsch, MM200). Total RNA was
602 extracted using the QIAamp Viral RNA Mini Kit (Quiagen, Cat. No. 52904), and RT-qPCR was performed
603 to detect transcripts of UL19 (lytic gene) and the latency-associated transcript (LAT). Custom-designed
604 primers (Eurofins) were used for LAT, and validated primer-probe sets for UL19 were kindly provided
605 by Dr. Conrad Freuling, Friedrich-Loeffler-Institut, Greifswald-Insel Riems. Primer sequences are listed
606 in Table 4. β-actin served as the internal housekeeping gene. A long LAT oligomer was used both as a
607 standard for generating the calibration curve and as a positive control. The threshold cycle (Ct) cutoff
608 was set at 40, based on dilution series of the LAT standard. Reactions above this threshold were
609 considered negative.

610 A 200µl primer-mix was prepared, containing 100pmol each forward and reverse primer, 2,5µl of the
611 fluorophore-labelled probe, and 157,5µl of 0,1X TE buffer (pH 8,0). Each 20 µl PCR reaction consisted
612 of:10 µl ready-to-use mix (2x SensiFast Probe No-ROX One-Step mix), 0,2 reverse transcriptase, 0,4
613 RiboSafe RNase inhibitor, 0,6 µl RNase-free water, 1,6µl of each primer-mix and 4µl RNA template.
614 Amplification was performed using a Bio-Rad CFX96 thermal cycler under the following conditions:
615 reverse transcriptase treatment at 45 °C for 15 min, inactivation of the transcriptase at 95 °C for 2 min,
616 template denaturation at 95 °C for 15 sec, and annealing/amplification of the target cDNA at 60 °C for
617 40 sec (40 cycles). Fluorescence was measured during the elongation phase.

618

619 **Table 4. Primer sequences and characteristics for RT-qPCR detection of LAT and UL19**
620 **transcripts.**

name	sequence (5‘-> 3‘)	location*	size [bp]	G+C content [%]	annealing temperature
Lat2 Probe (411)	[FAM] GTC TTC ACC CCA GAT GAC CG [TAM]	95.994 – 96.013	20	60	61,4℃
LAT2 323 F	AGT TGA AGA CGG GGA CTC TG	95.906 – 95.925	20	55	59,4℃
LAT2 470 R	GTC GAC GGG GAA GAG GAT GA	96.034 – 96.053	20	60	61,4℃
LAT2-template (Oligomer)	CAG TTG AAG ACG GGG ACT CTG GGG CGG GCG CGA GAC CCA GAC CCG GAG CCC TGC CCT TCG GCC TCC TCG TGG CGC ACC TCC TCG GTA TAG TCT TCA CCC CAG ATG ACC GCG AAG CCC CCC CCT ACC GGC TCA TCC TCT TCC CCG TCG ACA	-	150	68	-
PrV-UL19-TEX	CGC AAC ACG CAC AAC GCC GCC	67.510 – 67.530	21	71,4	67,6
PrV-UL19 1817F	CGC AGT GCA TCC AGA GCT AC	67.487 – 67.506	20	60	61,4
PrV-UL19 1966R	CGT TGC CCA GGT AGG TGT TG	67.563 – 67.582	20	60	61,4

***| Genbank accession number: JF797218 (Suid herpesvirus 1 strain Kaplan, complete genome)**

Primer pairs were designed for quantitative PCR analysis targeting latency-associated transcript (LAT) and the lytic viral gene UL19 of PrV-ΔUL21/US3Δkin. The table lists primer sequences, expected amplicon sizes, GC content and melting temperatures (Tm) used for specific amplification.

Statistical analysis

Statistical analyses and graphical presentation were performed in GraphPad Prism 10.2.1 (GraphPad Software, Boston, USA).

Ct values obtained from RT-qPCR were analyzed by two-way analysis of variance (ANOVA) with Sidak's multiple comparison test. Geometric mean values of UL19 and LAT transcripts were compared between brain regions. Correlations between $CD3^+$ T-cell scores and UL19 RNA expression in corresponding brain regions were assessed using Spearman's rank correlation coefficient.

$p \leq 0.05$ was considered statistically significant and indicated by an asterisk in the figures.

Acknowledgements

The authors would like to thank Silvia Schuparis and Robin Brandt for their excellent technical assistance. We are particularly grateful to Conrad Freuling and Thomas Müller for their valuable advice on RT-qPCR methodology. We further acknowledge Angele Breithaupt, Tobias Britzke and Lukas M. Michaely for scientific discussion.

Ethics statement

Animal experiments were approved by the State Office for Agriculture, Food Safety and Fishery in Mecklenburg-Western Pomerania (LALFF M-V) with reference number 7221.3-1-034/ 22.

Data availability statement

All data supporting the findings of this study are included in the Supporting Information files and are available from the corresponding author upon request, in compliance with PLOS' data policy.

Conflict of interest

646 The authors have no conflicts of interest to declare that are relevant to the content of this article.

647 Funding statement

648 The project was funded by the Deutsche Forschungsgemeinschaft (DFG), grant number 466759708.

649 References

650 1. Koyuncu OO, MacGibeny MA, Enquist LW. Latent versus productive infection: the alpha herpesvirus
651 switch. Future Virol 2018; 13(6):431–43.

652 2. Spear PG, Eisenberg RJ, Cohen GH. Three classes of cell surface receptors for alphaherpesvirus
653 entry. Virology 2000; 275(1):1–8.

654 3. Mettenleiter TC. Pathogenesis of neurotropic herpesviruses: role of viral glycoproteins in
655 neuroinvasion and transneuronal spread. Virus Res 2003; 92(2):197–206.

656 4. Smith G. Herpesvirus transport to the nervous system and back again. Annu Rev Microbiol 2012;
657 66:153–76.

658 5. Hill JM, Lukiw WJ, Gebhardt BM, Higaki S, Loutsch JM, Myles ME et al. Gene Expression Analyzed
659 by Microarrays in HSV-1 Latent Mouse Trigeminal Ganglion Following Heat Stress. Virus Genes 2001;
660 23:273–80.

661 6. Hill TJ, Field HJ, Blyth WA. Acute and Recurrent Infection with Herpes Simplex Virus in the Mouse: a
662 Model for Studying Latency and Recurrent Disease. J. gen. ViroL 1975; 28:341–53.

663 7. Duarte LF, Farías MA, Álvarez DM, Bueno SM, Riedel CA, González PA. Herpes Simplex Virus Type
664 1 Infection of the Central Nervous System: Insights Into Proposed Interrelationships With
665 Neurodegenerative Disorders. Front Cell Neurosci 2019; 13:46.

666 8. Gutekunst DE, Pirtle EC, Miller LD, Stewart WC. Isolation of pseudorabies virus from trigeminal
667 ganglia of a latently infected sow. Am J Vet Res 1980; 41(8):1315–6.

668 9. Ben-Porat T, Kaplan AS. Molecular Biology of Pseudorabies Virus. In: Roizman B, editor. The
669 Herpesviruses: Volume 3. Boston, MA: Springer US; 1985. p. 105–73.

670 10. Pomeranz LE, Reynolds AE, Hengartner CJ. Molecular biology of pseudorabies virus: impact on
671 neurovirology and veterinary medicine. Microbiol Mol Biol Rev 2005; 69(3):462–500.

672 11. Mahjoub N, Dhorne-Pollet S, Fuchs W, Endale Ahanda M-L, Lange E, Klupp B et al. A 2.5-kilobase
673 deletion containing a cluster of nine microRNAs in the latency-associated-transcript locus of the

674 pseudorabies virus affects the host response of porcine trigeminal ganglia during established latency. J
675 Virol 2015; 89(1):428–42.

676 12. Anselmo A, Flori L, Jaffrezic F, Rutigliano T, Cecere M, Cortes-Perez N et al. Co-Expression of Host
677 and Viral MicroRNAs in Porcine Dendritic Cells Infected by the Pseudorabies Virus. PLoS One 2011;
678 6(3):e17374.

679 13. Gupta A, Gartner JJ, Sethupathy P, Hatzigeorgiou AG, Fraser NW. Anti-apoptotic function of a
680 microRNA encoded by the HSV-1 latency-associated transcript. Nature 2006; 442(7098):82–5.

681 14. Perng G-C, Jones C, Ciacci-Zanella J, Stone M, Henderson G, Yukht A et al. Virus-Induced Neuronal
682 Apoptosis Blocked by the Herpes Simplex Virus Latency-Associated Transcript. Science 2000;
683 287:1500–3.

684 15. Umbach JL, Kramer MF, Jurak I, Karnowski HW, Coen DM, Cullen BR. MicroRNAs expressed by
685 herpes simplex virus 1 during latent infection regulate viral mRNAs. Nature 2008; 454(7205):780–3.

686 16. Shen W, Sa e Silva M, Jaber T, Vitvitskaia O, Li S, Henderson G et al. Two small RNAs encoded
687 within the first 1.5 kilobases of the herpes simplex virus type 1 latency-associated transcript can inhibit
688 productive infection and cooperate to inhibit apoptosis. J Virol 2009; 83(18):9131–9.

689 17. Divito S, Cherpes TL, Hendricks RL. A Triple Entente: Virus, Neurons, and CD8+ T Cells Maintain
690 HSV-1 Latency. Immunologic Research 2006; 36:119–26.

691 18. Harrison K, Jones C. Regulation of herpes simplex virus type 1 latency-reactivation cycle and ocular
692 disease by cellular signaling pathways. Exp Eye Res 2022; 218:109017.

693 19. Cohen JI. Herpesvirus latency. J Clin Invest 2020; 130(7):3361–9.

694 20. Yao H-W, Ling P, Tung Y-Y, Hsu S-M, Chen S-H. In vivo reactivation of latent herpes simplex virus
695 1 in mice can occur in the brain before occurring in the trigeminal ganglion. J Virol 2014; 88(19):11264–
696 70.

697 21. Sivasubramanian MK, Monteiro R, Harrison KS, Plakkot B, Subramanian M, Jones C. Herpes
698 Simplex Virus Type 1 Preferentially Enhances Neuro-Inflammation and Senescence in Brainstem of
699 Female Mice. J Virol 2022; 96(17):e0108122.

700 22. Marcocci ME, Napoletani G, Protto V, Kolesova O, Piacentini R, Li Puma DD et al. Herpes Simplex
701 Virus-1 in the Brain: The Dark Side of a Sneaky Infection. Trends Microbiol 2020; 28(10):808–20.

702 23. Stahl JP, Mailles A. Herpes simplex virus encephalitis update. Curr Opin Infect Dis 2019; 32(3):239–
703 43.

704 24. Bradshaw MJ, Venkatesan A. Herpes Simplex Virus-1 Encephalitis in Adults: Pathophysiology,
705 Diagnosis, and Management. Neurotherapeutics 2016; 13(3):493–508.

706 25. Feng S, Liu Y, Zhou Y, Shu Z, Cheng Z, Brenner C et al. Mechanistic insights into the role of herpes
707 simplex virus 1 in Alzheimer's disease. Front Aging Neurosci 2023; 15:1245904.

708 26. Protto V, Marcocci ME, Miteva MT, Piacentini R, Li Puma DD, Grassi C et al. Role of HSV-1 in
709 Alzheimer's disease pathogenesis: A challenge for novel preventive/therapeutic strategies. Curr Opin
710 Pharmacol 2022; 63:102200.

711 27. Mettenleiter TC. Aujeszky's disease (pseudorabies) virus: the virus and molecular pathogenesis -
712 State of the art, June 1999. Vet. Res. 2000; 31(1):99–115.

713 28. Babic N, Mettenleiter TC, Ugolini G, Flamand A, Coulon P. Propagation of Pseudorabies Virus in
714 the Nervous System of the Mouse after Intranasal Inoculation. Virology 1994; 204:616–25.

715 29. Sehl J, Hölper JE, Klupp BG, Baumbach C, Teifke JP, Mettenleiter TC. An improved animal model
716 for herpesvirus encephalitis in humans. PLoS Pathog 2020; 16(3):e1008445.

717 30. Sehl-Ewert J, Schwaiger T, Schäfer A, Hölper JE, Klupp BG, Teifke JP et al. Clinical,
718 neuropathological, and immunological short- and long-term feature of a mouse model mimicking human
719 herpes virus encephalitis. Brain Pathol 2022; 32(3):e13031.

720 31. Armien AG, Hu S, Little MR, Robinson N, Lokensgard JR, Low WC et al. Chronic cortical and
721 subcortical pathology with associated neurological deficits ensuing experimental herpes encephalitis.
722 Brain Pathol 2010; 20(4):738–50.

723 32. Asenbauer B, McEntagart M, King MD, Gallagher P, Burke M, Farrell MA. Chronic active destructive
724 herpes simplex encephalitis with recovery of viral DNA 12 years after disease onset. Neuropediatrics
725 1998; 29(3):120–3.

726 33. Armangue T, Spatola M, Vlagea A, Mattozzi S, Cárceles-Cordon M, Martinez-Heras E et al.
727 Frequency, symptoms, risk factors, and outcomes of autoimmune encephalitis after herpes simplex
728 encephalitis: a prospective observational study and retrospective analysis. Lancet Neurol 2018;
729 17(9):760–72.

730 34. Osorio FA, Rock DL. A murine model of pseudorabies virus latency 1992; 12:39–42.

731 35. Wang F, Flanagan J, Su N, Wang L-C, Bui S, Nielson A et al. RNAscope: a novel in situ RNA
732 analysis platform for formalin-fixed, paraffin-embedded tissues. J Mol Diagn 2012; 14(1):22–9.

733 36. Niemeyer CS, Merle L, Bubak AN, Baxter BD, Gentile Polese A, Colon-Reyes K et al. Olfactory and
734 trigeminal routes of HSV-1 CNS infection with regional microglial heterogeneity. J Virol 2024:e0096824.

735 37. McFarland DJ, Hotchin J. Contrasting patterns of virus spread and neuropathology following
736 microinjection of herpes simplex virus into the hippocampus or cerebellum of mice. Journal of the
737 Neurological Sciences 1987; 79:255–65.

738 38. Wu H-M, Huang C-C, Chen S-H, Liang Y-C, Tsai J-J, Hsieh C-L et al. Herpes simplex virus type 1
739 inoculation enhances hippocampal excitability and seizure susceptibility in mice. Eur J Neurosci 2003;
740 18(12):3294–304.

741 39. Chee K, Razmara A, Geller AS, Harris WB, Restrepo D, Thompson JA et al. The role of the piriform
742 cortex in temporal lobe epilepsy: A current literature review. Front Neurol 2022; 13:1042887.

743 40. Costa B, Vale N. Virus-Induced Epilepsy vs. Epilepsy Patients Acquiring Viral Infection: Unravelling
744 the Complex Relationship for Precision Treatment. Int J Mol Sci 2024; 25(7).

745 41. Wouk J, Rechenchoski DZ, Rodrigues BCD, Ribelato EV, Faccin-Galhardi LC. Viral infections and
746 their relationship to neurological disorders. Archives of Virology 2021; 166(3):733–53.

747 42. Held K, Derfuss T. Control of HSV-1 latency in human trigeminal ganglia--current overview. J
748 Neurovirol 2011; 17(6):518–27.

749 43. Sivasubramanian MK, Monteiro R, Harrison KS, Plakkot B, Subramanian M, Jones C. Herpes
750 Simplex Virus Type 1 Preferentially Enhances Neuro-Inflammation and Senescence in Brainstem of
751 Female Mice. J Virol 2022; 96(17):e0108122.

752 44. Zhang S, Zeng J, Zhou Y, Gao R, Rice S, Guo X et al. Simultaneous Detection of Herpes Simplex
753 Virus Type 1 Latent and Lytic Transcripts in Brain Tissue. ASN Neuro 2022; 14:17590914211053505.

754 45. Kramer MF, Coen DM. Quantification of transcripts from the ICP4 and thymidine kinase genes in
755 mouse ganglia latently infected with herpes simplex virus. J Virol 1995; 69(3):1389–99.

756 46. Feldman LT, Ellison AR, Voytek CC, Yang L, Krause P, Margolis TP. Spontaneous molecular
757 reactivation of herpes simplex virus type 1 latency in mice. Proc Natl Acad Sci U S A 2002; 99(2):978–
758 83.

759 47. Liu T, Khanna KM, Chen X, Fink DJ, Hendricks RL. CD8(+) T cells can block herpes simplex virus
760 type 1 (HSV-1) reactivation from latency in sensory neurons. J Exp Med 2000; 191(9):1459–66.

761 48. Sawtell NM. Quantitative analysis of herpes simplex virus reactivation in vivo demonstrates that
762 reactivation in the nervous system is not inhibited at early times postinoculation. J Virol 2003;
763 77(7):4127–38.

764 49. Menendez CM, Jinkins JK, Carr DJJ. Resident T Cells Are Unable To Control Herpes Simplex Virus-
765 1 Activity in the Brain Ependymal Region during Latency. J Immunol 2016; 197(4):1262–75.

766 50. Sawtell NM, Poon DK, Tansky CS, Thompson RL. The latent herpes simplex virus type 1 genome
767 copy number in individual neurons is virus strain specific and correlates with reactivation. J Virol 1998;
768 72(7):5343–50.

769 51. Sawtell NM. The probability of in vivo reactivation of herpes simplex virus type 1 increases with the
770 number of latently infected neurons in the ganglia. J Virol 1998; 72(8):6888–92.

771 52. Jiang X, Chentoufi AA, Hsiang C, Carpenter D, Osorio N, BenMohamed L et al. The herpes simplex
772 virus type 1 latency-associated transcript can protect neuron-derived C1300 and Neuro2A cells from
773 granzyme B-induced apoptosis and CD8 T-cell killing. J Virol 2011; 85(5):2325–32.

774 53. Valyi-Nagy T, Olson SJ, Valyi-Nagy K, Montine TJ, Dermody TS. Herpes Simplex Virus Type 1
775 Latency in the Murine Nervous System Is Associated with Oxidative Damage to Neurons. Virology 2000;
776 278(2):309–21. Available from: URL:
777 https://www.sciencedirect.com/science/article/pii/S0042682200906780.

778 54. Nicoll J, Love S, Kinrade E. Distribution of herpes simplex virus DNA in the brains of human long-
779 term survivors of encephalitis. Neurosci Lett 1993; 157:215–8.

780 55. Cleaver J, Jeffery K, Klenerman P, Lim M, Handunnetthi L, Irani SR et al. The immunobiology of
781 herpes simplex virus encephalitis and post-viral autoimmunity. Brain 2024; 147(4):1130–48.

782 56. Himmelein S, St Leger AJ, Knickelbein JE, Rowe A, Freeman ML, Hendricks RL. Circulating herpes
783 simplex type 1 (HSV-1)-specific CD8+T cells do not access HSV-1 latently infected trigeminal ganglia.
784 Herpesviridae 2011; 2(1):5.

785 57. Kaplan AS, Vatter AE. A Comparison of Herpes Simplex and Pseudorabies Viruses. Virology 1959;
786 7:394–407.

787 58. Fuchs W, Backovic M, Klupp BG, Rey FA, Mettenleiter TC. Structure-based mutational analysis of
788 the highly conserved domain IV of glycoprotein H of pseudorabies virus. J Virol 2012; 86(15):8002–13.

789 59. Gage GJ, Kipke DR, Shain W. Whole animal perfusion fixation for rodents. J Vis Exp 2012; (65).

790 60. Rao DB, Little PB, Malarkey DE, Herbert RA, Sills RC. Histopathological evaluation of the nervous
791 system in National Toxicology Program rodent studies: a modified approach. Toxicol Pathol 2011;
792 39(3):463–70.

793 61. Paxinos G, Franklin KBJ. The Mouse Brain in Stereotaxic Coordinates. 2nd ed. San Diego:
794 Academic Press; 2001.

795

Supporting information

S1 Fig. Clinical condition of PrV-infected mice at euthanasia and corresponding heatmaps of UL19 and LAT gene expression across defined brain regions. (A) The clinical condition of each mouse at the time of euthanasia is shown in relation to corresponding gene expression. Mice marked with an asterisk (*) exhibited severe clinical signs and reached predefined humane endpoint criteria, necessitating euthanasia. (B, C) RT-qPCR was performed to quantify RNA transcripts of UL19 (B) and LAT (C) of PrV in selected brain regions (OB = olfactory bulb, Pir = piriform cortex, TL = temporal lobe, TG = trigeminal ganglion, Cb = cerebellum, BS = brainstem) at defined time points. Heatmaps were generated from Ct values to illustrate spatial and temporal patterns of viral gene expression. Lower Ct values (darker color intensity) indicate higher transcript abundance.

S2 Fig. Delineation of brain regions for semiquantitative analysis of immunohistochemistry and in situ hybridization. Anatomical boundaries of each brain region were defined according to The Mouse Brain in Stereotaxic Coordinates (Paxinos & Franklin, 2001). Colored overlays indicate the specific areas analyzed within coronal sections at levels 1-6. Yellow: olfactory bulb (OB); light green: primary somatosensory cortex (S1); orange: agranular insular cortex (AI); blue: piriform cortex (Pir); grey: trigeminal ganglion (TG); pink: hippocampus (Hpc); purple: lateral entorhinal cortex (LEnt); brown: cerebellum (Cb); dark green: spinal trigeminal nucleus (Sp5). Brain atlas images adapted from The Mouse Brain in Stereotaxic Coordinates (Paxinos & Franklin, 2001).

S3 Fig. Representative images of RNAscope™ detection in the murine brain. (A) Negative control probe targeting Escherichia coli DapB shows absence of specific signals, confirming assay specificity. (B) Positive control probes for murine Ppib (C1, green) and Ubc (C2, red) demonstrate robust and widespread expression in neuronal tissue, validating RNA integrity and hybridization efficiency. Scale bar = 250 µm.

S1 Table. Summary of clinical findings, histopathological diagnoses, and molecular analyses. Each mouse is listed with clinical signs, HE-based pathological evaluation, and corresponding scores from IHC and RNAscope™ (ISH). Animals that reached the humane endpoint are indicated with an asterisk (*). TG = trigeminal ganglion, Cb = cerebellum, Sp5 = spinal trigeminal nucleus, S1 = primary somatosensory cortex, Hpc = hippocampus, LEnt = lateral entorhinal cortex, Pir = piriform cortex, AI = agranular insular cortex, OB = olfactory bulb.

A

mouse	brain region	Ct value [LAT]	Ct value [UL19]	euthanasia [dpi]	clinical signs at time point of euthanasia
M18*	OB	20,95	19,22	10	Severely hunched back, weight loss >20%, moderate pruritus, seizure with recovery
	Pir	23,48	21,55		
	TL	25,47	23,59		
	TG	40	32,97		
	Cb	40	33,36		
	BS	40	29,63		
M19*	OB	21,31	19,05	10	seizure with recovery, severe hair loss (cheek)
	Pir	21,82	19,68		
	TL	23,24	21,2		
	TG	33,51	30,69		
	Cb	40	28,15		
	BS	31,18	28,79		
M20*	OB	21,09	19,51	10	severely hunched back, weight loss >20%
	Pir	20,98	19,12		
	TL	22,82	21,11		
	TG	31,09	29,11		
	Cb	40	32,57		
	BS	40	29,05		
M21*	OB	23,65	21,81	10	seizure with recovery, severely hunched back
	Pir	25,46	23,67		
	TL	27,14	25,27		
	TG	32,87	30,34		
	Cb	40	40		
	BS	33,09	28,38		
M22*	OB	20,26	18,65	9	severely hunched back
	Pir	23,21	21,18		
	TL	26,49	24,66		
	TG	33,9	29,94		
	Cb	40	30,92		
	BS	31,21	28,16		
M23	OB	40	40	21	-
	Pir	40	40		
	TL	40	40		
	TG	40	39,5		
	Cb	40	35,98		
	BS	40	36,15		
M24	OB	40	36,25	21	'stargazing', mild hunched back, ruffled fur
	Pir	40	35,24		
	TL	31,18	28,31		
	TG	40	37,71		
	Cb	40	40		
	BS	40	34,5		
M25	OB	31,39	29,5	21	focal seizures, focal hair loss on the head
	Pir	30,98	29,39		
	TL	32,43	29,17		
	TG	32,91	30,53		
	Cb	40	31,73		
	BS	31,02	29,56		
M26	OB	40	30,27	21	Unilateral blepharitis
	Pir	40	30,04		
	TL	40	30,83		
	TG	40	40		
	Cb	40	32,31		
	BS	40	32,96		
M27	OB	40	29,12	21	-
	Pir	40	34,24		
	TL	40	40		
	TG	40	32,56		
	Cb	40	33,13		
	BS	40	30,27		
M28	OB	29,82	27,86	21	-
	Pir	33,23	28,54		
	TL	32,51	29,09		
	TG	40	32,17		
	Cb	40	30,2		
	BS	29,15	27,66		

M29	OB	30,81	28,59	42	-
	Pir	29,62	28,07		
	TL	29,36	27,76		
	TG	31,52	30,09		
	Cb	40	40		
	BS	34,15	30,59		
M30	OB	40	29,24	42	-
	Pir	40	29,49		
	TL	40	29,37		
	TG	40	33,58		
	Cb	40	40		
	BS	40	30,1		
M31	OB	40	29,93	42	-
	Pir	40	29,34		
	TL	40	29,99		
	TG	40	40		
	CB	40	40		
	BS	40	30,61		
M32	OB	40	28,53	42	Focal hair loss on the nasal bridge and flank
	Pir	40	30,13		
	TL	40	28,41		
	TG	40	36,08		
	Cb	40	40		
	BS	40	32,42		
M33	OB	40	36,75	42	-
	Pir	40	38,25		
	TL	40	29,99		
	TG	40	38,84		
	Cb	40	40		
	BS	40	35,7		
M34	OB	30,06	28,91	42	-
	Pir	31,83	30,29		
	TL	32.37	29,51		
	TG	40	36,21		
	Cb	40	40		
	BS	40	30,86		
M35	OB	40	28,59	105	nasal bridge edema
	Pir	40	29,17		
	TL	40	31,33		
	TG	40	33,19		
	Cb	40	40		
	BS	40	31,1		
M36	OB	40	29,72	105	ruffled fur
	Pir	33,72	29,41		
	TL	40	30,37		
	TG	40	32,05		
	Cb	40	40		
	BS	32,26	30,23		
M37	OB	40	29,24	105	-
	Pir	40	30,46		
	TL	40	30,28		
	TG	40	36,28		
	Cb	40	40		
	BS	32,46	32,79		
M38	OB	40	27,91	105	-
	Pir	40	29,37		
	TL	40	28,95		
	TG	40	34,13		
	Cb	40	40		
	BS	40	31,2		
M39	OB	40	28,67	105	-
	Pir	40	30,22		
	TL	40	30,73		
	TG	40	34,81		
	Cb	40	40		
	BS	40	31,47		
M40	OB	40	32,22	105	-
	Pir	40	28,95		
	TL	40	30,09		
	TG	40	37,19		
	Cb	40	40		
	BS	40	35,42		

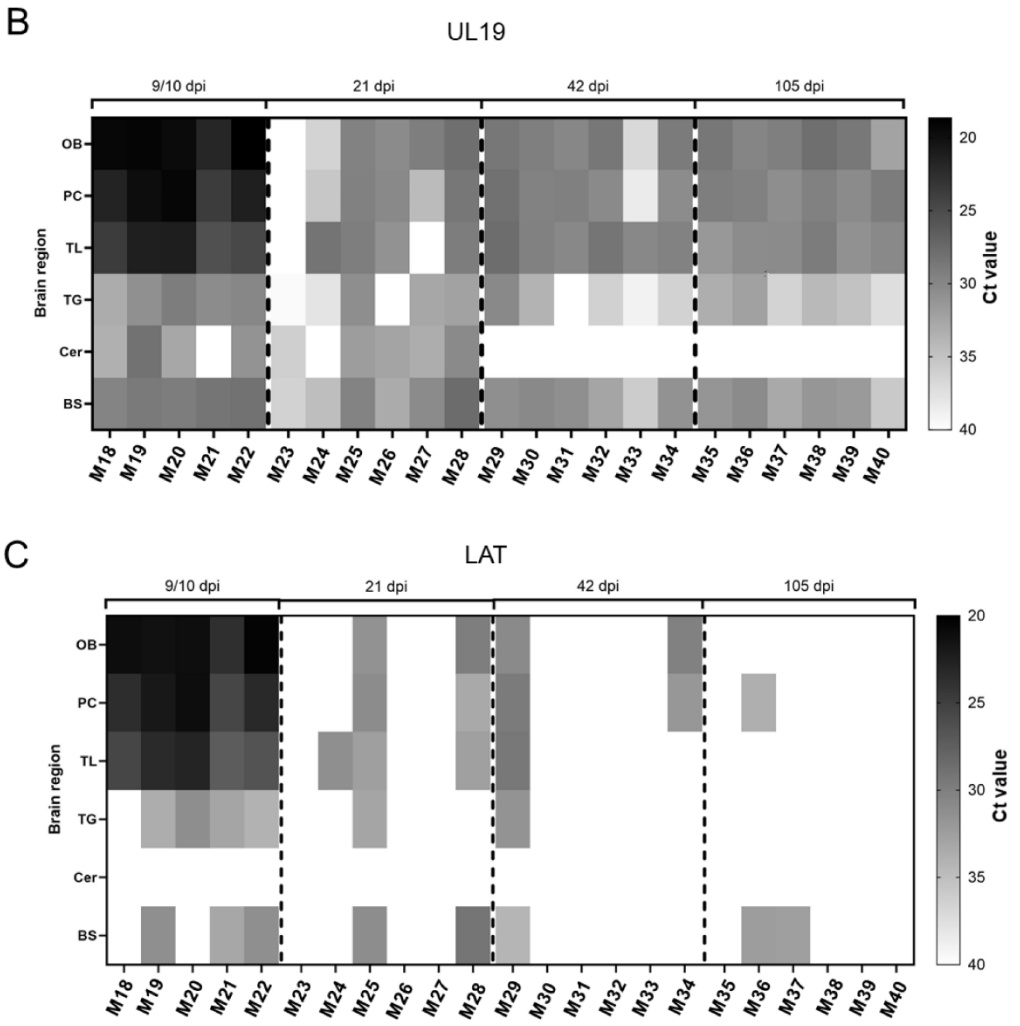

S1 Fig: Clinical condition of PrV-infected mice at euthanasia and corresponding heatmaps of UL19 and LAT gene expression across defined brain regions. (A) The clinical condition of each mouse at the time of euthanasia is shown in relation to corresponding gene expression. Mice marked with an asterisk (*) exhibited severe clinical signs and reached predefined humane endpoint criteria, necessitating euthanasia. (B, C) RT-qPCR was performed to quantify RNA transcripts of UL19 (B) and LAT (C) of PrV in selected brain regions (OB = olfactory bulb, Pir = piriform cortex, TL = temporal lobe, TG = trigeminal ganglion, Cb = cerebellum, BS = brainstem) at defined time points. Heatmaps were generated from Ct values to illustrate spatial and temporal patterns of viral gene expression. Lower Ct values (darker color intensity) indicate higher transcript abundance.

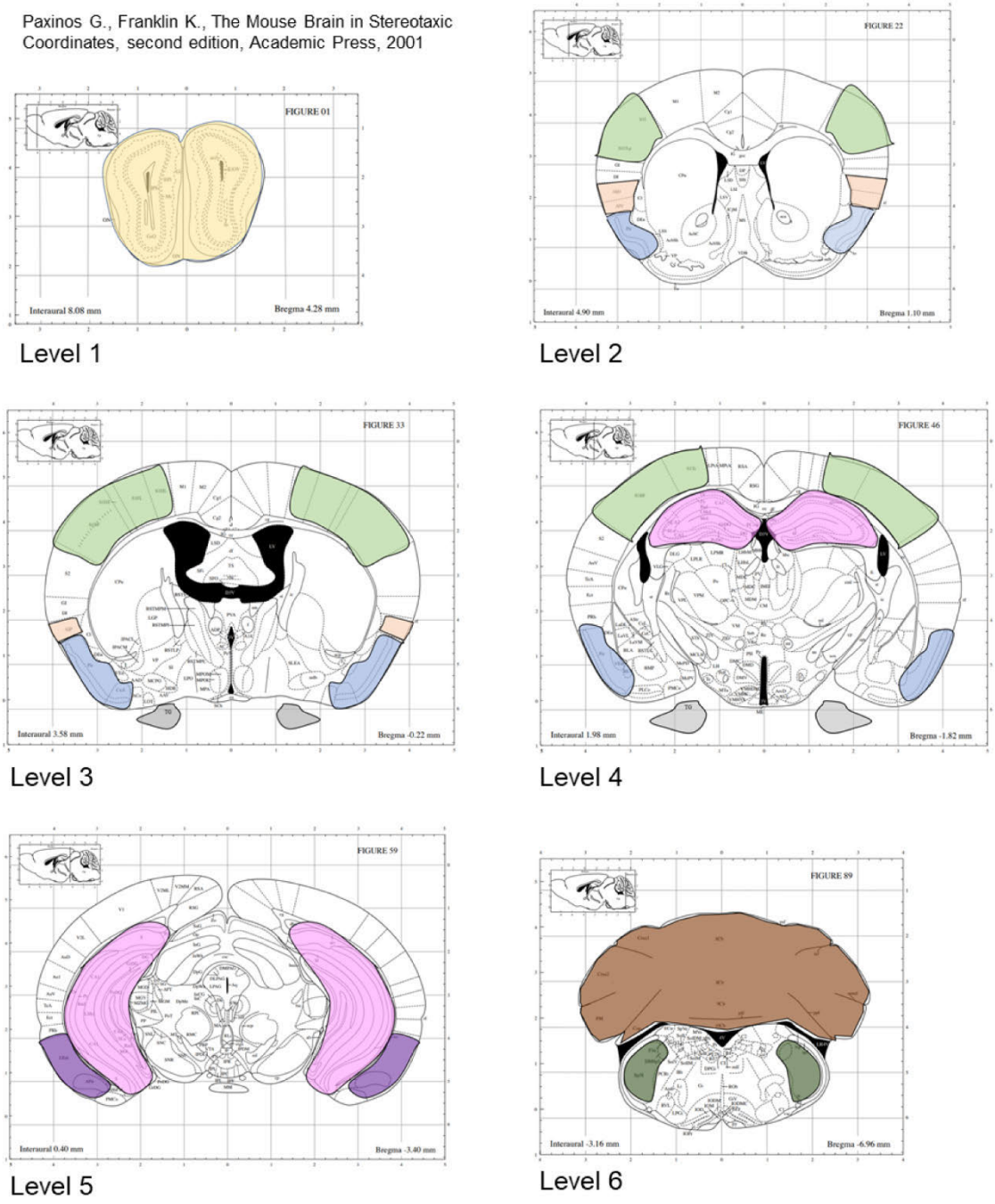

S2 Fig: Delineation of brain regions for semiquantitative analysis of immunohistochemistry and in situ hybridization. Anatomical boundaries of each brain region were defined according to The Mouse Brain in Stereotaxic Coordinates (Paxinos & Franklin, 2001). Colored overlays indicate the specific areas analyzed within coronal sections at levels 1-6. Yellow: olfactory bulb (OB); light green: primary somatosensory cortex (S1); orange: agranular insular cortex (AI); blue: piriform cortex (Pir); grey: trigeminal ganglion (TG); pink: hippocampus (Hpc); purple: lateral entorhinal cortex (LEnt); brown: cerebellum (Cb); dark green: spinal trigeminal nucleus (Sp5). Brain atlas images adapted from The Mouse Brain in Stereotaxic Coordinates (Paxinos & Franklin, 2001).

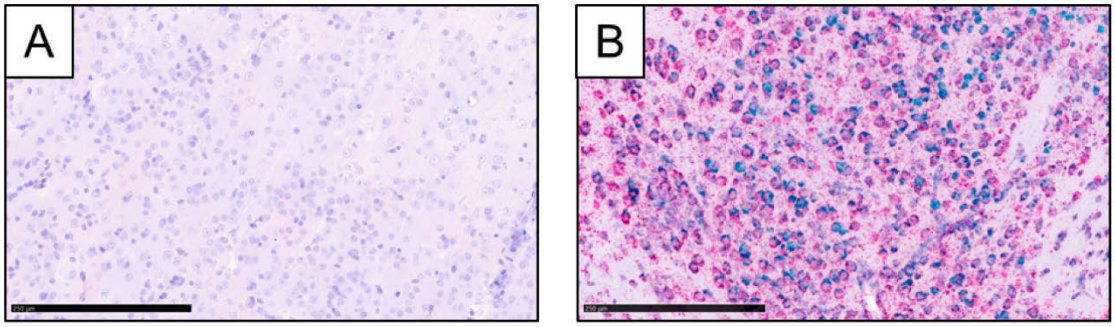

S3 Fig: Representative images of RNAscope™ detection in the murine brain. (A) Negative control probe targeting Escherichia coli DapB shows absence of specific signals, confirming assay specificity. (B) Positive control probes for murine Ppib (C1, green) and Ubc (C2, red) demonstrate robust and widespread expression in neuronal tissue, validating RNA integrity and hybridization efficiency. Scale bar = 250 µm.

mouse	inoculum, treatment	euthanasia [dpi]	clinical signs at euthanasia day	H&E	IHC/ RNAScope™ (ISH) Scoring/ brain region		OB	AI	Pir	Hpc	LEnt	S1	Sp5	TG	Cb
M1	PrV-ΔUL21/US3Δkin	11*	severely hunched back, ruffled and dull fur, hemorrhagic skin erosions, apathy	severe meningoencephalitis with extensive neuronal necrosis in Pir, Hpc and LEnt, meningeal and perivascular infiltrates of T-lymphocytes and histiocytes as well as glial activation in the temporal lobe (Pir, Hpc, LEnt), prefrontal cortex (AI) and Sp5	IHC	CD3	1	2	2	3	3	1	3	2	0
						Iba1	+	-	-	+	+	-	+	-	-
						GFAP	+	-	-	-	+	-	+	-	-
					ISH	LLT	1	4	5	4	5	4	1	0	0
						UL19	2	4	5	5	5	4	1	0	0
M2	PrV-ΔUL21/US3Δkin	14*	severely hunched back, ruffled and soiled fur, hemorrhagic skin erosions, seizure with recovery, moderate pruritus	severe meningoencephalitis with extensive neuronal necrosis in Pir and LEnt, meningeal and perivascular infiltrates of T-lymphocytes and histiocytes as well as glial activation in the temporal lobe (Pir, Hpc, LEnt), parietal lobe (S1), prefrontal cortex (AI) and Sp5	IHC	CD3	1	2	3	2	3	2	3	1	0
						Iba1	-	-	+	+	+	-	+	-	-
						GFAP	-	-	-	+	+	-	+	-	-
					ISH	LLT	1	4	4	4	4	0	1	0	0
						UL19	1	4	5	4	5	0	0	0	0
M3	PrV-ΔUL21/US3Δkin	14*	moderately hunched back, ruffled and dull fur, neck hair loss, nasal bridge edema, seizure with recovery	severe meningoencephalitis with extensive neuronal necrosis in S1, AI, Pir, Lent and Hpc, meningeal and perivascular infiltrates of T-lymphocytes and histiocytes as well as glial activation in the temporal lobe (Pir, Hpc, LEnt), parietal lobe (S1) and prefrontal cortex (AI)	IHC	CD3	1	3	3	3	3	3	1	1	1
						Iba1	-	+	+	+	+	+	+	-	-
						GFAP	-	+	+	+	+	+	-	-	-
						Cas3	0	3	3	2	3	1	0	0	0
					ISH	LLT	1	4	5	1	5	4	1	0	1
						UL19	1	4	5	4	5	5	4	0	1
M4	PrV-ΔUL21/US3Δkin	28	calm	Mild meningoencephalitis with single cell necrosis in Pir and LEnt, meningeal and perivascular infiltrates of T-lymphocytes and histiocytes as well as glial activation in the temporal lobe (Pir, Hpc, LEnt) and prefrontal cortex (AI)	IHC	CD3	0	2	2	2	2	1	0	1	0
						Iba1	-	+	+	-	+	-	+	-	+
						GFAP	-	+	+	-	+	-	+	-	-
						Cas3	0	0	1	0	1	0	0	0	0
					ISH	LLT	1	1	1	0	0	1	1	0	1
						UL19	1	1	1	1	1	1	1	1	0
M5	PrV-ΔUL21/US3Δkin	28	calm	Mild meningoencephalitis with single cell necrosis in Pir and LEnt, meningeal and perivascular infiltrates of T-lymphocytes and histiocytes as well as glial activation in the temporal lobe (Pir, Hpc, LEnt) and prefrontal cortex (AI)	IHC	CD3	1	3	3	3	3	0	1	1	0
						Iba1	+	-	+	+	+	-	+	-	-
						GFAP	-	-	+	+	+	-	-	-	-
					ISH	LLT	1	1	1	1	1	0	0	0	0
						UL19	1	2	2	3	2	2	0	1	0
M6	PrV-ΔUL21/US3Δkin	28	-	Mild meningoencephalitis with infiltrates of T-lymphocytes in the temporal lobe (Pir, Hpc)	IHC	CD3	0	1	2	2	1	0	1	0	0
						Iba1	-	-	-	-	-	-	-	-	-
						GFAP	+	-	-	-	-	-	+	-	-
					ISH	LLT	1	0	1	0	0	1	1	0	1

						UL19	0	1	1	2	1	1	1	1	1
M7	PrV-ΔUL21/US3Δkin	42	-	Mild meningoencephalitis with single cell necrosis in Pir and Hpc, meningeal and perivascular infiltrates of T-lymphocytes and histiocytes as well as glial activation in the temporal lobe (Pir, Hpc, LEnt), parietal lobe (S1) and prefrontal cortex (AI)	IHC	CD3	0	2	3	2	2	2	1	1	0
						Iba1	-	+	+	-	+	+	+	-	-
						GFAP	-	+	+	+	+	+	+	-	-
						Cas3	0	0	1	1	1	0	0	1	0
					ISH	LLT	1	2	2	3	1	2	4	0	1
						UL19	0	1	1	1	1	1	1	1	0
M8	PrV-ΔUL21/US3Δkin	42	-	Moderate meningoencephalitis with single cell necrosis in Pir, meningeal and perivascular infiltrates of T-lymphocytes and histiocytes as well as glial activation in the temporal lobe (Pir, Hpc, LEnt), parietal lobe (S1), prefrontal cortex (AI) and Cb	IHC	CD3	0	3	3	3	3	2	1	1	2
						Iba1	-	-	+	+	+	+	+	-	+
						GFAP	-	+	+	+	+	+	+	-	+
						Cas3	0	0	2	1	3	1	0	0	0
					ISH	LLT	0	1	1	1	1	1	1	0	0
						UL19	1	5	5	4	4	5	4	1	1
M9	PrV-ΔUL21/US3Δkin	42	'star gazing'	Moderate meningoencephalitis with single cell necrosis in Pir, LEnt and neuron loss in Hpc, meningeal and perivascular infiltrates of T-lymphocytes and histiocytes as well as glial activation in the temporal lobe (Pir, Hpc, LEnt)	IHC	CD3	1	2	3	3	3	2	1	1	1
						Iba1	-	-	+	+	+	-	+	-	+
						GFAP	-	-	+	+	+	-	+	-	-
						Cas3	0	1	3	3	3	0	0	0	0
					ISH	LLT	0	1	1	1	1	1	1	0	1
						UL19	1	2	3	2	2	2	2	1	1
M10	PrV-ΔUL21/US3Δkin	105	-	Mild meningoencephalitis with single cell necrosis in Pir and LEnt, meningeal and perivascular infiltrates of T-lymphocytes and histiocytes as well as glial activation in the temporal lobe (Pir, Hpc, LEnt)	IHC	CD3	0	1	3	2	3	2	1	n/a	1
						Iba1	-	+	+	+	+	-	-	n/a	-
						GFAP	-	-	+	+	+	-	-	n/a	-
					ISH	LLT	1	1	1	1	1	1	4	n/a	0
						UL19	1	3	4	3	3	4	3	n/a	1
M11	PrV-ΔUL21/US3Δkin	105	back hair loss	Mild meningoencephalitis with single cell necrosis in Pir and LEnt, meningeal and perivascular infiltrates of T-lymphocytes and histiocytes as well as glial activation in the temporal lobe (Pir, LEnt), prefrontal cortex (AI) and Sp5	IHC	CD3	1	2	3	1	3	2	2	n/a	1
						Iba1	-	+	+	-	+	-	+	n/a	-
						GFAP	-	+	+	-	+	-	-	n/a	-
					ISH	LLT	1	2	2	1	1	1	4	n/a	1
						UL19	1	1	2	2	3	3	1	n/a	0
M12	PrV-ΔUL21/US3Δkin	105	-	Mild meningoencephalitis with single cell necrosis in Pir and Hpc, meningeal and perivascular infiltrates of T-lymphocytes and histiocytes as well as glial activation in the	IHC	CD3	0	0	3	2	3	3	1	n/a	0
						Iba1	-	-	+	+	-	+	+	n/a	-

				temporal lobe (Pir, Hpc, Lent) and parietal lobe (S1)		GFAP	-	-	+	+	-	+	-	n/a	-
						Cas3	0	0	1	1	0	0	0	0	1
					ISH	LLT	0	1	1	2	1	1	4	n/a	0
						UL19	1	3	3	4	4	3	4	n/a	1
M13	PrV-ΔUL21/US3Δkin+ 170dpi cyclophosphamide/ dexamethasone treatment	190	-	Mild meningoencephalitis with single cell necrosis in Hpc, meningeal and perivascular infiltrates of T-lymphocytes and histiocytes as well as glial activation in the temporal lobe (Pir, Hpc, Lent) and parietal lobe (S1) and OB	IHC	CD3	2	1	2	3	2	2	1	1	0
						Iba1	+	-	+	+	+	+	-	-	-
						GFAP	-	-	+	+	+	-	-	-	-
					ISH	LLT	1	0	1	1	1	1	1	0	0
						UL19	0	0	1	1	0	1	0	1	0
M14	PrV-ΔUL21/US3Δkin+ 170dpi cyclophospahmide/ dexamethasone treatment	190	-	Mild meningoencephalitis with meningeal and perivascular infiltrates of T-lymphocytes and histiocytes as well as glial activation in the temporal lobe (Pir, Hpc) and prefrontal cortex (AI)	IHC	CD3	1	2	2	3	1	1	1	1	0
						Iba1	-	+	+	+	-	+	+	-	-
						GFAP	-	-	-	+	+	+	-	-	-
						Cas3	0	0	3	2	2	0	0	0	0
					ISH	LLT	1	1	1	1	1	1	1	0	0
						UL19	1	1	2	2	2	1	0	1	0
M15	PrV-ΔUL21/US3Δkin+ 170dpi cyclophospahmide/ dexamethasone treatment	190	calm	Mild meningoencephalitis with meningeal and perivascular infiltrates of T-lymphocytes and histiocytes as well as glial activation in the temporal lobe (Pir, LEnt) and OB	IHC	CD3	1	1	1	1	1	1	1	1	0
						Iba1	+	+	+	-	+	+	-	-	-
						GFAP	+	-	+	-	-	-	-	-	-
					ISH	LLT	2	1	2	2	1	2	1	0	1
						UL19	0	1	0	0	0	0	0	0	0
M16	mock + 170dpi cyclophospahmide/ dexamethasone treatment	190	-	-	IHC	CD3	0	0	0	0	0	0	0	0	0
						Iba1	-	-	-	-	-	-	-	-	-
						GFAP	-	-	-	-	-	-	-	-	-
						Cas3	0	0	3	1	1	0	0	0	0
					ISH	LLT	0	0	0	0	0	0	0	0	0
						UL19	0	0	0	0	0	0	0	0	0
M17	mock	21	-	-	IHC	CD3	0	0	0	0	0	0	0	0	0
						Iba1	-	-	-	-	-	-	-	-	-
						GFAP	-	-	-	-	-	-	-	-	-
						Cas3	0	0	0	0	0	0	0	0	0

					ISH	LLT	0	0	0	0	0	0	0	0	0
						UL19	0	0	0	0	0	0	0	0	0

S1 Table: Summary of clinical findings, histopathological diagnoses, and molecular analyses. Each mouse is listed with clinical signs, HE-based pathological evaluation, and corresponding scores from IHC and RNAscope™ (ISH). Animals that reached the humane endpoint are indicated with an asterisk (*). TG = trigeminal ganglion, Cb = cerebellum, Sp5 = spinal trigeminal nucleus, S1 = primary somatosensory cortex, Hpc = hippocampus, LEnt = lateral entorhinal cortex, Pir = piriform cortex, AI = agranular insular cortex, OB = olfactory bulb.

4 Contribution to publications

[I] Korff V, El-Debs I, Bröer S, Klupp BG, Teifke JP, Mettenleiter TC, Sehl-Ewert J (2025) Neurotropism of alphaherpesviruses is most prominent in the mesiotemporal, piriform and prefrontal cortices in mice. *Neuroscience* 584: 367–381, doi: 10.1016/j.neuroscience.2025.08.024,
Erratum: https://doi.org/10.1016/j.neuroscience.2025.10.037

Viktoria Korff	Generation of virus mutant PrV-ΔUL21gfp/US3Δkin; Mutant characterization in cell culture by growth kinetics, plaque assays and western blot analysis; Culturing and infection of primary neurons: analysis of growth kinetics and immunofluorescence; Conduction of animal experiments; Histological preparation of mouse brains; Preparation of brain sections with the vibratome; Examination of virus spread and nectin-1 distribution using immunofluorescence techniques; Imaging of immunofluorescence staining; Interpretation of data; Visualization of data; Writing and correction of the manuscript
Issam El-Debs	Participation in animal experiments; Correction and review of the manuscript
Sonja Bröer	Methodology
Barbara G. Klupp	Provision of mutant PrV-ΔUL21/US3Δkin and PrV-Kaplan-ΔgGgfp; Interpretation of data; Correction and review of the manuscript
Jens P. Teifke	Interpretation of data; Correction and review of the manuscript
Thomas C. Mettenleiter	Interpretation of data; Correction and review of the manuscript

Julia Sehl-Ewert	Conceptualization of the study; Interpretation of data; Preparation, correction and review of the manuscript; Corresponding authorship

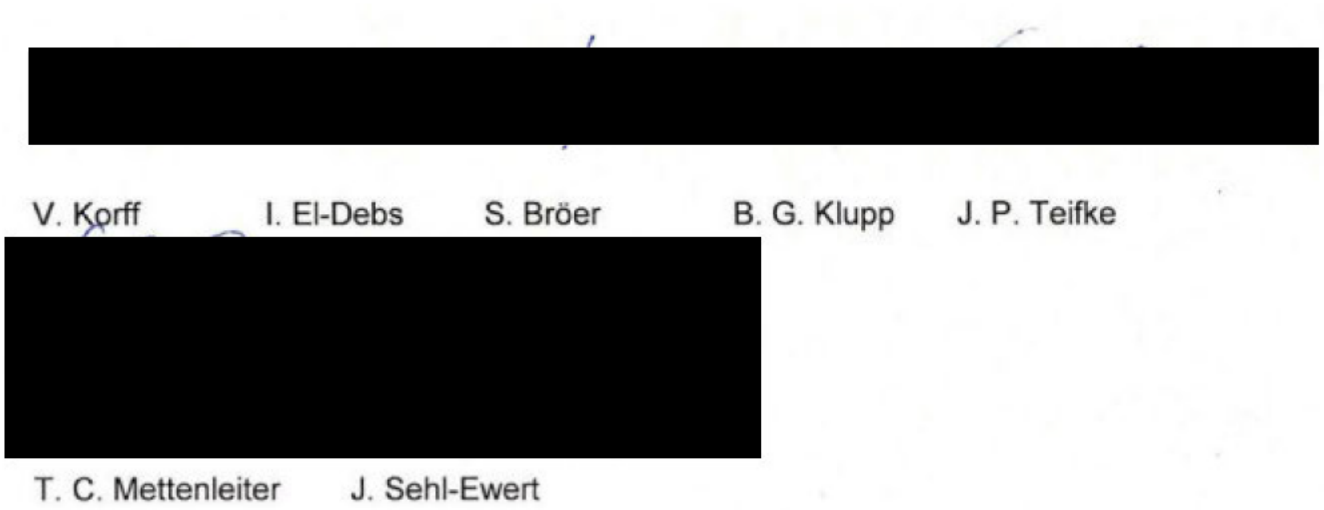

[II] Korff V, El-Debs I, Sehl-Ewert J (2025) Spatial and temporal mapping of early alphaherpesvirus invasion routes into the mouse central nervous system. J Neurovirol, doi: 10.1007/s13365-025-01278-3

Viktoria Korff	Conduction of animal experiments; Histological preparation of mouse brains; Preparation of brain sections with the cryostat; Examination of virus spread using immunofluorescence and in situ hybridization techniques; Imaging of immunofluorescence staining; Interpretation of data; Visualization of data; Writing and correction of the manuscript
Issam El-Debs	Participation in animal experiments; Correction and review of the manuscript
Julia Sehl-Ewert	Conceptualization of the study; Interpretation of data; Preparation, correction and review of the manuscript; Corresponding authorship

V. Korff I. El-Debs J. Sehl-Ewert

[III] Korff V, El-Debs I, Klupp BG, Teifke JP, Mettenleiter TC, Sehl-Ewert J (2025) Spatiotemporal dynamics of alphaherpesviral latency and reactivation in the murine central nervous system. bioRxiv, doi: 10.1101/2025.09.11.675502

Viktoria Korff	Conduction of animal experiments; Histological preparation of mouse brains; Examination of virus spread using in situ hybridization techniques; Pathohistological examination of inflammation using hematoxylin and eosin stain as well as immunohistochemistry; Interpretation of data; Visualization of data; Writing and correction of the manuscript
Issam El-Debs	Conduction of animal experiments, RT-qPCR analysis of infected brain tissue; Visualization of data; Writing and correction of the manuscript
Barbara G. Klupp	Interpretation of data; Correction and review of the manuscript
Jens P. Teifke	Interpretation of data; Correction and review of the manuscript
Thomas C. Mettenleiter	Interpretation of data; Correction and review of the manuscript
Julia Sehl-Ewert	Conceptualization of the study; Interpretation of data; Preparation, correction and review of the manuscript; Corresponding authorship

[redacted]

V. Korff I. El-Debs B. G. Klupp J. P. Teifke T. C. Mettenleiter

[redacted]

J. Sehl-Ewert

5 Results and general discussion

Alphaherpesviruses are characterized by their pronounced neurotropism and capacity to establish both acute and latent infections in the nervous system (Koyuncu et al., 2018). The closely related alphaherpesviruses HSV-1 and PrV are capable of invading neural tissues and triggering life-threatening encephalitis (Mettenleiter et al., 2019; Stahl and Mailles, 2019). In humans, HSV-1 infection can cause HSE, which predominantly affects the frontal and temporal lobes and manifests with severe inflammation, and subsequent acute neurological deficits as well as persistent cognitive and functional impairments (Raschilas et al., 2002; Steiner and Benninger, 2013; Gnann and Whitley, 2017):

Despite decades of research, key questions remain regarding (i) why distinct brain regions are selectively vulnerable, (ii) which anatomical pathways permit CNS access and (iii) how long-term infection dynamics unfold with respect to latency and reactivation? To address these gaps, we used a recently established CD-1 mouse model infected with the attenuated mutant PrV-ΔUL21/US3Δkin, which reproduces hallmark features of HSE (Sehl et al., 2020; Sehl-Ewert et al., 2022). Within this thesis, three complementary studies interrogated region- and cell type–specific susceptibility (**paper I**), the earliest routes of CNS entry after intranasal infection (**paper II**), and long-term brain infection dynamics including latency/reactivation (**paper III**). The following sections synthesize these results in a stepwise framework (clinical course → target regions and receptor biology → entry routes → long-term dynamics) to maintain logical continuity.

Before addressing the specific experimental objectives, we first characterized the clinical course of PrV-ΔUL21/US3Δkin infection to establish the temporal framework and biological reproducibility of the model.

5.1 Clinical course of PrV-ΔUL21/US3Δkin infection in mice

Across **papers I-III**, the clinical phenotype of PrV-ΔUL21/US3Δkin-infected mice was consistent. During the acute phase of infection, animals displayed nonspecific clinical signs (hunching, ruffled fur, reduced activity) plus neurological manifestations (seizures, “stargazing”) compatible with dysfunction in piriform and mesiotemporal structures (Hokkanen et al., 1997; Wu et al., 2003; Chee et al., 2022). Pruritus likely

reflected lesions in peripheral and central sensory pathways, with the neuroinflammatory response contributing to the pathophysiology (Laval and Enquist, 2020).

Differences in the onset of clinical signs and severity were closely linked to the inoculation route and target region. In **paper I**, stereotactic temporal lobe inoculation precipitated severe signs around 5 dpi, one to two days earlier than cerebellar inoculation, plausibly due to shorter network distance to susceptible limbic targets in the temporal lobe. Temporal inoculation produced seizures/behavioral changes early, while cerebellar inoculation yielded initial pruritus then behavioral abnormalities. Wild-type PrV-Ka caused severe pruritus and seizures ≤2 dpi underscoring the mutants attenuated phenotype (**paper I**). When compared to intranasal inoculation (Klopfleisch et al., 2004; Klopfleisch et al., 2006; Sehl et al., 2020), intracranial infection accelerated disease and increased severity, likely because direct parenchymal deposition of viral particles bypasses peripheral barriers and permits rapid neuroinvasion (McLean et al., 1989; Speck and Simmons, 1998).

In **paper II** (≤4 dpi after intranasal infection) no clinical signs were expectedly observed, consistent with first mild signs around 6 dpi (Sehl et al., 2020).

Paper III extended to 190 dpi and confirmed a multiphasic course (Sehl-Ewert et al., 2022): an acute phase (9-14dpi), followed by a partial recovery and possible late recurrences, including immunosuppression-triggered return of clinical signs around 170 dpi, paralleling long-term sequelae known from HSE (Marcocci et al., 2020; Wouk et al., 2021; Costa and Vale, 2024).

5.2 Objective 1: predilection sites - mesiotemporal lobe, piriform, and prefrontal cortex

Papers I–III (Sehl et al., 2020; Sehl-Ewert et al., 2022), consistently identified MTL, piriform, and prefrontal cortex as core targets, irrespective of the inoculation site – matching classic HSE pathology (Esiri, 1982; Taylor et al., 2005; Armien et al., 2010; Yong et al., 2021).

In **paper I**, both temporal and cerebellar stereotactic inoculations ultimately converged on MTL, Pir, and prefrontal cortices via brainstem – midbrain – thalamus/hypothalamus

between 5 and 7 dpi. Temporal lobe inoculation did not result in spread to the cerebellum, and cerebellar inoculation produced only sparse local infection, confirming low cerebellar permissiveness (McFarland and Hotchin, 1987; Sehl et al., 2020). Wild-type PrV-Ka showed a similar distribution, but appeared more restricted, likely because early euthanasia (rapid clinical decline) precluded full cortical spread. Future refinements (additional inoculation sites, lower titers) could test whether spread invariably converges on these cortical areas. **Paper II** showed that peripheral infection reaches the MTL within 72 hpi via ascending routes from peripheral sites, the OE and brainstem nuclei, corroborated by antigen and RNA detection. **Paper III** detected high viral transcript loads in MTL and Pir during 9–14 dpi in animals that reached humane endpoint criteria, with long-term histopathology showing transition from severe necrotizing meningoencephalitis to persistent lymphohistiocytic inflammation, gliosis and focal neuronal necrosis predominantly affecting MTL/Pir/prefrontal cortex.

Studies on the difference of cell-intrinsic susceptibility supported this pattern: in vitro infection of primary cerebral vs. cerebellar neurons (**paper I**) yielded higher titers in cerebral cultures for both mutant and wild-type PrV, suggesting intrinsic permissiveness differences. Analogous region-specificity is known for West Nile virus (Cho et al., 2013) and may relate to basal interferon-stimulated gene programs (Zhang et al., 2021) a candidate mechanism of future work.

Nectin-1 as a determinant of cortical vulnerability

To explain regional tropism mechanistically, **paper I** analyzed nectin-1, a key entry receptor for PrV/HSV-1 (Geraghty et al., 1998; Shukla et al., 2000; Spear et al., 2000). Nectin-1 is broadly expressed in brain tissue, but its regional distribution varies considerably (Haarr et al., 2001; Horváth et al., 2006; Lathe and Haas, 2017). In vitro, cerebral vs. cerebellar neurons showed no nectin-1 difference, likely reflecting model limitations (lack of cytoarchitecture and region-specific cellular composition). In vivo, high nectin-1 was mapped to MTL, Pir and prefrontal regions (high antigen levels) and low expression to cerebellum and V2 (minimal to no antigen detection), which align with murine/ human reference data (Prandovszky et al., 2008; Lathe and Haas, 2017). Our analysis showed no significant difference in nectin-1 distribution between PrV-infected and mock-treated mice, supporting inherent region-specific receptor levels - rather than infection-induced changes - as a major driver of tropism. This is

substantiated by recent work showing that nectin-1 knockout mice exhibit significantly improved survival following intranasal PrV challenge, underscoring the receptor's critical role in viral entry and pathogenesis (Tomioka et al., 2024). These findings indicate that both regional and neuronal population–specific factors, including receptor distribution, contribute to selective cortical vulnerability. Building on this, future studies employing genetically modified mouse models with reduced or altered nectin-1 expression may help to resolve remaining questions about its role in shaping neuroinvasion patterns and clinical outcomes.

5.3 Objective 2: entry routes - a multimodal cranial-nerve network with brainstem integration

Alphaherpesviruses invade the CNS via a multimodal network of cranial nerves that includes trigeminal, olfactory, glossopharyngeal–vagal, and hypoglossal pathways. These routes collectively enable widespread viral dissemination from peripheral entry sites into higher-order brain regions. Among them, the trigeminal and olfactory systems represent the principle conduits (Held and Derfuss, 2011; Steiner and Benninger, 2013; Mori, 2015; Sehl and Teifke, 2020; Niemeyer et al., 2024). Across **papers I-III** both pathways were prominently represented.

Trigeminal system

The trigeminal pathway emerges as one of the most reliable routes of CNS entry and spread. Across **papers I-III**, viral signals were consistently identified in Sp5 and S1, both core components of the trigeminal projection network (Landisman and Connors, 2007; García-Guillén et al., 2021). In **paper I**, additional viral antigen was found in the VPM, while **paper III** revealed viral transcripts in the TG, reinforcing the canonical anatomical chain TG - Sp5 - VPM - S1 (Shigenaga et al., 1979; Hattox and Nelson, 2007; Donovan and McCasland, 2008). These structures have previously been shown to harbor viral antigen in PrV-infected mice (Klopfleisch et al., 2004; Klopfleisch et al., 2006; Sehl et al., 2020). **Paper II** extended this trajectory to the periphery, demonstrating viral antigen in regions innervated by the maxillary, mandibular, and ophthalmic branches of the trigeminal nerve, including the palate, nasal mucosa and incisors (Grunditz et al., 1994; Naftel et al., 1999; Shankland, 2001; Prendergast, 2013; Fried and Gibbs, 2014; Yun et al., 2024).

Olfactory system

The olfactory pathway represents a second, equally critical route for CNS entry, particularly following intranasal infection. **Paper II** identified viral antigen in the OE and OB within 72 hpi, indicating rapid access to the forebrain. **Paper III** confirmed these findings by detecting viral transcripts in the OB, providing molecular evidence of olfactory neuroinvasion. While PrV-associated OE involvement had previously been documented only in pigs (Verpoest et al., 2017), our data demonstrate that PrV-ΔUL21/US3Δkin also targets these regions in mice - consistent with HSV-1 findings (Shivkumar et al., 2013; Niemeyer et al., 2024). Downstream of the OB, viral antigen was consistently found in MTL structures, particularly in the lateral entorhinal cortex (LEnt) and Pir, both of which maintain dense reciprocal connectivity with olfactory regions (Neville and Haberly, 2004; Kajiwara et al., 2007; Gretenkord et al., 2019; Stenwall et al., 2025). These areas serve as key relay stations linking olfactory input to limbic and prefrontal targets. Supporting this, **papers I** and **III** reported strong antigen signals in Pir, Hpc, MO and AI - regions engaged in odor information processing and emotion-related behavior (Boggian et al., 2000; Shivkumar et al., 2013; Menendez and Carr, 2017b).

Glossopharyngeal, vagal, and hypoglossal projections/pathways

Beyond these major routes, findings from **paper II** suggest that additional cranial nerves contribute to CNS entry and dissemination. Evidence for glossopharyngeal involvement (CN IX) includes viral antigen in the palate - a region innervated by glossopharyngeal fibers (Mu et al., 2021), and in the Sol and Amb, which represent primary sensory and motor nuclei of this nerve relay (Mizuno and Nomura, 1986; Standring, 2016). Both nuclei are functionally coupled to the vagus nerve (CN X): the Sol receive dense vagal afferents, and the Amb houses vagal motor neurons (Isabella and Moens, 2024; Chen and Liu, 2025). Hence, glossopharyngeal and vagal circuits likely cooperate in mediating ascending viral transport within the brainstem. Moreover, the detection of viral antigen in the 12N in **papers I** and **II** suggests that PrV may exploit overlapping motor pathways. This observation is consistent with the known connectivity between 12N, Sp5, and Sol (Borke et al., 1983; Guan et al., 1998; Okada et al., 2019; Guo et al., 2020) and supports the concept of cross-nerve dissemination.

Also, these findings correspond with previously documented neuroinvasion profiles of related alphaherpesviruses, including HSV-1 (Niemeyer et al., 2024).

Brainstem relay networks and ascending viral spread

The brainstem serves as a central hub and integrates these multimodal cranial-nerve circuits. Across **papers I-III**, the FR consistently exhibited viral antigen detection and appears to function as a key intersection linking trigeminal, glossopharyngeal-vagal, and hypoglossal networks, as well as MTL structures connected to the olfactory pathway (Baker et al., 1990; Hornung, 2003; Panneton and Gan, 2014). The FR is densely interconnected with the Sol, Amb, and 12N (Holstege and Kuypers, 1982; Borke et al., 1983; Streppel et al., 2000; Ruggiero et al., 2000; Nasse et al., 2008), providing a pipeline for viral exchange between sensory and motor systems.

Beyond the brainstem, thalamic and hypothalamic regions also exhibited viral antigen presence in **papers I** and **III**, implicating them as potential relay centers for ascending spread. The VPM of the thalamus, connects to the S1, while both the thalamus and hypothalamus maintain reciprocal projections with MTL, Pir, and prefrontal areas (Gehrlach et al., 2020; O'Leary et al., 2022; Qiu et al., 2024). Both structures are anatomically linked to the FR (Milsom et al., 2004; Wang, 2009), suggesting that once viral particles reach the reticular network, they can propagate toward higher cortical targets through established ascending pathways.

Experimental considerations

The choice of inoculation method becomes critical for accurately capturing neuroinvasion pathways. While stereotactic CNS injection (**paper I**) enables precise targeting, it bypasses physiologically relevant entry points such as the olfactory and trigeminal systems, and thus does not fully replicate natural exposure patterns. In contrast, the intranasal inoculation (**papers II** and **III)** closely replicates peripheral exposure, engaging both olfactory and trigeminal routes and, potentially, secondary activation of glossopharyngeal and hypoglossal circuits through accidental ingestion and swallowing reflexes (Jean, 2001; Milsom et al., 2004). Together, these findings support a multimodal entry model in which multiple cranial nerves cooperate in establishing CNS infection. The FR functions as an integration node, coordinating bidirectional spread between cranial-nerve nuclei and higher-order limbic regions. This

expanded view moves beyond the traditional dual-route concept and underscores the complex neuroanatomical basis of alphaherpesviral neuroinvasion.

5.4 Objective 3: long-term alphaherpesviral CNS infection dynamics - latent vs. lytic programs and immune correlates

In **paper III** long-term infection dynamics of PrV-ΔUL21/US3Δkin were analyzed up to 105 dpi using RNAscope™ and RT-qPCR for the latency marker LAT and the lytic gene UL19, encoding the major capsid protein (Hill et al., 1975; Klupp et al., 2004; Koyuncu et al., 2018).

During the acute phase (9–14 dpi), both transcripts were abundantly expressed in mesiotemporal, frontal and parietal lobes, consistent with high viral loads detected by RT-qPCR. By 28 dpi, transcript levels markedly declined. From 42 dpi onward, LAT stabilized at low levels, while UL19 varied among animals, indicating heterogenous reactivation propensities. These differences may reflect individual variation in latent genome copy numbers, which are known to influence reactivation likelihood (Sawtell, 1998; Sawtell et al., 1998). Accumulating evidence also suggests that abortive reactivations, defined by the initiation of lytic transcription without completion of the replication cycle, occur frequently. In such cases, lytic transcripts are detectable, but corresponding proteins are absent, indicating that viral replication is halted prematurely. This interruption likely results from robust intrinsic antiviral responses within neurons, which possess cell-intrinsic mechanisms capable of sensing and suppressing viral gene expression (Ma et al., 2014).

Importantly, the consistency between RNAscope™ and RT-qPCR data reinforces the reliability of these findings. However, minor discrepancies particularly observed in the olfactory bulb likely arise from methodological resolution, as whole-tissue analysis captures viral genomes below the detection threshold of section-based imaging.

Unexpectedly, LAT was not detected in the trigeminal ganglion, the canonical site of alphaherpesviral latency (Pomeranz et al., 2005; Held and Derfuss, 2011; Koyuncu et al., 2018). Instead, LAT was consistently present in brainstem regions, particularly in Sp5, supporting previous reports suggesting that brainstem neurons may preferentially harbor latent genomes (Yao et al., 2014; Sivasubramanian et al., 2022).

Single-cell analysis revealed a temporal shift from frequent co-expression of LAT and UL19 during early infection toward mutually exclusive transcription of either LAT or UL19 after 28 dpi, indicating a transition from an initial mixed state to stable latent or lytic programs (Kramer and Coen, 1995; Liu et al., 2000; Feldman et al., 2002; Sawtell, 2003; Zhang et al., 2022).

Long-term histopathology focusing on immune correlates, further substantiated these findings. The pattern of CNS pathology evolved from an acute necrotizing meningoencephalitis to a persistent state characterized by lymphohistiocytic infiltration, gliosis, and focal neuronal necrosis in anatomically predisposed regions. T-cell aggregates co-localized with UL19-rich regions at 11–14 and 42 dpi, indicating sites where viral reactivation has likely occurred and elicited an immune response (Held and Derfuss, 2011). Consistent with HSV-1 studies, $CD8^+$ T cells are thought to suppress further viral reactivation in an antigen-specific manner (Liu et al., 2000), whereas LAT transcripts may counteract immune pressure by inhibiting apoptosis through caspase-3 modulation (Jiang et al., 2011). Positive regions of cleaved caspase-3 overlapped with areas of high UL19 expression and dense T-cell infiltration, indicating that lytic activity triggers immune effector engagement, and subsequent apoptotic neuronal loss. Collectively, these findings indicate that alphaherpesviral persistence within the brain is accompanied by sustained neuroinflammatory processes that may modulate the dynamics of viral reactivation.

Future studies should refine these correlations by immunophenotyping infiltrating T cells ($CD4^+$ vs. $CD8^+$), evaluating effector markers such as granzyme B and intracellular IFN-γ, and profiling chemokine axes (CXCL9/10, CCL5) to discriminate between abortive, subclinical, and productive reactivation.

In a targeted reactivation experiment (**paper III)**, long-term infected mice received cyclophosphamide and dexamethasone at 170 dpi, followed by euthanasia 20 days post-treatment (dpt). Moderate clinical signs emerged around 5 dpt, and by 20 dpt low-level LAT and UL19 signals were detectable accompanied by sparse T-cell infiltration — consistent with glucocorticoid-induced lymphodepletion (Himmelein et al., 2011). These findings suggest that reactivation may have occurred earlier than sampling, highlighting the need for shorter treatment-to-sampling intervals to accurately capture peak lytic activity.

Together, these results support three non-exclusive patterns of long-term CNS infection: (i) episodic, abortive reactivation or (ii) episodic, often subclinical reactivation marked by focal UL19 expression and T-cell clustering, and (iii) chronic, low-grade infection with persistent inflammation and low-level viral transcription. Both scenarios (ii, iii) parallel findings from long-term HSV-1 studies (Nicoll et al., 1993; Asenbauer et al., 1998; Valyi-Nagy et al., 2000; Armien et al., 2010).

Beyond direct viral effects, long-term CNS infections may have broader implications. Recurrent HSV-1 reactivations have been associated with cognitive decline, amnestic mild cognitive impairment (aMCI) and Alzheimer's disease (AD). Epidemiological and molecular evidence links HSV-1 reactivation to altered APP metabolism, amyloid-β deposition, and increased anti-HSV-1 IgG avidity (Kobayashi et al., 2013; Readhead et al., 2018; Marcocci et al., 2020).

In addition, post-infectious autoimmune responses such as anti-NMDAR encephalitis may further exacerbate cognitive impairment (Cleaver et al., 2024). Given its limbic predilection and intermittent lytic activity, the PrV-ΔUL21/US3Δkin model provides a translational framework to investigate such mechanisms. Future long-term studies combining transcriptomic profiling, serology, amyloid-β immunohistochemistry, and screening for anti-NMDAR antibodies could elucidate how recurrent alphaherpesviral reactivation contributes to progressive neurodegeneration.

5.5 Conclusion

This thesis provides an integrated analysis of alphaherpesviral neuroinvasion, persistence, and neuropathogenesis using the PrV-ΔUL21/US3Δkin mouse model, which closely reproduces key clinical and histopathological features of human HSE. Across three complementary studies, the work delineates a coherent framework that links regional and cellular susceptibility (**paper I**), multimodal cranial-nerve–mediated entry routes (**paper II**), receptor-dependent cortical tropism (**paper I**), and the long-term balance between latent and lytic viral programs (**paper III**).

The results identify the mesiotemporal lobe, piriform, and prefrontal cortices as core target regions, reflecting both anatomical connectivity and high nectin-1 expression as determinants of cortical vulnerability (**paper I**). Neuroanatomical tracing across multiple inoculation routes demonstrates that PrV accesses the CNS through a

complex cranial-nerve network — including trigeminal, olfactory, glossopharyngeal-vagal, and hypoglossal pathways — that converge in the brainstem and enable ascending viral dissemination (**paper II**). This integrated circuitry provides a structural basis for the selective involvement of limbic and associative cortices characteristic of HSE.

Long-term analyses reveal persistent low-grade infection and episodic abortive or subclinical reactivation events within the CNS, associated with T-cell infiltration, apoptotic neuronal loss, and region-specific viral transcription patterns (**paper III**). The identification of LAT expression within brainstem nuclei rather than trigeminal ganglia supports an expanded concept of central latency reservoirs. Together, these findings underscore that alphaherpesviral persistence in the brain represents a dynamic equilibrium between immune control and viral reactivation potential, accompanied by neuroinflammatory processes that may shape long-term outcomes.

Beyond its mechanistic insights, the PrV-ΔUL21/US3Δkin model establishes a translationally relevant system to study post-infectious sequelae, including neuroinflammation, cognitive decline, and putative links to neurodegenerative and autoimmune disorders. As such, it provides a robust platform for future investigations into the molecular and immunological determinants of alphaherpesvirus-induced neuropathology and long-term CNS dysfunction.

6 Summary

Alphaherpesviruses such as HSV-1 and PrV exhibit pronounced neurotropism and the ability to establish acute and latent infections within the nervous system. To elucidate key determinants of alphaherpesviral neuroinvasion and persistence, this thesis employed the attenuated mutant PrV-ΔUL21/US3Δkin in CD-1 mice, which reproduces hallmark features of human HSE.

Through a combination of targeted stereotactic and intranasal infection models, three principal aspects were addressed: (i) regional and cell type–specific neuronal susceptibility, (ii) anatomical pathways of early CNS entry, and (iii) long-term infection dynamics including latency and reactivation.

The studies identified the mesial temporal, piriform, and prefrontal cortices as core targets, linked to high nectin-1 expression and specific anatomical connectivity. Neuroanatomical mapping revealed that PrV gains CNS access via a multimodal cranial-nerve network encompassing trigeminal, olfactory, glossopharyngeal-vagal, and hypoglossal routes converging in the brainstem. Long-term analyses demonstrated persistent, low-grade infection and episodic abortive or subclinical reactivation associated with neuroinflammatory responses, indicating a predominantly central establishment of viral latency that extends the current understanding of alphaherpesviral persistence to include central neuronal reservoirs in addition to peripheral ganglia.

Collectively, these findings establish the PrV-ΔUL21/US3Δkin model as a robust and translationally relevant system for dissecting regional and receptor-dependent neurotropism, multimodal cranial-nerve-mediated CNS entry, and the central dynamics of alphaherpesviral latency and reactivation.

7 Zusammenfassung

Alphaherpesviren wie HSV-1 und PrV zeichnen sich durch ihren ausgeprägten Neurotropismus sowie die Fähigkeit aus, sowohl akute als auch latente Infektionen im Nervensystem zu etablieren. Zur Identifizierung zentraler Determinanten der alphaherpesviralen Neuroinvasion und Persistenz wurden in dieser Arbeit CD-1-Mäuse mit der attenuierten Pseudorabiesvirusmutante PrV-ΔUL21/US3Δkin infiziert, die charakteristischen Merkmale der humanen Herpes-simplex-Enzephalitis (HSE) reproduziert.

Mittels einer Kombination aus gezielten stereotaktischen und intranasalen Infektionsmodellen wurden drei Hauptaspekte untersucht: (i) regionale und zelltypspezifische neuronale Vulnerabilität, (ii) anatomische Eintrittspfade in das ZNS sowie (iii) Langzeitverläufe der Infektion einschließlich Latenz und Reaktivierung.

Die Untersuchungen identifizierten die mesialen Temporallappen, den piriformen und den präfrontalen Kortex als zentrale Zielregionen alphaherpesviraler Infektion, die mit einer hohen Nectin-1-Expression und spezifischer anatomischer Konnektivität korrelierten. Eine neuroanatomische Kartierung zeigte, dass PrV über ein multimodales Hirnnervennetzwerk Zugang zum ZNS erhält, das trigeminale, olfaktorische, glossopharyngeal-vagale und hypoglossale Bahnen umfasst und im Hirnstamm konvergiert. Langzeitanalysen belegten eine geringgradige, persistierende Infektion sowie episodische, abortive oder subklinische Reaktivierungen, die mit neuroinflammatorischen Reaktionen einhergingen. Die Befunde sprechen für eine überwiegend zentrale Etablierung viraler Latenz und erweitern damit das bisherige Verständnis alphaherpesviraler Persistenz in peripheren Ganglien um zentrale neuronale Reservoirs.

Zusammenfassend etabliert das PrV-ΔUL21/US3Δkin-Modell ein robustes und translational relevantes System zur Untersuchung regionaler und rezeptorabhängiger Neurotropie, multimodaler hirnnervenvermittelter ZNS-Invasion sowie zentraler Dynamiken alphaherpesviraler Latenz und Reaktivierung.

8 References

Albà, M. M., Das, R., Orengo, C. A. and Kellam, P. (2001) 'Genomewide function conservation and phylogeny in the Herpesviridae', *Genome research*, vol. 11, no. 1, pp. 43–54.

Alsweed, A., Alsuhibani, M., Casanova, J.-L. and Al-Hajjar, S. (2018) 'Approach to recurrent Herpes Simplex Encephalitis in children', *International journal of pediatrics & adolescent medicine*, vol. 5, no. 2, pp. 35–38.

Amunts, K., Kedo, O., Kindler, M., Pieperhoff, P., Mohlberg, H., Shah, N. J., Habel, U., Schneider, F. and Zilles, K. (2005) 'Cytoarchitectonic mapping of the human amygdala, hippocampal region and entorhinal cortex: intersubject variability and probability maps', *Anatomy and Embryology*, vol. 210, 5-6, pp. 343–352.

Angeloni, C. and Geffen, M. N. (2018) 'Contextual modulation of sound processing in the auditory cortex', *Current opinion in neurobiology*, vol. 49, pp. 8–15.

Arbuthnot, W., MacLeod, N. K., Maxwell, D. J. and Wright, A. K. (1990) 'istribution and synaptic contacts of the cortical terminals arising from neurons in the rat ventromedial thalamic nucleus', *Neuroscience*, vol. 38, pp. 47–60.

Armien, A. G., Hu, S., Little, M. R., Robinson, N., Lokensgard, J. R., Low, W. C. and Cheeran, M. C.-J. (2010) 'Chronic cortical and subcortical pathology with associated neurological deficits ensuing experimental herpes encephalitis', *Brain pathology (Zurich, Switzerland)*, vol. 20, no. 4, pp. 738–750.

Asenbauer, B., McEntagart, M., King, M. D., Gallagher, P., Burke, M. and Farrell, M. A. (1998) 'Chronic active destructive herpes simplex encephalitis with recovery of viral DNA 12 years after disease onset', *Neuropediatrics*, vol. 29, no. 3, pp. 120–123.

Aubert, M., Krantz, E. M. and Jerome, K. R. (2006) 'Herpes Simplex Virus Genes Us3, Us5, and Us12 Differentially Regulate Cytotoxic T Lymphocyte-Induced Cytotoxicity', *Viral Immunology*, vol. 19, no. 3, pp. 391–408.

Babic, N., Mettenleiter, T. C., Ugolini, G., Flamand, A. and Coulon, P. (1994) 'Propagation of Pseudorabies Virus in the Nervous System of the Mouse after Intranasal Inoculation', *Virology*, vol. 204, pp. 616–625.

Baines, J. D., Koyama, A. H., Huang, T. and Roizman, B. (1994) 'The UL21 gene products of herpes simplex virus 1 are dispensable for growth in cultured cells', *Journal of Virology*, vol. 68, no. 5, pp. 2929–2936.

Baker, K. G., Halliday, G. M. and Törk, I. (1990) 'Cytoarchitecture of the human dorsal raphe nucleus', *The Journal of comparative neurology*, vol. 301, no. 2, pp. 147–161.

Baringer, J. R. and Pisani, P. (1994) 'Herpes simplex virus genomes in human nervous system tissue analyzed by polymerase chain reaction', *Annals of neurology*, vol. 36, no. 6, pp. 823–829.

Barrios, A. W., Núñez, G., Sánchez Quinteiro, P. and Salazar, I. (2014) 'Anatomy, histochemistry, and immunohistochemistry of the olfactory subsystems in mice', *Frontiers in neuroanatomy*, vol. 8, p. 63.

Baumel, J. J. (1974) 'Trigeminal-facial nerve communications. Their function in facial muscle innervation and reinnervation', *Archives of otolaryngology (Chicago, Ill.: 1960)*, vol. 99, no. 1, pp. 34–44.

Bearer, E. L. (2012) 'HSV, Axonal Transport and Alzheimer ‘s Disease: in Vitro and in Vivo Evidence for Causal Relationships', *Future virology*, vol. 7, no. 9, pp. 885–899.

Begemann, K., Rawashdeh, O., Olejniczak, I., Pilorz, V., Assis, L. V. M. de, Osorio-Mendoza, J. and Oster, H. (2025) 'Endocrine regulation of circadian rhythms', *npj Biological Timing and Sleep*, vol. 2, no. 1, p. 10.

Benetti, L., Munger, J. and Roizman, B. (2003) 'The Herpes Simplex Virus 1 US3 Protein Kinase Blocks Caspase-Dependent Double Cleavage and Activation of the Proapoptotic Protein BAD', *Journal of Virology*, vol. 77, no. 11, pp. 6567–6573.

Benetti, L. and Roizman, B. (2007) 'In Transduced Cells, the US3 Protein Kinase of Herpes Simplex Virus 1 Precludes Activation and Induction of Apoptosis by Transfected Procaspase 3', *Journal of Virology*, vol. 81, no. 19, pp. 10242–10248.

Ben-Porat, T. and Kaplan, A. S. (1985) 'Molecular Biology of Pseudorabies Virus', in Roizman, B. (ed) *The Herpesviruses: Volume 3,* Boston, MA, Springer US, pp. 105–173.

Ben-Porat, T., Ann Veach, R. and Ihara, S. (1983) 'Localization of the regions of homology between the genomes of herpes simplex virus, type 1, and pseudorabies virus', *Virology*, 127 1, pp. 194–204 [Online]. Available at https:// api.semanticscholar.org/CorpusID:32746619.

Boggian, I., Buzzacaro, E., Calistri, A., Calvi, P., Cavaggioni, A., Mucignat-Caretta, C. and Palu, G. (2000) 'Asymptomatic herpes simplex type 1 virus infection of the mouse brain', *Journal of neurovirology*, vol. 6, no. 4, pp. 303–313.

Booss, J. and Kim, J. H. (1984) 'Biopsy histopathology in herpes simplex encephalitis and in encephalitis of undefined etiology', *The Yale journal of biology and medicine*, vol. 57, no. 5, pp. 751–755.

Borich, M. R., Brodie, S. M., Gray, W. A., Ionta, S. and Boyd, L. A. (2015) 'Understanding the role of the primary somatosensory cortex: Opportunities for rehabilitation', *Neuropsychologia*, vol. 79, Pt B, pp. 246–255.

Borke, R. C., Nau, M. E. and Ringler, R. L., JR (1983) 'Brain stem afferents of hypoglossal neurons in the rat', *Brain Research*, vol. 269, no. 1, pp. 47–55.

Bradshaw, M. J. and Venkatesan, A. (2016) 'Herpes Simplex Virus-1 Encephalitis in Adults: Pathophysiology, Diagnosis, and Management', *Neurotherapeutics: the journal of the American Society for Experimental NeuroTherapeutics*, vol. 13, no. 3, pp. 493–508.

Brdovčak, M. C., Zubković, A. and Jurak, I. (2018) 'Herpes Simplex Virus 1 Deregulation of Host MicroRNAs', *Non-coding RNA*, vol. 4, no. 4.

Briscoe, S. D. and Ragsdale, C. W. (2019) 'Evolution of the Chordate Telencephalon', *Current biology : CB*, vol. 29, no. 13, R647-R662.

Brozzetti, L., Sacchetto, L., Cecchini, M. P., Avesani, A., Perra, D., Bongianni, M., Portioli, C., Scupoli, M., Ghetti, B., Monaco, S., Buffelli, M. and Zanusso, G. (2020) 'Neurodegeneration-Associated Proteins in Human Olfactory Neurons Collected by Nasal Brushing', *Frontiers in neuroscience*, Volume 14 - 2020 [Online]. DOI: 10.3389/fnins.2020.00145.

Bruner, E., Amano, H., de la Cuétara, José Manuel and Ogihara, N. (2015) 'The brain and the braincase: a spatial analysis on the midsagittal profile in adult humans', *Journal of Anatomy*, vol. 227, no. 3, pp. 268–276.

Cabezas, R., Avila, M., Gonzalez, J., El-Bachá, R. S., Báez, E., García-Segura, L. M., Jurado Coronel, J. C., Capani, F., Cardona-Gomez, G. P. and Barreto, G. E. (2014) 'Astrocytic modulation of blood brain barrier: perspectives on Parkinson's disease', *Frontiers in cellular neuroscience*, vol. 8, p. 211.

Cao, S., Zhou, M., Ji, S., Ma, D. and Zhu, S. (2024) 'Recent Advances in the Study of Alphaherpesvirus Latency and Reactivation: Novel Guidance for the Design of Herpesvirus Live Vector Vaccines', *Pathogens (Basel, Switzerland)*, vol. 13, no. 9.

Card, J. P. (2001) 'Pseudorabies virus neuroinvasiveness: a window into the functional organization of the brain', *Advances in virus research*, vol. 56, pp. 39–71.

Card, J. P. and Enquist, L. W. (1995) 'Neurovirulence of pseudorabies virus', *Critical reviews in neurobiology*, vol. 9, 2-3, pp. 137–162.

Cartier, A., Broberg, E., Komai, T., Henriksson, M. and Masucci, M. G. (2003) 'The herpes simplex virus-1 Us3 protein kinase blocks CD8T cell lysis by preventing the cleavage of Bid by granzyme B', *Cell Death & Differentiation*, vol. 10, no. 12, pp. 1320–1328.

Cartier, A., Komai, T. and Masucci, M. G. (2003) 'The Us3 protein kinase of herpes simplex virus 1 blocks apoptosis and induces phosporylation of the Bcl-2 family member Bad', *Experimental Cell Research*, vol. 291, no. 1, pp. 242–250 [Online]. DOI: 10.1016/S0014-4827(03)00375-6.

Cartier, A. and Masucci, M. G. (2004) 'Differential Regulation of MHC Class-I-Restricted and Unrestricted Cytotoxicity by the Us3 Protein Kinase of Herpes Simplex Virus-1', *Scandinavian Journal of Immunology*, vol. 60, no. 6, pp. 592–599.

Catani, M., Dell'acqua, F. and Thiebaut de Schotten, M. (2013) 'A revised limbic system model for memory, emotion and behaviour', *Neuroscience and Biobehavioral Reviews*, vol. 37, no. 8, pp. 1724–1737.

Cavarretta, F., Burton, S. D., Igarashi, K. M., Shepherd, G. M., Hines, M. L. and Migliore, M. (2018) 'Parallel odor processing by mitral and middle tufted cells in the olfactory bulb', *Scientific Reports*, vol. 8, no. 1, p. 7625.

Chee, K., Razmara, A., Geller, A. S., Harris, W. B., Restrepo, D., Thompson, J. A. and Kramer, D. R. (2022) 'The role of the piriform cortex in temporal lobe epilepsy: A current literature review', *Frontiers in neurology*, vol. 13, p. 1042887.

Chen, J. J., Gershon, A. A., Li, Z., Cowles, R. A. and Gershon, M. D. (2011) 'Varicella zoster virus (VZV) infects and establishes latency in enteric neurons', *Journal of neurovirology*, vol. 17, no. 6, pp. 578–589.

Chen, Y., Gao, J., Hua, R. and Zhang, G. (2025) 'Pseudorabies virus as a zoonosis: scientific and public health implications', *Virus Genes*, vol. 61, no. 1, pp. 9–25.

Chen, Z. and Liu, K. (2025) 'Mechanism and Applications of Vagus Nerve Stimulation', *Current issues in molecular biology*, vol. 47, no. 2.

Chentoufi, A. A., Kritzer, E., Yu, D. M., Nesburn, A. B. and BenMohamed, L. (2012) 'Towards a rational design of an asymptomatic clinical herpes vaccine: the old, the new, and the unknown', *Clinical & developmental immunology*, vol. 2012, p. 187585.

Cho, H., Proll, S. C., Szretter, K. J., Katze, M. G., Gale, M. and Diamond, M. S. (2013) 'Differential innate immune response programs in neuronal subtypes determine susceptibility to infection in the brain by positive-stranded RNA viruses', *Nature medicine*, vol. 19, no. 4, pp. 458–464.

Cleaver, J., Jeffery, K., Klenerman, P., Lim, M., Handunnetthi, L., Irani, S. R. and Handel, A. (2024) 'The immunobiology of herpes simplex virus encephalitis and post-viral autoimmunity', *Brain: a journal of neurology*, vol. 147, no. 4, pp. 1130–1148.

Colonna, M. and Butovsky, O. (2017) 'Microglia Function in the Central Nervous System During Health and Neurodegeneration', *Annual review of immunology*, vol. 35, pp. 441–468.

Corkin, S., Milner, B. and Rasmussen, T. (1970) 'Somatosensory thresholds--contrasting effects of postcentral-gyrus and posterior parietal-lobe excisions', *Archives of neurology*, vol. 23, no. 1, pp. 41–58.

Costa, B. and Vale, N. (2024) 'Virus-Induced Epilepsy vs. Epilepsy Patients Acquiring Viral Infection: Unravelling the Complex Relationship for Precision Treatment', *International journal of molecular sciences*, vol. 25, no. 7.

Curanović, D., Lyman, M. G., Bou-Abboud, C., Card, J. P. and Enquist, L. W. (2009) 'Repair of the UL21 Locus in Pseudorabies Virus Bartha Enhances the Kinetics of Retrograde, Transneuronal Infection In Vitro and In Vivo', *Journal of Virology*, vol. 83, no. 3, pp. 1173–1183.

Damasio, A. R. and van Hoesen, G. W. (1985) 'The limbic system and the localisation of herpes simplex encephalitis', *Journal of Neurology, Neurosurgery & Psychiatry*, vol. 48, no. 4, p. 297.

Dando, S. J., Mackay-Sim, A., Norton, R., Currie, B. J., St. John, J. A., Ekberg, J. A. K., Batzloff M., Ulett G. C. and Beacham I. R. (2014) 'Pathogens Penetrating the Central Nervous System: Infection Pathways and the Cellular and Molecular Mechanisms of Invasion', *Clinical Microbiology Reviews*, vol. 27, no. 4, pp. 691–726.

Davison, A. J. (2002) 'Evolution of the herpesviruses', *Veterinary microbiology*, vol. 86, 1-2, pp. 69–88.

Davison, A. J., Eberle, R., Ehlers, B., Hayward, G. S., McGeoch, D. J., Minson, A. C., Pellett, P. E., Roizman, B., Studdert, M. J. and Thiry, E. (2009) 'The order Herpesvirales', *Archives of Virology*, vol. 154, no. 1, pp. 171–177.

Deng, S., Gan, L., Liu, C., Xu, T., Zhou, S., Guo, Y., Zhang, Z., Yang, G.-Y., Tian, H. and Tang, Y. (2023) 'Roles of Ependymal Cells in the Physiology and Pathology of the Central Nervous System', *Aging and disease*, vol. 14, no. 2, pp. 468–483.

Deshmane, S. L. and Fraser, N. W. (1989) 'During latency, herpes simplex virus type 1 DNA is associated with nucleosomes in a chromatin structure', *Journal of Virology*, vol. 63, no. 2, pp. 943–947.

Dhama, K., Kumar, N., Saminathan, M., Tiwari, R., Karthik, K., Kumar, M. A., Palanivelu, M., Shabbir, M. Z., Malik, Y. S. and Singh, R. K. (2017) 'Duck virus enteritis (duck plague) – a comprehensive update', *The veterinary quarterly*, vol. 37, no. 1, pp. 57–80.

Diek, D., Smidt, M. P. and Mesman, S. (2022) 'Molecular Organization and Patterning of the Medulla Oblongata in Health and Disease', *International journal of molecular sciences*, vol. 23, no. 16 [Online]. DOI: 10.3390/ijms23169260.

Divito, S., Cherpes, T. L. and Hendricks, R. L. (2006) 'A Triple Entente: Virus, Neurons, and CD8+ T Cells Maintain HSV-1 Latency', *Immunologic Research*, vol. 36, pp. 119–126.

Doll, J. R., Thompson, R. L. and Sawtell, N. M. (2019) 'Infectious Herpes Simplex Virus in the Brain Stem Is Correlated with Reactivation in the Trigeminal Ganglia', *Journal of Virology*, vol. 93, no. 8.

Donovan, S. L. and McCasland, J. S. (2008) 'GAP-43 is critical for normal targeting of thalamocortical and corticothalamic, but not trigeminothalamic axons in the whisker barrel system', *Somatosensory & motor research*, vol. 25, no. 1, pp. 33–47.

Duarte, L. F., Farías, M. A., Álvarez, D. M., Bueno, S. M., Riedel, C. A. and González, P. A. (2019) 'Herpes Simplex Virus Type 1 Infection of the Central Nervous System: Insights Into Proposed Interrelationships With Neurodegenerative Disorders', *Frontiers in cellular neuroscience*, vol. 13, p. 46.

Durrant, D. M., Ghosh, S. and Klein, R. S. (2016) 'The Olfactory Bulb: An Immunosensory Effector Organ during Neurotropic Viral Infections', *ACS chemical neuroscience*, vol. 7, no. 4, pp. 464–469.

Eichenbaum, H. (2000) 'A cortical–hippocampal system for declarative memory', *Nature Reviews Neuroscience*, vol. 1, no. 1, pp. 41–50.

Epstein, R. and Kanwisher, N. (1998) 'A cortical representation of the local visual environment', *Nature*, vol. 392, no. 6676, pp. 598–601.

Esiri, M. (1982) 'Herpes Simplex Encephalitis An Immunohistological Study of the Distribution of Viral Antigen within the Brain', *Journal of the Neurological Sciences*, vol. 54, pp. 209–226.

Evrard, H. C. (2019) 'The Organization of the Primate Insular Cortex', *Frontiers in neuroanatomy*, Volume 13 - 2019 [Online]. DOI: 10.3389/fnana.2019.00043.

Ezure, H., Goto, N., Nonaka, N., Goto, J. and Tani, H. (2001) 'Morphometric analysis of the human trigeminal nerve', *Okajimas folia anatomica Japonica*, vol. 78, 2-3, pp. 49–53.

Fama, R. and Sullivan, E. V. (2015) 'Thalamic structures and associated cognitive functions: Relations with age and aging', *Neuroscience and Biobehavioral Reviews*, vol. 54, pp. 29–37.

Fehrenbach, M. J. (2015) *Illustrated Anatomy of the Head and Neck - E-Book* [Online], 5th edn, Saintt Louis, Elsevier - Health Sciences Division. Available at https:// ebookcentral.proquest.com/lib/kxp/detail. action?docID=5517354.

Feldman, E. L., Russell, J. W., Löscher, W. N., Grisold, W. and Meng, S. (2021) 'Cranial Nerves', in Feldman, E. L., Russell, J. W., Löscher, W. N., Grisold, W. and Meng, S. (eds) *Atlas of Neuromuscular Diseases: A Practical Guideline,* Cham, Springer International Publishing, pp. 69–102.

Feldman, L. T., Ellison, A. R., Voytek, C. C., Yang, L., Krause, P. and Margolis, T. P. (2002) 'Spontaneous molecular reactivation of herpes simplex virus type 1 latency in mice', *Proceedings of the National Academy of Sciences of the United States of America*, vol. 99, no. 2, pp. 978–983.

Finnen, R. L. and Banfield, B. W. (2018) 'CRISPR/Cas9 Mutagenesis of UL21 in Multiple Strains of Herpes Simplex Virus Reveals Differential Requirements for pUL21 in Viral Replication', *Viruses*, vol. 10, no. 5.

Fitzgerald, M. (2005) 'The development of nociceptive circuits', *Nature Reviews Neuroscience*, vol. 6, no. 7, pp. 507–520.

Fraser, N. W., Lawrence, W. C., Wroblewska, Z., Gilden, D. H. and Koprowski, H. (1981) 'Herpes simplex type 1 DNA in human brain tissue', *Proceedings of the National Academy of Sciences*, vol. 78, no. 10, pp. 6461–6465.

Fried, K. and Gibbs, J. L. (2014) 'Dental Pulp Innervation', in Goldberg, M. (ed) *The Dental Pulp: Biology, Pathology, and Regenerative Therapies,* Berlin, Heidelberg, Springer Berlin Heidelberg, pp. 75–95.

Funahashi, S. (2017) 'Prefrontal Contribution to Decision-Making under Free-Choice Conditions', *Frontiers in neuroscience*, vol. 11, p. 431.

Gandar, F., Wilkie, G. S., Gatherer, D., Kerr, K., Marlier, D., Diez, M., Marschang, R. E., Mast, J., Dewals, B. G., Davison, A. J. and Vanderplasschen, A. F. C. (2015) 'The Genome of a Tortoise Herpesvirus (Testudinid Herpesvirus 3) Has a Novel Structure and Contains a Large Region That Is Not Required for Replication In Vitro or Virulence In Vivo', *Journal of Virology*, vol. 89, no. 22, pp. 11438–11456.

García-Guillén, I. M., Martínez-de-la-Torre, M., Puelles, L., Aroca, P. and Marín, F. (2021) 'Molecular Segmentation of the Spinal Trigeminal Nucleus in the Adult Mouse Brain', *Frontiers in neuroanatomy*, vol. 15, p. 785840.

Gaskell, R., Susan Dawson, Alan Radford and Etienne Thiry (2007) 'Feline herpesvirus', *Veterinary Research*, vol. 38, no. 2, pp. 337–354.

Gebhart, G. F. and Schmidt, R. F. (eds) (2013) *Encyclopedia of Pain*, Berlin, Heidelberg, Springer Berlin Heidelberg.

Geenen, K., Favoreel, H. W., Olsen, L., Enquist, L. W. and Nauwynck, H. J. (2005) 'The pseudorabies virus US3 protein kinase possesses anti-apoptotic activity that protects cells from apoptosis during infection and after treatment with sorbitol or staurosporine', *Virology*, vol. 331, no. 1, pp. 144–150 [Online]. DOI: 10.1016/j.virol.2004.10.027.

Gehrlach, D. A., Weiand, C., Gaitanos, T. N., Cho, E., Klein, A. S., Hennrich, A. A., Conzelmann, K.-K. and Gogolla, N. (2020) 'A whole-brain connectivity map of mouse insular cortex', *eLife*, vol. 9.

Geraghty, R. J., Krummenacher, C., Cohen, G. H., Eisenberg, R. J. and Spear, P. G. (1998) 'Entry of Alphaherpesviruses Mediated by Poliovirus Receptor-Related Protein 1 and Poliovirus Receptor', *Science*, vol. 280, pp. 1618–1620.

Gershon, A. A., Chen, J. and Gershon, M. D. (2015) 'Use of Saliva to Identify Varicella Zoster Virus Infection of the Gut', *Clinical infectious diseases: an official publication of the Infectious Diseases Society of America*, vol. 61, no. 4, pp. 536–544.

Glocker, F. X., Rösler, K. M. and Hopf, H. C. (2006) '5.1 Anatomie und Funktion', in *Erkrankungen der Hirnnerven,* Stuttgart, Georg Thieme Verlag KG.

Gnann, J. W. and Whitley, R. J. (2017) 'Herpes Simplex Encephalitis: an Update', *Current infectious disease reports*, vol. 19, no. 3, p. 13.

Gornatti-Churria, C. D., Loukopoulos, P., Stoute, S. T., Shivaprasad, H. L. and Uzal, F. A. (2023) 'A retrospective study of pigeon herpesviral infection in domestic pigeons in California (1991-2014) and literature review', *Journal of veterinary diagnostic investigation: official publication of the American Association of Veterinary Laboratory Diagnosticians, Inc*, vol. 35, no. 3, pp. 252–257.

Gowthaman, V., Kumar, S., Koul, M., Dave, U., Murthy, T R Gopala Krishna, Munuswamy, P., Tiwari, R., Karthik, K., Dhama, K., Michalak, I. and Joshi, S. K. (2020) 'Infectious laryngotracheitis: Etiology, epidemiology, pathobiology, and advances in diagnosis and control - a comprehensive review', *The veterinary quarterly*, vol. 40, no. 1, pp. 140–161.

Graham, D. A. (2013) 'Bovine herpes virus-1 (BoHV-1) in cattle-a review with emphasis on reproductive impacts and the emergence of infection in Ireland and the United Kingdom', *Irish veterinary journal*, vol. 66, no. 1, p. 15.

Gretenkord, S., Kostka, J. K., Hartung, H., Watznauer, K., Fleck, D., Minier-Toribio, A., Spehr, M. and Hanganu-Opatz, I. L. (2019) 'Coordinated electrical activity in the olfactory bulb gates the oscillatory entrainment of entorhinal networks in neonatal mice', *PLoS biology*, vol. 17, no. 1, e2006994.

Grunditz, T., Uddman, R. and Sundler, F. (1994) 'Origin and peptide content of nerve fibers in the nasal mucosa of rats', *Anatomy and Embryology*, vol. 189, pp. 327–337.

Guan, Z.-L., Ding, Y.-Q., Li, J.-L. and Lü, B.-Z. (1998) 'Substance P receptor-expressing neurons in the medullary and spinal dorsal horns projecting to the nucleus of the solitary tract in the rat', *Neuroscience Research*, vol. 30, no. 3, pp. 213–218 [Online]. DOI: 10.1016/S0168-0102(97)00131-4.

Guo, H., Yuan, X.-S., Zhou, J.-C., Chen, H., Li, S.-Q., Qu, W.-M. and Huang, Z.-L. (2020) 'Whole-Brain Monosynaptic Inputs to Hypoglossal Motor Neurons in Mice', *Neuroscience bulletin*, vol. 36, no. 6, pp. 585–597.

Gupta, A., Gartner, J. J., Sethupathy, P., Hatzigeorgiou, A. G. and Fraser, N. W. (2006) 'Anti-apoptotic function of a microRNA encoded by the HSV-1 latency-associated transcript', *Nature*, vol. 442, no. 7098, pp. 82–85.

Haanen, C. and Vermes, I. (1995) 'Apoptosis and inflammation', *Mediators of Inflammation*, vol. 4, no. 1, p. 614169.

Haarr, L., Shukla, D., Rødahl, E., Dal Canto, M. C. and Spear, P. G. (2001) 'Transcription from the gene encoding the herpesvirus entry receptor nectin-1 (HveC) in nervous tissue of adult mouse', *Virology*, vol. 287, no. 2, pp. 301–309.

Hadland, K. A., Rushworth, M. F. S., Gaffan, D. and Passingham, R. E. (2003) 'The effect of cingulate lesions on social behaviour and emotion', *Neuropsychologia*, vol. 41, no. 8, pp. 919–931.

Hamza, M. A., Higgins, D. M., Feldman, L. T. and Ruyechan, W. T. (2007) 'The latency-associated transcript of herpes simplex virus type 1 promotes survival and stimulates axonal regeneration in sympathetic and trigeminal neurons', *Journal of neurovirology*, vol. 13, no. 1, pp. 56–66.

Hargreaves, E. L., Rao, G., Lee, I. and Knierim, J. J. (2005) 'Major dissociation between medial and lateral entorhinal input to dorsal hippocampus', *Science*, vol. 308, no. 5729, pp. 1792–1794.

Hariri, A. R., Bookheimer, S. Y. and Mazziotta, J. C. (2000) 'Modulating emotional responses: effects of a neocortical network on the limbic system', *Neuroreport*, vol. 11, no. 1, pp. 43–48.

Harrison, K. and Jones, C. (2022) 'Regulation of herpes simplex virus type 1 latency-reactivation cycle and ocular disease by cellular signaling pathways', *Experimental eye research*, vol. 218, p. 109017.

Hattox, A. M. and Nelson, S. B. (2007) 'Layer V neurons in mouse cortex projecting to different targets have distinct physiological properties', *Journal of Neurophysiology*, vol. 98, no. 6, pp. 3330–3340.

Hayden, B. Y. and Platt, M. L. (2010) 'Neurons in anterior cingulate cortex multiplex information about reward and action', *The Journal of neuroscience : the official journal of the Society for Neuroscience*, vol. 30, no. 9, pp. 3339–3346.

Held, K. and Derfuss, T. (2011) 'Control of HSV-1 latency in human trigeminal ganglia--current overview', *Journal of neurovirology*, vol. 17, no. 6, pp. 518–527.

Henssen, D., Derks, B., van Doorn, M., Verhoogt, N. C., Staats, P., Vissers, K. and van Cappellen Walsum, A. M. (2019) 'Visualizing the trigeminovagal complex in the human medulla by combining ex-vivo ultra-high resolution structural MRI and polarized light imaging microscopy', *Scientific Reports*, vol. 9, no. 1, p. 11305.

Hill, J. M., Lukiw, W. J., Gebhardt, B. M., Higaki, S., Loutsch, J. M., Myles, M. E., Thompson, H. W., Kwon, B. S., Bazan, N. G. and Kaufman, H. E. (2001) 'Gene Expression Analyzed by Microarrays in HSV-1 Latent Mouse Trigeminal Ganglion Following Heat Stress', *Virus Genes*, vol. 23, pp. 273–280.

Hill, T. J., Field, H. J. and Blyth, W. A. (1975) 'Acute and Recurrent Infection with Herpes Simplex Virus in the Mouse: a Model for Studying Latency and Recurrent Disease', *J. gen. ViroL*, vol. 28, pp. 341–353.

Himmelein, S., St Leger, A. J., Knickelbein, J. E., Rowe, A., Freeman, M. L. and Hendricks, R. L. (2011) 'Circulating herpes simplex type 1 (HSV-1)-specific CD8+T cells do not access HSV-1 latently infected trigeminal ganglia', *Herpesviridae*, vol. 2, no. 1, p. 5.

Hintiryan, H., Gou, L., Zingg, B., Yamashita, S., Lyden, H. M., Song, M. Y., Grewal, A. K., Zhang, X., Toga, A. W. and Dong, H.-W. (2012) 'Comprehensive connectivity of the mouse main olfactory bulb: analysis and online digital atlas', *Frontiers in neuroanatomy*, vol. 6, p. 30.

Ho, M.-L., Juliano, A., Eisenberg, R. L. and Moonis, G. (2015) 'Anatomy and Pathology of the Facial Nerve', *American Journal of Roentgenology*, vol. 204, no. 6, W612-W619.

Hogue, I. B., Bosse, J. B., Hu, J.-R., Thiberge, S. Y. and Enquist, L. W. (2014) 'Cellular mechanisms of alpha herpesvirus egress: live cell fluorescence microscopy of pseudorabies virus exocytosis', *PLOS Pathogens*, vol. 10, no. 12, e1004535.

Hokkanen, L., Launes, J., Poutiainen, E., Valanne, L., Salonen, O., Siren, J. and Iivanainen, M. (1997) 'Subcortical type cognitive impairment in herpes zoster encephalitis', *journal of neurology*, vol. 244, pp. 239–245.

Holstege, G. and Kuypers, H. G. (1982) 'The Anatomy of Brain Stem Pathways to the Spinal Cord in Cat. A Labeled Amino Acid Tracing Study', in Kuypers, H. and Martin, G. F. (eds) *Progress in Brain Research,* Elsevier, pp. 145–175.

Honess, R. W. and Roizman, B. (1974) 'Regulation of herpesvirus macromolecular synthesis. I. Cascade regulation of the synthesis of three groups of viral proteins', *Journal of Virology*, vol. 14, no. 1, pp. 8–19.

Hooi, Y. T., Fu, T. L., Tan, S. H., Ong, K. C., Tan, C. Y. and Wong, K. T. (2025) 'Neuroinvasion via Peripheral Nerves in Epidemic Viral Encephalitis Caused by Enterovirus, Orthoflavivirus and SARS-Coronavirus', *Neuropathology and applied neurobiology*, vol. 51, no. 1, e70005.

Horn-Bochtler, A. K. E. and Büttner-Ennever, J. A. (2011) 'Neuroanatomy of the Brainstem', in Urban, P. and Caplan, L. R. (eds) *Brainstem Disorders,* Berlin, Heidelberg, Springer Berlin Heidelberg, pp. 1–35.

Hornung, J.-P. (2003) 'The human raphe nuclei and the serotonergic system', *Journal of chemical neuroanatomy*, vol. 26, no. 4, pp. 331–343.

Horváth, S., Prandovszky, E., Kis, Z., Krummenacher, C., Eisenberg, R. J., Cohen, G. H., Janka, Z. and Toldi, J. (2006) 'Spatiotemporal changes of the herpes simplex virus entry receptor nectin-1 in murine brain during postnatal development', *Journal of neurovirology*, vol. 12, no. 3, pp. 161–170.

Hovis, K. R., Ramnath, R., Dahlen, J. E., Romanova, A. L., LaRocca, G., Bier, M. E. and Urban, N. N. (2012) 'Activity regulates functional connectivity from the vomeronasal organ to the accessory olfactory bulb', *The Journal of neuroscience : the official journal of the Society for Neuroscience*, vol. 32, no. 23, pp. 7907–7916.

(2007) *Human Herpesviruses: Biology, Therapy, and Immunoprophylaxis,* Cambridge University Press.

Illig, K. R. and Wilson, D. A. (2014) 'Olfactory Cortex: Comparative Anatomy', in *Reference Module in Biomedical Sciences,* Elsevier.

Imai, T., Koyanagi, N., Ogawa, R., Shindo, K., Suenaga, T., Sato, A., Arii, J., Kato, A., Kiyono, H., Arase, H. and Kawaguchi, Y. (2013) 'Us3 Kinase Encoded by Herpes Simplex Virus 1 Mediates Downregulation of Cell Surface Major Histocompatibility Complex Class I and Evasion of CD8+ T Cells', *PloS one*, vol. 8, no. 8, e72050.

Isabella, A. J. and Moens, C. B. (2024) 'Development and regeneration of the vagus nerve', *Seminars in cell & developmental biology*, vol. 156, pp. 219–227.

Jacobs, J., Kahana, M. J., Ekstrom, A. D., Mollison, M. V. and Fried, I. (2010) 'A sense of direction in human entorhinal cortex', *Proceedings of the National Academy of Sciences of the United States of America*, vol. 107, no. 14, pp. 6487–6492.

Jay, V., Becker, L. E., Blaser, S., Hwang, P., Hoffman, H. J., Humphreys, R. and Zielenska, M. (1995) 'Pathology of chronic herpes infection associated with seizure disorder: a report of two cases with tissue detection of herpes simplex virus 1 by the polymerase chain reaction', *Pediatric pathology & laboratory medicine : journal of the Society for Pediatric Pathology, affiliated with the International Paediatric Pathology Association*, vol. 15, no. 1, pp. 131–146.

Jean, A. (2001) 'Brain Stem Control of Swallowing: Neuronal Network and Cellular Mechanisms', *Physiological Reviews*, vol. 81, no. 2, pp. 929–969.

Jiang, X., Chentoufi, A. A., Hsiang, C., Carpenter, D., Osorio, N., BenMohamed, L., Fraser, N. W., Jones, C. and Wechsler, S. L. (2011) 'The herpes simplex virus type 1 latency-associated transcript can protect neuron-derived C1300 and Neuro2A cells from granzyme B-induced apoptosis and CD8 T-cell killing', *Journal of Virology*, vol. 85, no. 5, pp. 2325–2332.

Johns, P. (2014) *Clinical Neuroscience: An Illustrated Colour Text* [Online], Churchill Livingstone/Elsevier. Available at https://books.google.de/books?id=0MninQEACAAJ.

Kajiwara, R., Tominaga, T. and Takashima, I. (2007) 'Olfactory information converges in the amygdaloid cortex via the piriform and entorhinal cortices: observations in the guinea pig isolated whole-brain preparation', *The European journal of neuroscience*, vol. 25, no. 12, pp. 3648–3658.

Kamel, H. A. M. and Toland, J. (2001) 'Trigeminal Nerve Anatomy', *American Journal of Roentgenology*, vol. 176, no. 1, pp. 247–251.

Kapoor, S., Sharma, H., Singh, M., Kumar, P., Ranjan, K., Kumari, A. and Khirbat, R. (2014) 'Equine Herpesviruses: a Brief Review', *Advances in Animal and Veterinary Sciences*, vol. 2, 2S, pp. 46–54.

Kato, A. and Kawaguchi, Y. (2018) 'Us3 Protein Kinase Encoded by HSV: The Precise Function and Mechanism on Viral Life Cycle', in Kawaguchi, Y., Mori, Y. and Kimura, H. (eds) *Human Herpesviruses,* Singapore, Springer Singapore, pp. 45–62.

Kennedy, P. G., Adams, J. H., Graham, D. I. and Clements, G. B. (1988) 'A clinico-pathological study of herpes simplex encephalitis', *Neuropathology and applied neurobiology*, vol. 14, no. 5, pp. 395–415.

Kimman, T. G., Wind, N. de, Bruin, T. de, Visser, Y. de and Voermans, J. (1994) 'Inactivation of Glycoprotein gE and Thymidine Kinase or the US3-Encoded Protein Kinase Synergistically Decreases in Vivo Replication of Pseudorabies Virus and the Induction of Protective Immunity', *Virology*, vol. 205, no. 2, pp. 511–518 [Online]. DOI: 10.1006/viro.1994.1672.

Klopfleisch, R., Klupp, B. G., Fuchs, W., Kopp, M., Teifke, J. P. and Mettenleiter, T. C. (2006) 'Influence of pseudorabies virus proteins on neuroinvasion and neurovirulence in mice', *Journal of virology*, vol. 80, no. 11, pp. 5571–5576.

Klopfleisch, R., Teifke, J. P., Fuchs, W., Kopp, M., Klupp, B. G. and Mettenleiter, T. C. (2004) 'Influence of tegument proteins of pseudorabies virus on neuroinvasion and transneuronal spread in the nervous system of adult mice after intranasal inoculation', *Journal of virology*, vol. 78, no. 6, pp. 2956–2966.

Klupp, B. G., Böttcher, S., Granzow, H., Kopp, M. and Mettenleiter, T. C. (2005) 'Complex Formation between the UL16 and UL21 Tegument Proteins of Pseudorabies Virus', *Journal of Virology*, vol. 79, no. 3, pp. 1510–1522.

Klupp, B. G., Granzow, H. and Mettenleiter, T. C. (2001) 'Effect of the pseudorabies virus US3 protein on nuclear membrane localization of the UL34 protein and virus egress from the nucleus', *The Journal of general virology*, vol. 82, Pt 10, pp. 2363–2371.

Klupp, B. G., Hengartner, C. J., Mettenleiter, T. C. and Enquist, L. W. (2004) 'Complete, annotated sequence of the pseudorabies virus genome', *Journal of virology*, vol. 78, no. 1, pp. 424–440.

Klupp, B. G., Lomniczi, B., Visser, N., Fuchs, W. and Mettenleiter, T. C. (1995) 'Mutations affecting the UL21 gene contribute to avirulence of pseudorabies virus vaccine strain Bartha', *Virology*, vol. 212, no. 2, pp. 466–473.

Knipe, D. M. (1989) 'The role of viral and cellular nuclear proteins in herpes simplex virus replication', *Advances in virus research*, vol. 37, pp. 85–123.

Kobayashi, N., Nagata, T., Shinagawa, S., Oka, N., Shimada, K., Shimizu, A., Tatebayashi, Y., Yamada, H., Nakayama, K. and Kondo, K. (2013) 'Increase in the IgG avidity index due to herpes simplex virus type 1 reactivation and its relationship with cognitive function in amnestic mild cognitive impairment and Alzheimer's disease', *Biochemical and Biophysical Research Communications*, vol. 430, no. 3, pp. 907–911 [Online]. DOI: 10.1016/j.bbrc.2012.12.054.

Koyuncu, O. O., MacGibeny, M. A. and Enquist, L. W. (2018) 'Latent versus productive infection: the alpha herpesvirus switch', *Future virology*, vol. 13, no. 6, pp. 431–443.

Kramer, M. F. and Coen, D. M. (1995) 'Quantification of transcripts from the ICP4 and thymidine kinase genes in mouse ganglia latently infected with herpes simplex virus', *Journal of Virology*, vol. 69, no. 3, pp. 1389–1399.

Kramer, T. and Enquist, L. W. (2013) 'Directional spread of alphaherpesviruses in the nervous system', *Viruses*, vol. 5, no. 2, pp. 678–707.

Krummenacher, C., Baribaud, F., Ponce de Leon, M., Baribaud, I., Whitbeck, J. C., Xu, R., Cohen, G. H. and Eisenberg, R. J. (2004) 'Comparative usage of herpesvirus entry mediator A and nectin-1 by laboratory strains and clinical isolates of herpes simplex virus', *Virology*, vol. 322, no. 2, pp. 286–299.

Krusemark, E. A., Novak, L. R., Gitelman, D. R. and Li, W. (2013) 'When the Sense of Smell Meets Emotion: Anxiety-State-Dependent Olfactory Processing and Neural Circuitry Adaptation', *The Journal of Neuroscience*, vol. 33, no. 39, p. 15324.

Ku, C.-C., Besser, J., Abendroth, A., Grose, C. and Arvin, A. M. (2005) 'Varicella-Zoster virus pathogenesis and immunobiology: new concepts emerging from investigations with the SCIDhu mouse model', *Journal of Virology*, vol. 79, no. 5, pp. 2651–2658.

Kubat, N. J., Tran, R. K., McAnany, P. and Bloom, D. C. (2004) 'Specific histone tail modification and not DNA methylation is a determinant of herpes simplex virus type 1 latent gene expression', *Journal of Virology*, vol. 78, no. 3, pp. 1139–1149.

Lanave, G., Larocca, V., Losurdo, M., Catella, C., Capozza, P., Tempesta, M., Martella, V., Buonavoglia, C. and Camero, M. (2020) 'Isolation and characterization of bovine alphaherpesvirus 2 strain from an outbreak of bovine herpetic mammillitis in a dairy farm', *BMC veterinary research*, vol. 16, no. 1, p. 103.

Landau, Z., Miller, E. B. and Roif, M. (2005) 'Recurrent herpes simplex encephalitis', *European journal of internal medicine*, vol. 16, no. 7, pp. 513–514.

Landisman, C. E. and Connors, B. W. (2007) 'VPM and PoM nuclei of the rat somatosensory thalamus: intrinsic neuronal properties and corticothalamic feedback', *Cerebral cortex (New York, N.Y.: 1991)*, vol. 17, no. 12, pp. 2853–2865.

Laohathai, C., Weber, D. J., Hayat, G. and Thomas, F. P. (2016) 'Chronic herpes simplex type-1 encephalitis with intractable epilepsy in an immunosuppressed patient', *Infection*, vol. 44, no. 1, pp. 121–125.

Lathe, R. and Haas, J. G. (2017) 'Distribution of cellular HSV-1 receptor expression in human brain', *Journal of neurovirology*, vol. 23, no. 3, pp. 376–384.

Laval, K. and Enquist, L. W. (2020) 'The Neuropathic Itch Caused by Pseudorabies Virus', *pathogens*, vol. 9, no. 4, p. 254.

Laval, K., van Cleemput, J., Vernejoul, J. B. and Enquist, L. W. (2019) 'Alphaherpesvirus infection of mice primes PNS neurons to an inflammatory state regulated by TLR2 and type I IFN signaling', *PLOS Pathogens*, vol. 15, no. 11, e1008087.

Laval, K., Vernejoul, J. B., van Cleemput, J., Koyuncu, O. O. and Enquist, L. W. (2018) 'Virulent Pseudorabies Virus Infection Induces a Specific and Lethal Systemic Inflammatory Response in Mice', *Journal of Virology*, vol. 92, no. 24.

Leopardi, R., van Sant, C. and Roizman, B. (1997) 'The herpes simplex virus 1 protein kinase US3 is required for protection from apoptosis induced by the virus', *Proceedings of the National Academy of Sciences*, vol. 94, no. 15, pp. 7891–7896.

Li, S., Carpenter, D., Hsiang, C., Wechsler, S. L. and Jones, C. (2010) 'Herpes simplex virus type 1 latency-associated transcript inhibits apoptosis and promotes neurite sprouting in neuroblastoma cells following serum starvation by maintaining protein kinase B (AKT) levels', *The Journal of general virology*, vol. 91, Pt 4, pp. 858–866.

Liebich, H.-G. (2010) *Funktionelle Histologie der Haussäugetiere und Vögel*, Stuttgart, Schattauer GmbH.

Lin, H. C. and Barkhaus, P. E. (2009) 'Cranial nerve XII: the hypoglossal nerve', *Seminars in neurology*, vol. 29, no. 1, pp. 45–52.

Liu, T., Khanna, K. M., Chen, X., Fink, D. J. and Hendricks, R. L. (2000) 'CD8(+) T cells can block herpes simplex virus type 1 (HSV-1) reactivation from latency in sensory neurons', *The Journal of experimental medicine*, vol. 191, no. 9, pp. 1459–1466.

Lövblad, K.-O., Schaller, K. and Vargas, M. I. (2014) 'The fornix and limbic system', *Seminars in ultrasound, CT, and MR*, vol. 35, no. 5, pp. 459–473.

Lyman, M. G., Demmin, G. L. and Banfield, B. W. (2003) 'The Attenuated Pseudorabies Virus Strain Bartha Fails To Package the Tegument Proteins Us3 and VP22', *Journal of Virology*, vol. 77, no. 2, pp. 1403–1414.

Ma, J. Z., Russell, T. A., Spelman, T., Carbone, F. R. and Tscharke, D. C. (2014) 'Lytic Gene Expression Is Frequent in HSV-1 Latent Infection and Correlates with the Engagement of a Cell-Intrinsic Transcriptional Response', *PLOS Pathogens*, vol. 10, no. 7, e1004237.

Magyar, G., Tanyi, J., Hornyák, A. and Bartha, A. (1993) 'Restriction endonuclease analysis of Hungarian bovine herpesvirus isolates from different clinical forms of IBR, IPV and encephalitis', *Acta veterinaria Hungarica*, vol. 41, 1-2, pp. 159–170.

Mahjoub, N., Dhorne-Pollet, S., Fuchs, W., Endale Ahanda, M.-L., Lange, E., Klupp, B., Arya, A., Loveland, J. E., Lefevre, F., Mettenleiter, T. C. and Giuffra, E. (2015) 'A 2.5-kilobase deletion containing a cluster of nine microRNAs in the latency-associated-

transcript locus of the pseudorabies virus affects the host response of porcine trigeminal ganglia during established latency', *Journal of virology*, vol. 89, no. 1, pp. 428–442.

Mancini, M. and Vidal, S. M. (2018) 'Insights into the pathogenesis of herpes simplex encephalitis from mouse models', *Mammalian genome: official journal of the International Mammalian Genome Society*, vol. 29, 7-8, pp. 425–445.

Marcocci, M. E., Napoletani, G., Protto, V., Kolesova, O., Piacentini, R., Li Puma, D. D., Lomonte, P., Grassi, C., Palamara, A. T. and Chiara, G. de (2020) 'Herpes Simplex Virus-1 in the Brain: The Dark Side of a Sneaky Infection', *Trends in microbiology*, vol. 28, no. 10, pp. 808–820.

Maresch, C. (2011) 'Studien zur Neuroinvasion und zum axonalen Transport von Mutanten des Pseudorabiesvirus im Tiermodell und an Neuronenkulturen', *VVB Laufersweiler*.

Martínez Pascual, P., Maranillo, E., Vázquez, T., Simon de Blas, C., Lasso, J. M. and Sañudo, J. R. (2019) 'Extracranial Course of the Facial Nerve Revisited', *Anatomical record (Hoboken, N.J. : 2007)*, vol. 302, no. 4, pp. 599–608.

Masuda, T., Sankowski, R., Staszewski, O., Böttcher, C., Amann, L., Sagar, Scheiwe, C., Nessler, S., Kunz, P., van Loo, G., Coenen, V. A., Reinacher, P. C., Michel, A., Sure, U., Gold, R., Grün, D., Priller, J., Stadelmann, C. and Prinz, M. (2019) 'Spatial and temporal heterogeneity of mouse and human microglia at single-cell resolution', *Nature*, vol. 566, no. 7744, pp. 388–392.

Mathiasen, M. L., Aggleton, J. P. and Witter, M. P. (2023) 'Projections of the insular cortex to orbitofrontal and medial prefrontal cortex: A tracing study in the rat', *Frontiers in neuroanatomy*, Volume 17 - 2023 [Online]. DOI: 10.3389/fnana.2023.1131167.

Mbong, E. F., Woodley, L., Frost, E., Baines, J. D. and Duffy, C. (2012) 'Deletion of UL21 Causes a Delay in the Early Stages of the Herpes Simplex Virus 1 Replication Cycle', *Journal of Virology*, vol. 86, no. 12, pp. 7003–7007.

McDonald, B., Highley, J. R., Walker, M. A., Herron, B. M., Cooper, S. J., Esiri, M. M. and Crow, T. J. (2000) 'Anomalous asymmetry of fusiform and parahippocampal gyrus

gray matter in schizophrenia: A postmortem study', *The American journal of psychiatry*, vol. 157, no. 1, pp. 40–47.

McFarland, D. J. and Hotchin, J. (1987) 'Contrasting patterns of virus spread and neuropathology following microinjection of herpes simplex virus into the hippocampus or cerebellum of mice', *Journal of the Neurological Sciences*, vol. 79, pp. 255–265.

McGrath, N., Anderson, N. E., Croxson, C. M. and Powell, K. F. (1997) 'Herpes simplex encephalitis treated with acyclovir: diagnosis and long-term outcome', *Journal ofNeurology, Neurosurgery, and Psychiatry*, vol. 63, pp. 321–326.

McLean, J. H., Shipley, M. T. and Bernstein, D. I. (1989) 'Golgi-Like, Transneuronal Retrograde Labelling With CNS Injections of Herpes Simplex Virus Type 1', *Brain Research Bulletin*, vol. 22, pp. 867–881.

Mena, W., Baker, K., Rubin, A., Kohli, S., Yoo, Y., Bathellier, B., Ziv, Y., Rezaei-Mazinani, S. and Fleischmann, A. (2025) 'Differential encoding of odor and place in mouse piriform and entorhinal cortex', *bioRxiv: the preprint server for biology*.

Menendez, C. M. and Carr, D. J. J. (2017a) 'Defining nervous system susceptibility during acute and latent herpes simplex virus-1 infection', *Journal of neuroimmunology*, vol. 308, pp. 43–49.

Menendez, C. M. and Carr, D. J. J. (2017b) 'Herpes simplex virus-1 infects the olfactory bulb shortly following ocular infection and exhibits a long-term inflammatory profile in the form of effector and HSV-1-specific T cells', *Journal of neuroinflammation*, vol. 14, no. 1, p. 124.

Messlinger, K., Balcziak, L. K. and Russo, A. F. (2020) 'Cross-talk signaling in the trigeminal ganglion: role of neuropeptides and other mediators', *Journal of neural transmission (Vienna, Austria: 1996)*, vol. 127, no. 4, pp. 431–444.

Mettenleiter, T. C. (2000) 'Aujeszky’s disease (pseudorabies) virus: the virus and molecular pathogenesis - State of the art, June 1999', *Veterinary Research*, vol. 31, no. 1, pp. 99–115.

Mettenleiter, T. C. (2002) 'Herpesvirus assembly and egress', *Journal of Virology*, vol. 76, no. 4, pp. 1537–1547.

Mettenleiter, T. C. (2003) 'Pathogenesis of neurotropic herpesviruses: role of viral glycoproteins in neuroinvasion and transneuronal spread', *Virus research*, vol. 92, no. 2, pp. 197–206.

Mettenleiter, T. C. (2004) 'Budding events in herpesvirus morphogenesis', *Virus research*, vol. 106, no. 2, pp. 167–180 [Online]. DOI: 10.1016/j.virusres.2004.08.013.

Mettenleiter, T. C., Ehlers, B., Müller, T., Yoon, K.-J. and Teifke, J. P. (2019) 'Herpesviruses', in *Diseases of Swine*, pp. 548–575.

Mettenleiter, T. C., Klupp, B. G. and Granzow, H. (2009) 'Herpesvirus assembly: an update', *Virus research*, vol. 143, no. 2, pp. 222–234.

Michael, K., Klupp, B. G., Karger, A. and Mettenleiter, T. C. (2007) 'Efficient Incorporation of Tegument Proteins pUL46, pUL49, and pUS3 into Pseudorabies Virus Particles Depends on the Presence of pUL21', *Journal of Virology*, vol. 81, no. 2, pp. 1048–1051.

Milsom, W. K., Chatburn, J. and Zimmer, M. B. (2004) 'Pontine influences on respiratory control in ectothermic and heterothermic vertebrates', *Respiratory physiology & neurobiology*, vol. 143, 2-3, pp. 263–280.

Miranda-Saksena, M., Denes, C. E., Diefenbach, R. J. and Cunningham, A. L. (2018) 'Infection and Transport of Herpes Simplex Virus Type 1 in Neurons: Role of the Cytoskeleton', *Viruses*, vol. 10, no. 2.

Mizuno, N. and Nomura, S. (1986) 'Primary afferent fibers in the glossopharyngeal nerve terminate in the dorsal division of the principal sensory trigeminal nucleus: An HRP study in the cat', *Neuroscience letters*, vol. 66, no. 3, pp. 338–340 [Online]. DOI: 10.1016/0304-3940(86)90042-X.

Moerel, M., Martino, F. de, Uğurbil, K., Yacoub, E. and Formisano, E. (2019) 'Processing complexity increases in superficial layers of human primary auditory cortex', *Scientific Reports*, vol. 9, no. 1, p. 5502.

Mogenson, G. J., Jones, D. L. and Yim, C. Y. (1980) 'From motivation to action: functional interface between the limbic system and the motor system', *Progress in neurobiology*, vol. 14, 2-3, pp. 69–97.

Moreno-Bravo, J. A., Martinez-Lopez, J. E. and Puelles, E. (2012) 'Mesencephalic neuronal populations: new insights on the ventral differentiation programs', *Histology and histopathology*, vol. 27, no. 12, pp. 1529–1538.

Mori, I. (2015) 'Transolfactory neuroinvasion by viruses threatens the human brain', *Acta virologica*, vol. 59, no. 4, pp. 338–349.

Mu, L., Chen, J., Li, J., Fowkes, M., Benson, B., Nyirenda, T., Sobotka, S., Christopherson, M. and Sanders, I. (2021) 'Innervation of human soft palate muscles', *Anatomical record (Hoboken, N.J.: 2007)*, vol. 304, no. 5, pp. 1054–1070.

Munger, J. and Roizman, B. (2001) 'The US3 protein kinase of herpes simplex virus 1 mediates the posttranslational modification of BAD and prevents BAD-induced programmed cell death in the absence of other viral proteins', *Proceedings of the National Academy of Sciences*, vol. 98, no. 18, pp. 10410–10415.

Naftel, J. P., Richards, L. P., Pan, M. and Bernanke, J. M. (1999) 'Course and composition of the nerves that supply the mandibular teeth of the rat', *The Anatomical Record*, vol. 256, no. 4, pp. 433–447.

Nagayama, S., Igarashi, K. M., Manabe, H. and Mori, K. (2014) 'Parallel Tufted Cell and Mitral Cell Pathways from the Olfactory Bulb to the Olfactory Cortex', in Mori, K. (ed) *The Olfactory System: From Odor Molecules to Motivational Behaviors,* Tokyo, Springer Japan, pp. 133–160.

Nahmias, A. J., Whitley, R. J., Visintine, A. N., Takei, Y., Alford, C. A., Jr. and Collaborative Antiviral Study Group (1982) 'Herpes Simplex Virus Encephalitis: Laboratory Evaluations and Their Diagnostic Significance', *The Journal of infectious diseases*, vol. 145, no. 6, pp. 829–836.

Narayanan, S. and Thirumalai, V. (2019) 'Contributions of the cerebellum for predictive and instructional control of movement', *Current Opinion in Physiology*, vol. 8, pp. 146–151 [Online]. DOI: 10.1016/j.cophys.2019.01.011.

Nash, P. G., Macefield, V. G., Klineberg, I. J., Gustin, S. M., Murray, G. M. and Henderson, L. A. (2010) 'Bilateral activation of the trigeminothalamic tract by acute orofacial cutaneous and muscle pain in humans', *Pain*, vol. 151, no. 2, pp. 384–393.

Nasse, J., Terman, D., Venugopal, S., Hermann, G., Rogers, R. and Travers, J. B. (2008) 'Local circuit input to the medullary reticular formation from the rostral nucleus of the solitary tract', *American journal of physiology. Regulatory, integrative and comparative physiology*, vol. 295, no. 5, R1391-408.

Neville, K. R. and Haberly, L. B. (2004) 'Olfactory Cortex', in Shepherd, G. M. (ed) *The Synaptic Organization of the Brain,* Oxford University Press, p. 0.

Nicoll, J., Love, S. and Kinrade, E. (1993) 'Distribution of herpes simplex virus DNA in the brains of human long-term survivors of encephalitis', *Neuroscience letters*, vol. 157, pp. 215–218.

Nicoll, M. P., Proença, J. T. and Efstathiou, S. (2012) 'The molecular basis of herpes simplex virus latency', *FEMS microbiology reviews*, vol. 36, no. 3, pp. 684–705.

Niemeyer, C. S., Merle, L., Bubak, A. N., Baxter, B. D., Gentile Polese, A., Colon-Reyes, K., Vang, S., Hassell, J. E., Bruce, K. D., Nagel, M. A. and Restrepo, D. (2024) 'Olfactory and trigeminal routes of HSV-1 CNS infection with regional microglial heterogeneity', *Journal of virology*, e0096824.

Ogg, P. D., McDonell, P. J., Ryckman, B. J., Knudson, C. and Roller, R. J. (2004) 'The HSV-1 Us3 protein kinase is sufficient to block apoptosis induced by overexpression of a variety of Bcl-2 family members', *Virology*, vol. 319, no. 2, pp. 212–224 [Online]. DOI: 10.1016/j.virol.2003.10.019.

Ohbayashi, M. (2021) 'The Roles of the Cortical Motor Areas in Sequential Movements', *Frontiers in Behavioral Neuroscience*, Volume 15 - 2021 [Online]. DOI: 10.3389/fnbeh.2021.640659.

Okada, S., Katagiri, A., Saito, H., Lee, J., Ohara, K., Iinuma, T. and Iwata, K. (2019) 'Functional involvement of nucleus tractus solitarii neurons projecting to the parabrachial nucleus in trigeminal neuropathic pain', *Journal of oral science*, vol. 61, no. 2, pp. 370–378.

O'Leary, T. P., Kendrick, R. M., Bristow, B. N., Sullivan, K. E., Wang, L., Clements, J., Lemire, A. L. and Cembrowski, M. S. (2022) 'Neuronal cell types, projections, and spatial organization of the central amygdala', *iScience*, vol. 25, no. 12, p. 105497.

Owens, Flores, Di Serio, F., Li, S., Pallás, V., Randles, J., Sano and Vidalakis (2012) 'Virus Taxonomy: Ninth Report of the International Committee on Taxonomy of Viruses', in, pp. 1221–1234.

Panneton, W. M. and Gan, Q. (2014) 'Direct reticular projections of trigeminal sensory fibers immunoreactive to CGRP: potential monosynaptic somatoautonomic projections', *Frontiers in neuroscience*, vol. 8, p. 136.

Patel, N. M., Jozsa, F. and Das, J. M. (2025) 'Neuroanatomy, Spinal Trigeminal Nucleus', in *StatPearls,* Treasure Island (FL).

Patestas, M. A. and Gartner, L. P. (2016) *A textbook of neuroanatomy / Maria A. Patestas, Leslie P. Gartner*, Hoboken, New Jersey, Wiley Blackwell.

Paxinos, G. and Franklin, K. B. J. (2001) *The Mouse Brain in Stereotaxic Coordinates*, 2nd edn, San Diego, Academic Press.

Perng, G.-C., Jones, C., Ciacci-Zanella, J., Stone, M., Henderson, G., Yukht, A., Slanina, S. M., Hofman, F. M., Ghiasi, H., Nesburn, A. B. and Wechsler, S. L. (2000) 'Virus-Induced Neuronal Apoptosis Blocked by the Herpes Simplex Virus Latency-Associated Transcript', *Science*, vol. 287, pp. 1500–1503.

Phelan, D., Barrozo, E. R. and Bloom, D. C. (2017) 'HSV1 latent transcription and non-coding RNA: A critical retrospective', *Journal of neuroimmunology*, vol. 308, pp. 65–101.

Pilling, A., Mark F. Rosenberg, Sharon H. Willis, Joachim Jäger, Gary H. Cohen, Roselyn J Eisenberg, David M. Meredith and Andreas Holzenburg (1999) 'Three-Dimensional Structure of Herpes Simplex Virus Type 1 Glycoprotein D at 2.4-Nanometer Resolution', *Journal of Virology*, vol. 73, pp. 7830–7834 [Online]. Available at https://api.semanticscholar.org/CorpusID:20369801.

Pomeranz, L. E., Reynolds, A. E. and Hengartner, C. J. (2005) 'Molecular biology of pseudorabies virus: impact on neurovirology and veterinary medicine', *Microbiology and molecular biology reviews : MMBR*, vol. 69, no. 3, pp. 462–500.

Poonam, Khatri, R., Mohan, H., Prasad, M. and CS, P. (2017) 'Etiology, Epidemiology, Pathogenesis and Diagnosis of Marek's Disease in Chickens: A Mini Review', *Journal of Veterinary Science & Medical Diagnosis*, vol. 06.

Prandovszky, E., Horváth, S., Gellért, L., Kovács, S. K., Janka, Z., Toldi, J., Shukla, D. and Vályi-Nagy, T. (2008) 'Nectin-1 (HveC) is expressed at high levels in neural subtypes that regulate radial migration of cortical and cerebellar neurons of the developing human and murine brain', *Journal of neurovirology*, vol. 14, no. 2, pp. 164–172.

Prendergast, P. M. (2013) 'Neurologic Anatomy of the Nose', in Shiffman, M. A. and Di Giuseppe, A. (eds) *Advanced Aesthetic Rhinoplasty: Art, Science, and New Clinical Techniques,* Berlin, Heidelberg, Springer Berlin Heidelberg, pp. 17–23.

Puelles, L. (2019) 'Survey of Midbrain, Diencephalon, and Hypothalamus Neuroanatomic Terms Whose Prosomeric Definition Conflicts With Columnar Tradition', *Frontiers in neuroanatomy*, Volume 13 - 2019 [Online]. DOI: 10.3389/fnana.2019.00020.

Qin, J., Ma, Z., Chen, X. and Shu, S. (2023) 'Microglia activation in central nervous system disorders: A review of recent mechanistic investigations and development efforts', *Frontiers in neurology*, Volume 14 - 2023 [Online]. DOI: 10.3389/fneur.2023.1103416.

Qiu, S., Hu, Y., Huang, Y., Gao, T., Wang, X., Wang, D., Ren, B., Shi, X., Chen, Y., Wang, X., Wang, D., Han, L., Liang, Y., Liu, D., Liu, Q., Deng, L., Chen, Z., Zhan, L., Chen, T., Huang, Y., Wu, Q., Xie, T., Qian, L., Jin, C., Huang, J., Deng, W., Jiang, T., Li, X., Jia, X., Yuan, J., Li, A., Yan, J., Xu, N., Xu, L., Luo, Q., Poo, M.-M., Sun, Y., Li, C. T., Yao, H., Gong, H., Sun, Y.-G. and Xu, C. (2024) 'Whole-brain spatial organization of hippocampal single-neuron projectomes', *Science (New York, N.Y.)*, vol. 383, no. 6682, eadj9198.

Ramchandani, M., Kong, M., Tronstein, E., Selke, S., Mikhaylova, A., Magaret, A., Huang, M.-L., Johnston, C., Corey, L. and Wald, A. (2016) 'Herpes simplex virus type 1 shedding in tears and nasal and oral mucosa of healthy adults', *Sexually Transmitted Diseases*, vol. 43, no. 12, pp. 756–760 [Online]. DOI: 10.1097/OLQ.0000000000000522.

Rao, P., Wen, X., Lo, J. H., Kim, S., Li, X., Chen, S., Feng, X., Akbari, O. and Yuan, W. (2018) 'Herpes Simplex Virus 1 Specifically Targets Human CD1d Antigen Presentation To Enhance Its Pathogenicity', *Journal of Virology*, vol. 92, no. 22, 10.1128/jvi.01490-18.

Raschilas, F., Wolff, M., Delatour, F., Chaffaut, C., Broucker, T. de, Chevret, S., Lebon, P., Canton, P. and Rozenberg, F. (2002) 'Outcome of and Prognostic Factors for Herpes Simplex Encephalitis in Adult Patients: Results of a Multicenter Study', *Clin Infect Dis*, vol. 35, pp. 254–260.

Readhead, B., Haure-Mirande, J.-V., Funk, C. C., Richards, M. A., Shannon, P., Haroutunian, V., Sano, M., Liang, W. S., Beckmann, N. D., Price, N. D., Reiman, E. M., Schadt, E. E., Ehrlich, M. E., Gandy, S. and Dudley, J. T. (2018) 'Multiscale Analysis of Independent Alzheimer's Cohorts Finds Disruption of Molecular, Genetic, and Clinical Networks by Human Herpesvirus', *Neuron*, vol. 99, no. 1, 64 – 82.e7 [Online]. DOI: 10.1016/j.neuron.2018.05.023.

Remington, L. A. (2012) 'Chapter 4 - Retina', in Remington, L. A. (ed) *Clinical Anatomy and Physiology of the Visual System (Third Edition),* Saint Louis, Butterworth-Heinemann, pp. 61–92.

Roizman, B., Knipe, D. M. and Whitley, R. J. (2007) 'Herpes simplex viruses', *Herpes Simplex Viruses*, pp. 1823–1897 [Online]. Available at https://www.scopus.com/inward/record.uri?eid=2-s2.0-51849135855&partnerID=40&md5=4710ae0f1993cab6e3e37729fae2a5c5.

Roizman, B. and Whitley, R. J. (2013) 'An inquiry into the molecular basis of HSV latency and reactivation', *Annual review of microbiology*, vol. 67, pp. 355–374.

Roller, R. J. and Baines, J. D. (2017) 'Herpesvirus Nuclear Egress', *Advances in anatomy, embryology, and cell biology*, vol. 223, pp. 143–169.

Rolls, M. M. and Jegla, T. J. (2015) 'Neuronal polarity: an evolutionary perspective', *The Journal of experimental biology*, vol. 218, Pt 4, pp. 572–580.

Royet, J.-P. and Plailly, J. (2004) 'Lateralization of olfactory processes', *Chemical senses*, vol. 29, no. 8, pp. 731–745.

Ruggiero, D. A., Underwood, M. D., Mann, J. J., Anwar, M. and Arango, V. (2000) 'The human nucleus of the solitary tract: visceral pathways revealed with an ‘‘in vitro’’ postmortem tracing method', *Journal of the Autonomic Nervous System*, vol. 79, pp. 181–190.

Salinas, S., Schiavo, G. and Kremer, E. J. (2010) 'A hitchhiker's guide to the nervous system: the complex journey of viruses and toxins', *Nature reviews. Microbiology*, vol. 8, no. 9, pp. 645–655.

Sawchenko, P. E. and Swanson, L. W. (1981) 'Central noradrenergic pathways for the integration of hypothalamic neuroendocrine and autonomic responses', *Science*, vol. 214, no. 4521, pp. 685–687.

Sawtell, N. M. (1998) 'The probability of in vivo reactivation of herpes simplex virus type 1 increases with the number of latently infected neurons in the ganglia', *Journal of virology*, vol. 72, no. 8, pp. 6888–6892.

Sawtell, N. M. (2003) 'Quantitative analysis of herpes simplex virus reactivation in vivo demonstrates that reactivation in the nervous system is not inhibited at early times postinoculation', *Journal of Virology*, vol. 77, no. 7, pp. 4127–4138.

Sawtell, N. M., Poon, D. K., Tansky, C. S. and Thompson, R. L. (1998) 'The latent herpes simplex virus type 1 genome copy number in individual neurons is virus strain specific and correlates with reactivation', *Journal of virology*, vol. 72, no. 7, pp. 5343–5350.

Schang, L. M., Rosenberg, A. and Schaffer, P. A. (1999) 'Transcription of herpes simplex virus immediate-early and early genes is inhibited by roscovitine, an inhibitor specific for cellular cyclin-dependent kinases', *Journal of Virology*, vol. 73, no. 3, pp. 2161–2172.

Schoenbaum, G., Chiba, A. A. and Gallagher, M. (1999) 'Neural encoding in orbitofrontal cortex and basolateral amygdala during olfactory discrimination learning', *The Journal of neuroscience: the official journal of the Society for Neuroscience*, vol. 19, no. 5, pp. 1876–1884.

Sehl, J., Hölper, J. E., Klupp, B. G., Baumbach, C., Teifke, J. P. and Mettenleiter, T. C. (2020) 'An improved animal model for herpesvirus encephalitis in humans', *PLoS pathogens*, vol. 16, no. 3, e1008445.

Sehl, J. and Teifke, J. P. (2020) 'Comparative Pathology of Pseudorabies in Different Naturally and Experimentally Infected Species-A Review', *Pathogens (Basel, Switzerland)*, vol. 9, no. 8.

Sehl-Ewert, J., Schwaiger, T., Schäfer, A., Hölper, J. E., Klupp, B. G., Teifke, J. P., Blohm, U. and Mettenleiter, T. C. (2022) 'Clinical, neuropathological, and immunological short- and long-term feature of a mouse model mimicking human herpes virus encephalitis', *Brain pathology (Zurich, Switzerland)*, vol. 32, no. 3, e13031.

Sehrawat, S., Kumar, D. and Rouse, B. T. (2018) 'Herpesviruses: Harmonious Pathogens but Relevant Cofactors in Other Diseases?', *Frontiers in Cellular and Infection Microbiology*, Volume 8 - 2018 [Online]. DOI: 10.3389/fcimb.2018.00177.

Seidel, K., Mahlke, J., Siswanto, S., Krüger, R., Heinsen, H., Auburger, G., Bouzrou, M., Grinberg, L. T., Wicht, H., Korf, H.-W., Dunnen, W. den and Rüb, U. (2015) 'The brainstem pathologies of Parkinson's disease and dementia with Lewy bodies', *Brain pathology (Zurich, Switzerland)*, vol. 25, no. 2, pp. 121–135.

Shahin, V., Hafezi, W., Oberleithner, H., Ludwig, Y., Windoffer, B., Schillers, H. and Kühn, J. E. (2006) 'The genome of HSV-1 translocates through the nuclear pore as a condensed rod-like structure', *Journal of cell science*, vol. 119, Pt 1, pp. 23–30.

Shankland, W. E. (2001) 'The trigeminal nerve. Part III: The maxillary division', *Cranio : the journal of craniomandibular practice*, vol. 19, no. 2, pp. 78–83.

Shen, W., Sa e Silva, M., Jaber, T., Vitvitskaia, O., Li, S., Henderson, G. and Jones, C. (2009) 'Two small RNAs encoded within the first 1.5 kilobases of the herpes simplex virus type 1 latency-associated transcript can inhibit productive infection and cooperate to inhibit apoptosis', *Journal of virology*, vol. 83, no. 18, pp. 9131–9139.

Shigenaga, Y., Takabatake, M., Sugimoto, T. and Sakai, A. (1979) 'Neurons in marginal layer of trigeminal nucleus caudalis ventrobasal complex (VB) and posterior

nuclear group (PO) by retrograde labeling with horseradish peroxidase Y', *Brain Research*, vol. 166, pp. 391–396.

Shivkumar, M., Milho, R., May, J. S., Nicoll, M. P., Efstathiou, S. and Stevenson, P. G. (2013) 'Herpes simplex virus 1 targets the murine olfactory neuroepithelium for host entry', *Journal of virology*, vol. 87, no. 19, pp. 10477–10488.

Shukla, D., Dal Canto, M. C., Rowe, C. L. and Spear, P. G. (2000) 'Striking similarity of murine nectin-1alpha to human nectin-1alpha (HveC) in sequence and activity as a glycoprotein D receptor for alphaherpesvirus entry', *Journal of virology*, vol. 74, no. 24, pp. 11773–11781.

Shukla, N. D., Tiwari, V. and Valyi-Nagy, T. (2012) 'Nectin-1-specific entry of herpes simplex virus 1 is sufficient for infection of the cornea and viral spread to the trigeminal ganglia', *Molecular vision*, vol. 18, pp. 2711–2716.

Simon, E. and Mertens, P. (2009) 'Functional anatomy of the glossopharyngeal, vagus, accessory and hypoglossal cranial nerves', *Neuro-Chirurgie*, vol. 55, no. 2, pp. 132–135.

Simons, M. and Nave, K.-A. (2015) 'Oligodendrocytes: Myelination and Axonal Support', *Cold Spring Harbor perspectives in biology*, vol. 8, no. 1, a020479.

Singletary, M. and Hagerty, S. (2023) 'Neuroanatomy and Neurophysiology of the Olfactory Signal Transduction Pathway', in Lazarowski, L. (ed) *Olfactory Research in Dogs,* Cham, Springer International Publishing, pp. 39–51.

Sivasubramanian, M. K., Monteiro, R., Harrison, K. S., Plakkot, B., Subramanian, M. and Jones, C. (2022) 'Herpes Simplex Virus Type 1 Preferentially Enhances Neuro-Inflammation and Senescence in Brainstem of Female Mice', *Journal of virology*, vol. 96, no. 17, e0108122.

Sköldenberg, B., Aurelius, E., Hjalmarsson, A., Sabri, F., Forsgren, M., Andersson, B., Linde, A., Strannegård, O., Studahl, M., Hagberg, L. and Rosengren, L. (2006) 'Incidence and pathogenesis of clinical relapse after herpes simplex encephalitis in adults', *journal of neurology*, vol. 253, no. 2, pp. 163–170.

Smith, G. (2012) 'Herpesvirus transport to the nervous system and back again', *Annual review of microbiology*, vol. 66, pp. 153–176.

Sodeik, B., Ebersold, M. W. and Helenius, A. (1997) 'Microtubule-mediated transport of incoming herpes simplex virus 1 capsids to the nucleus', *The Journal of cell biology*, vol. 136, no. 5, pp. 1007–1021.

Sosulski, D. L., Bloom, M. L., Cutforth, T., Axel, R. and Datta, S. R. (2011) 'Distinct representations of olfactory information in different cortical centres', *Nature*, vol. 472, no. 7342, pp. 213–216.

Spear, P. G., Eisenberg, R. J. and Cohen, G. H. (2000) 'Three classes of cell surface receptors for alphaherpesvirus entry', *Virology*, vol. 275, no. 1, pp. 1–8.

Spear, P. G. and Longnecker, R. (2003) 'Herpesvirus entry: an update', *Journal of virology*, vol. 77, no. 19, pp. 10179–10185.

Speck, P. and Simmons, A. (1998) 'Precipitous clearance of herpes simplex virus antigens from the peripheral nervous systems of experimentally infected C57BL/10 mice', *Journal of General Virology*, vol. 79, pp. 561–654.

Squire, L. R. (1992) 'Memory and the hippocampus: a synthesis from findings with rats, monkeys, and humans', *Psychological review*, vol. 99, no. 2, pp. 195–231.

Squire, L. R. and Zola-Morgan, S. (1991) 'The medial temporal lobe memory system', *Science*, vol. 253, no. 5026, pp. 1380–1386.

Stahl, J. P. and Mailles, A. (2019) 'Herpes simplex virus encephalitis update', *Current opinion in infectious diseases*, vol. 32, no. 3, pp. 239–243.

Standring, S. (2016) *Gray's Anatomy: The Anatomical Basis of Clinical Practice. 41st Edition.: Cranial nerves: functional components and nuclei p. 806–807*, Elsevier.

Standring, S. and Gray, H. (eds) (2005) *Gray's anatomy: The anatomical basis of clinical practice*, 39th edn, Edinburgh, Elsevier Churchill Livingstone.

Steiner, I. and Benninger, F. (2013) 'Update on herpes virus infections of the nervous system', *Current neurology and neuroscience reports*, vol. 13, no. 12, p. 414.

Stenwall, A., Uggla, A.-L., Weibust, D., Fahlström, M., Ryttlefors, M. and Latini, F. (2025) 'The Bulb, the Brain and the Being: New Insights into Olfactory System Anatomy, Organization and Connectivity', *Brain sciences*, vol. 15, no. 4.

Stewart, P. A. (1989) 'The sensory component of the trigeminal nerve. Maxillary and mandibular divisions', *University of Toronto dental journal*, vol. 2, no. 2, pp. 32–35.

Streppel, M., Popratiloff, A., Gruart, A., Angelov, D. N., Guntinas-Lichius, O., Delgado-Garcia, J. M., Neiss, W. F. and Stennert, E. (2000) 'Morphologische Verbindungen zwischen N. hypoglossus und N.facialis im Hirnstamm der Ratte', *HNO*, vol. 48, pp. 911–916.

Struyf, F., Posavad, C. M., Keyaerts, E., van Ranst, M., Corey, L. and Spear, P. G. (2002) 'Search for Polymorphisms in the Genes for Herpesvirus Entry Mediator, Nectin-1, and Nectin-2 in Immune Seronegative Individuals', *The Journal of infectious diseases*, vol. 185, no. 1, pp. 36–44 [Online]. Available at http://www.jstor.org/stable/30138123.

Sunderland, M. A. (2001) 'Neural Circuits', in Purves, D., Augustine, G. J. and Fitzpatrick, D. (eds) *Neuroscience. 2nd edition,* Sinauer Associates.

Taub, D. G., Jiang, Q., Pietrafesa, F., Su, J., Carroll, A., Greene, C., Blanchard, M. R., Jain, A., El-Rifai, M., Callen, A., Yager, K., Chung, C., He, Z., Chen, C. and Woolf, C. J. (2024) 'The secondary somatosensory cortex gates mechanical and heat sensitivity', *Nature Communications*, vol. 15, no. 1, p. 1289.

Taylor, M. P. and Enquist, L. W. (2015) 'Axonal spread of neuroinvasive viral infections', *Trends in microbiology*, vol. 23, no. 5, pp. 283–288.

Taylor, S. W., Smith, R. M., Pari, G., Wobeser, W., Rossiter, J. P. and Jackson, A. C. (2005) 'Herpes simplex encephalitis', *The Canadian journal of neurological sciences. Le journal canadien des sciences neurologiques*, vol. 32, no. 2, pp. 246–247.

Thompson, N., Mastitskaya, S. and Holder, D. (2019) 'Avoiding off-target effects in electrical stimulation of the cervical vagus nerve: Neuroanatomical tracing techniques to study fascicular anatomy of the vagus nerve', *Journal of Neuroscience Methods*, vol. 325, p. 108325 [Online]. DOI: 10.1016/j.jneumeth.2019.108325.

Thompson, R. L., Preston, C. M. and Sawtell, N. M. (2009) 'De Novo Synthesis of VP16 Coordinates the Exit from HSV Latency In Vivo', *PLOS Pathogens*, vol. 5, no. 3, e1000352.

Tomioka, Y., Takeda, K., Ozaki, K., Inoue, H., Yamamoto, S., Takeuchi, T. and Ono, E. (2024) 'Single amino acid mutation of nectin-1 provides remarkable resistance against lethal pseudorabies virus infection in mice', *The Journal of veterinary medical science*, vol. 86, no. 1, pp. 120–127.

Traurig, H. H. (2008) 'The Brain Stem Reticular Formation', in Conn, P. M. (ed) *Neuroscience in Medicine,* Totowa, NJ, Humana Press, pp. 273–286.

Turcotte, S., Letellier, J. and Lippé, R. (2005) 'Herpes simplex virus type 1 capsids transit by the trans-Golgi network, where viral glycoproteins accumulate independently of capsid egress', *Journal of Virology*, vol. 79, no. 14, pp. 8847–8860.

Twomey, J. A., Barker, C. M., Robinson, G. and Howell, D. A. (1979) 'Olfactory mucosa in herpes simplex encephalitis', *Journal of Neurology, Neurosurgery, and Psychiatry*, vol. 42, pp. 983–987.

Tyler, K. L. (2004) 'Update on herpes simplex encephalitis', *Reviews in neurological diseases*, vol. 1, no. 4, pp. 169–178.

Tyler, K. L. (2009) 'Emerging viral infections of the central nervous system: part 2', *Archives of neurology*, vol. 66, no. 9, pp. 1065–1074.

Umbach, J. L., Kramer, M. F., Jurak, I., Karnowski, H. W., Coen, D. M. and Cullen, B. R. (2008) 'MicroRNAs expressed by herpes simplex virus 1 during latent infection regulate viral mRNAs', *Nature*, vol. 454, no. 7205, pp. 780–783.

Uysal, S. (2023) '168The Occipital Lobes and Visual Processing', in Uysal, S. (ed) *Functional Neuroanatomy and Clinical Neuroscience: Foundations for Understanding Disorders of Cognition and Behavior,* Oxford University Press, p. 0.

Vallbracht, M., Backovic, M., Klupp, B. G., Rey, F. A. and Mettenleiter, T. C. (2019) 'Chapter Seven - Common characteristics and unique features: A comparison of the fusion machinery of the alphaherpesviruses Pseudorabies virus and Herpes simplex

virus', in Kielian, M., Mettenleiter, T. C. and Roossinck, M. J. (eds) *Advances in Virus Research: Virus Entry,* Academic Press, pp. 225–281.

Valyi-Nagy, T., Olson, S. J., Valyi-Nagy, K., Montine, T. J. and Dermody, T. S. (2000) 'Herpes Simplex Virus Type 1 Latency in the Murine Nervous System Is Associated with Oxidative Damage to Neurons', *Virology*, vol. 278, no. 2, pp. 309–321 [Online]. DOI: 10.1006/viro.2000.0678.

Verpoest, S., Cay, B., Favoreel, H. and Regge, N. de (2017) 'Age-Dependent Differences in Pseudorabies Virus Neuropathogenesis and Associated Cytokine Expression', *Journal of virology*, vol. 91, e02058-16.

Verzosa, A. L., McGeever, L. A., Bhark, S.-J., Delgado, T., Salazar, N. and Sanchez, E. L. (2021) 'Herpes Simplex Virus 1 Infection of Neuronal and Non-Neuronal Cells Elicits Specific Innate Immune Responses and Immune Evasion Mechanisms', *Frontiers in immunology*, vol. 12, p. 644664.

Wagenaar, F., Pol, J. M., Wind, N. de and Kimman, T. G. (2001) 'Deletion of the UL21 gene in Pseudorabies virus results in the formation of DNA-deprived capsids: an electron microscopy study', *Veterinary Research*, vol. 32, no. 1, pp. 47–54.

Wang, D. (2009) 'Reticular formation and spinal cord injury', *Spinal Cord*, vol. 47, 204-212 [Online]. Available at doi://10.1038/sc.2008.105;.

Wang, X., Patenode, C. and Roizman, B. (2011) 'US3 protein kinase of HSV-1 cycles between the cytoplasm and nucleus and interacts with programmed cell death protein 4 (PDCD4) to block apoptosis', *Proceedings of the National Academy of Sciences*, vol. 108, no. 35, pp. 14632–14636.

Wang, Y., Nian, H., Li, Z., Wang, W., Wang, X. and Cui, Y. (2019) 'Human encephalitis complicated with bilateral acute retinal necrosis associated with pseudorabies virus infection: A case report', *International journal of infectious diseases: IJID : official publication of the International Society for Infectious Diseases*, vol. 89, pp. 51–54.

Whitley, R. and Baines, J. (2018) 'Clinical management of herpes simplex virus infections: past, present, and future', *F1000Research*, 7(F1000 Faculty Rev): 1726.

Whitley, R., Lakeman, A. D., Nahmias, A. and Roizman, B. (1982) 'Dna restriction-enzyme analysis of herpes simplex virus isolates obtained from patients with encephalitis', *The New England journal of medicine*, vol. 307, no. 17, pp. 1060–1062.

Whitley, R. J. and Lakeman, F. (1995) 'Herpes simplex virus infections of the central nervous system: therapeutic and diagnostic considerations', *Clin Infect Dis*, vol. 20, no. 2, pp. 414–420.

Whitmore, L., Yetsko, K., Farrell, J. A., Page-Karjian, A., Daniel, W., Shaver, D. J., Frandsen, H. R., Walker, J. S., Crowder, W., Bovery, C., Rollinson Ramia, D., Burkhalter, B., Ryan, E. and Duffy, D. J. (2021) 'Evolutionary Comparisons of Chelonid Alphaherpesvirus 5 (ChHV5) Genomes from Fibropapillomatosis-Afflicted Green (Chelonia mydas), Olive Ridley (Lepidochelys olivacea) and Kemp's Ridley (Lepidochelys kempii) Sea Turtles', *Animals : an open access journal from MDPI*, vol. 11, no. 9.

Wilcox, S. L., Gustin, S. M., Macey, P. M., Peck, C. C., Murray, G. M. and Henderson, L. A. (2015) 'Anatomical changes at the level of the primary synapse in neuropathic pain: evidence from the spinal trigeminal nucleus', *The Journal of neuroscience: the official journal of the Society for Neuroscience*, vol. 35, no. 6, pp. 2508–2515.

Wild, P., Kaech, A., Schraner, E., Walser, L. and Ackermann, M. (2018) 'Endoplasmic reticulum-to-Golgi transitions upon herpes virus infection', *F1000Research*, vol. 6, p. 1804.

Wilson, A. C. and Mohr, I. (2012) 'A cultured affair: HSV latency and reactivation in neurons', *Trends in microbiology*, vol. 20, no. 12, pp. 604–611 [Online]. DOI: 10.1016/j.tim.2012.08.005.

Wind, N. de, Wagenaar, F., Pol, J., Kimman, T. and Berns, A. (1992) 'The pseudorabies virus homology of the herpes simplex virus UL21 gene product is a capsid protein which is involved in capsid maturation', *Journal of Virology*, vol. 66, no. 12, pp. 7096–7103.

Wnęk, M., Ressel, L., Ricci, E., Rodriguez-Martinez, C., Guerrero, J. C. V., Ismail, Z., Smith, C., Kipar, A., Sodeik, B., Chinnery, P. F., Solomon, T. and Griffiths, M. J. (2016)

'Herpes simplex encephalitis is linked with selective mitochondrial damage; a post-mortem and in vitro study', *Acta neuropathologica*, vol. 132, no. 3, pp. 433–451.

Wouk, J., Rechenchoski, D. Z., Rodrigues, B. C. D., Ribelato, E. V. and Faccin-Galhardi, L. C. (2021) 'Viral infections and their relationship to neurological disorders', *Archives of Virology*, vol. 166, no. 3, pp. 733–753.

Wu, H.-M., Huang, C.-C., Chen, S.-H., Liang, Y.-C., Tsai, J.-J., Hsieh, C.-L. and Hsu, K.-S. (2003) 'Herpes simplex virus type 1 inoculation enhances hippocampal excitability and seizure susceptibility in mice', *The European journal of neuroscience*, vol. 18, no. 12, pp. 3294–3304.

Wurst, W. and Bally-Cuif, L. (2001) 'Neural plate patterning: upstream and downstream of the isthmic organizer', *Nature reviews. Neuroscience*, vol. 2, no. 2, pp. 99–108.

Xiong, R., Rao, P., Kim, S., Li, M., Wen, X. and Yuan, W. (2015) 'Herpes Simplex Virus 1 US3 Phosphorylates Cellular KIF3A To Downregulate CD1d Expression', *Journal of Virology*, vol. 89, no. 13, pp. 6646–6655.

Yamada, S., Kameyama, T., Nagaya, S., Hashizume, Y. and Yoshida, M. (2003) 'Relapsing herpes simplex encephalitis: pathological confirmation of viral reactivation', *Journal of Neurology, Neurosurgery & Psychiatry*, vol. 74, no. 2, pp. 262–264.

Yan, K., Liu, J., Guan, X., Yin, Y.-X., Peng, H., Chen, H.-C. and Liu, Z.-F. (2019) 'The Carboxyl Terminus of Tegument Protein pUL21 Contributes to Pseudorabies Virus Neuroinvasion', *Journal of Virology*, vol. 93, no. 7.

Yang, Y., Wu, S., Wang, Y., Pan, S., Lan, B., Liu, Y., Zhang, L., Leng, Q., Da Chen, Zhang, C., He, B. and Cao, Y. (2015) 'The Us3 Protein of Herpes Simplex Virus 1 Inhibits T Cell Signaling by Confining Linker for Activation of T Cells (LAT) Activation via TRAF6 Protein*', *The Journal of biological chemistry*, vol. 290, no. 25, pp. 15670–15678 [Online]. DOI: 10.1074/jbc.M115.646422.

Yao, H.-W., Ling, P., Tung, Y.-Y., Hsu, S.-M. and Chen, S.-H. (2014) 'In vivo reactivation of latent herpes simplex virus 1 in mice can occur in the brain before occurring in the trigeminal ganglion', *Journal of virology*, vol. 88, no. 19, pp. 11264–11270.

Yong, S. J., Yong, M. H., Teoh, S. L., Soga, T., Parhar, I., Chew, J. and Lim, W. L. (2021) 'The Hippocampal Vulnerability to Herpes Simplex Virus Type I Infection: Relevance to Alzheimer's Disease and Memory Impairment', *Frontiers in cellular neuroscience*, vol. 15, p. 695738.

Yoshida, E., Kondo, M., Nakae, K., Ako, R., Terada, S., Hatano, N., Liu, L., Kobayashi, K., Ishii, S. and Matsuzaki, M. (2025) 'Whether or not to act is determined by distinct signals from motor thalamus and orbitofrontal cortex to secondary motor cortex', *Nature Communications*, vol. 16, no. 1, p. 3106.

Yuan, T.-F., Liang, Y.-X. and So, K.-F. (2014) 'Occurrence of new neurons in the piriform cortex', *Frontiers in neuroanatomy*, vol. 8, p. 167.

Yun, H., Gerges, P. H., Moghbeli, K., Das, J., Singh, H., Davis, B. M. and St. Leger, A. (2024) 'Dissecting Mouse Trigeminal Ganglia: A Comprehensive Analysis through Anatomical, Immunohistochemical, and Transcriptomic Approaches', *Investigative Ophthalmology & Visual Science*, vol. 65, no. 7, p. 3880.

Zhang, P., Yang, Y., Zou, J., Yang, X., Liu, Q. and Chen, Y. (2020) 'Seizures and epilepsy secondary to viral infection in the central nervous system', *Acta Epileptologica*, vol. 2, no. 1, p. 12.

Zhang, S., Zeng, J., Zhou, Y., Gao, R., Rice, S., Guo, X., Liu, Y., Feng, P. and Zhao, Z. (2022) 'Simultaneous Detection of Herpes Simplex Virus Type 1 Latent and Lytic Transcripts in Brain Tissue', *ASN neuro*, vol. 14, 17590914211053505.

Zhang, S.-Y., Harschnitz, O., Studer, L. and Casanova, J.-L. (2021) 'Neuron-intrinsic immunity to viruses in mice and humans', *Current opinion in immunology*, vol. 72, pp. 309–317.

Zhu, S. and Viejo-Borbolla, A. (2021) 'Pathogenesis and virulence of herpes simplex virus', *Virulence*, vol. 12, no. 1, pp. 2670–2702.

9 Appendix

9.1 Eigenständigkeitserklärung

"Ich erkläre: Ich habe die vorgelegte Dissertation selbständig und ohne unerlaubte fremde Hilfe und nur mit den Hilfen angefertigt, die ich in der Dissertation angegeben habe. Alle Textstellen, die wörtlich oder sinngemäß aus veröffentlichten oder nicht veröffentlichten Schriften entnommen sind, und alle Angaben, die auf mündlichen Auskünften beruhen, sind als solche kenntlich gemacht. Bei den von mir durchgeführten und in der Dissertation erwähnten Untersuchungen habe ich die Grundsätze guter wissenschaftlicher Praxis, wie sie in der "Satzung der Justus-Liebig-Universität Gießen zur Sicherung guter wissenschaftlicher Praxis" niedergelegt sind, eingehalten."

Viktoria Korff

9.2 Publications

[I] Korff V, El-Debs I, Bröer S, Klupp BG, Teifke JP, Mettenleiter TC, Sehl-Ewert J (2025) Neurotropism of alphaherpesviruses is most prominent in the mesiotemporal, piriform and prefrontal cortices in mice. *Neuroscience* 584: 367–381, doi: 10.1016/j.neuroscience.2025.08.024
Erratum: https://doi.org/10.1016/j.neuroscience.2025.10.037

[II] Korff V, El-Debs I, Sehl-Ewert J (2025) Spatial and temporal mapping of early alphaherpesvirus invasion routes into the mouse central nervous system. J Neurovirol, doi: 10.1007/s13365-025-01278-3

[III] Korff V, El-Debs I, Klupp BG, Teifke JP, Mettenleiter TC, Sehl-Ewert J (2025) Spatiotemporal dynamics of alphaherpesviral latency and reactivation in the murine central nervous system. bioRxiv, doi: 10.1101/2025.09.11.675502

9.3 Poster presentations

03/2025	**Korff, V**.; El-Debs, I.; Klupp, B.G.; Teifke, J.P.; Mettenleiter, T.C.; Sehl-Ewert, J. (2025), Neurotropism in a murine model of alphaherpesvirus infection is most prominent within the temporal lobe. 34th Annual Meeting of the Society for Virology, Hamburg, 04.03.-07.03.2025
11/2024	**Korff, V**.; El-Debs, I.; Klupp, B.G.; Teifke, J.P.; Mettenleiter, T.C.; Sehl-Ewert, J. (2024), Neurotropism in a murine model of alphaherpesvirus infection is most prominent within the temporal lobe. Junior Scientist Symposium, Friedrich-Loeffler-Institut, Braunschweig, 20.11.-22.11.2024
03/2024	**Korff, V**.; El-Debs, I.; Klupp, B.G.; Teifke, J.P.; Mettenleiter, T.C.; Sehl-Ewert, J. (2024), Brain region-specific susceptibility upon alphaherpesviral infection. 33rd Annual Meeting of the Society for Virology, Wien, 25.03.-28.03.2024
11/2023	**Korff, V**.; El-Debs, I.; Klupp, B.G.; Teifke, J.P.; Mettenleiter, T.C.; Sehl-Ewert, J. (2023), Why infect alphaherpesviruses only very specific regions in the brain? Junior Scientist Symposium, Friedrich-Loeffler-Institut, Jena, 15.11.-17.11.2023
11/2022	**Korff, V**.; El-Debs, I.; Klupp, B.G.; Teifke, J.P.; Mettenleiter, T.C.; Sehl-Ewert, J. (2022), Characterization of the invasion route and susceptibility of neural tissue upon alphaherpesviral infection. Junior Scientist Symposium, Friedrich-Loeffler-Institut, Greifswald – Insel Riems, 14.11.-16.11.2022

9.4 Acknowledgement

Diese Dissertation ist nicht nur das Ergebnis wissenschaftlicher Arbeit, sondern auch Ausdruck der Unterstützung, des Vertrauens und der Zusammenarbeit vieler Menschen, denen ich von Herzen danken möchte.

Mein tiefster Dank gilt **Dr. Julia Sehl-Ewert** für ihre außergewöhnliche und engagierte Betreuung während meiner Promotionszeit. Ihre konstante Unterstützung – selbst während Schwangerschaft und Mutterschaft – sowie ihre offene, klare Kommunikation, schnelle Rückmeldung und zielführenden Anregungen haben mir in vielerlei Hinsicht enorm geholfen. Julia, deine Begeisterung für neurovirologische und neuropathologische Themen war ansteckend und hat mich nachhaltig inspiriert. Deine Verlässlichkeit und dein bemerkenswerter Ehrgeiz haben mich nicht nur fachlich, sondern auch persönlich entscheidend geprägt. Du warst jederzeit bereit für ein Gespräch, das oft von inspirierenden Diskussionen getragen wurde. Du hast mir Raum zur Selbstentfaltung gegeben und mir den Einstieg in die wissenschaftliche Arbeit durch deine Begleitung spürbar erleichtert. Dafür danke ich dir von Herzen.

Herrn **Prof. Dr. Jens P. Teifke** danke ich besonders für seine Betreuung, die konstruktiven Gespräche, seine wertvollen Ratschläge sowie die Möglichkeit, meine Doktorarbeit am Friedrich-Loeffler-Institut und der Universität Gießen durchführen zu dürfen.

Mein herzlicher Dank geht an Frau **Dr. Barbara G. Klupp** für die Möglichkeit, meine molekularvirologischen Arbeiten in ihrem Labor durchführen zu dürfen. Ihre geduldige Unterstützung beim Erlernen molekularvirologischer Methoden sowie ihre fachkundige Begleitung bei der Interpretation meiner Ergebnisse haben mir sehr geholfen.

Herrn **Prof. Dr. Dr. h.c. Thomas C. Mettenleiter** danke ich für die wertvollen Diskussionen und seinen wissenschaftlichen Input. Von seinem umfassenden Wissen konnte ich in hohem Maße profitieren.

Frau **Dr. Angele Breithaupt** danke ich für ihre Unterstützung während meiner gesamten Zeit am FLI, insbesondere während Julias Mutterschaft. Ihr wissenschaftlicher Input und die angenehme Zusammenarbeit und ihr stets offenes Ohr waren für mich von großem Wert.

Mein besonderer Dank gilt den technischen Assistenten Frau **Silvia Schuparis**, Herrn **Robin Brandt**, Frau **Cindy Krüper** und Frau **Karla Günther**, die mich mit viel Geduld und Fachkenntnis bei molekularvirologischen und pathohistologischen Techniken unterstützt und eingearbeitet haben.

Ein großer Dank geht an alle Mitglieder der „AG-Pathologie“ für die wunderbare Zeit und das kollegiale Miteinander. Ich habe mich in unserem Team stets wohl und unterstützt gefühlt. Herrn **Issam El-Debs** danke ich für seine tatkräftige Hilfe bei den täglichen Tierkontrollen und stereotaktischen Operationen – und für die vielen gemeinsamen Stunden im Stall, die trotz Stress immer von gegenseitiger Unterstützung und guter Laune geprägt waren. Herrn **Tobias Britzke** danke ich für seine Hilfe bei der bildgebenden Analyse und bei pathohistologischen Auswertungen. Herrn **L. Mathias Michaely** danke ich für seine Unterstützung bei statistischen Fragestellungen und seine stets hilfsbereite Art.

Für die Einführung und Unterstützung bei bildgebenden Verfahren wie dem Thunder Imaging System und der konfokalen Laser-Scanning Mikroskopie danke ich Herrn **Dr. Dmitry Ushakov**, Frau **Henriette Schwotzer** und Herrn **Sebastian Gaßmann** ganz herzlich.

Frau **Prof. Dr. Sonja Bröer** danke ich für ihre wertvolle Hilfe bei den stereotaktischen Operationen und ihre geduldige Einarbeitung.

Mein Dank gilt auch den **Tierpflegern** des FLI, die mich bei der Einstallung und Pflege meiner Mäuse stets zuverlässig unterstützt haben, sowie den Sektionshelfern Herrn **Thomas Pieper** und Herrn **Ralf Redmer** für ihre Hilfsbereitschaft und tatkräftige Unterstützung in den Stallungen.

Ein herzliches Dankeschön geht an meine **Mitdoktoranden**, die im Laufe der Zeit zu engen Freunden geworden sind. Ohne euch wäre diese Zeit nur halb so schön gewesen. Die gemeinsamen Mittagspausen, Fahrten zum FLI und die Treffen am Hafen oder Strand werde ich sehr vermissen.

Mein letzter und größter Dank gilt meiner **Familie** und engen **Freunden**. Eure bedingungslose Unterstützung, euer Vertrauen und euer Verständnis haben mir die

Kraft gegeben, diesen Weg zu gehen. Ohne euch wäre diese Arbeit nicht möglich gewesen.